# Aspects of Lasers for the Illumination of Interferometric Gravitational Wave Detectors

Sheila Rowan

Department of Physics and Astronomy

University of Glasgow

Presented as a thesis for the degree of Ph.D.

in the University of Glasgow

July 27, 1995

# Contents

# List of Figures

# List of Tables

# Acknowledgements

Firstly I would like to thank my supervisor Prof. Jim Hough for his extreme patience, help and encouragement throughout the research for this thesis.

Thanks are also due to Anne Campbell for her help and support during the period of this work.

I would also like to thank the other members of the Gravitational Waves Group at Glasgow University namely, Gavin Newton, Norna Robertson, Harry Ward, Jennifer Logan, David Robertson, Kenneth Strain, Stuart Killbourn, Alison McLaren, Paul McNamara, Kenneth Skeldon, Sharon Twyford, Alistair Grant and Ray Hutchins for their advice and interest in my work.

Thanks are also due to Colin Craig, David Edwards, Allan Latta and Angus McKellar for excellent technical support.

I am grateful for the support given by Prof. R.P. Ferrier during the period of this work. During the time this work was carried out I was in receipt of financial support from PPARC (formerly SERC).

Lastly I would like my family and in particular my mother, for their support during my years at university.

# Preface

Chapter 1 of this thesis contains an introduction to the nature, sources and methods proposed for the detection of gravitational waves. Emphasis is placed on the techniques and noise sources associated with laser interferometric gravitational wave detectors and the resulting implications for the choice of a laser source for this type of detector. This information is mainly derived from the literature.

Chapter 2 contains details of experiments to construct electronic feedback systems to stabilise the intensity at both low and high frequencies of a miniature diode-pumped monolithic Nd:YAG ring laser. This work was performed in collaboration with Dr Anne Campbell and Prof. Jim Hough, with advice on directly driving the diode laser from Charles Harb, (Australian National University, Canberra). Also described are investigations into the factors limiting the performance of the stabilisation systems. This was carried out with the added help of Ken Skeldon.

Chapter 3 describes experiments to measure the frequency noise of a Nd:YAG ring laser at relaxation oscillation frequencies. Also described are investigations into the noise of a commercial Nd:YAG ring laser. These experiments were carried out in collaboration with Dr. Anne Campbell and Prof. Jim Hough.

Chapter 4 describes experiments on the intracavity frequency doubling of a high power flashlamp-pumped Nd:YAG rod laser using different cavity designs. These experiments were carried out mainly by the author with some advice from Prof. Jim Hough, Dr. Anne Campbell, Dr. Gavin Newton and Dr. Malcolm Gray (Australian National University, Canberra) and with some invaluable experimental help from Dr. J. Hong (formerly of the University of St. Andrews).

This thesis concludes with Chapter 5 describing the prospects for the use of Nd:YAG lasers and frequency doubled Nd:YAG lasers as sources of illumination for

interferometric gravitational wave detectors.

# Summary

Gravitational waves are one of the predictions of Einstein's General Theory of Relativity. Observation by Hulse and Taylor of the changes in the orbit of the binary pulsar PSR 1913+16 provided indirect evidence for the existence of gravitational waves, but direct detection has yet to be achieved. Over the past few years much progress has been made in developing methods which centre on sensing the minute changes in the curvature of spacetime resulting from violent astrophysical phenomena. In particular, the most promising type of detector currently under development uses laser interferometry to sense the displacement of freely suspended masses caused by their interaction with gravitational radiation, and construction of the first of several large scale detectors of this type is already underway.

There are many potential sources of noise which may limit the sensitivity of this type of detector, one of these being noise associated with the light used to illuminate the detector. Currently most prototype gravitational wave detectors are illuminated by argon-ion lasers but laser sources proposed for large scale detectors include Nd:YAG lasers and frequency doubled Nd:YAG lasers. It is thus important that the properties of these laser sources are investigated. This thesis details investigations into aspects of Nd:YAG and frequency doubled Nd:YAG lasers for use in interferometric gravitational wave detectors.

Monolithic Nd:YAG ring lasers are compact efficient sources of light at 1064 nm and are proposed as seed lasers for the high power injection locked Nd:YAG systems designed for use in large scale detectors. It has been previously shown by Farinas et al in Stanford that the noise properties of the light from the slave laser are dominated by those of the seed laser light. This type of laser is prone to a particular type of high frequency intensity noise in the form of relaxation oscillations. Significant amounts

of noise at high frequencies may couple into measurements at low frequencies as a result of any nonlinearities in the detection process so it is important to be able to control noise at the relaxation oscillation frequencies. In this thesis previous work by Kane at Stanford on the damping of relaxation oscillations in low power monolithic Nd:YAG ring lasers is extended to higher power lasers suitable for use as master oscillators. Experiments are described which resulted in fluctuations in laser intensity due to relaxation oscillations being suppressed to a level of $1.9 \times 10^{-6}/\sqrt{Hz}$ at 250 kHz.

A broadband electronic feedback system was designed and constructed to simultaneously reduce intensity noise to acceptable levels both at the relaxation oscillation frequencies and at the lower frequencies of direct interest for gravitational wave detection. Resulting stabilised levels of $2.3 \times 10^{-6}/\sqrt{Hz}$ at the relaxation oscillation frequency of around 260 kHz to 270 kHz and $4.6 \times 10^{-8}/\sqrt{Hz}$ at 500 Hz were low enough to make this type of laser a good candidate for a seed laser.

Investigations were also made into the frequency noise levels of this type of laser at both low and relaxation oscillation frequencies.

The level of frequency noise at the relaxation oscillation frequency was found to lower than 1 $Hz/\sqrt{Hz}$ and this is considered to be unlikely to cause problems with measurements at lower frequencies. The upper limit to the level of low frequency noise of $\simeq 200$ $Hz/\sqrt{Hz}$ at 500 Hz was measured, and this was acceptable as the laser light would undergo further stabilisation before injection into an interferometric detector.

Investigations were made into the intra-cavity frequency doubling of light from a high power flashlamp pumped Nd:YAG laser using linear and ring designs of cavity. The linear cavity design allowed both the fundamental and second harmonic light to leave the crystal and reenter it - i.e. to pass twice through the doubling crystal - before the second harmonic light was extracted from the cavity. If the second harmonic and fundamental beams reentered the doubling crystal in phase, then in theory the beams of second harmonic light could add to produce up to four times the power which was expected on a single pass through a doubling crystal. Results were obtained using different types of doubling crystal.

The maximum second harmonic power obtained was 4.6 W using a 23 mm crystal of LBO. The light obtained was in several spatial and longitudinal modes and no single mode operation of the laser was achieved. It was concluded that while the linear design of doubling cavity was a relatively simple and efficient way of obtaining reasonably high powers of multi-mode frequency doubled light it was not suitable for producing single frequency green light.

It seemed desirable to use a ring cavity design to obtain the frequency doubled light in the single longitudinal mode necessary for the illumination of gravitational wave detectors. Experiments were thus carried out to investigate intra-cavity doubling using a 4 mirror ring cavity. In this case the maximum second harmonic power obtained was 2.8 W again in several longitudinal and spatial modes. The maximum single frequency second harmonic power obtained (980 mW) appeared to be limited by the intra-cavity power of the laser. This was less than would be required to replace the argon-ion lasers which are currently used in prototype gravitational wave detectors.

It is possible that increased second harmonic power could be obtained by isolating the laser cavity from sources of acoustic and vibrational noise to allow higher powers of fundamental intra-cavity light in $TEM_{00q}$ mode. An alternative approach to improving performance would be to use an external resonant doubling as has been successfully demonstrated by Yang and colleagues in Stanford. This would allow the lasing and doubling processes to be separated so each process could be more easily optimised. It is also possible that high powers of second harmonic light may be more easily achieved through the use of new nonlinear materials currently under development. These areas of development will be pursued further in the future.

# Chapter 1

# The Nature, Sources and Detection of Gravitational Waves

## 1.1 Introduction

In a Newtonian model of the universe, any change in gravitational field caused by a body moving occurs instantly. However, the description of gravity contained in the General Theory of Relativity developed by Einstein, implies that changes in gravitational fields propagate at the speed of light, with solutions to the weak-field approximation of this theory obeying a wave equation.

Analysis carried out by Taylor and Weisberg [1] of observations of the orbital period of the binary pulsar PSR 1913 + 16 provided indirect evidence for the existence of these gravitational waves. These observations, which used the pulsar signals as a clock to time the binary orbit, showed the orbital period of the system to be decreasing at a rate consistent with the predictions of General Relativity and in particular with the loss of energy from the system by gravitational waves.

Direct observation of gravitational waves has however yet to be achieved and several research groups world-wide are currently working towards this end. Indeed the detection of gravitational waves is one of the most challenging and potentially rewarding goals of experimental physics. It will not only allow direct confirmation of one of the more exotic predictions of General Relativity, but will provide information about violent astrophysical events in the Universe obtainable in no other way, and

will lead to the opening of a new field of astronomy.

This chapter will describe briefly the nature, sources and proposed methods for detection of gravitational waves.

## 1.2 The Nature, Sources and Detection of Gravitational Waves

The wave nature of the propagation of changes in the gravitational field can be derived from the weak field approximation to Einstein's General Theory of Relativity, in which space-time is considered to be described by the sum of a background term which is nearly flat, and a perturbation. From this assumption the curvature of space-time resulting from the perturbation can be described by equation 1.1 [2].

$$\nabla^2 h_{\alpha\beta} - \frac{1}{c^2}\frac{\partial^2}{\partial t^2} h_{\alpha\beta} = 0 \tag{1.1}$$

This is a three-dimensional wave equation implying the existence of waves travelling with velocity $c$ equal to the speed of light. $h_{\alpha\beta}$ can be thought of as the gravitational wave field and is a tensor describing the strain in space-time caused by the changing gravitational field.

Waves reaching us from distant sources will be approximately plane so it is appropriate to think of the waves as propagating linearly in some direction, $z$. These transverse waves, which are quadrupole in nature, can be split into two independent polarisation states normally denoted $h_+$ and $h_\times$.

To visualise the strain in space caused by plane polarised gravitational waves it is useful to imagine the effects of the gravitational waves on a ring of test particles. The deformations of this ring by waves of polarisation $h_+$ and $h_\times$ respectively are shown in figure 1.1.

It can be seen that in both cases the ring is stretched and compressed in orthogonal directions. If the ring of particles originally has radius $L$, the passage of a gravitational wave travelling in a direction perpendicular to the plane of the ring causes the radius of the ring to be stretched in one direction by an amount $\Delta L$, and compressed in the orthogonal direction by $\Delta L$. The amplitude of the gravitational

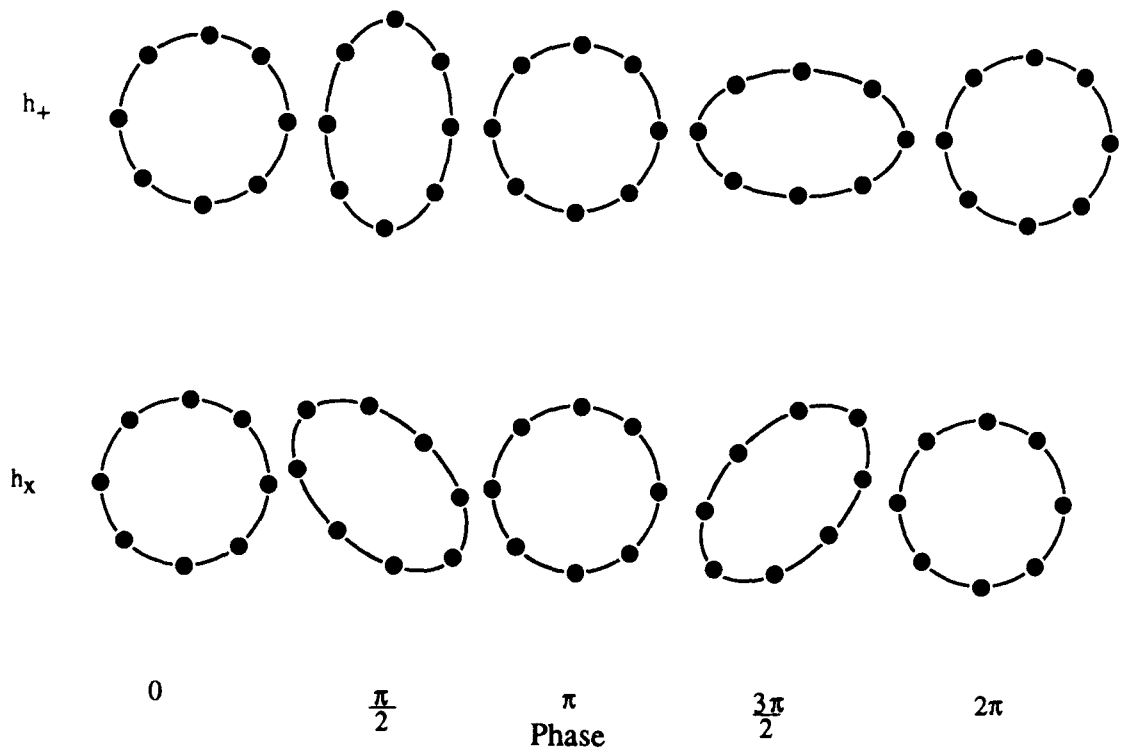


Figure 1.1: *The effects of plane polarised gravitational waves of polarisations $h_+$ and $h_\times$ on a ring of test particles in space. Reproduced from D. Blair, The detection of gravitational waves, Cambridge University Press, Cambridge, (1991)*

wave may be defined in terms of the induced strain as

$$h = \frac{2\Delta L}{L} \tag{1.2}$$

## 1.3 Sources of Gravitational Waves

Gravitational waves are produced by the acceleration of mass with, however, the requirement that the acceleration must in some way be asymmetric. The amplitude of gravitational waves generated by any laboratory source has been shown to be too small to make detection feasible [2]. However the large masses and accelerations involved in astrophysical processes mean that a variety of astrophysical systems can be considered as powerful sources of gravitational waves. Sources can be split into several categories: burst sources, producing gravitational waves over a relatively short time interval; periodic sources, producing continuous gravitational wave signals; and stochastic sources. These are briefly described below. A more complete review of sources may be found in [3] [4] and [5].

### 1.3.1 Burst Sources

#### Gravitational Collapse

The possibility of gravitational wave production by stellar collapses (supernovae) was one of the motivations behind early experiments in gravitational wave detection [6]. Supernovae are classified as either type I or type II events. It is believed that a type I supernova is the nuclear explosion of a white dwarf which has been accreting matter from a companion star, with the core of the white dwarf possibly collapsing to form a neutron star. A type II supernova involves the collapse of the core of a massive star when the radiation pressure is no longer sufficient to balance gravitational attraction. The properties of gravitational waves produced by these types of event would depend on the speed, and crucially, the symmetry of the collapse. No gravitational waves would result from a perfectly spherical collapse. If, however, the core has reasonably high angular momentum then an asymmetric collapse will occur [3] with the possibility of strong emission of gravitational waves. Recently evidence from the observation of the velocities of pulsars [7], considered to be formed in supernovae explosions, suggests that asymmetries are larger than was previously thought and it is reasonable that signals of amplitude $h \simeq 10^{-21}$ over time scales of several milliseconds, might be expected from events at the distance of the Virgo cluster [8]. It is plausible that several events per year of this type might be observable on earth [8].

It is also possible that gravitational collapse occurs on much larger scales and has led to the formation of massive and super massive black holes now thought to exist at the centres of some galaxies. Gravitational waves of very low frequency are likely to have been emitted during the formation phase and may also be emitted during possible black hole interactions associated with galaxy mergers [9]. Such signals are not likely to be candidates for detection by earth bound detectors for reasons which will be discussed later.

#### Coalescing Binaries

Coalescing binary systems, consisting of neutron stars (or black holes) rotating about a common centre of mass, experience decay of their orbital periods as the systems

inspiral due to loss of energy in the form of gravitational waves generated by their orbital motion.

These systems, which can range from two neutron stars each of $\simeq 1.4$ solar masses to two black holes each of several million solar masses, are attractive candidates for gravitational wave generation both at high and low frequencies.

The expected wave forms of the gravitational radiation emitted may be predicted relatively easily. For example in the few seconds prior to the final coalescence the gravitational wave signal will have a distinctive form as both the frequency and amplitude of the signal increase towards a maximum [8].

Coalescing binaries are of particular interest as Schutz [10] has shown that the distance and position of a coalescing binary system may be obtained from detecting the strength and form of the gravitational wave signal produced. This requires the signal to be sensed by three or more detectors. Coalescing binary systems may thus be used as distance indicators. If an optical signal is also detected at this distance, the red shift in the detected spectrum then allows the calculation of an unambiguous value for Hubble's Constant.

Recently there has been some discussion as to the event rate associated with binary coalescences. This depends on the type and mass of the components of the binary system. For the case of neutron star-neutron star (NS-NS) binaries the statistics of observed pulsars in neutron star binary systems would suggest an event rate of, on average, one every 8 years out to a distance of 100 Mpc [11]. However Tutukov and Yungelson [12] suggest that there may exist a large population of short lived neutron star binaries leading to a coalescence rate of 100 a year out to a distance of $\simeq$200 Mpc. These predictions are not in conflict as the pulsar searches would be unlikely to detect candidates with short lifetimes [11]. For black hole binaries, or black hole-neutron star binaries, the coalescence rate is, within a given volume, expected to be less but the signals are expected to be stronger than for the NS-NS case [9]. Thus for a detection system of given sensitivity these types of coalescences may give signals at a rate comparable to the NS-NS coalescences.

Possible signal strengths for supernovae and coalescing binaries are shown in figure 1.2.

### 1.3.2 Periodic Sources

There are a number of possible types of periodic sources, the most predictable of these being white dwarf binary systems which radiate at frequencies below $\simeq 10^{-2}$ Hz. [13] Of more interest for ground based detectors are pulsars and spinning accreting neutron stars.

#### Pulsars

Pulsars are sources of gravitational radiation through any asymmetry they may have about their axis of rotation. Such asymmetries must be present because of off axis magnetic field alignment but their size depends on unknown quantities, such as the properties of the crust and the surface magnetic field pattern [14]. It is interesting to note that if the newly discovered nearby pulsar PSR J0437-4715 radiates gravitational energy at a rate comparable to the rate at which it is losing rotational energy, then it would produce a signal of amplitude up to $h = 3 \times 10^{-26}$ at 346 Hz, depending on orientation [3]. If this signal is integrated for a year it has an effective strength (with respect to background detector noise) of $\simeq 3 \times 10^{-21}$. Most other pulsars are expected to produce a somewhat weaker signal.

#### Spinning Accreting Neutron Stars (Wagoner Stars)

Neutron stars with high angular momentum may, as a result of accretion, reach a gravitational radiation instability point causing asymmetries in the star and gravitational wave production. Further accretion drives the instability until a steady state is reached in which the angular momentum lost by radiation of gravitational waves equals the angular momentum gained by accretion. Radiation at frequencies of several hundred Hz is expected from this process at levels somewhat weaker than for the pulsar discussed above. The exact frequencies of the signals are unknown but in a particular instance may be determined by directly measuring the periodicity in the X-ray flux which may be radiated from such a system [15].

### 1.3.3 Stochastic Background

It is expected that a random background of gravitational radiation will exist as a result of the signals from many sources. This may contain information about cosmic strings or other processes in the early universe connected with galaxy formation.

Since stochastic sources are defined to be randomly distributed, the energy density of the sources in some frequency range may be defined as some fraction of the closure density, $\Omega_{gw}$ of the universe. The results of searches for the stochastic background, using the cross-correlation of measurements by two or more detectors, will thus allow an upper limit to be set on the closure density of the universe [16]. Current cosmic string theories require $\Omega_{gw} \simeq 10^{-7}$ per decade of frequency [17] so the results of stochastic observations could help with the interpretation of these theories.

### 1.3.4 Summary

Some of the relevant sources of gravitational waves and their expected strengths are shown in figure 1.2 along with design sensitivities for two projects currently proposed to detect gravitational waves.

## 1.4 The Detection of Gravitational Waves

As was seen in section 1.2, the effect of gravitational waves on a system of particles was to induce a strain in space which resulted in relative movement of the particles. Proposed methods of gravitational wave detection are based on detecting and measuring this strain using various techniques for precision measurement of the motions of test masses.

Laboratory based techniques are split into two different approaches: those which involve attempting to measure the mechanical modes of a carefully chosen piece of massive material excited by a suitably oriented gravitational wave, and those involving the use of laser interferometry to measure changes in the separation of freely suspended masses. Space based experiments in gravitational wave detection have also been of interest for a number of years [18]. In this section several of these techniques are considered.

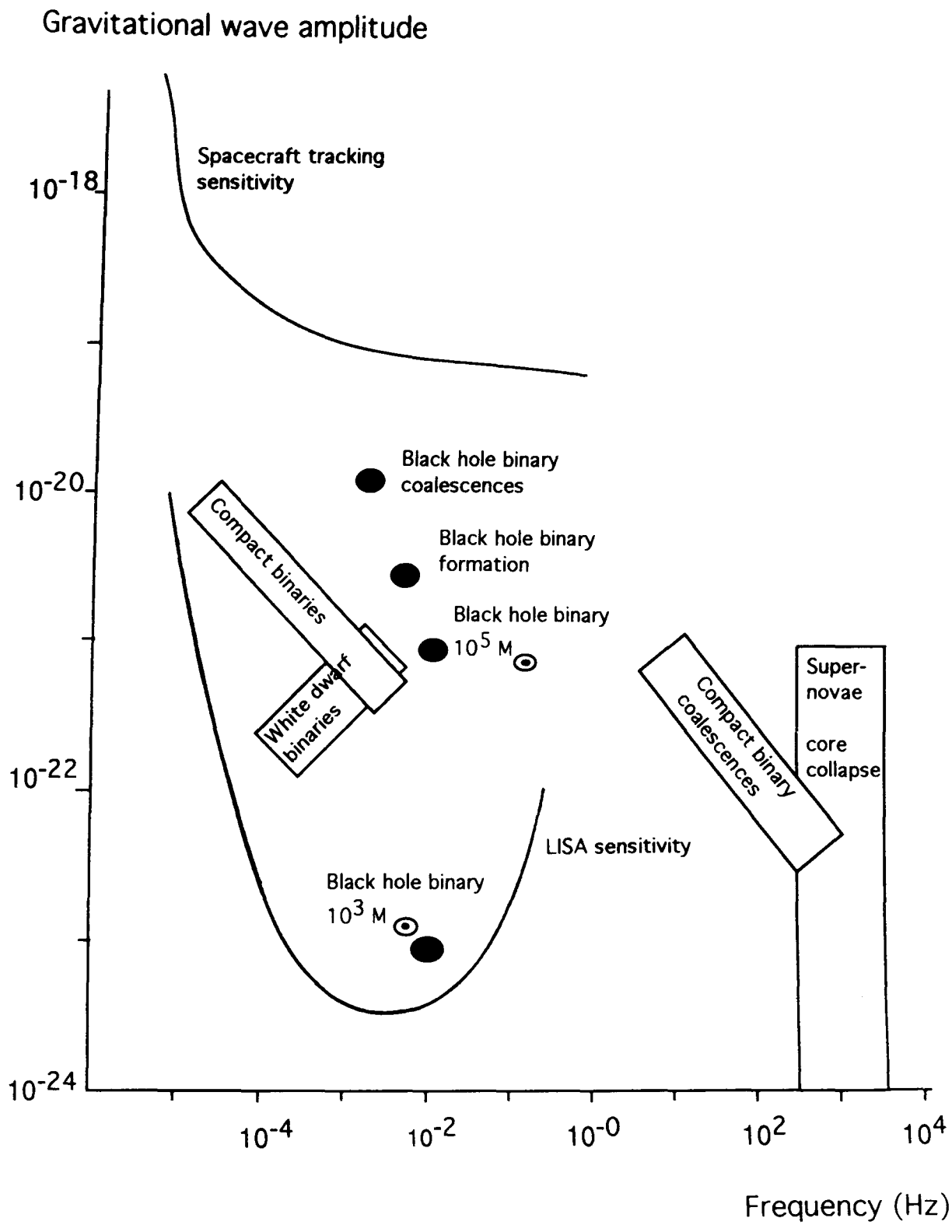


Figure 1.2: *Some astrophysical sources of gravitational waves. The circular markers and rectangular boxes show the approximate signal strengths from a range of sources.*

Figure 1.2 shows the frequencies and relative strengths of some of the expected gravitational wave signals from various sources. It can be seen that such signals are expected to occur over a wide frequency range, from $\simeq$ 0.1 mHz to 10 kHz and that the amplitude of these signals corresponds to strains in space that are extremely small. For example, to detect gravitational waves occurring at $\simeq$ 1 kHz would require a detector capable of measuring strains at this frequency of the order of $h \simeq 10^{-21}$ or better in a 1 kHz bandwidth. It is thus important that motions of the test masses caused by gravitational waves are not masked by noise from other sources, for example acoustic or seismic noise.

### 1.4.1 Space Based Detectors

As can be seen from figure 1.2, several promising sources of gravitational waves produce signals at frequencies below 1 Hz. There are however significant sources of noise which would act on any test masses situated on the earth to make signals at these very low frequencies inaccessible to ground based detectors. Motions of the masses due to the effects of seismic noise at low frequencies are difficult to eliminate and in particular it is impossible to shield the test masses from changes in the surrounding gravity gradient.

A solution to these problems is to operate a gravitational wave detector in the quiet environment of space. In addition to the possible avoidance of these noise sources, using space based detectors provides another benefit. As can be seen from equation 1.2, the change in separation of two test masses, $\Delta L$, caused by a gravitational wave of amplitude $h$ is proportional to the separation of the masses; thus to maximise the sensitivity of the system, it is desirable that the test masses be as far apart as possible. Space based detectors allow the possibility of using test masses separated by distances far greater than is possible with any terrestrial detector.

#### Pulsar timing

At very low frequencies, 1 cycle per year or lower, pulsar timing is being used to set limits on the gravitational wave background. This is done by using the pulsar as a very stable clock and searching for the effects of a very low frequency gravitational

wave on the phase of the radio signals from the pulsar. Timing observations of the pulsars B1855+09 and B1937+21 by Kaspi et al [19] have set a limit on the energy density per logarithmic frequency interval (defined as $d\Omega_{gw}/(d \ln f)$) in a cosmic background of stochastic gravitational waves of $\Omega_{gw} < 6 \times 10^{-8}$ .

**Spacecraft Tracking - ULYSSES**

Using a stable clock on Earth as a reference, a method similar to that adopted in pulsar timing experiments has been in use at higher frequencies in spacecraft tracking experiments. Searches for gravitational wave signals in the mHz region have been carried out by using Doppler tracking of the motion of spacecraft (Voyager I [18], ULYSSES [20]). Recent experiments using the ULYSSES spacecraft have set an upper limit on the gravitational wave amplitude in this frequency range of $h \simeq 3 \times 10^{-15}$.

**LISA**

The LISA (Laser Interferometer Space Antenna) experiment is a space based Michelson type interferometer proposed to detect and observe gravitational waves occurring in the 0.1 mHz to 1 Hz range which, for reasons described earlier, are not detectable by ground based detectors [13].

LISA consists of an array of 6 spacecraft, arranged in 3 pairs, with each pair of spacecraft at the corner of an equilateral triangle with sides of length 5 million km. This array would be placed in solar orbit (following the Earth). Each spacecraft contains a test mass and laser transponder so that the arms of the triangle form three separate but not fully independent interferometers. The passage of a gravitational wave will change the separations of the test masses (and spacecraft) and result in changes in the arm lengths of the interferometers. These changes are measured by comparing the phases of laser beams sent out from each spacecraft with those of beams returning from the distant spacecraft and, from this, information about the possible gravitational wave sources may be extracted.

LISA is proposed as a Cornerstone Mission for the European Space Agency Horizon 2000 Program.

Figure 1.2 shows the expected sensitivity of LISA to gravitational wave signals.

### 1.4.2 Ground Based Detectors

#### Bar Detectors

The first experiments in gravitational wave detection were carried out by Joseph Weber of the University of Maryland. These experiments were designed to detect the vibrations induced in massive bars of material (usually several tons of aluminium) caused by the passage of suitably oriented gravitational waves [6].

Early resonant bar detectors were designed so that the fundamental longitudinal mode of the bar was resonant at 1600 Hz, a frequency at which one might expect there to be gravitational waves. The motion of the bar was sensed using piezoelectric transducers (pzts), with the bar being acoustically and seismically isolated.

Weber carried out experiments designed to look for coincident excitations of two bar detectors separated by about 1000 km. Results from these experiments were published in 1969 claiming coincident excitations consistent with the detection of gravitational waves [6]. However no subsequent experiments were able to repeat these findings [21] [22] [23]. These experiments did however stimulate interest in the field of gravitational wave detection resulting in significant increases in detector sensitivity. Development of Weber bar type detectors has continued with the emphasis being on cooling the detector (to $\simeq 4K$) to reduce the noise level. Currently systems at the Universities of Rome, Louisiana and Perth are achieving sensitivities of better than $h \simeq 10^{-18}$ for millisecond pulses [24]. Currently very massive 'spherical' detectors are being proposed to achieve higher sensitivities [25]. Bar detectors have the disadvantage, however, of being sensitive only to signals which have significant spectral components occurring in a narrow frequency range around their resonant frequency.

An alternative method of gravitational wave detection offering the possibility of very high sensitivity over a wide range of frequencies is to use laser interferometery to measure the displacements of freely suspended test masses.

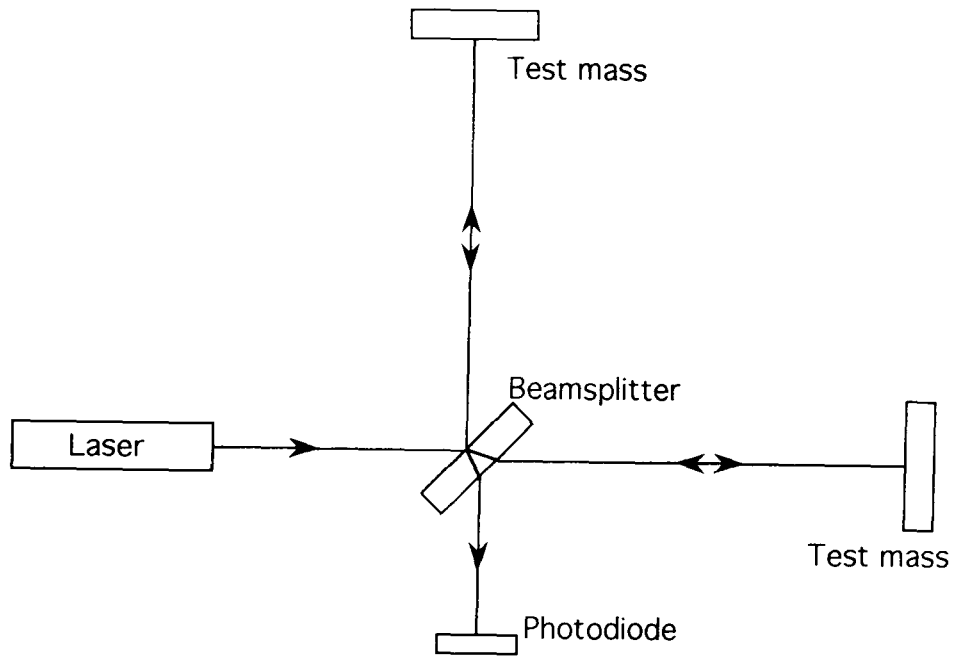


Figure 1.3: *Schematic diagram of a simple Michelson interferometer.*

### Interferometric Detectors

Gravitational wave detectors based on laser interferometry were first proposed by Forward [26], and Weiss [27].

This technique is based on the Michelson interferometer as shown in figure 1.3. A simple Michelson interferometer consists of two mirrors and a beamsplitter, with light from a laser, usually continuous wave (cw), incident on the beamsplitter and divided equally between the two arms of the interferometer. Light reflected from each of the mirrors recombines at the beamsplitter and the resultant interference pattern is detected at the interferometer output. Any differential change in the lengths of the interferometer arms will produce a change in the intensity of the detected light.

This type of detector is particularly suited to the detection of gravitational waves given their quadrupole nature. Consider gravitational waves propagating in a direction perpendicular to the plane of the interferometer arms. These will result in one arm of the interferometer being stretched by an amount $\Delta L$ whilst the other arm is compressed by $\Delta L$, resulting in a differential change of $2\Delta L$. To use this arrangement as a gravitational wave detector requires that the test masses are mirrors and

are isolated from noise sources such as acoustic or ground vibrations or fluctuations in air pressure which might mask the movement of the masses caused by gravitational waves. Towards this end, the masses and beamsplitter are suspended as pendulums in vacuum so that above the pendulum resonant frequencies the masses are essentially free in space.

Prototype detectors based on this principle have been constructed by various research groups, at the University of Glasgow [28], the Max-Planck-Institut für Quantenoptik (MPQ) [29], California Institute for Technology (Caltech) [30], Massachusetts Institute of Technology [31], the Institute of Space and Astronautical Science, Japan [32], and construction of a prototype at Perth, Australia [33] is planned as part of the Australian Gravitational Wave Consortium. These prototype detectors have arm lengths ranging from a few metres to 100 metres.

To increase the effective arm length of these prototypes, methods of folding the optical path in the interferometer arms are used. This may be achieved by the use of either multi-beam delay lines or resonant cavities.

An international network of interferometric gravitational wave detectors is currently under construction. The American LIGO project to construct two detectors with arms of 4 km, one in Hanford, Washington and one in Livingston, Louisiana is fully funded with construction of the Hanford detector underway. Also close to the start of construction are the French/Italian VIRGO detector and the British/German GEO 600 detector. The VIRGO collaboration will construct an interferometer with 3 km arms near Pisa, Italy and the GEO 600 project will result in the construction of an interferometer with 600 m arms near Hannover, Germany. The design of the GE0 600 interferometer includes advanced technology which should enable this medium scale interferometer to operate with a sensitivity comparable to that of the full sized detectors in their initial configuration. This will allow the interferometer to be used as a test bed for these advanced techniques which may find applications in the later stages of the LIGO and VIRGO projects

To enable coverage of the whole sky a detector in the Southern Hemisphere would be desirable and indeed research groups in Japan and Australia are currently involved in research and development directed towards the construction of large

scale gravitational wave detectors [34] [35].

## 1.5 Noise and Techniques in Ground Based Laser Interferometric Gravitational Wave Detectors

### 1.5.1 Introduction

To observe gravitational waves occurring at $\simeq 1$ kHz would require a detector capable of measuring strains over a bandwidth of $\simeq 1$ kHz around 1 kHz of the order of $h \simeq 10^{-21}$ or better. It is clearly essential that the effects of apparent displacements due to noise in the frequency range of interest for gravitational wave detection are acceptably small. Limitations to detector sensitivity may be split into two types,

1. fundamental limitations

2. technical limitations

In the first category are limitations such as the Heisenberg Uncertainty Principle applied to the test masses, thermal noise in the test masses and suspensions, and photo-electron shot noise in the detected light. The second category includes noise sources such as seismic and mechanical vibrations, acoustic noise and noise associated with the laser source. In this section the implications of these noise sources for detector sensitivity will be considered briefly.

### 1.5.2 Fundamental Limitations

#### The Heisenberg Uncertainty Principle

The Heisenberg Uncertainty Principle sets a limit on the accuracy with which the position of any free mass may be measured. For a simple Michelson interferometer, assuming a heavy beamsplitter, the minimum root mean square (r.m.s.) differential displacement, $\delta x_d$, of the two end test masses, each of mass m, in a one Hertz

bandwidth at frequency f, is given by [36]

$$< \delta x_d >= \left[\frac{\hbar}{m\pi^2 f^2}\right]^{\frac{1}{2}} m/\sqrt{Hz} \tag{1.3}$$

The sensitivity of an interferometer of arm length L is thus given by

$$< h >= \frac{1}{L}\left[\frac{\hbar}{m\pi^2 f^2}\right]^{\frac{1}{2}} /\sqrt{Hz} \tag{1.4}$$

where $\hbar = \frac{Plancks\ constant}{2\pi}$. Thus using typical values proposed for the test masses of m = 16 kg [37] it can be seen that for signals of magnitude $h \simeq 10^{-21}$ at 1 kHz to be detected at a three standard deviation level requires an interferometer to have an arm length in excess of 78 m.

While the Uncertainty Principle represents a fundamental limit to the detector sensitivity, other noise sources will present more immediate limitations to the sensitivity of proposed detectors.

### Thermal Noise

Another significant source of noise is the thermal motion associated with the modes of each of the test masses and the pendulum modes of the suspensions. This is a result of thermal motions of the constituent atoms exciting vibrational modes at the resonant frequencies of the test masses and suspensions.

To minimise the effects of this noise on the interferometer sensitivity it is desirable that the test mass and suspension have resonant frequencies which are not in the frequency ranges of interest for gravitational wave measurements and have resonances of high quality factor, Q, where Q is defined as

$$Q = \frac{f_0}{\Delta f} \tag{1.5}$$

$f_0$ being the resonant frequency and $\Delta f$ the full width of the resonance peak at half maximum power. This can be achieved by careful design and choice of materials for the test masses and suspensions.

The predicted level of thermal noise for the GEO 600 interferometer is shown in figure 1.4.

There is evidence that current prototypes may be close to being limited by thermal noise and work in this area is continuing [30] [38].

### Photon Shot Noise

As described in section 1.4.2 light from the interferometer arms recombines at the beamsplitter with the resulting interference fringes detectable at the interferometer output. A gravitational wave of suitable polarisation would produce differential changes in the length of the two arms resulting in a relative phase change of the light from the arms. This would cause a very small change in the interference fringe pattern produced and thus a change in the number of photons detected at the interferometer output. The minimum change in arm length which can be detected thus depends on the minimum detectable change in the light at the output.

Inherent in the use of an interferometer is the fact that vacuum fluctuations may enter the interferometer through the unused port. This results in an uncertainty in the number of photons detected at the output. This can be treated as equivalent to the uncertainty associated with photon shot noise counting statistics and will be discussed in detail in section 1.6.

## 1.5.3 Technical Noise

### Seismic and Mechanical Noise

At low frequencies, seismic noise will affect the performance of all terrestrial detectors. Some degree of isolation of the test masses is achieved by suspending the interferometer components as pendulums. The suspension point of each component may then itself be isolated from ground movement by an isolation stack [39] as is proposed for the GEO 600 project, or by a further multistage chain of pendulums as is proposed for the VIRGO project [40]. Even with measures such as these in place, it is likely that at frequencies below a few tens of Hertz, earth based gravitational wave detectors will be limited by seismic noise.

The expected isolated level of seismic noise for the GEO 600 interferometer is shown in figure 1.4.

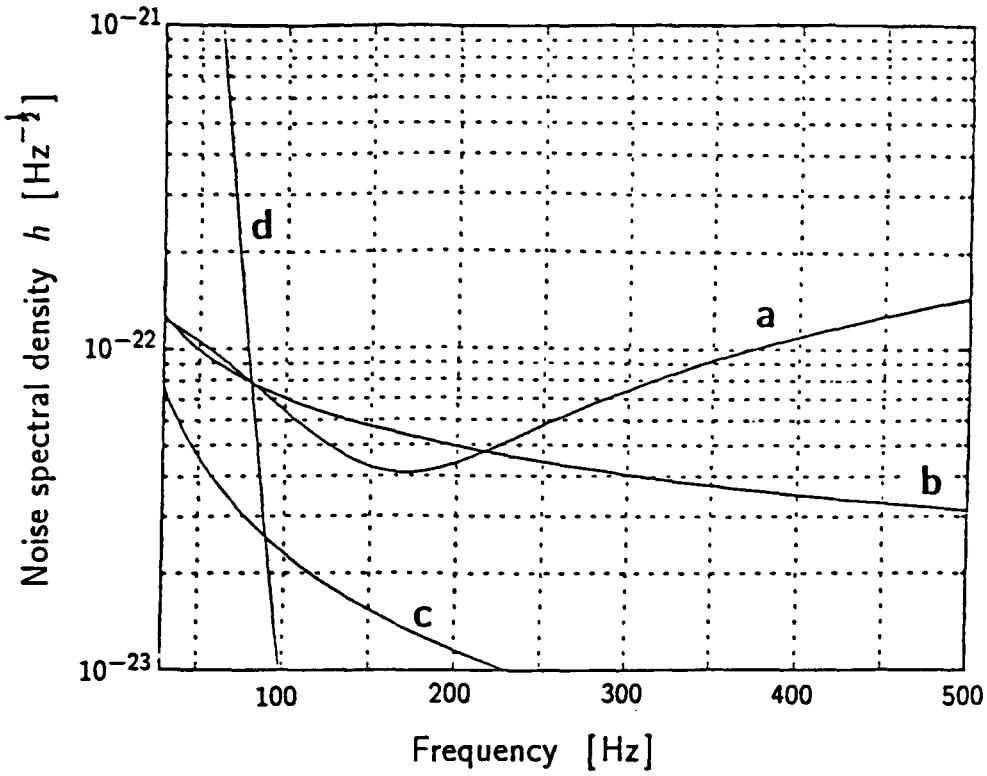


Figure 1.4: *Schematic diagram of the expected noise budget for the GEO 600 detector. Curve* **a** *is the photoelectron shot noise with 5 W of laser light. Curve* **b** *is the thermal noise. Curve* **c** *is the limit set by the Heisenberg Uncertainty Principle. Curve* **d** *represents a likely seismic noise limit.*

### Other Noise Sources

There are a variety of other sources of noise which may affect the sensitivity of a laser interferometric gravitational wave detector. For example, variations in air pressure could result in refractive index fluctuations and thus changes in optical path length. This effect and that of acoustic noise requires that the test masses and beamsplitter are suspended in vacuum. Light scattered from the pipes of the vacuum system may couple back into the detection process and cause noise. This effect may be minimised by the placing of baffles in the optical path [41]. Variations in the frequency, intensity and position of the laser beam illuminating the detector may also result in spurious signals being produced, and these noise sources will be discussed in detail in section 1.7.

## 1.6 Signal Detection

### 1.6.1 Photon Shot Noise

For gravitational wave signals to be detected, the interferometer must be held at a particular point on an output interference fringe. An obvious point to choose is halfway up an interference fringe since the change in photon number produced by a given differential change in arm length is greatest at this point. The interferometer may be stabilised to this point by sensing any changes in intensity at the interferometer output with a photodiode and feeding the resulting signal back, with suitable phase, to a piezoelectric transducer (pzt) mounted on one of the interferometer mirrors. Provided the laser power does not fluctuate significantly, information about changes in length of the interferometer arms can then be obtained by monitoring the signal fed back to the pzt.

It has been shown by Edelstein et al [36] that the sensitivity of a Michelson interferometer may be obtained from the equation

$$(\delta x)^2 \geq \frac{hc\lambda\Delta f}{8\pi^2 I_0 \cos(\phi/2)^2} \tag{1.6}$$

where: $\delta x$ is the relative change in arm length of the interferometer; $\phi - \pi$ is the phase difference between the light beams from the arms at the point of recombination: $I_0$ is the effective input light power to the interferometer and is equal to the total input power times the quantum efficiency of the detection photodiode; $\Delta f$ is the bandwidth corresponding to an observing time $\tau = \frac{1}{2\Delta f}$; $h$ is Planck's constant and $\lambda$ is the wavelength of the light. From equation 1.6 it can be seen that the sensitivity of a Michelson interferometer is best when the interferometer is operated near a null in the interference pattern, and is approximately a factor of $\sqrt{2}$ better than when operated half way up an interference fringe.

To operate an interferometer close to a null in the interference pattern it is usual to make use of a modulation technique.

An example of a simple modulation scheme is shown in figure 1.5. An electro-optic phase modulator can be placed in one arm of the interferometer to phase modulate the light in that arm. This will cause a modulation of the relative phase of the light beams on recombination. With the interferometer arranged to operate

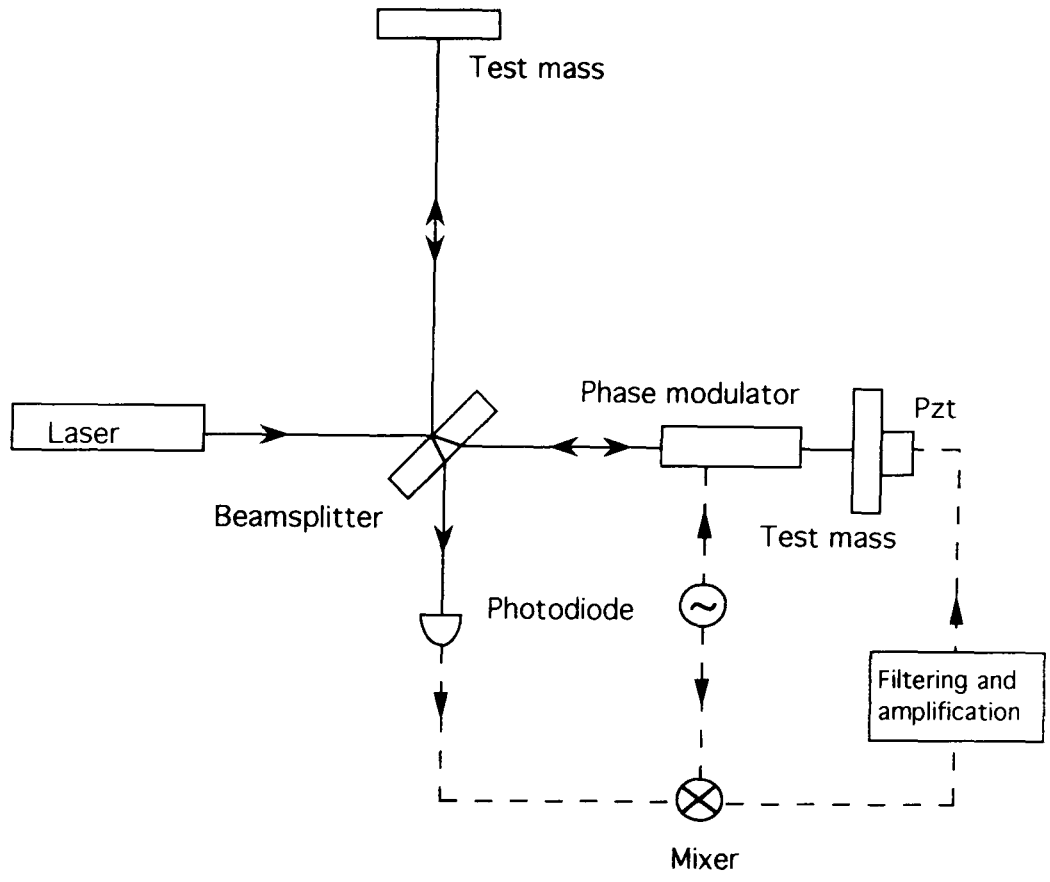


Figure 1.5: *Basic internal modulation scheme for a Michelson interferometer.*

at a point near a null fringe, this phase modulation will result in output signals at the modulation frequency proportional to the size of the deviations from the null fringe. The detected signal can then be demodulated by mixing it with a signal from the reference oscillator driving the phase modulator. The shape of a typical interference fringe and corresponding demodulated signal obtained by sweeping the interferometer path difference through approximately one half wavelength is shown in figure 1.6. The demodulated signal is zero with the cavity exactly on a null fringe and changes sign on different sides of the null providing a bipolar error signal; this can be fed back to a pzt on one interferometer mirror to hold the interferometer locked near to a null fringe.

Since the interferometer output is not exactly on a null fringe but is oscillating about the null point at the modulation frequency the signal to noise performance is not exactly that predicted by Edelstein et al but is degraded by a factor of approximately $\sqrt{(3/2)}$ [42]. This performance is still an improvement on the performance obtained by locking to the side of an interference fringe and can be improved by the use of more complicated demodulation techniques [43] [44]. To obtain high performance from these modulation techniques it is necessary that at the modulation frequency, the intensity of the laser light must be shot noise limited and that the

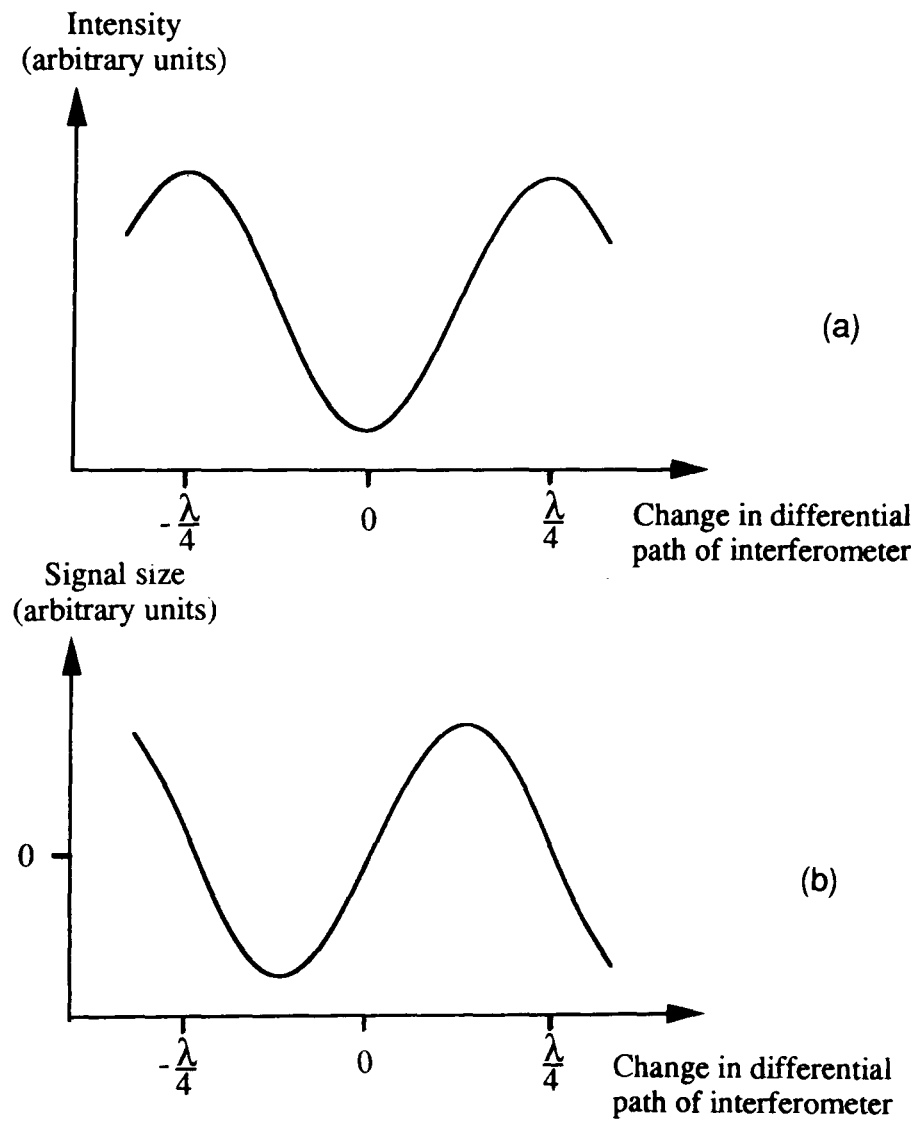


Figure 1.6: *Interference fringe and corresponding demodulated detected signal. Curve* **a** *shows the changes in the interference pattern and curve* **b** *the changes in the demodulated signal obtained when the differential path length of a Michelson interferometer is swept through one half wavelength.*

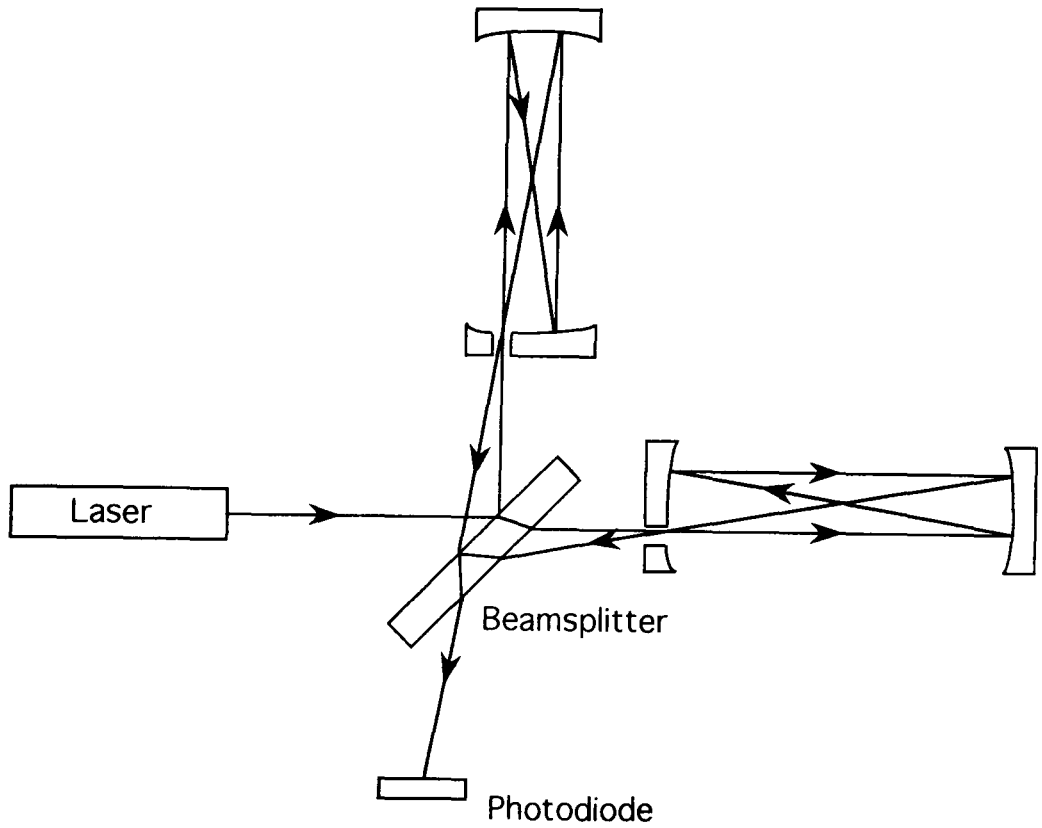


Figure 1.7: *Schematic diagram of an interferometric gravitational wave detector using delay lines.*

frequency noise of the laser be close to the Shawlow-Townes limit set by spontaneous emission.

Other advantages in locking to the null point of an interference fringe will be discussed in section 1.7.

### 1.6.2 Interferometer Configurations

There are various techniques which may be used to improve the sensitivity of a simple interferometer. One approach is to increase the effective arm length of the interferometer by folding the optical path in the interferometer arms using either delay lines or resonant cavities. Further improvement may be obtained by the use of various optical recycling techniques.

#### Folding Schemes

1. **Delay Lines**

   A schematic diagram of an interferometer employing delay lines is shown in figure 1.7. Mirrors are used to reflect the light repeatedly in each arm such

that the light traces a path in which the beams do not overlap. This effectively increases the effect of a gravitational wave signal on the path length for the light in each arm. Schemes of this type are employed in the detector prototypes at Garching, Germany [29] and at the Institute of Space and Astronautical Science, Japan [32]. There are however disadvantages to such a system. The increased number of light beams present in each arm leads to an increase in the amount of scattered light in the system. If the arm length is large, light which is scattered may resonate between the mirrors and then recombine with the main beam after having followed a different optical path in the arms and cause noise in the phase of the output light. In practice, only a small number of beams can be used as a result of this problem [45].

2. **Resonant Cavities**

Another multi-pass scheme used in interferometric detectors has Fabry-Perot cavities in the arms of the interferometer. This technique was first developed at Glasgow [46] on a prototype with 10 m arms and later at Caltech using a 40 m prototype. A schematic diagram showing this interferometer configuration is shown in figure 1.8. In this scheme the laser beams in each Fabry-Perot cavity lie on top of one another. One cavity is held on resonance by locking the frequency of the laser to a resonance of the cavity. The length of the second cavity is then altered to keep it resonant for the laser frequency. Any relative changes in the lengths of the interferometer arms will tend to move the secondary cavity off resonance. This movement is compensated for by a control signal which would contain the gravitational wave signal. This method of operating an interferometer requires sophisticated control systems to hold each of the cavities on resonance and depends on the laser frequency being highly stabilised. It does however significantly reduce the problems caused by scattered light.

**Recycling Techniques**

1. **Standard Recycling**

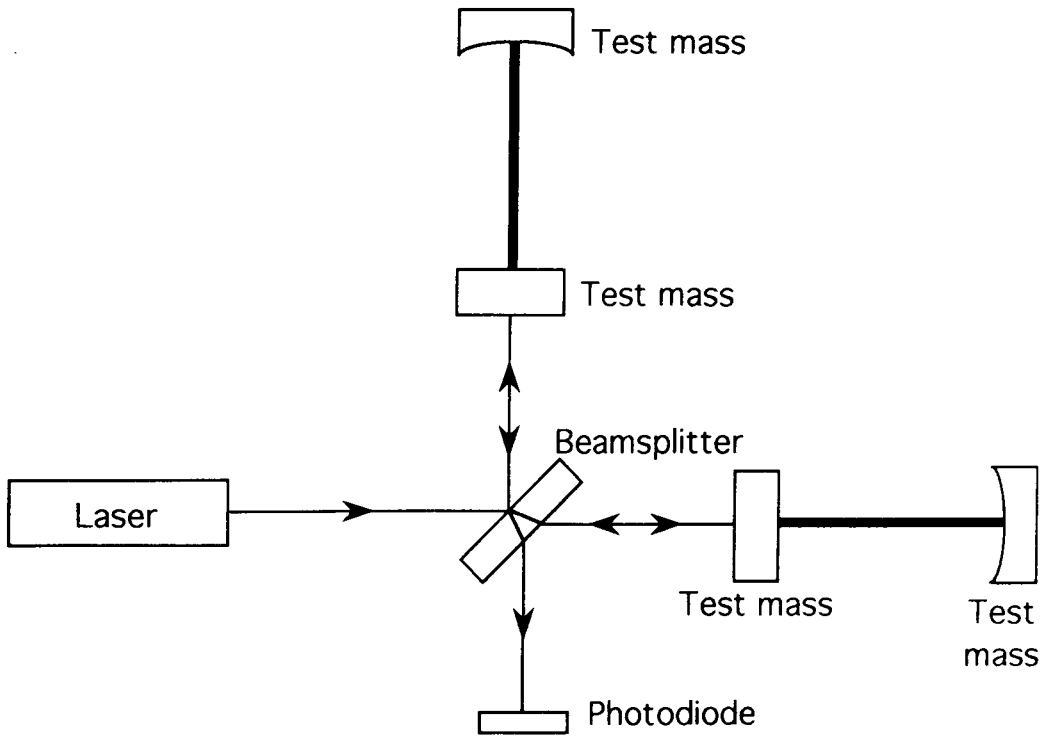


Figure 1.8: *Schematic diagram of an interferometric gravitational wave detector using Fabry-Perot cavities in the interferometer arms.*

It can be seen from equation 1.6 that the shot noise limited sensitivity of an interferometer is optimised by using high laser powers. Since the interferometer is usually operated locked to the null of a fringe then if very low loss mirrors are used almost all the input laser power is directed back towards the laser. By positioning a mirror of suitable reflectivity at the input to the interferometer as shown in figure 1.9 this previously unused light may be coherently added to the input light so that the whole interferometer effectively behaves as a cavity.

This increases the light power in the interferometer and thus reduces photon shot noise and increases the signal to noise response of the system. This technique is known as standard recycling [47].

2. **Signal Recycling**

This technique involves the positioning of a mirror at the output of the interferometer such that the interferometer effectively forms a cavity for the optical sidebands which result from the effect of a gravitational wave signal. One sideband thus resonates and is effectively increased in size; thus the shot noise limited sensitivity of the interferometer may be enhanced over a partic-

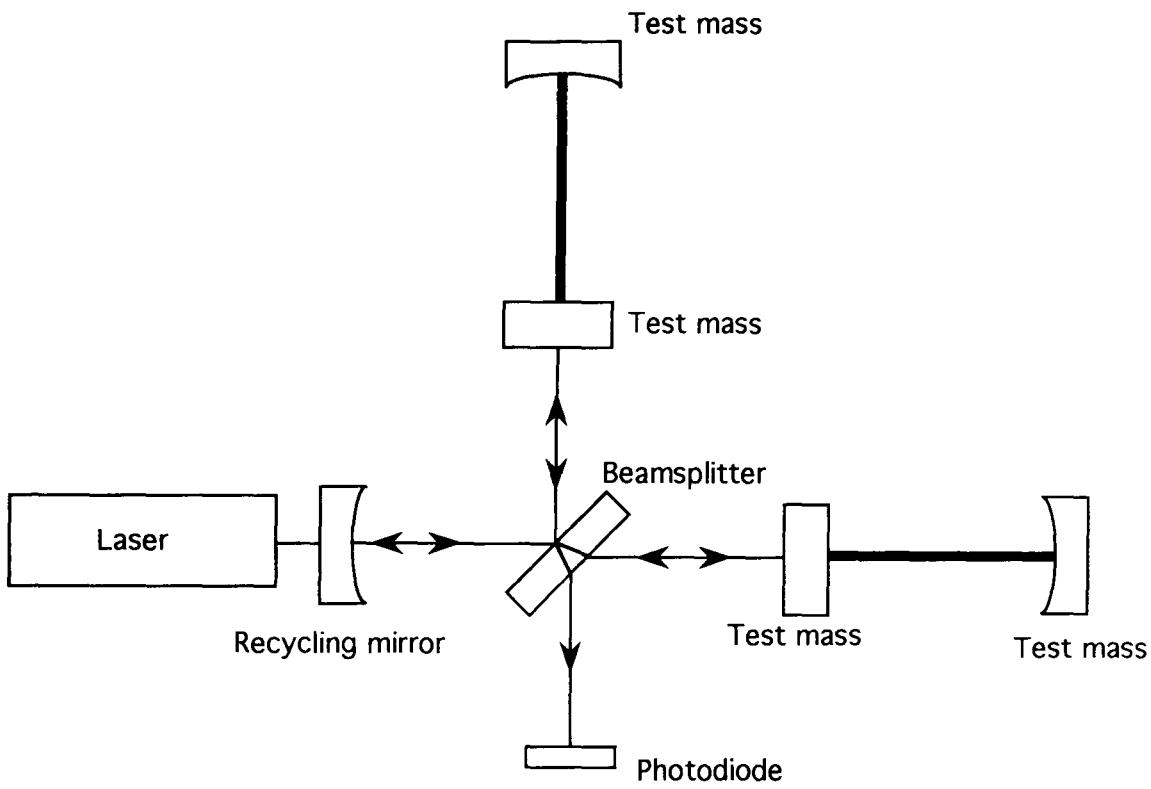


**Figure 1.9:** *Schematic diagram of an interferometric gravitational wave detector using Fabry-Perot cavities and standard recycling.*

ular frequency range [48]. It is proposed that both power and signal recycling (dual recycling) will be used in the GEO 600 detector, as shown in figure 1.10, with the expected detector sensitivity shown as curve **a** in figure 1.4.

3. **Resonant Sideband Extraction**

In the case of interferometers using resonant Fabry-Perot cavities there is an optimum time of $\tau_s$ = half the period of a gravitational wave, for which the light may be stored in the arms of the interferometer. For storage times longer than $\tau_s$ the gravitational wave signal becomes distorted. Normally systems are designed to operate with appropriately short storage times, times much shorter than the quality of available mirrors would allow. However a different approach is possible using the technique of resonant sideband extraction. This technique involves the careful positioning of a suitable mirror at the output of the interferometer such that a cavity is formed in which the gravitational wave sidebands may resonate. This then allows the extraction of the gravitational wave signal [49]. The advantage of this method is that the long storage time in the arms leads to very high power in the arms and leads to power recycling

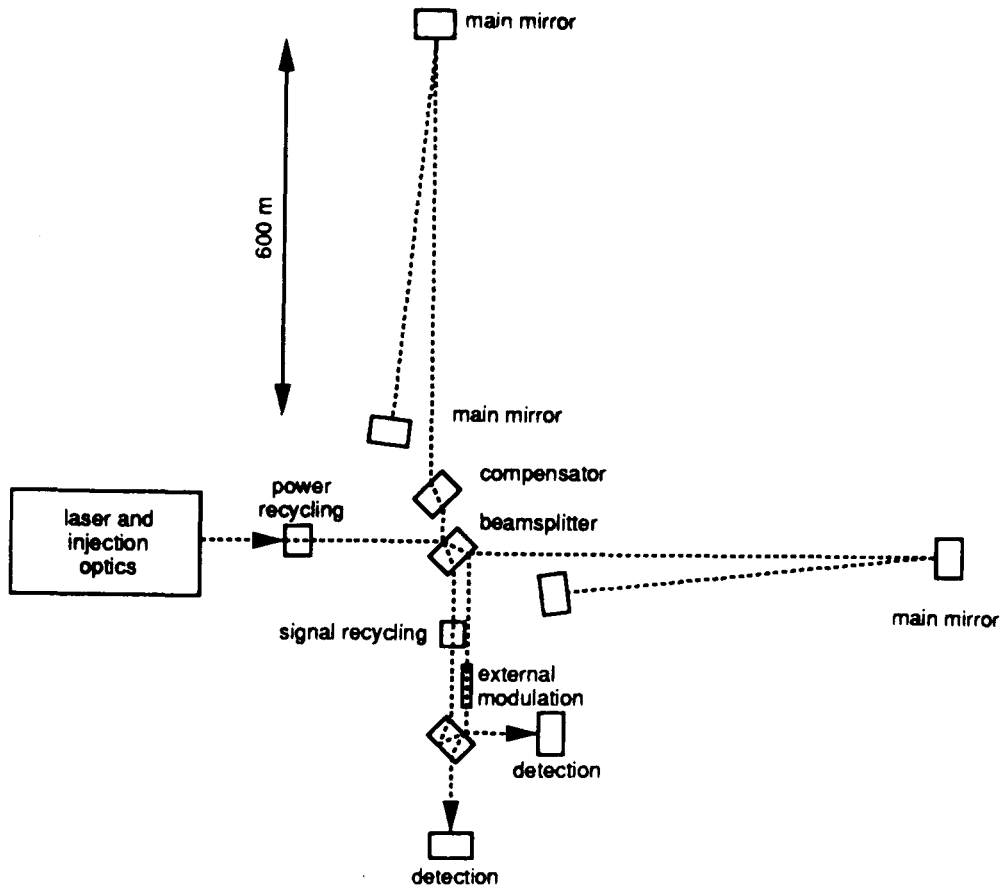


Figure 1.10: *Schematic diagram of the optical layout for the proposed GEO 600 interferometric gravitational wave detector.*

being unnecessary.

## 1.7 Laser Noise

### 1.7.1 Intensity Noise/Power Fluctuations

[1] In general, fluctuations in the output power of the laser source may be detected as fluctuations in the number of photons detected at the interferometer output and thus represent a source of experimental noise.

When using an interferometer locked to the side of an interference fringe the effect of the intensity noise may be reduced by, for example, independently measuring the noise and subtracting this signal from the signal detected at the interferometer output. Alternatively if the line-up of the interferometer is slightly offset the laser power returning to the laser from the beamsplitter can be used. The signal obtained by detecting this light is 180 degrees out of phase with that at the interferometer

[1] It should be noted that by convention, power fluctuations are normally referred to as intensity noise. While this is not strictly correct this terminology will be used in this thesis to follow convention.

output and by subtracting these signals the effects of intensity noise can be reduced while doubling the size of a signal due to a change in path length. These techniques, however, can in practice normally only reduce the effects of intensity noise present by a factor of up to several hundred [50].

Operating the interferometer locked to the null point on a fringe means that, in principle, the interferometer output is insensitive to intensity noise; however in practice there will be small displacements of the output from the locking point causing some sensitivity to this noise. In this case it can be shown that the required intensity stability of the laser in the frequency range of interest for gravitational wave detection may be estimated to be [52]

$$\frac{\delta P}{P} = h\left(\frac{\delta l}{l}\right)^{-1} \tag{1.7}$$

where $\frac{\delta P}{P}$ are the relative intensity fluctuations of the laser, and $\delta l$ is the offset in position from the correct locking point for an interferometer of arm length $l$. From calculations for long baseline detectors [52] it can be estimated that for the proposed GEO 600 interferometer arm length of 600 m, $\delta l$ might be approximately a few times $10^{-13}$ m (depending on the gain of the locking servo). Thus for $h \simeq 10^{-21}$ over millisecond time scales this suggests a required

$$\frac{\delta P}{P} \leq 3 \times 10^{-8}/\sqrt{Hz} \tag{1.8}$$

at approximately 1 kHz. This level of intensity noise may be achieved by the use of appropriate servo systems to stabilise the intensity of the laser. Some degree of passive intensity stabilisation is also provided for noise at high frequencies by the modecleaner and recycling cavities.

### 1.7.2 Frequency Noise

It can be shown that a change $\delta x$, in the differential path length $x$ of the interferometer arms causes a phase change $\delta\phi$ of the light at the interferometer output given by

$$\delta\phi = \frac{2\pi}{c}(f\delta x + x\delta f) \tag{1.9}$$

where $\delta f$ is a change in the laser frequency, $f$, and $c$ is the speed of light. From this it can be seen that if the lengths of the arms of the interferometer are exactly equal then $x = 0$, and the interferometer output is insensitive to fluctuations in the laser frequency. In practice however, differences in the curvatures of the interferometer mirrors are likely to mean that the arm lengths will be slightly different; thus frequency noise may couple in to the measurement. It can be shown that an estimate of the frequency stability required may be obtained from [52]

$$\frac{\delta f}{f} = h\left(\frac{x}{l}\right)^{-1} \tag{1.10}$$

where $\frac{\delta f}{f}$ is the relative frequency noise of the laser in a one Hertz bandwidth at 1kHz. Estimates suggest that $\frac{x}{l}$ may be about $10^{-3}$ [52], requiring

$$\frac{\delta f}{f} \simeq 3 \times 10^{-20}/\sqrt{Hz} \tag{1.11}$$

or $\delta f \simeq 9 \times 10^{-6} Hz/\sqrt{Hz}$ for Nd:YAG light at approximately 1 kHz. This level of frequency noise may be achieved by the use of appropriate laser frequency stabilisation systems. Some degree of passive frequency stabilisation is also provided for noise at high frequencies by the modecleaner and recycling cavities.

### 1.7.3 Beam Geometry Noise

Fluctuations in the geometry of the laser beam can also be a source of noise in an interferometer. Changes in the lateral and angular position of the beam, along with changes in its size and variations in its phasefront curvature, may all couple into the output signal and reduce the sensitivity. It is generally assumed that the dominant source of noise from beam geometry fluctuations is that caused by fluctuations in the lateral position of the beam. These fluctuations may couple in to interferometry measurements through a misalignment of the beamsplitter with respect to the interferometer mirrors. It can be shown that for an angular misalignment of the beamsplitter of $\frac{\alpha}{2}$ the phase mismatch $\delta\phi$ of the interfering beams caused by a lateral movement of the input beam $\delta z$ is [53] [54]

$$\delta\phi = \frac{4\pi}{\lambda}\alpha\delta z \tag{1.12}$$

Assuming a typical beamsplitter misalignment of approximately $10^{-7}$ radians means that to achieve the sensitivity required for the GEO 600 interferometer, a level of lateral beam geometry fluctuations of approximately $5 \times 10^{-14} m/\sqrt{Hz}$ at 1 kHz is required.

Typically this will mean that the beam positional fluctuations need to be suppressed by several orders of magnitude. The two main methods of reducing beam geometry fluctuations are:

1. passing the input beam through a single mode optical fibre, and

2. using a resonant cavity as a mode cleaner.

Passing the beam through a single mode fibre helps to eliminate beam geometry fluctuations as deviations of the beam from a Gaussian $TEM_{00}$ mode are equivalent to higher order spatial modes which are thus attenuated by the optical fibre. However there are problems in using optical fibres due to their limited power handling capacity ($\simeq$ 1 W) and care must also be taken to avoid introducing extra beam geometry fluctuations from movements of the fibre itself.

A cavity may be used to reduce beam geometry fluctuations of the laser light if it is adjusted to be resonant only for the $TEM_{00}$ mode of the light. Any higher order modes present should thus be suppressed [53]. The use of a resonant cavity as a mode cleaner should allow the handling of higher laser powers as well as having the added benefits of acting as a filter for fast fluctuations in laser frequency and power.

## 1.8 Implications for Laser Sources

As mentioned earlier a suitable source of illumination for an interferometric gravitational wave detector is a cw laser. There are a variety of possible laser sources but stringent requirements on power, reliability and low technical noise must be satisfied. The photon-noise limited sensitivity of an interferometric gravitational wave detector is proportional to $(P_0)^{-\frac{1}{2}}$ where $P_0$ is the laser power incident on the interferometer, and proportional to $(\lambda)^{\frac{1}{2}}$ where $\lambda$ is the wavelength of the laser

light. It can thus be seen that the best sensitivity is obtained using a laser source of high power with a relatively short wavelength. Thus, for example, diode lasers and helium neon lasers are unsuitable due to their low output powers, and carbon dioxide lasers are unsuitable because they produce light of a relatively long wavelength. Currently the best candidates for laser sources are argon-ion lasers and Nd:YAG lasers. Argon-ion lasers, emitting single frequency light at 514 nm, are currently used in several interferometric gravitational wave detector prototypes [55] [56] [29]. They have an output power in the required single spatial, single frequency ($TEM_{00q}$) mode of operation typically of around several watts, which is sufficient for this type of laser to be proposed as the laser source for the gravitational wave interferometers currently under construction in the first stage of the LIGO project [56]. For advanced detectors higher laser powers would be desirable and it has been demonstrated that the output of several argon-ion lasers could be coherently added for this purpose [57]. The main disadvantage of this type of laser is its relatively poor efficiency which means that only approximately 0.01% of the input electrical power is converted to laser light.

Nd:YAG lasers emitting at 1064 nm present an alternative candidate for use as a laser source. The longer wavelength of 1064 nm for Nd:YAG laser light is however less desirable than the 514 nm of the argon-ion laser as more power at 1064 nm is required to obtain the same sensitivity, and the resulting increase in beam diameter leads to a need for larger optical components.

Nd:YAG lasers are however significantly more efficient than argon-ion lasers. Typically 1 kW of flashlamp power produces approximately 5 W of $TEM_{00q}$ mode laser light in a ring cavity. Diode pumped Nd:YAG lasers are more efficient still. Nd:YAG lasers also allow the possibility of obtaining very high powers of $TEM_{00q}$ mode light at 1064 nm. Experiments with diode pumped Nd:YAG lasers at the Laser Zëntrum in Hannover have produced up to 20 W of light in $TEM_{00q}$ mode with efficiencies of around 1.5 % [58]. Experiments to develop high power Nd:YAG lasers as sources for gravitational wave detectors are currently underway in several research groups worldwide [59] [40].

Experiments have shown that Nd:YAG laser light may be successfully frequency

doubled with up to 6.5 W of single frequency green light having been obtained [60]. Reliable high power frequency doubled Nd:YAG lasers are not yet available, but research into their development is continuing [61] [62].

Nd:YAG lasers are the proposed light sources for the gravitational wave interferometers of the GEO 600 and VIRGO projects [63] [40]. Frequency doubled Nd:YAG light is proposed for the illumination of the LIGO interferometer at a later stage. This thesis will detail the results of investigations into aspects of Nd:YAG and frequency doubled Nd:YAG lasers for use in interferometric gravitational wave detectors.

# Chapter 2

# The Intensity Stabilisation of a Monolithic Nd:YAG Ring Laser

## 2.1 Introduction

The figures calculated in the previous chapter, and summarised in Table 2.1, set upper limits on the levels of tolerable laser noise (after appropriate stabilisation) at 1 kHz, this being an example of a typical frequency from the range of interest for gravitational wave detection (from a few tens of Hz to a few kHz). Although these calculations were carried out for the simplest example of a Michelson interferometer, more complicated interferometers require lasers of similar performance. It is clearly important to know the typical levels of fluctuations in frequency, power and beam geometry for any laser which may be used as a source of illumination for a detector. This then determines what level of stabilisation of the laser light is required at the

| Upper limits on the main forms of laser noise occurring at 1 kHz | | |
|---|---|---|
| Relative intensity noise | Frequency noise | Lateral beam geometry fluctuations |
| $3 \times 10^{-8}/\sqrt{Hz}$ | $9 \times 10^{-6} Hz/\sqrt{Hz}$ | $5 \times 10^{-14} m/\sqrt{Hz}$ |

Table 2.1: *Summary of the levels of tolerable laser noise which would allow a simple Michelson type interferometer to detect signals with* $h \simeq 3 \times 10^{-23}/\sqrt{Hz}$ *at 1 kHz*

frequencies of interest for gravitational wave detection and allows appropriate servo systems to be designed. This area has been addressed by a number of workers [52].

However, large amounts of laser noise occurring at higher frequencies, for example in the hundreds of kHz range, can also present a significant problem. Nonlinearities in the signal detection process can convert high frequency noise into signals at lower frequencies. This type of distortion is known as intermodulation distortion and the ratio of r.m.s. intermodulation products to total r.m.s. output voltage can vary from a few percent for a strongly driven double balanced mixer to a few thousandth of a percent for a very high quality amplifier. High frequency noise can be difficult to suppress since in general a servo system has a finite gain which tends to decrease at higher frequencies. This means it can be difficult to construct a servo system which will simultaneously reduce noise at the low frequencies of interest for gravitational wave detection and at much higher frequencies. It is thus important that the high frequency noise of any laser source is investigated.

As mentioned in chapter 1, it is proposed that Nd:YAG lasers will be used as the laser sources for the interferometers in the GEO 600 and VIRGO projects. In both cases a similar arrangement is proposed where a high power diode-pumped Nd:YAG slave laser is injection seeded with light from a lower power monolithic Nd:YAG master ring laser. It has been demonstrated that this technique allows high powers of light to be obtained from the slave laser; light generated in this way has noise properties which are dominated by those of the master laser light [65]. The proposed master laser in both the GEO 600 and VIRGO projects is a diode-pumped monolithic Nd:YAG ring laser [66]. This type of laser is however prone to a particular type of intensity fluctuation occurring at high frequencies and found in many solid-state lasers. These fluctuations, called relaxation oscillations, occur in lasers where the time taken to regain a population inversion after de-excitation is longer than the characteristic lifetime of a photon in the laser cavity [67].

The presence of these high frequency fluctuations in intensity is well known, and it has been shown that for a low power monolithic Nd:YAG ring laser, operating with an output power of 5.7 mW at 1.32$\mu$m, the fluctuations may be suppressed using electronic feedback [68]. If however this type of laser is to be used as the

master oscillator for illuminating an interferometric gravitational wave detector it is important to show that,

1. suppression of relaxation oscillations in intensity is possible in lasers having output powers of the order required for injection seeding, and

2. it is possible to construct a servo system which can simultaneously damp the relaxation oscillations in intensity occurring at high frequencies while reducing the intensity noise of the laser at low frequencies.

It is also important that investigations are made into the high frequency fluctuations in frequency and beam geometry of such lasers. It is particularly important to determine whether the relaxation oscillation processes in intensity couple in to the frequency or beam geometry noise for the laser, as these might represent significant sources of high frequency noise.

This chapter will describe experiments to measure and suppress the intensity noise at high frequencies in a single-mode monolithic Nd:YAG ring laser with a maximum output power of 400 mW, and experiments to suppress intensity noise in a similar laser at both high and low frequencies using a broadband feedback system.

Chapter 3 will describe experiments to measure the frequency noise and beam geometry fluctuations of the laser at relaxation oscillation frequencies.

## 2.2 Relaxation Oscillations

### 2.2.1 Laser Description

The laser used in these experiments was a monolithic diode-pumped Nd:YAG ring laser built at the Laser Zëntrum in Hannover, Germany, based on the original design by Kane and Byer [66], and capable of producing output powers of the order required for injection seeding ($\simeq 400\ mW$). The pump laser was a diode laser type SDL-2462-P1 from Spectra Diode Labs with a maximum output power of 1 W emitting at approximately 810 nm. The output from this pump laser, after passing through some focusing optics, was directed onto the front face of the monolithic Nd:YAG laser cavity. A schematic diagram of the laser resonator is shown in figure 2.1.

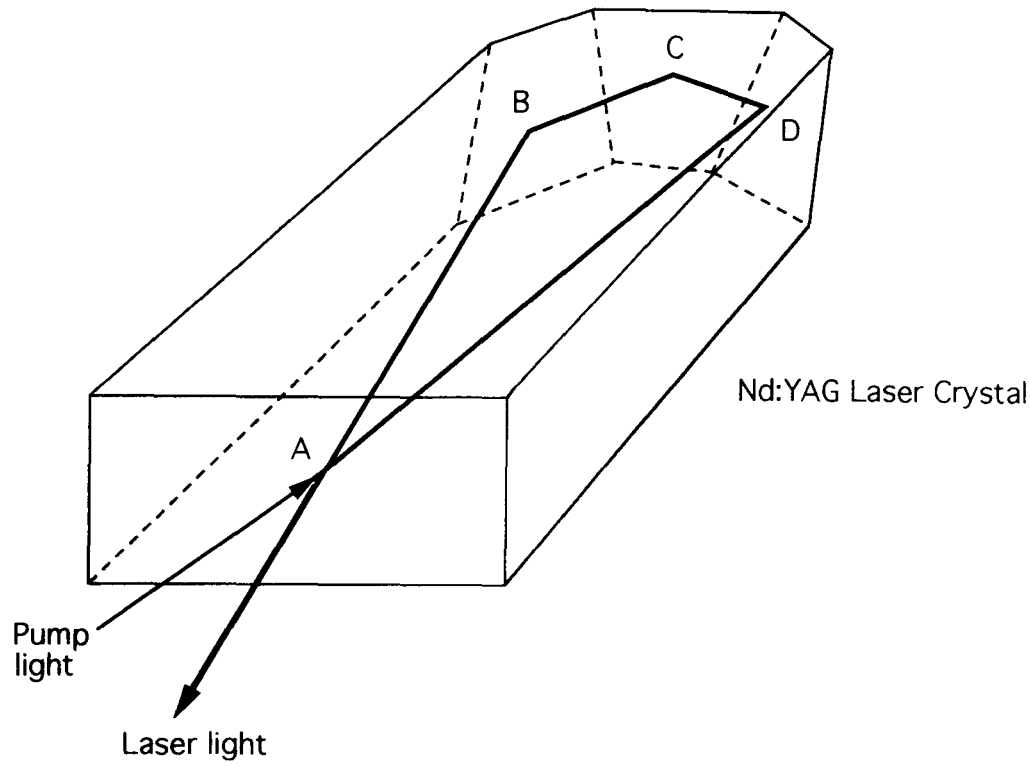


Figure 2.1: *Schematic diagram of a monolithic Nd:YAG laser resonator. A, B, C and D are the bounce points of the laser light inside the resonator.*

The monolithic laser resonator also acted as an optical diode. The polariser of this diode was formed by the non-normal angle of incidence of the beam at the output face, meaning that there was a greater transmission, and hence loss, for light of p polarisation allowing a preferential build up inside the cavity of the s polarisation. The non-planar lasing path inside the resonator caused a net rotation of the polarisation of the light in the cavity after one round trip. A magnetic field applied to the Nd:YAG crystal caused Faraday rotation of the resonant polarisation with the Faraday rotation adding to the rotation caused by the non-planar lasing path in one direction of travel round the resonator and in the other direction subtracting from the rotation. The combination of these effects allowed unidirectional operation of the laser [66].

The length of the beam path in the resonator was approximately 28.5 mm. The light from the cavity was emitted in a $TEM_{00q}$ mode, with the maximum output power of the laser being 400 mW. The output power of the laser could be altered by changing the current to the diode laser pump and thus the pump power. The diode driver was a Spectra diode driver model SDL-820, which included an input to allow modulation of the current to the diode laser.

### 2.2.2 Relaxation Oscillations

As mentioned in section 2.1, relaxation oscillations are periodic fluctuations in output intensity often found in solid-state lasers. The source of these oscillations can be described in terms of the initial behaviour of the laser when first turned on.

When the laser pump is switched on there are few photons in the laser cavity and the pump causes a population inversion. The lack of cavity photons means that the population inversion may increase above the threshold value for lasing since no radiation yet exists to cause de-excitation of the upper state by stimulated emission. Once the population inversion has passed the threshold level and de-excitation begins, this de-excitation occurs very rapidly and there is a rapid increase in cavity photon number further leading to de-excitation of the upper state. If this rate of de-excitation is greater that the rate of pumping the population inversion can fall below the threshold value for lasing. This will result in a subsequent drop in cavity photons, returning to a situation similar to the initial point when the pump was turned on. The cycle thus tends to continue, with these rapid changes in cavity photon number causing proportional changes in the output intensity of the laser, although damping mechanisms limit the amplitude of the oscillations.

Relaxation oscillations may be treated as perturbations of the steady-state rate equations for lasing, caused for example, by variations $R_1$ of the pumping rate in a laser. Starting with this premise the equation shown below describing the resulting fluctuations in cavity photon number, $q_1$, may be derived [69]:

$$\ddot{q}_1 + \frac{r}{\tau}\dot{q}_1 + \frac{r-1}{\tau t_c}q_1 = \frac{r-1}{\tau}R_1 \tag{2.1}$$

where r is the pumping ratio and

$$r = \frac{r_{actual}}{r_{threshold}} \tag{2.2}$$

$r_{threshold}$ is the rate of pumping at the threshold for lasing, $r_{actual}$ is the actual rate of pumping, $\tau$ is the fluorescence lifetime of the upper state and $t_c$ is the average lifetime for a photon in the laser cavity, dependent on the length of the lasing path and the losses in the cavity.

The form of equation 2.1 is that of a second order differential equation describing a driven damped simple harmonic oscillator. An equation for the frequency of the

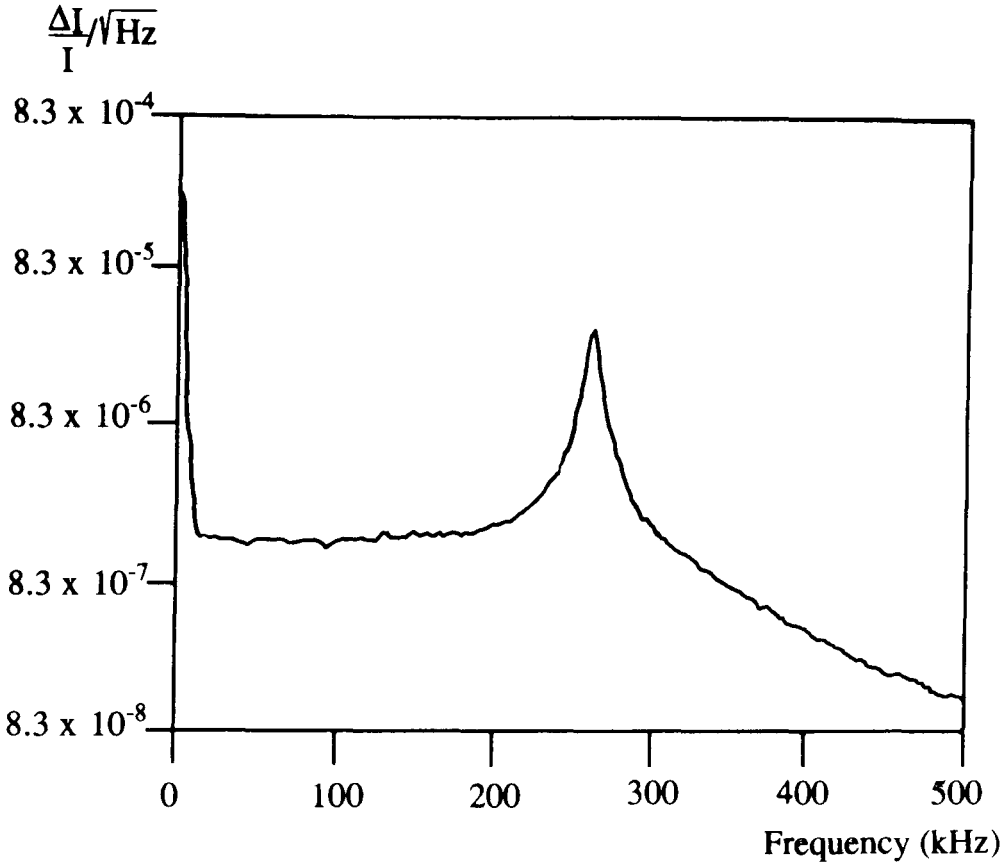


Figure 2.2: *Typical intensity spectrum from 0 to 500 kHz showing a peak in the intensity noise due to relaxation oscillations at approximately 260 kHz*

relaxation oscillations, $f_s$, may be obtained from equation 2.1 where

$$f_s = \frac{1}{2\pi}\left(\frac{r-1}{\tau t_c}\right)^{\frac{1}{2}} \tag{2.3}$$

A typical intensity noise spectrum for the laser is shown in figure 2.2. The relaxation oscillation peak can clearly be seen occurring at a frequency of approximately 260 kHz. The pumping rate of the laser was varied by varying the current to the laser diode pump and the variation of the frequency of the relaxation oscillations noted. This is shown in figure 2.3. It can be seen from equation 2.3 that by plotting $\omega^2$ against r-1 where $\omega = 2\pi f_s$, a graph can be obtained whose gradient is equal to $\frac{1}{\tau t_c}$. By finding a value for $t_c$, the total loss per round trip of the laser cavity, L, can be estimated using the relation

$$t_c = \frac{nl}{cL} \tag{2.4}$$

where $n$ is the refractive index for Nd:YAG (1.82 [70]), $l$ is the path length in the resonator (28.5 mm) and c is the speed of light.

A plot of $\omega^2$ against r-1 is shown in figure 2.4. The gradient of the graph is found to be

$$\frac{1}{\tau t_c} = 14.59 \times 10^{11} s^{-2} \tag{2.5}$$

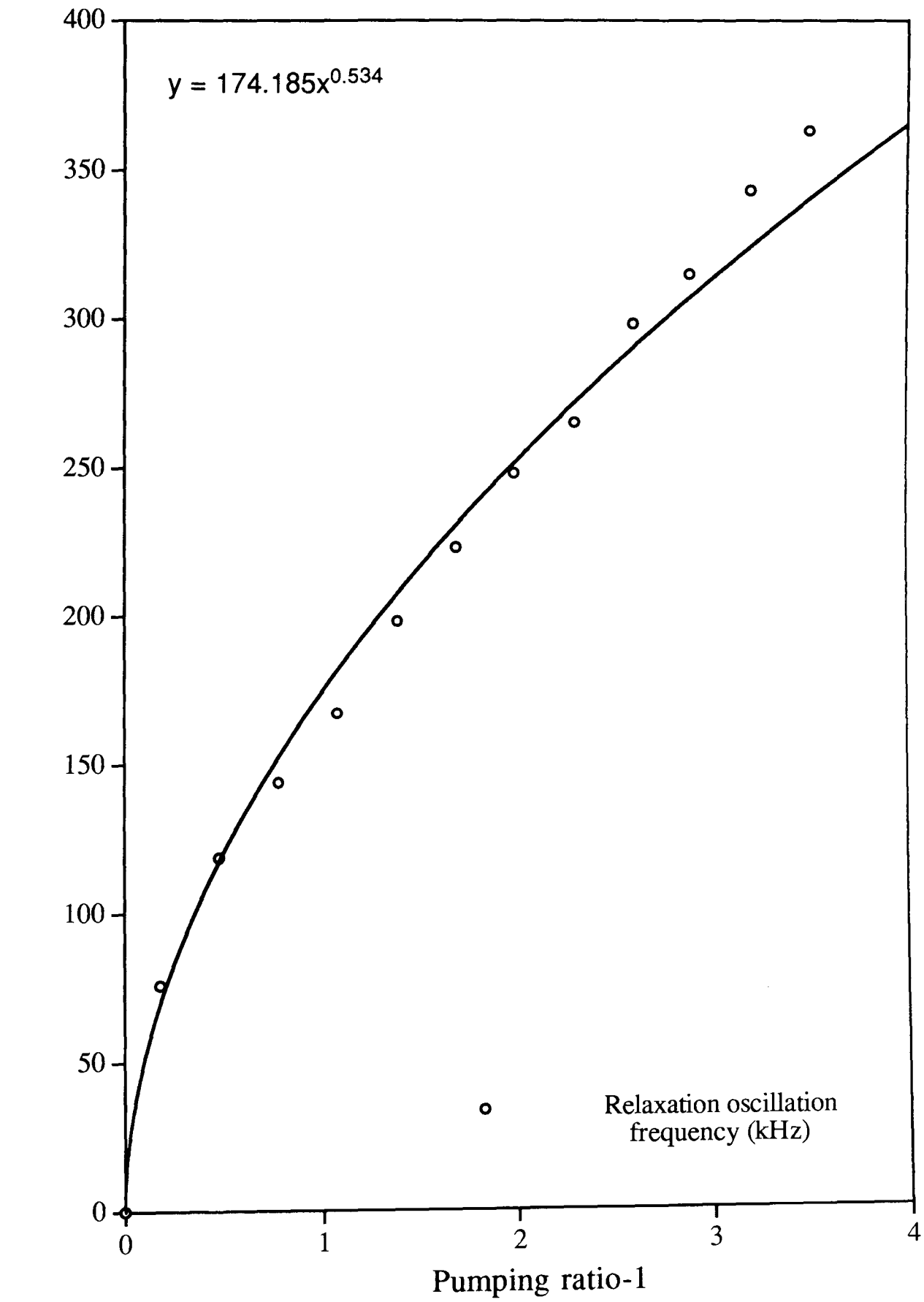


Figure 2.3: *Measured variation in relaxation oscillation frequency as a function of pumping ratio.*

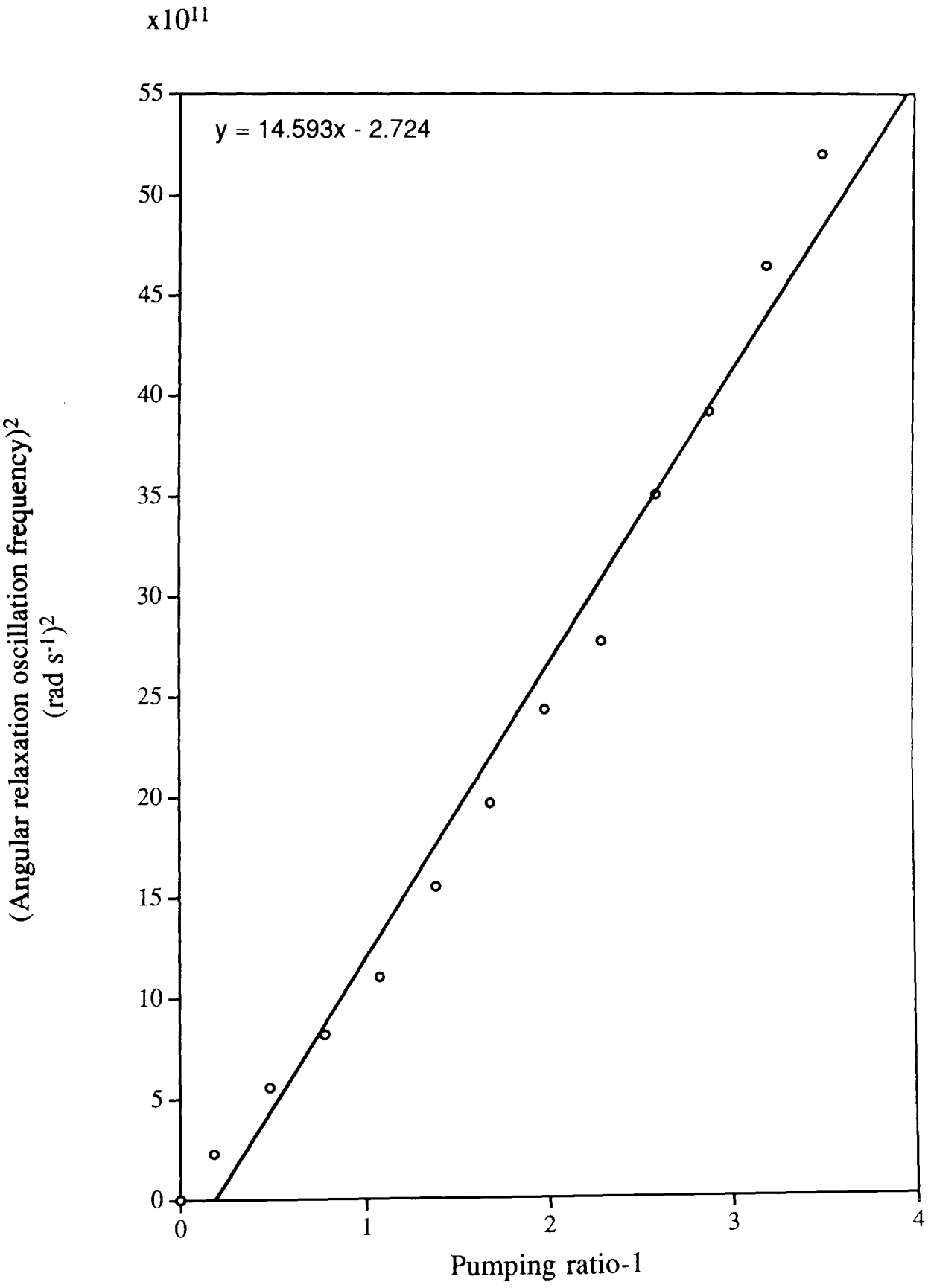


Figure 2.4: *Graph of the angular relaxation oscillation frequency squared, ($\omega^2$) plotted against pumping ratio-1, (r-1)*

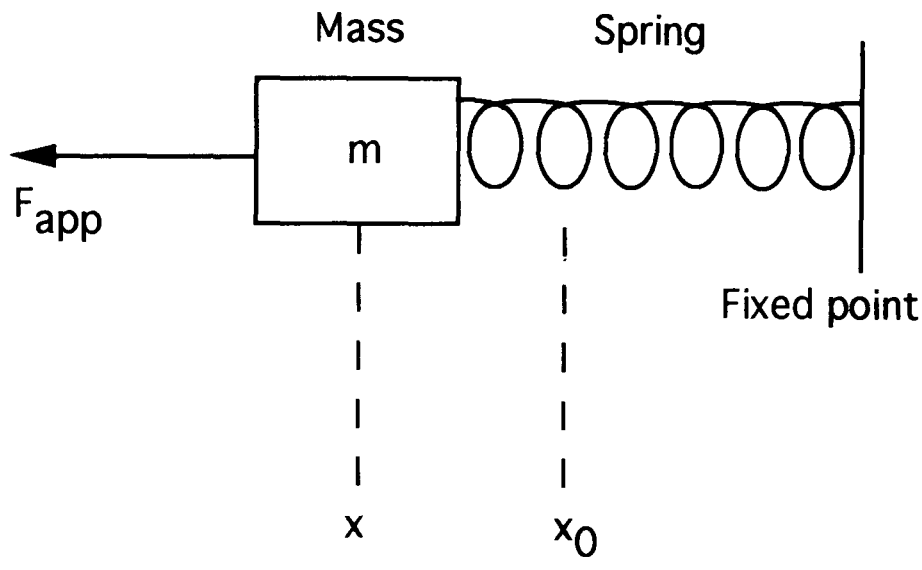


Figure 2.5: *Schematic diagram of a mass on a spring.*

Using $\tau = 230\mu s$ [70] thus gives $t_c = 6.8 \times 10^{-13} s$. From equation 2.4, the total loss in the laser cavity is thus found to be approximately 5.8%. This is in reasonable agreement with what might be expected for such a laser [71].

### 2.2.3 Principles of Damping Relaxation Oscillations

The shape of the intensity noise spectrum of the laser light shown in figure 2.2 is that of the frequency response of a driven damped simple harmonic oscillator as predicted by equation 2.1.

A possible method of damping the relaxation oscillation peak in intensity noise is suggested by considering a simpler example of a driven damped harmonic oscillator, that of a mass, $m$, on a spring under the action of an external force $F_{app}$, as shown in figure 2.5. It can be shown that the behaviour of the mass under the action of an applied force $F_{app}$ may be described by the second order differential equation given in equation 2.6.

$$\ddot{x} + \frac{b}{m}\dot{x} + \frac{k}{m}x = \frac{F_{app}}{m} \tag{2.6}$$

where

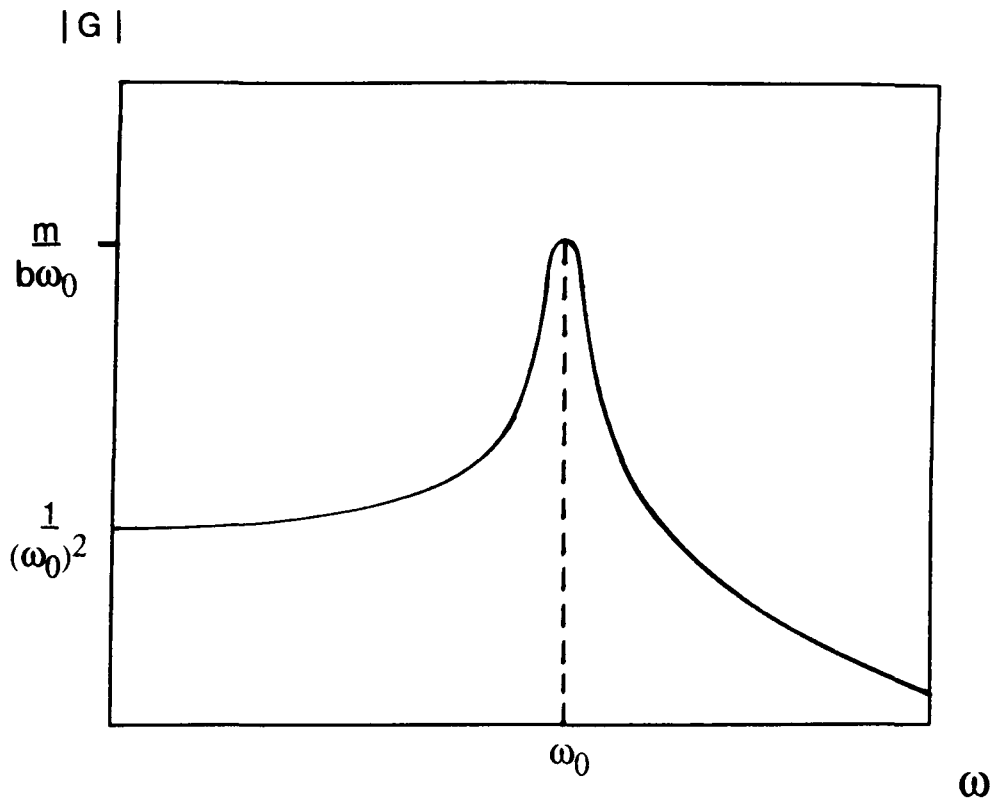


Figure 2.6: *Magnitude of frequency response of a mass on a spring.*

$\ddot{x}$ = acceleration of mass

$\dot{x}$ = velocity of mass

$x$ = relative displacement of the mass from its equilibrium position, $x_0$

$b$ = damping constant

$k$ = spring constant

An input force $F_{app}$ thus results in a displacement $x$ of the mass from its equilibrium position. Using standard Laplace techniques and replacing $\dot{x}$ by $sx$ and $\ddot{x}$ by $s^2x$, the transfer function $G(s)$ for this process may be written in the form

$$G(s) = \frac{x(s)}{F_{app}/m} = \frac{1}{s^2 + s\frac{b}{m} + \omega_0^2} \tag{2.7}$$

where $\omega_0^2 = \frac{k}{m}$ is the resonant frequency of the system.

By letting $s = j\omega$ it is possible to obtain an expression for the frequency response $G(j\omega)$ of the system. A Bode plot of the magnitude of this response, $|G|$, as function of frequency is shown in figure 2.6. It can be seen that the shape of the Bode plot is very similar to the shape of the intensity noise spectrum for the Nd:YAG ring laser shown in figure 2.2 with the relaxation oscillation peak corresponding to the peak at the resonant frequency of the mass/spring system. The size of the resonance

is dependent on the damping term $\frac{b}{m}$, and thus by increasing $\frac{b}{m}$ the size of the resonance can be decreased. One way to do this is to use a feedback system. In the schematic feedback loop shown in figure 2.7 a fraction of the output signal, $Hx$, is fed back and added to the input signal $F_{app}$, driving the mass. This modifies the

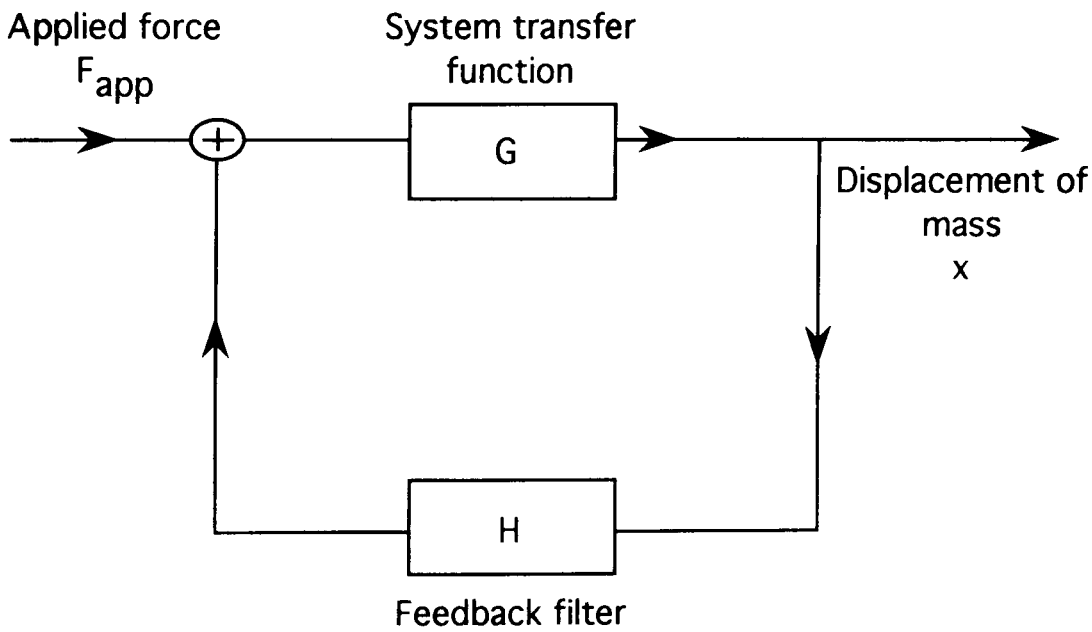


Figure 2.7: *Schematic feedback loop to damp the resonance of a mass on a spring.*

transfer function for the system which becomes

$$\frac{x(s)}{F_{app}/m} = \frac{1}{s^2 + \frac{b}{m}s - H + \omega_0^2} \tag{2.8}$$

It is possible to increase the damping factor by making H be negative and proportional to s. An appropriate feedback system to damp the resonance of the mass/spring system should thus sense the displacements of the mass from its equilibrium position, differentiate the signal obtained and feed this signal back, with the appropriate phase, to modify the force applied to the mass. Comparing equations 2.1 and 2.6 it can be seen that the displacements $x$, of the mass from its equilibrium position in the mass/spring system are analogous to the deviations in cavity photon number $q_1$, from equilibrium in the laser. Similarly the applied force $F_{app}$ driving the mass is analogous to the changes in pumping rate $R_1$ which sustain the relaxation oscillations. This suggests that a feedback system to damp the relaxation oscillation resonance should sense the changes in cavity photon number, differentiate the

signal obtained and feed this signal back to modify the pumping rate of the laser. A feedback system based on this principle was designed and is discussed in detail in the following section.

### 2.2.4 A Feedback System to Damp Relaxation Oscillations in Intensity

The previous section suggested a basis for designing a feedback system to damp the relaxation oscillations in the intensity of the Nd:YAG laser.

In practice the laser intensity fluctuations were monitored by sensing a fraction of the laser light using a photodiode. The resulting signal was amplified, filtered appropriately, and fed back to an input of the current driver for the laser diode pump. Using an input of the diode current driver as the feedback point meant however that when designing an appropriate feedback system the diode driver to laser transfer function had to be considered as well as the transfer function for the relaxation oscillation process.

#### Diode Driver Characteristics

The input resistance of the diode driver was measured by noting the drop in voltage of an input signal across a resistor of known value placed in series with the modulation input to the diode driver. The input resistance of the driver was found to be approximately 18 k$\Omega$.

The gain and phase responses of the laser including the diode driver were measured as shown in figure 2.8. The size and phase of sinusoidal signals produced by the signal generator were measured at point A, the input to the diode driver, and compared with signals produced by a photodiode sensing a fraction of the detected laser light at point B. The gain and phase of the laser system as a function of frequency were thus plotted and are shown in figures 2.9 and 2.10.

It can be seen that the gain response of the system in figure 2.9 looks similar to the response expected from a simple low pass filter but with a sudden increase in gain between 200 kHz and 300 kHz due to the relaxation oscillation peak in intensity. The slope of the gain curve in figure 2.9 was measured in the 50 kHz to 100kHz range

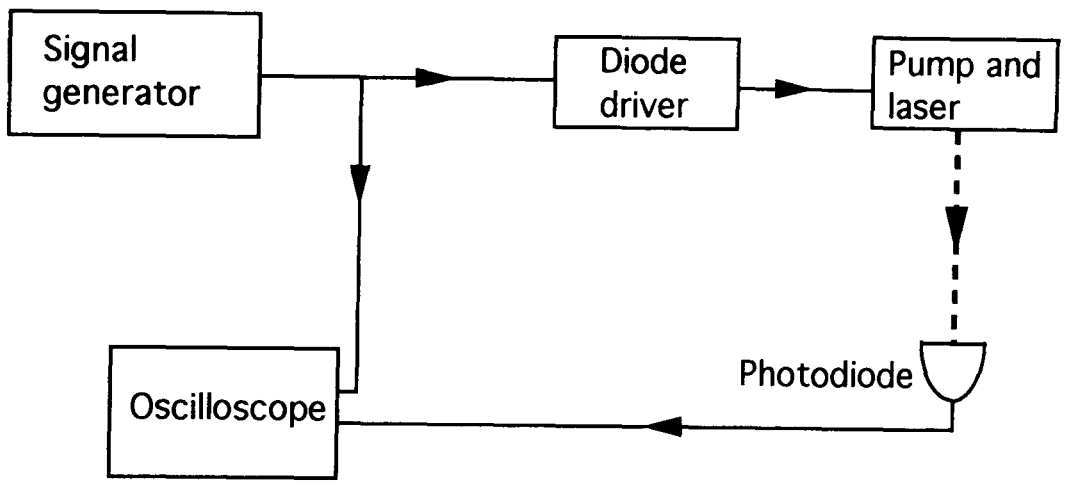


Figure 2.8: *System to measure transfer function of laser and driver for diode pump.*

and found to be approximately 15 dB per decade. This suggested that at higher frequencies the slope tended towards the 20 dB per decade expected for a low pass filter.

It is clear however from figure 2.10 that the phase response of the system was not that of a simple low pass filter. At 300 kHz the phase lag of the system was approximately 431 degrees. Of this, 180 degrees were due to the relaxation resonance at approximately 250 kHz. At this frequency the diode driver was thus responsible for a phase lag of approximately 251 degrees. Since the maximum phase lag which can be produced by a low pass filter is 90 degrees this suggested that the driver was behaving as a low pass filter plus some time delay. Close to the relaxation oscillation frequency this time delay, equivalent to a phase lag of approximately 161 degrees, was estimated to be approximately 1.6 $\mu s$ and is thus not too large to be compensated by filtering techniques.

### 2.2.5 Feedback System Design and Performance

From section 2.2.3, a feedback system to damp the relaxation oscillations in intensity should contain a differentiator and therefore some phase lead. However the

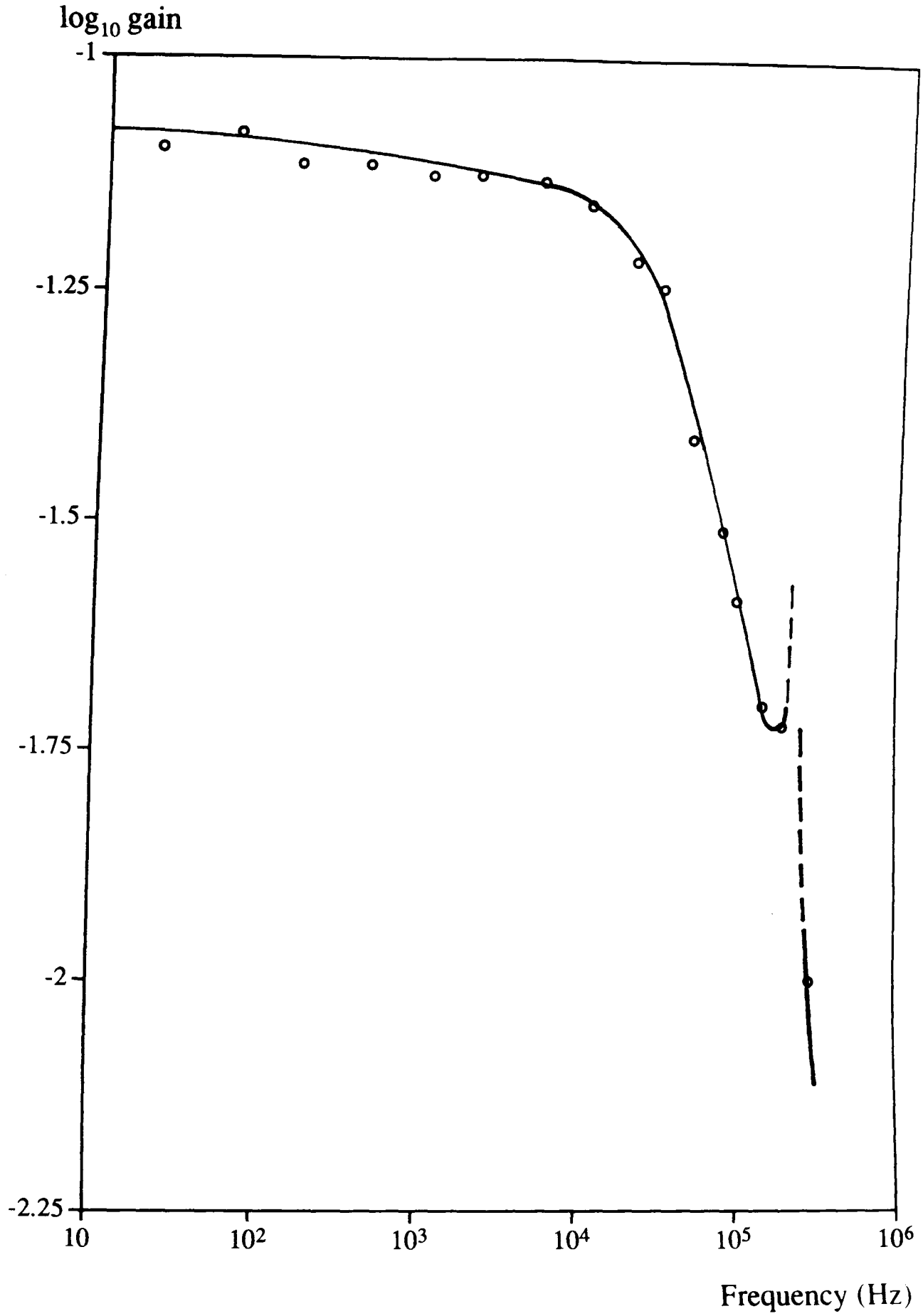


Figure 2.9: *Gain response of diode driver and laser as a function of frequency.*

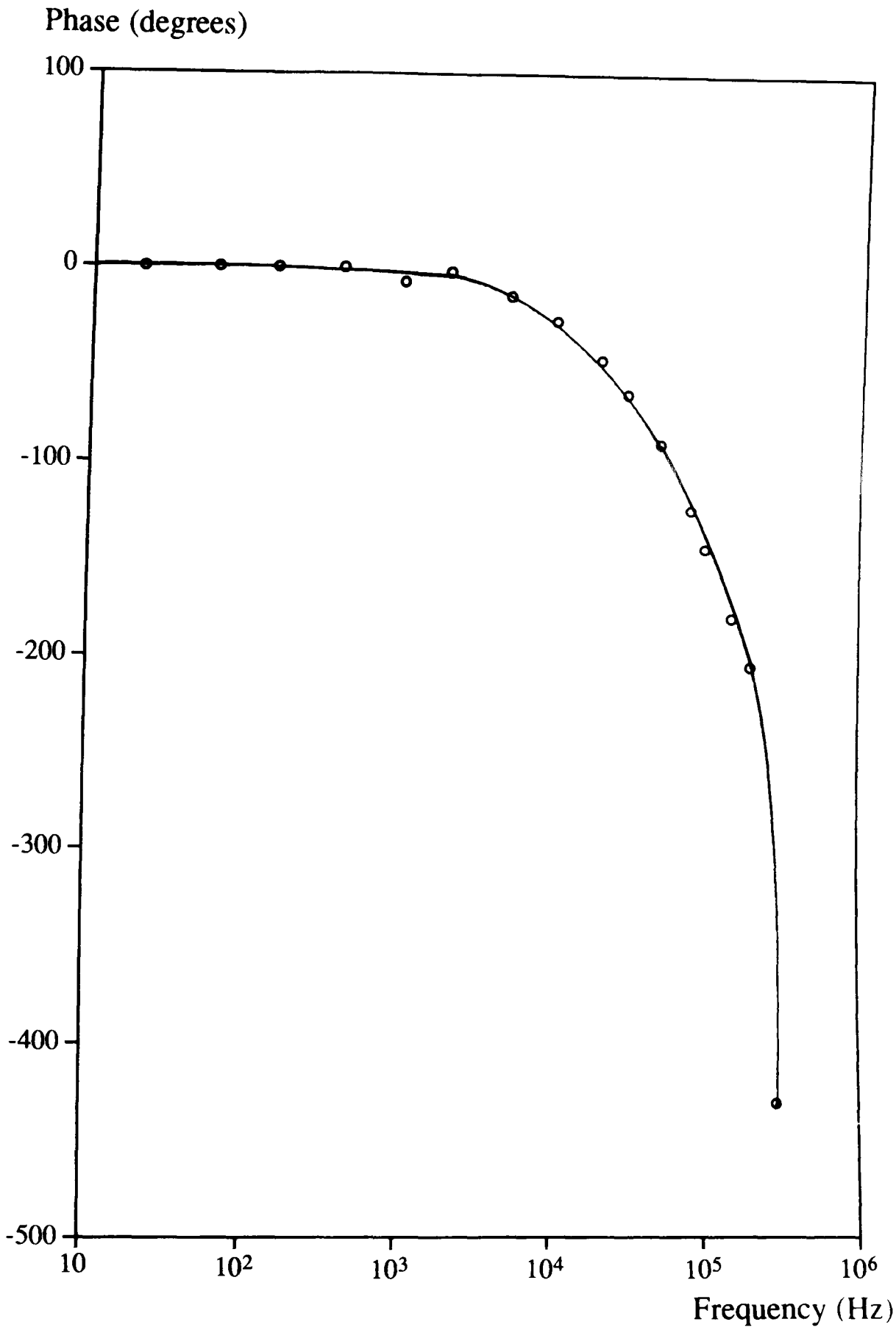


Figure 2.10: *Phase response of diode driver and laser as a function of frequency.*

added complication of the diode driver characteristics must be considered. One design of feedback system which takes these characteristics into account is shown in figure 2.11.

With the laser operating with an output power of approximately 200 mW, the relaxation oscillations were detected by sensing a fraction of the laser light using a photodiode. The signal from this photodiode was then amplified and filtered as shown in figure 2.11. The resulting signal was fed back to the input of the diode driver to modulate the diode pump current.

A fraction of the laser light was sensed on a photodiode external to the servo loop and the detected signal displayed on a spectrum analyser to monitor the effects of the feedback system on the intensity noise of the laser. Intensity noise spectra for the laser taken with and without the feedback system operating are shown in figure 2.12. It can be seen from figure 2.12 that the intensity noise at the relaxation oscillation frequency of approximately 250 kHz has been damped by 20 dB, from a level of $1.9 \times 10^{-5}/\sqrt{Hz}$ to $1.9 \times 10^{-6}/\sqrt{Hz}$. The corresponding dc photocurrent was approximately 0.54 mA.

At frequencies below approximately 150 kHz the servo system caused a slight increase in the intensity noise level of the laser of 1 to 2 dB. The reason for this can be seen by examining the schematic Nyquist plot of the open loop transfer function for the feedback system shown in figure 2.13. The inclusion of two inverting amplifiers and bandpass filters with low frequency corners at approximately 1 Hz and 1 kHz respectively meant that the phase of the negative feedback signal started close to 0 degrees. The phase lag of the feedback signal then started to increase as the phase lead from the bandpass filters decreased. Above a few kHz this lag was further increased due to the diode driver behaving as a low pass filter plus time delay with a corner frequency of approximately 30 kHz. To prevent this significant phase lag causing positive feedback at the relaxation oscillation frequency of approximately 250 kHz, four transitional differentiators were used to provide phase lead at frequencies between a few tens of kHz to a few hundreds of kHz range. Thus, at and close to the relaxation oscillation frequency, the feedback system had significant gain and was operating in a regime away from the point (-1,0) allowing stable operation of the

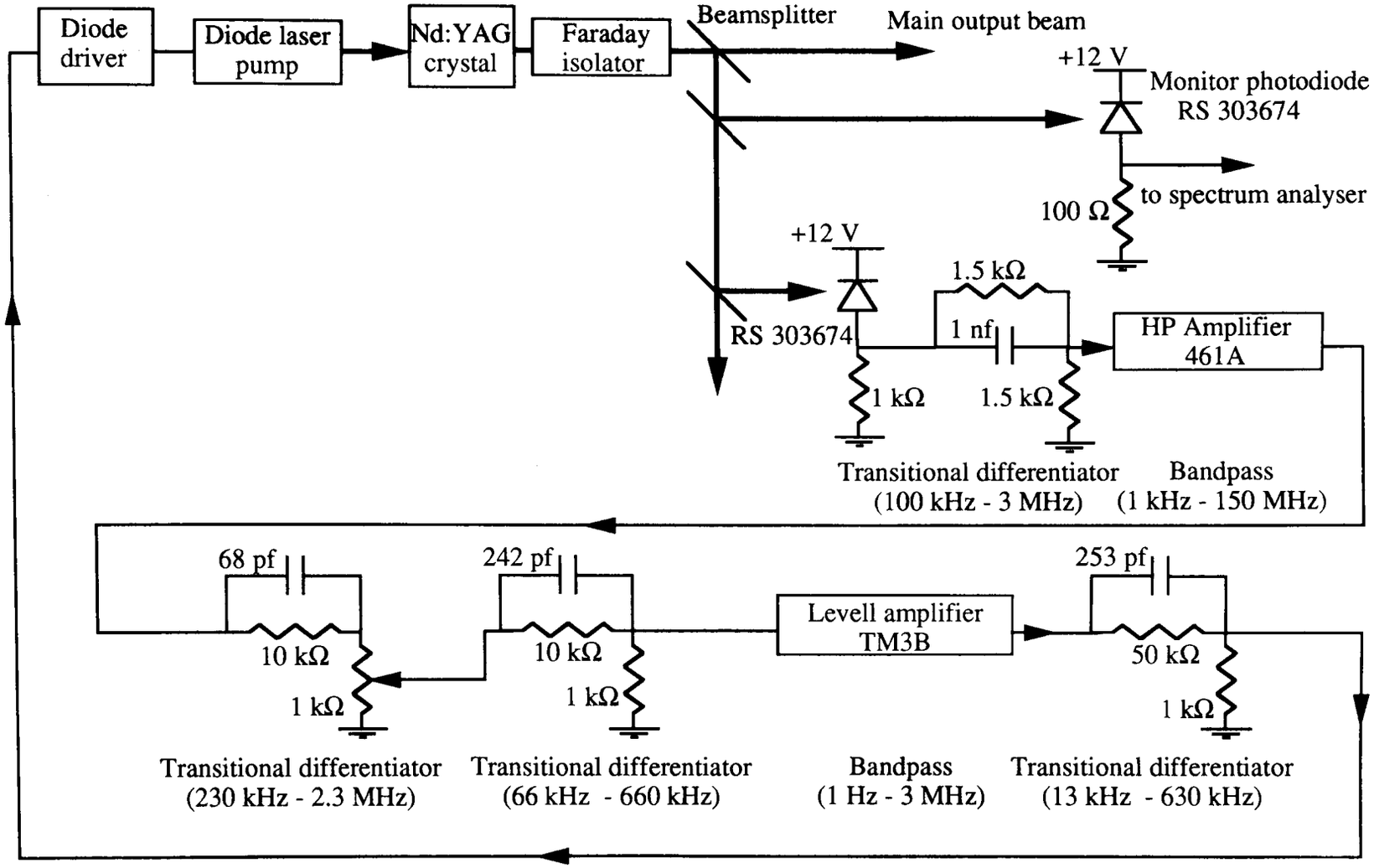


Figure 2.11: *Feedback system used to damp the relaxation oscillation peak in intensity noise of a monolithic Nd:YAG ring laser.*

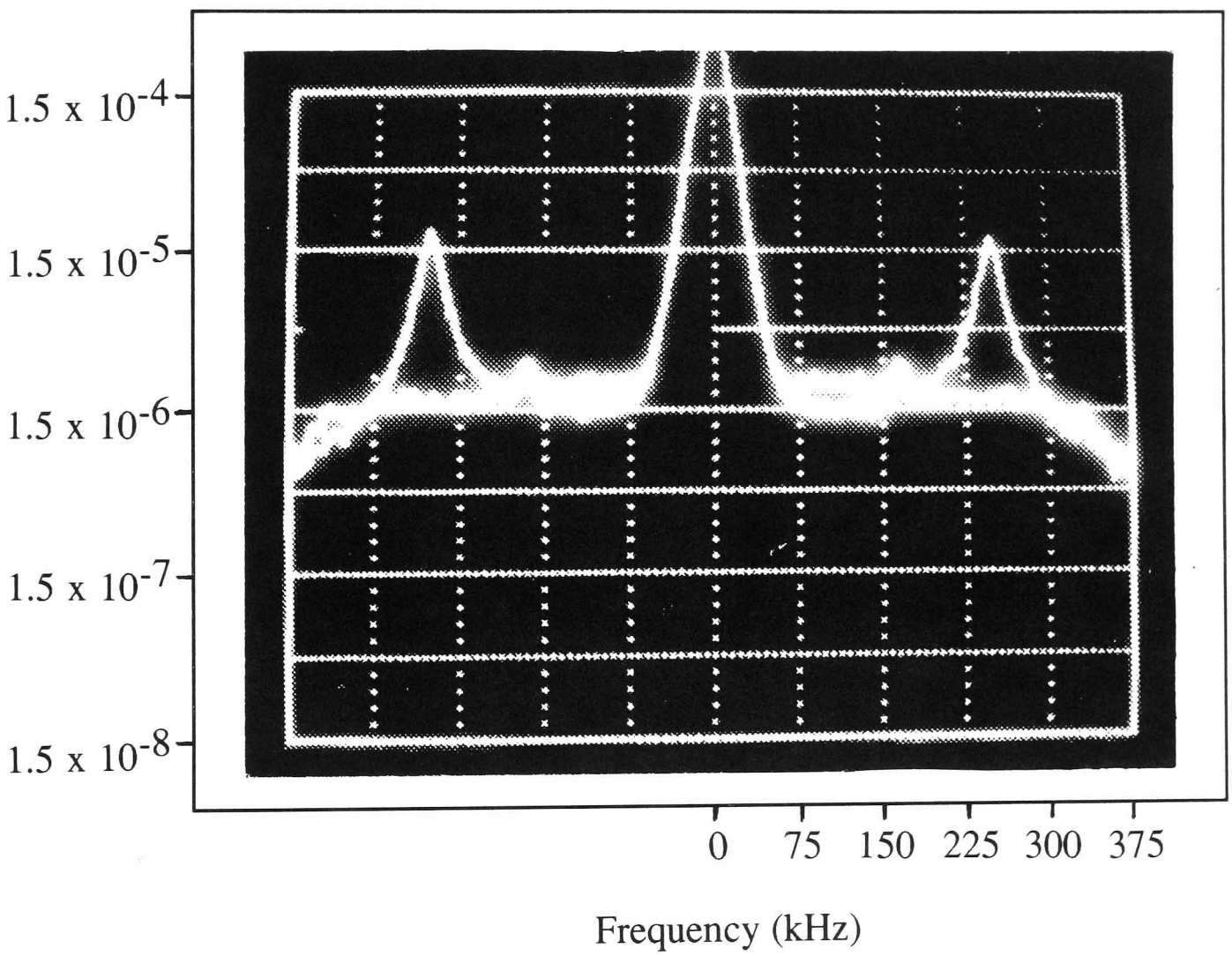


Figure 2.12: *Intensity noise spectra with and without the intensity noise feedback servo operating.*

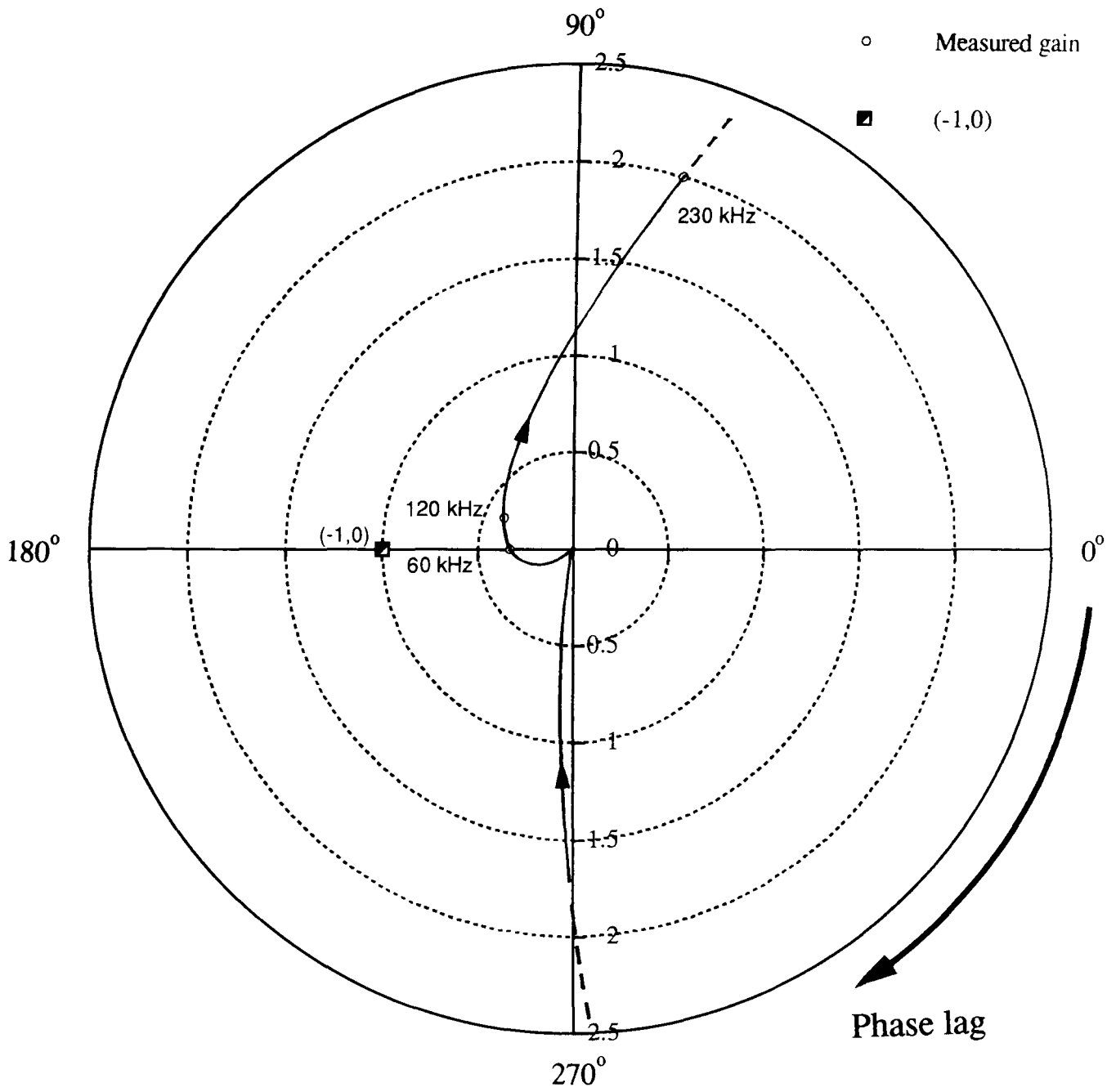


Figure 2.13: *Schematic Nyquist plot of open loop transfer function of the feedback system to damp relaxation oscillations in intensity. Gain is plotted on a linear scale.*

system. At lower frequencies - around 60 kHz to 150 kHz - the system operated in a regime closer to (-1,0) and there was a small amount of positive feedback resulting in the observed increase in intensity noise at these frequencies.

The feedback system described above damped the peak at 250 kHz in the intensity noise of the laser caused by relaxation oscillations to a level which would be acceptable were this type of laser to be used as the master oscillator for the illumination of an interferometric gravitational wave detector. The damped noise level of approximately $1.9 \times 10^{-6}/\sqrt{Hz}$ at 250 kHz was however approximately an order of magnitude above the background noise level set by electronic noise. It was thought that the increase in low frequency noise and limited servo performance was a result of the presence of the time delay in the feedback loop.

Further work on intensity noise reduction systems for this laser was thus carried out in an attempt to circumvent the problem of the measured time delay and low pass filter from the diode driver and laser system, and to show simultaneous reduction in the intensity noise at high and low frequencies.

## 2.3 A Broadband Intensity Stabilisation System

A feedback system was designed to reduce the intensity noise at high and low frequencies of a monolithic Nd:YAG ring laser very similar to that described in section 2.2. The laser had a maximum output power of 350 mW but for measurements described here was operated with an output power of approximately 200 mW, producing a relaxation oscillation frequency of approximately 260 kHz. In an attempt to avoid the time delay and low pass filter apparently introduced by the current driver, the feedback signal was connected directly to the power pins of the diode laser.

### 2.3.1 Design of Broadband Intensity Stabilisation Feedback System

It was desirable to damp the intensity noise of the laser over two separate frequency ranges: around the relaxation oscillation peak close to 260 kHz and at the frequencies

of interest for gravitational wave detection, from a few Hz up to several kHz. To do this a two-loop servo system was designed which operated over two frequency ranges simultaneously. A diagram of the feedback system is shown in figure 2.14. Light from the laser, after passing through a Faraday effect device to provide external isolation, was split from the main beam to provide two separate beams. Each beam was sensed by a photodiode, one to provide the low frequency correction signal and the other to provide the high frequency correction signal. The signal from each photodiode was then amplified and filtered and the resulting signals were added. The combined signal provided the feedback signal to modulate the current to the laser diode. A separate photodiode was used for each loop so that the loops could easily be operated independently: future systems would be likely to use one photodiode for both loops. A fraction of the light from the main laser beam was also sensed by a third independent photodiode and the detected signal displayed on a spectrum analyser to monitor the performance of the feedback system. The amount of light falling on the external photodiode was approximately 7 mW; approximately 7 mW of light was incident on the photodiode in the low frequency feedback loop; and 13 mW of light fell on the photodiode in the high frequency feedback loop.

### 2.3.2 Feedback Loop to Reduce Intensity Noise at Low Frequencies

One loop of the feedback system operated mainly at low frequencies, in the range from a few Hz to around 30 kHz, with most of the noise suppression occurring around a few hundred Hz. This loop, however, also had gain around the relaxation oscillation frequency, with a reduction of up to 10 dB in the noise at the relaxation oscillation peak being observed when this feedback loop was operated independently of the high frequency loop.

The low frequency loop consisted of two Princeton model 113 amplifiers in series, one operating over frequencies from 10 Hz to 100 Hz, and the other operating from dc to 300 kHz. This signal then passed through a high pass filter with a corner at 7 Hz before being added to the signal from the high frequency feedback loop. This loop did not contain a dc feedback path since any dc offsets in the feedback loop

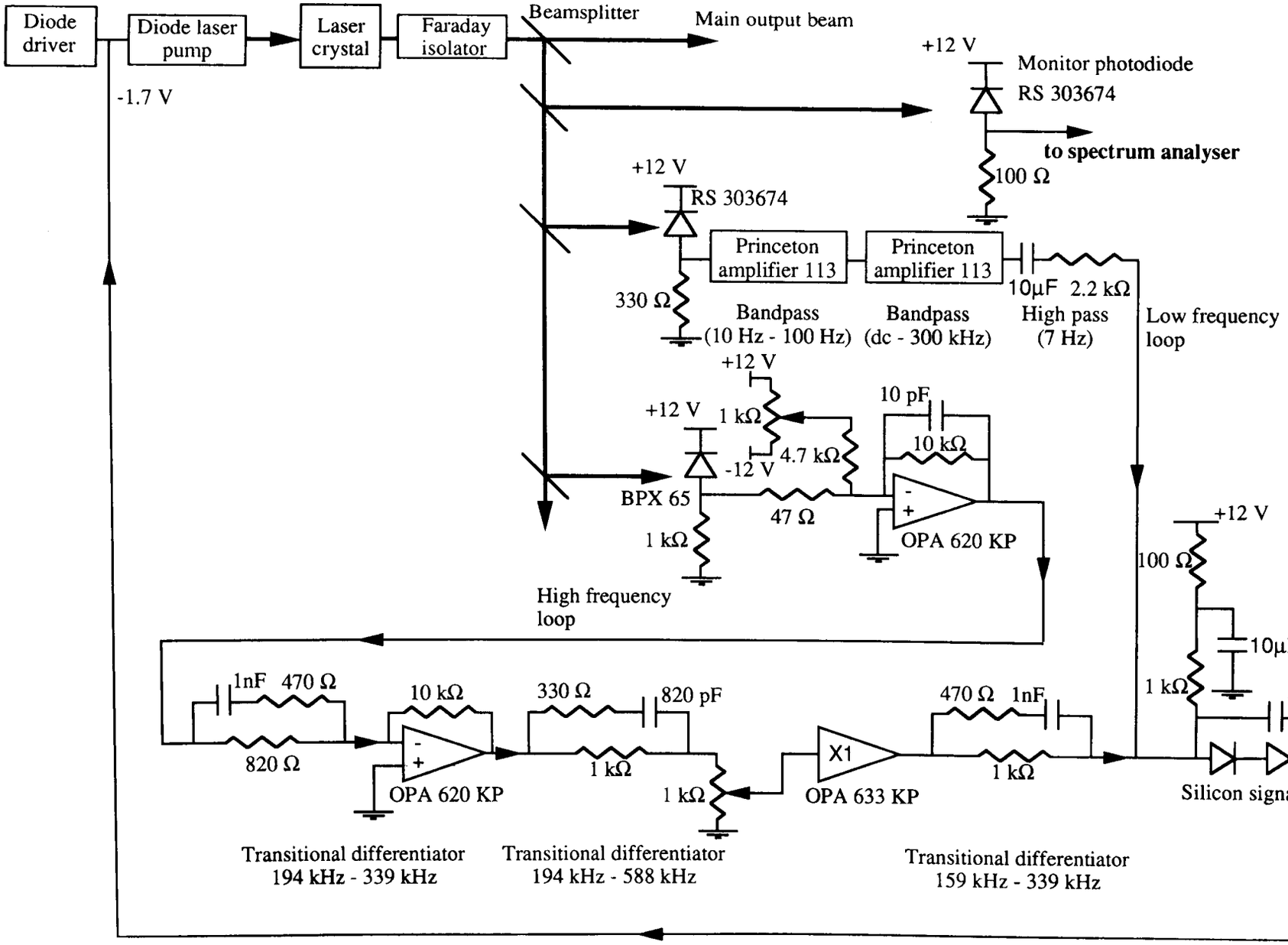


Figure 2.14: *Diagram of two-loop intensity stabilisation system.*

resulted in difficulties in locking the system.

A Nyquist plot of the measured open loop transfer function for the low frequency feedback loop is shown in figure 2.15, with the behaviour of the system close to the point (-1,0) shown in more detail in figure 2.16.

Figure 2.15 shows that this feedback loop had significant gain in two frequency ranges, from low frequencies up to approximately 30 kHz and from approximately 200 kHz to 300 kHz around the relaxation oscillation frequency.

At frequencies up to a few kHz, it can be seen that the phase of the transfer function was controlled, as might be expected, by the phase lag from the 100 Hz corner of the Princeton amplifier operating over the 10 Hz to 100 Hz frequency range. At frequencies of a few tens of kHz and above, however, the phase lag of the feedback signal increased faster than might be expected simply from the feedback electronics. The phase response of the system was in fact consistent with the presence of an extra phase delay similar to that produced by the time delay described in section 2.2.4; but the phase lag due to the low pass filter action of the diode driver had been removed. The extra phase lag meant that the phase of the feedback signal close to the relaxation oscillation frequency was correct to allow some suppression of the noise at these frequencies. It should be noted that a similar feedback system with similar performance could have been designed which included the diode driver system in the feedback loop.

### 2.3.3 Feedback Loop Operating at High Frequencies

The second loop of the feedback system operated solely at frequencies around the relaxation oscillation frequency.

To damp the intensity noise at the relaxation oscillation frequency, three transitional differentiators were required to provide phase lead in the ranges 194 kHz - 339 kHz, 194 kHz - 558 kHz and 159 kHz - 339 kHz as shown in figure 2.14. This was again consistent with the presence of a phase lag such as that produced by the time delay described in section 2.2.4.

Figure 2.17 shows the performance of the high frequency loop of the broadband intensity stabilisation system operating independently of the low frequency servo

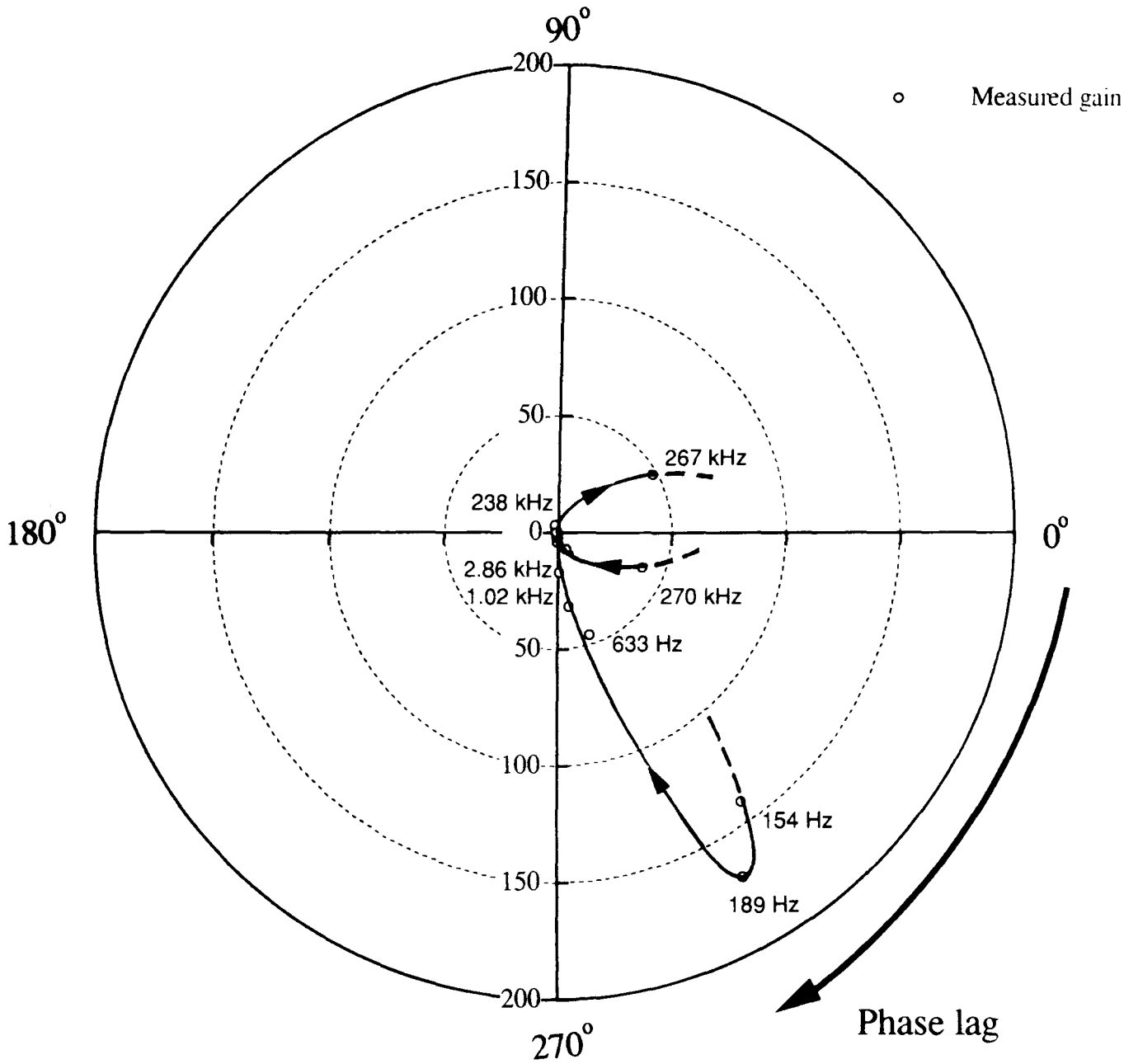


Figure 2.15: *Nyquist plot showing the open loop transfer function for the low frequency loop of the broadband intensity stabilisation system. Gain is plotted on a linear scale.*

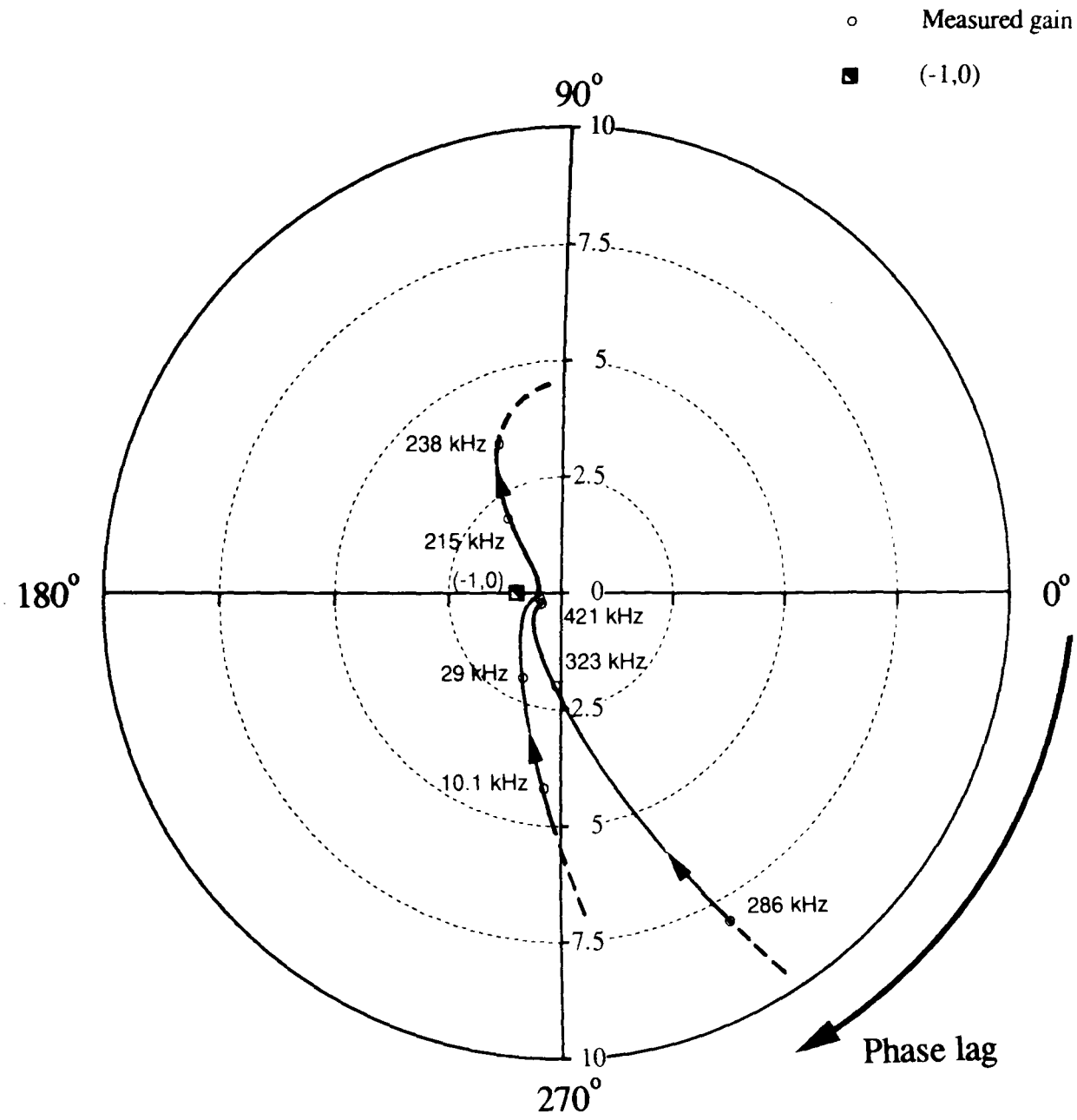


Figure 2.16: *Nyquist plot showing the behaviour of the open loop transfer function for the low frequency loop of the broadband intensity stabilisation system close to the point (-1,0). Gain is plotted on a linear scale.*

loop. It can be seen from figure 2.17 that the high frequency servo loop suppresses the noise at the relaxation oscillation frequency by approximately 17 dB, with no increase in the intensity noise at other frequencies. This could be expected from the shape of the Nyquist plot of the open loop transfer function for the high frequency feedback loop shown in figure 2.18.

The observation that directly driving the diode laser did not eliminate the time delay was a surprise. It seems that the delay is associated with some physical process associated with the pumping of the Nd:YAG. This will not be considered further in this thesis but will be investigated further at a later stage

### 2.3.4 Complete Broadband Intensity Stabilisation System

To provide broadband stabilisation of the intensity of the laser both the high and low frequency feedback loops were operated simultaneously.

In figures 2.19 and 2.20 Nyquist plots of the open loop transfer function for the two-loop feedback system are shown.

Figure 2.19 shows the Nyquist plot for the complete frequency range of operation of the system. From the shape of this plot it can be seen that the feedback system had significant gain in the frequency range from a few Hz to a few kHz, with maximum gain and thus maximum reduction in intensity noise, at a few hundred Hz. The complete system also had gain available in the range from approximately 200 kHz to 300 kHz which was desirable to allow damping of the intensity noise at and close to the relaxation oscillation frequency of around 260 kHz to 270 kHz. It is interesting to note the behaviour of the open loop transfer function around the point (-1,0) as shown in figure 2.20. For frequencies between approximately 30 kHz and 200 kHz the transfer function is close to the point (-1,0) but does not encircle it. It could thus be expected that the feedback system should be stable but cause a slight increase in the intensity noise in this frequency range.

#### Performance of Broadband Intensity Feedback System

The effect of the broadband feedback system on the laser intensity noise over different frequency ranges is shown in figure 2.21, 2.22, and 2.23.

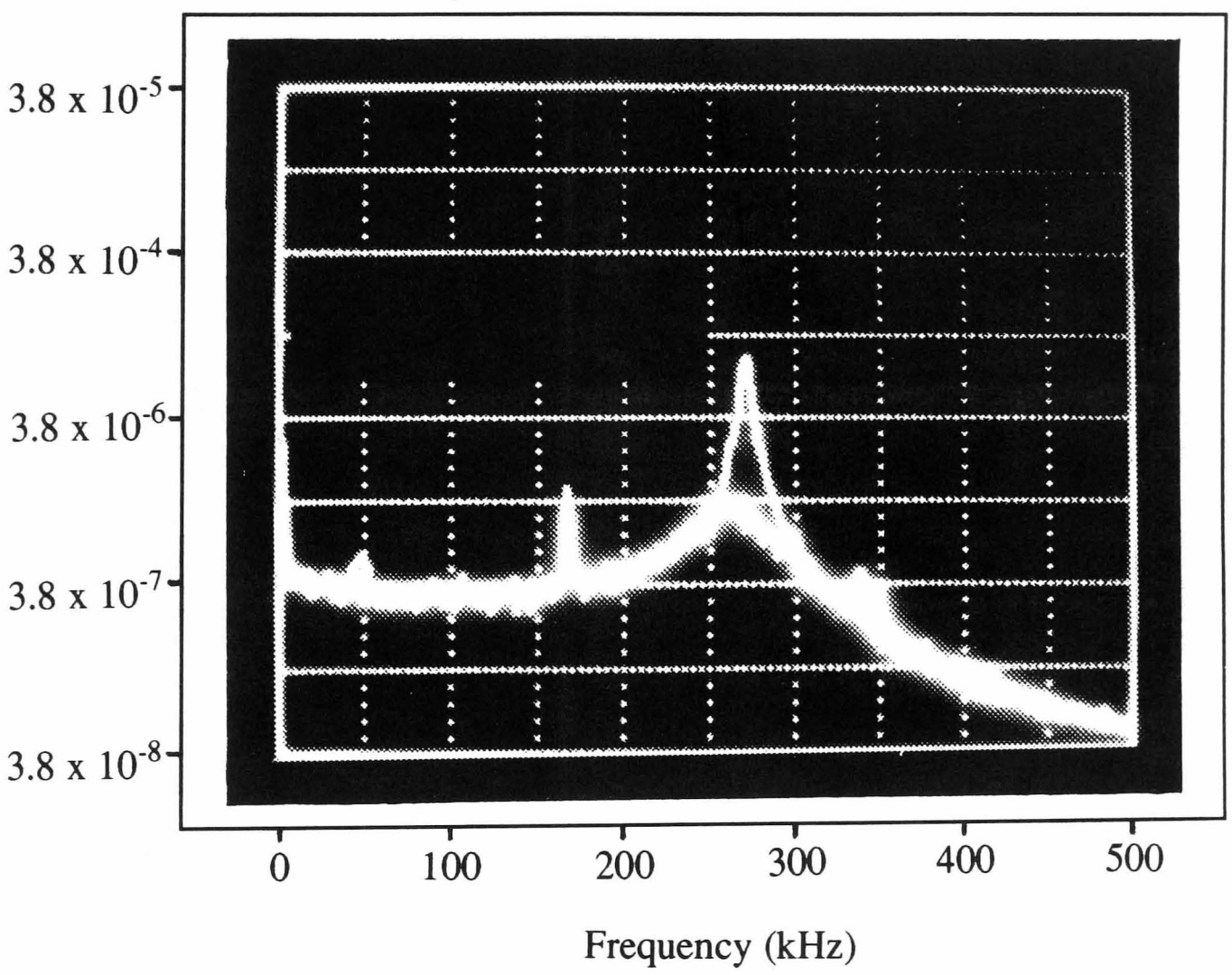


Figure 2.17: *Intensity noise spectra with and without the high frequency loop of the broadband intensity stabilisation system operating. The peaks at 170 kHz and 340 kHz are thought to be due to electronic pick-up.*

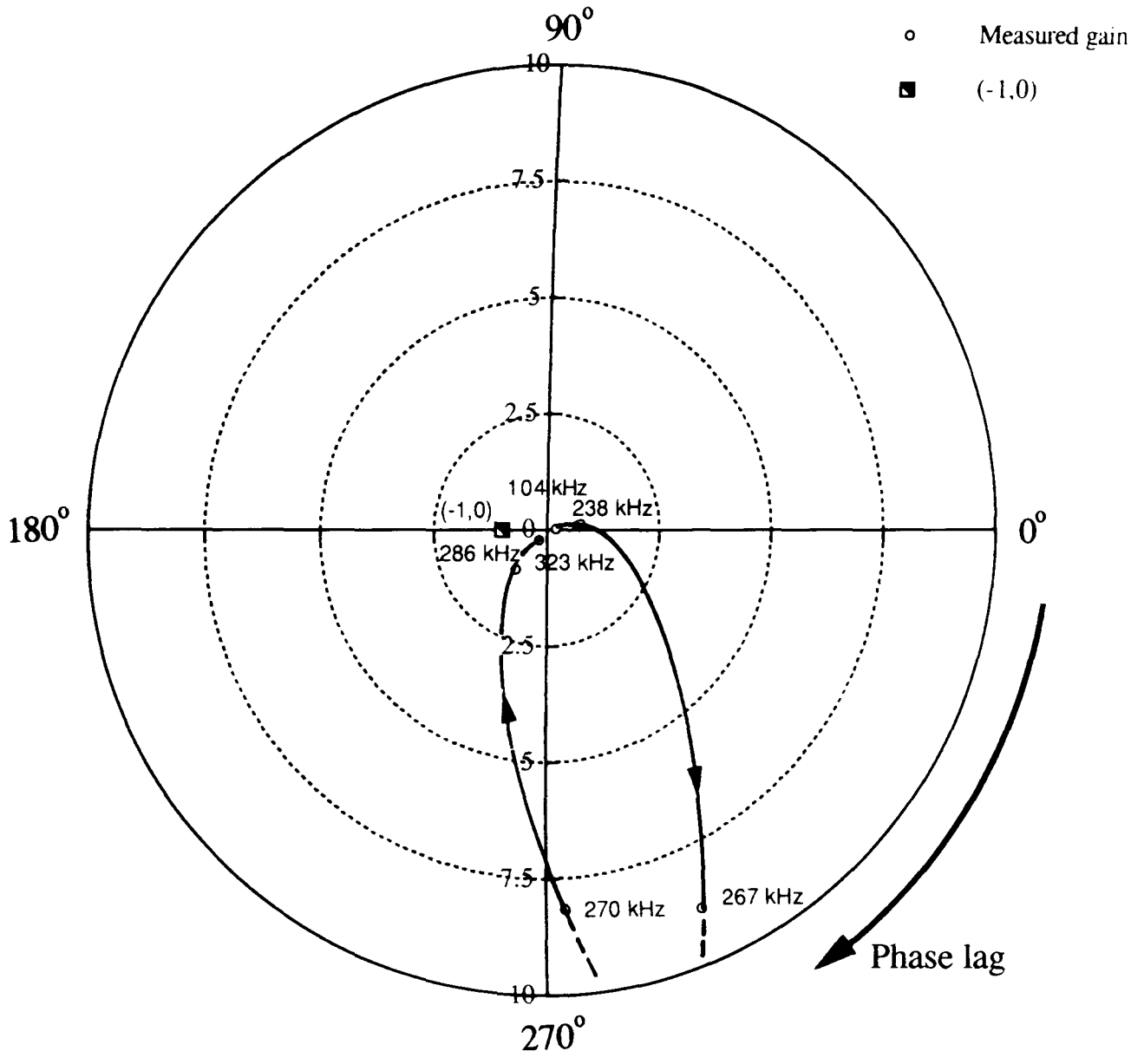


Figure 2.18: *Nyquist plot showing the open loop transfer function for the high frequency loop of the broadband intensity stabilisation system. Gain is plotted on a linear scale.*

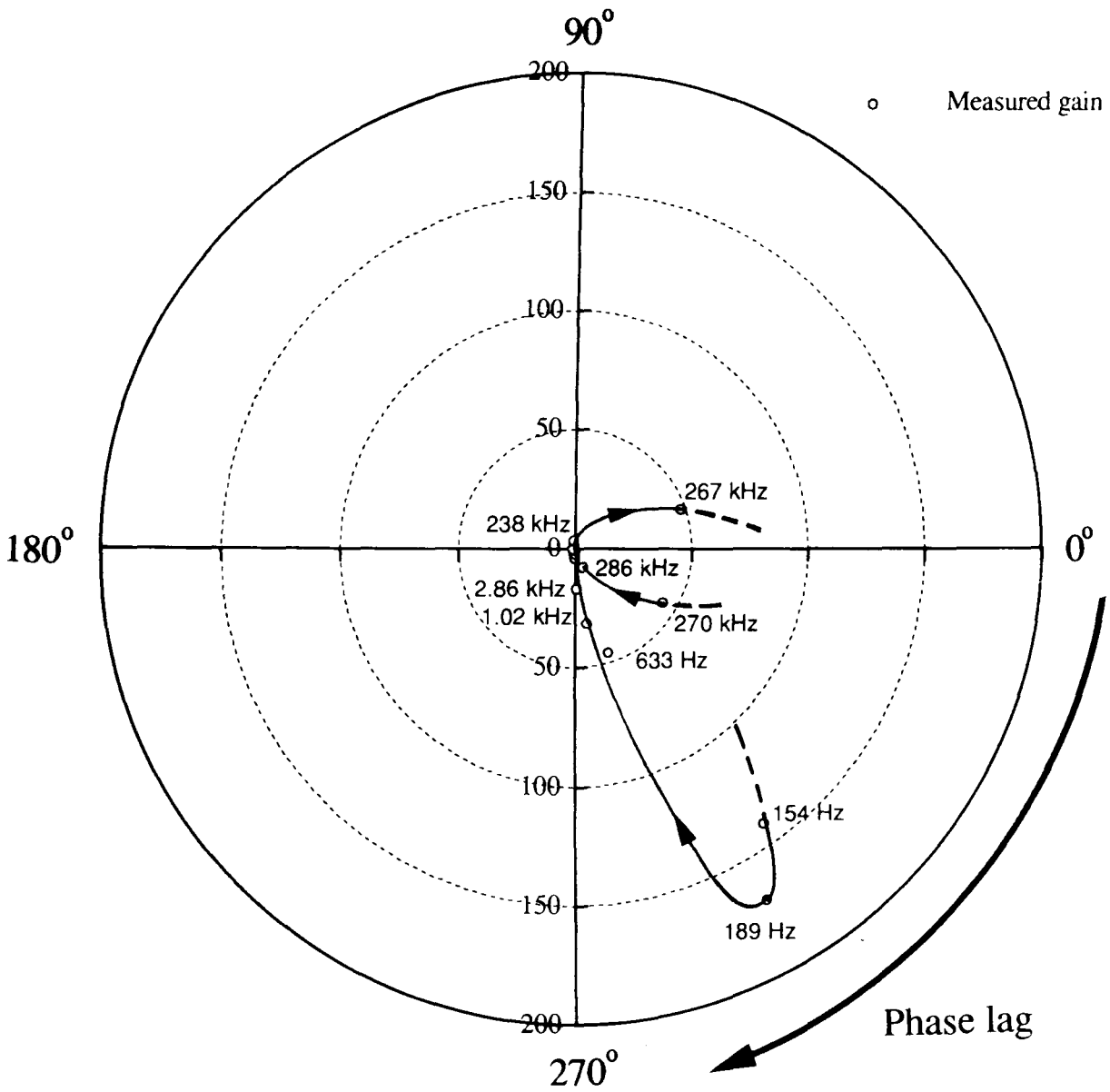


Figure 2.19: *Nyquist plot of the transfer function for the complete two-loop intensity stabilisation system. Gain is plotted on a linear scale.*

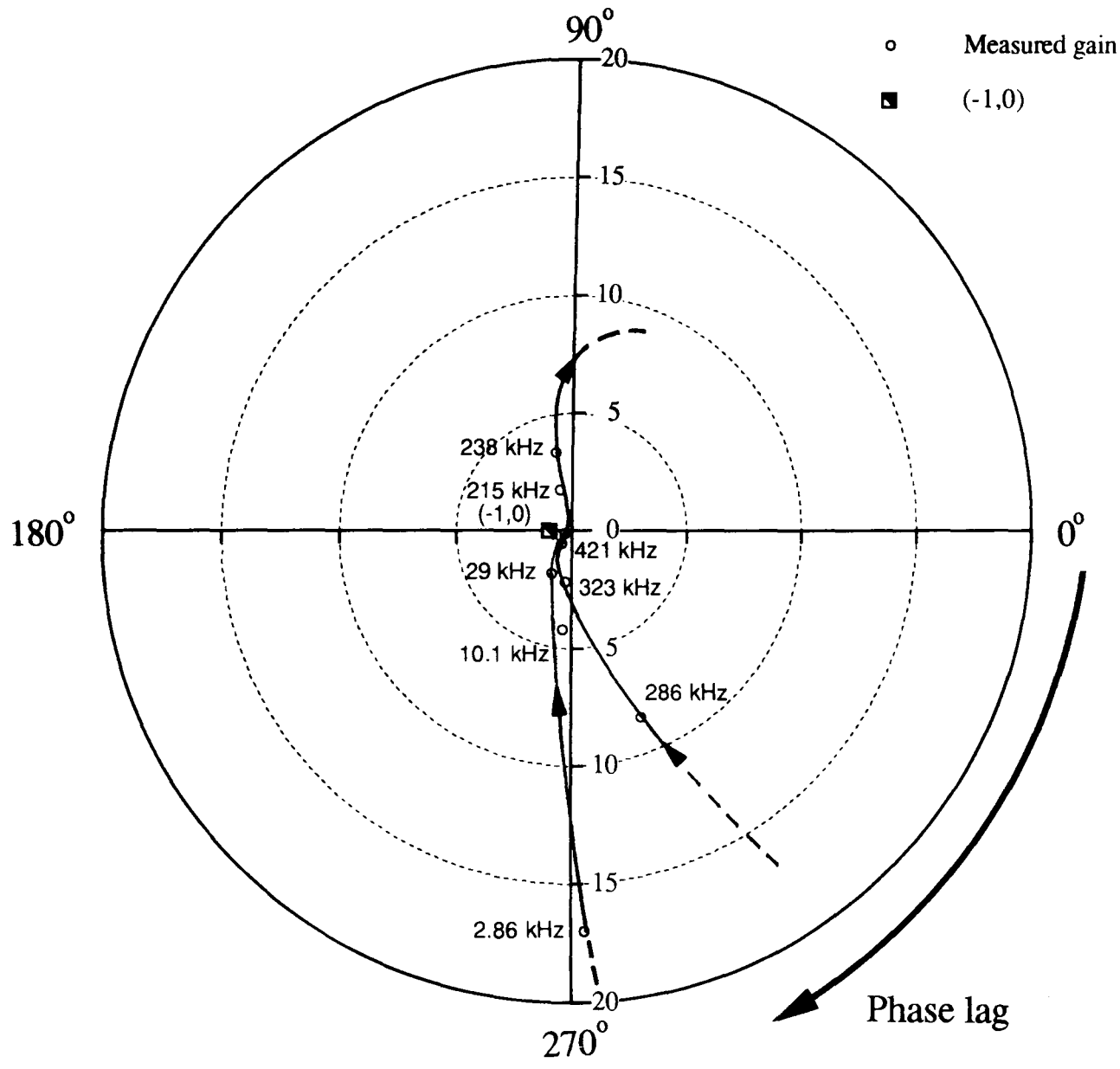


Figure 2.20: *Nyquist plot of the behaviour of the two-loop intensity stabilisation system close to the point (-1,0). Gain is plotted in linear units.*

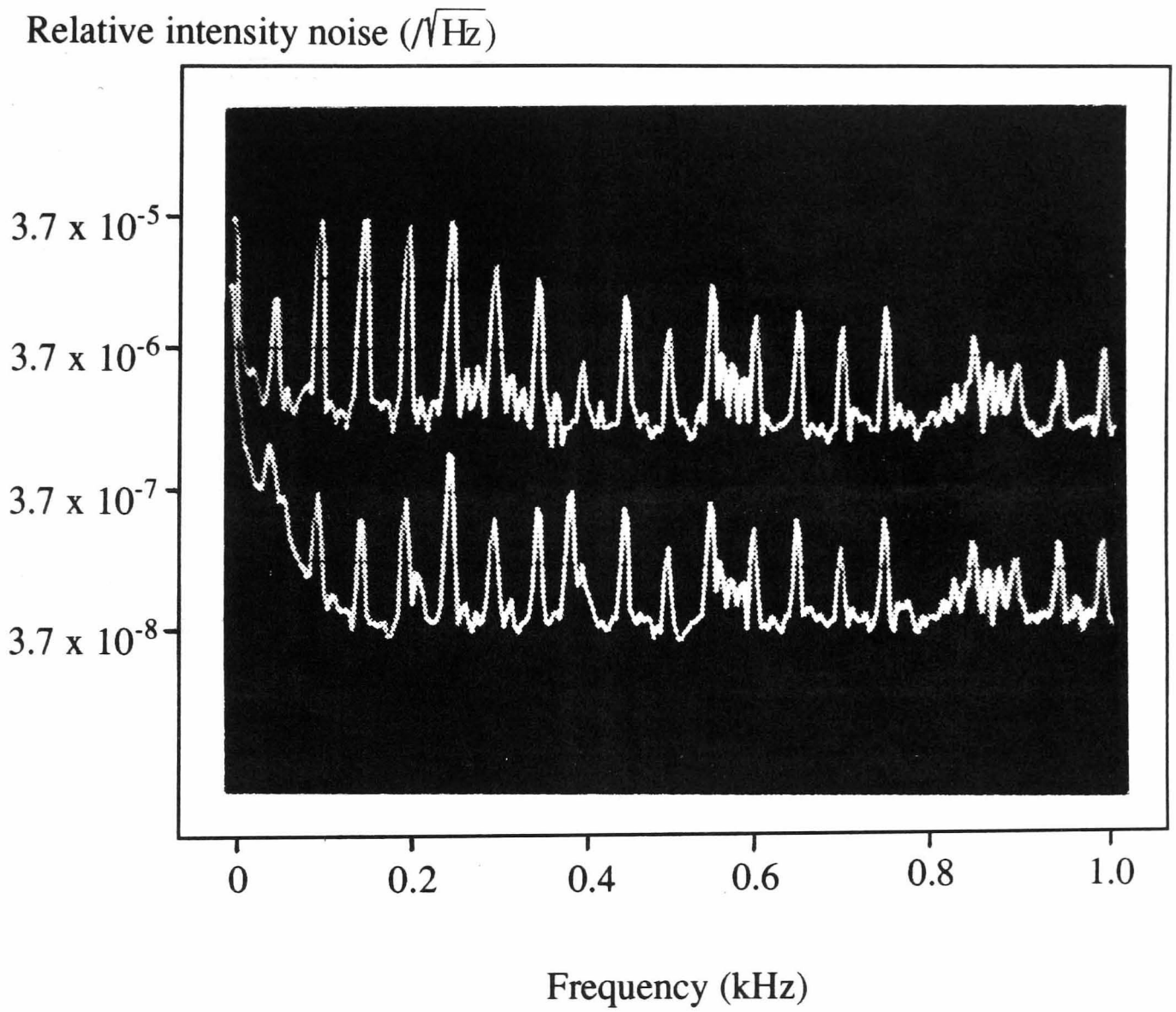


Figure 2.21: *Spectra showing intensity noise up to 1 kHz with and without the intensity stabilisation system. The intensity spikes at multiples of the 50 Hz mains frequency were imposed on the light by the laser power supply.*

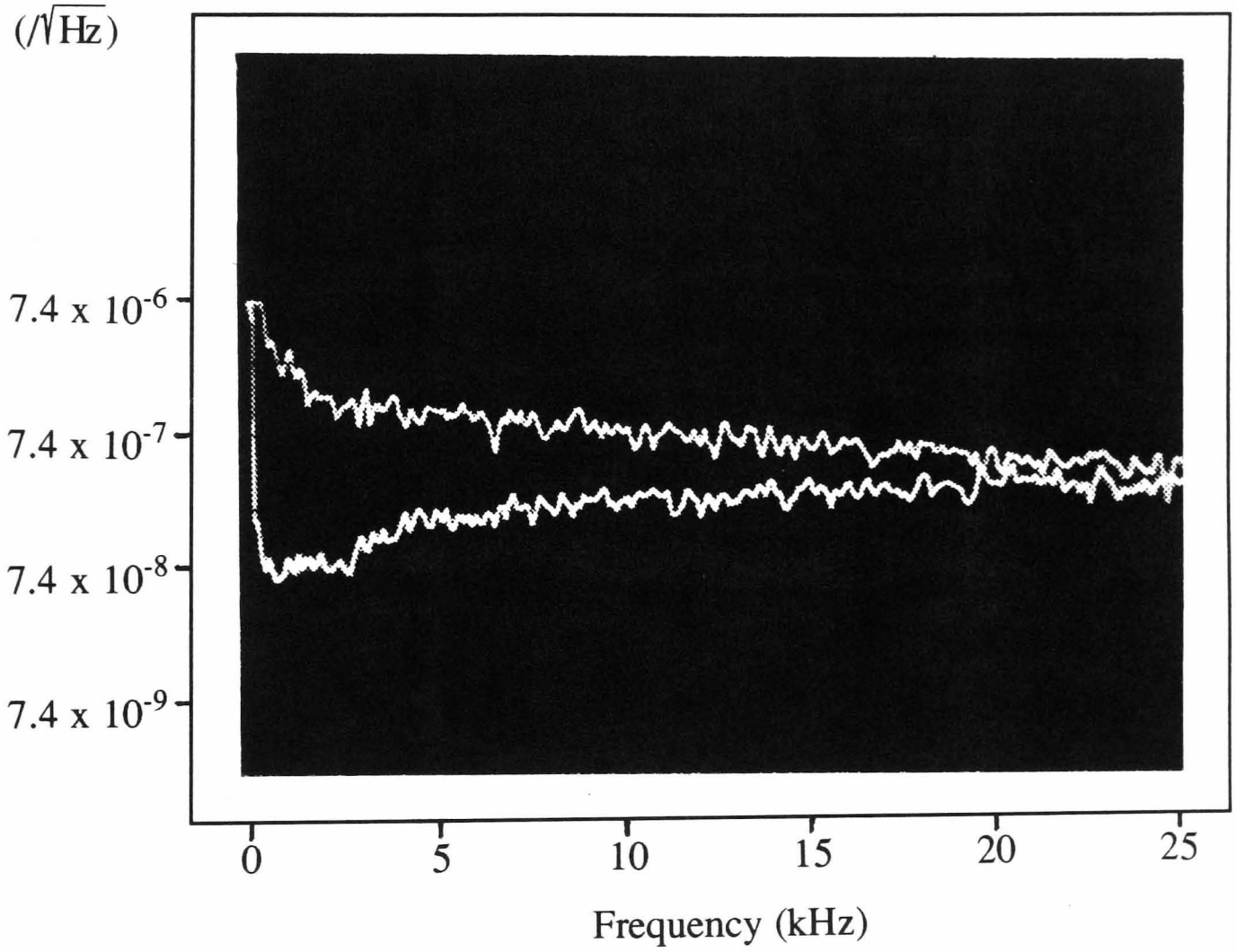


Figure 2.22: *Spectra showing intensity noise up to 25 kHz with and without the intensity stabilisation system.*

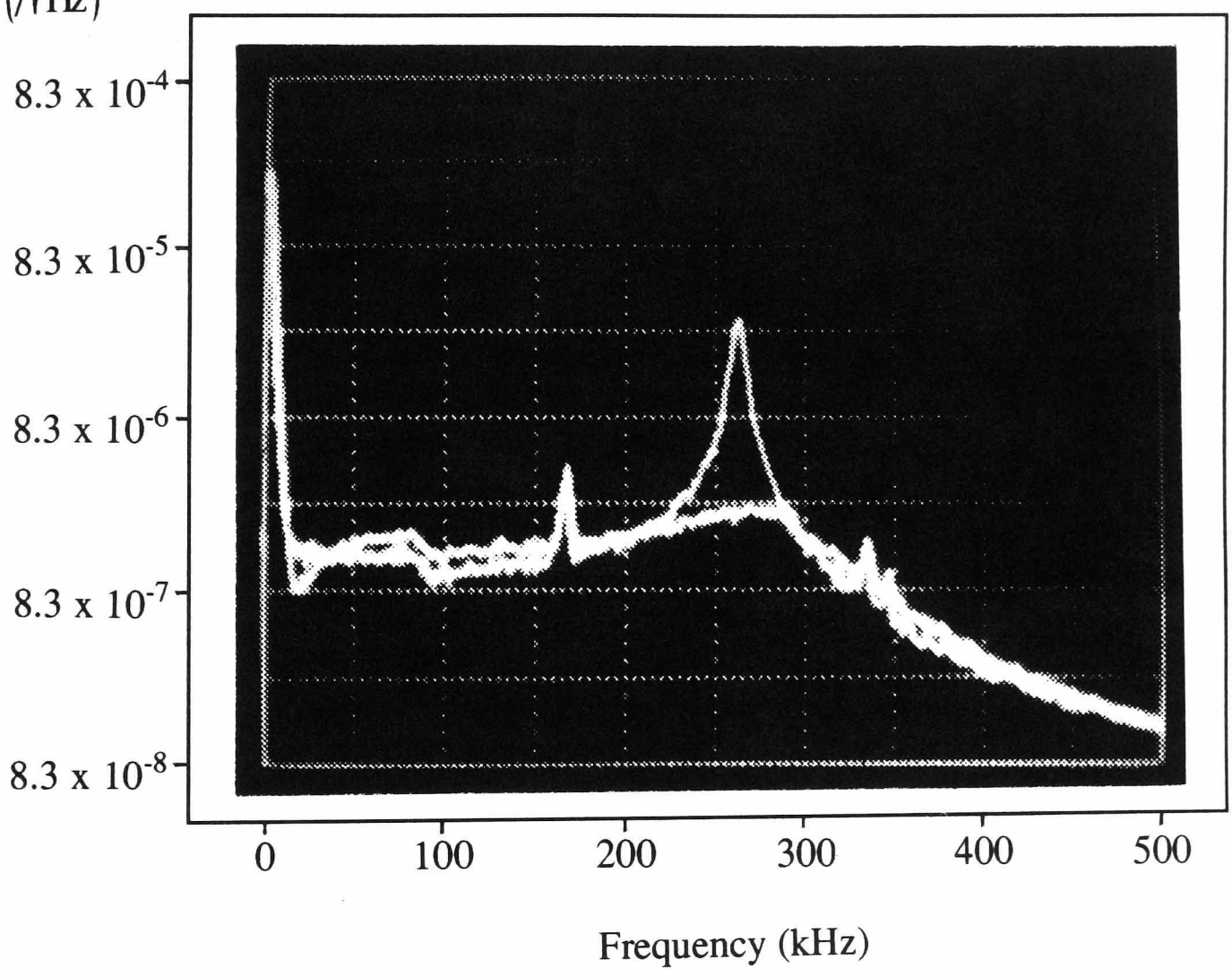


Figure 2.23: *Spectra showing intensity noise up to 500 kHz with and without the intensity stabilisation system.*

Figure 2.21 shows spectra of the laser intensity noise in the region 0 to 1 kHz with and without the intensity reduction system operating. The intensity noise was reduced by up to factor of 30 over this frequency range. The noise was reduced to $4.6 \times 10^{-8}/\sqrt{Hz}$ at 500 Hz of which $1.5 \times 10^{-8}/\sqrt{Hz}$ was photon shot noise in 7 mW of detected light. This stabilised level is close to that required of the source for the planned GEO 600 interferometer.

Figure 2.22 shows the reduction in intensity noise over the region 0 to 25 kHz caused by the intensity feedback system.

Intensity noise spectra for the frequency range 0 to 500 kHz, with and without the intensity feedback system operating are shown in figure 2.23. There was a slight increase in intensity noise with the feedback system operating for noise occurring at frequencies between approximately 30 kHz and 200 kHz. This is to be expected from the shape of the Nyquist plots in figures 2.19 and 2.20. The relaxation oscillation peak at approximately 260 kHz was reduced by a factor of 14, damping the relative intensity noise to $2.3 \times 10^{-6}/\sqrt{Hz}$ at that frequency.

### 2.3.5 Investigations into Servo Performance

From the results above it can be seen that in the frequency range 0 Hz to 1 kHz, with the servo operating, the intensity noise was reduced to a level within 10 dB of the shot noise limit for the detected light. We would not expect to be able to reduce the intensity noise further than to a level of about 5 dB above the shot noise limit for the light detected on the external photodiode due to a contribution to the laser noise from the shot noise and amplifier noise of the low frequency servo loop. (Note that due to the relatively low gain of the high frequency servo loop at low frequencies, noise in this loop did not contribute to the intensity noise discussed above).

### 2.3.6 Background Experiments

Initial experiments with a similar intensity noise feedback system saw the servo performance limited more severely at low frequencies, with the performance below approximately 500 Hz limited at around 20 dB above shot noise on the monitor

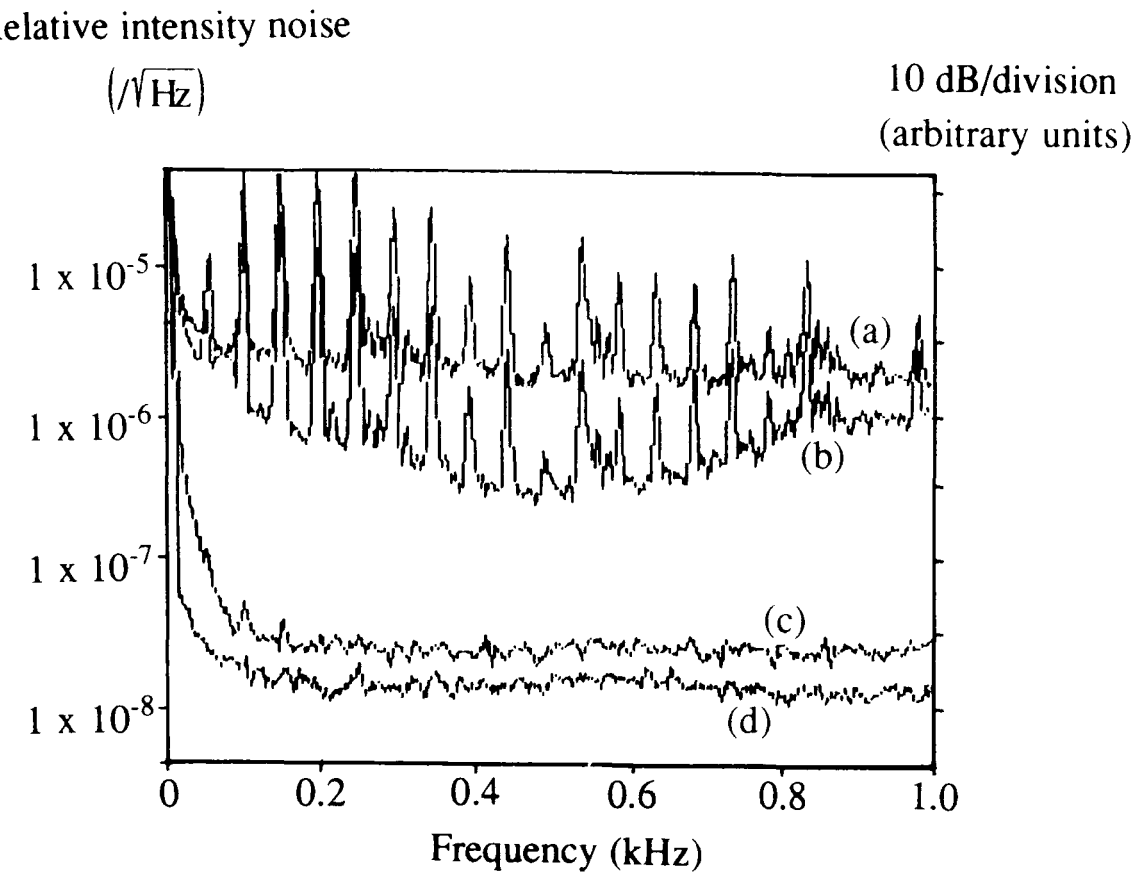


Figure 2.24: *Preliminary measurements of intensity spectra up to 1 kHz with and without the intensity feedback system operating are shown as curves* **(b)** *and* **(a)** *respectively. Corresponding levels of shot noise and electronic noise are shown as curves* **(c)** *and* **(d)** *respectively.*

photodiode. This is shown in figures 2.24 and 2.25. It can be seen in figure 2.24 that the stabilised intensity noise level is not limited by shot noise or electronic noise. Further, figure 2.25 shows that when the gain of the intensity servo was doubled, the noise above approximately 500 Hz was decreased, but that there was no further decrease in the intensity noise below 500 Hz.

Experiments with other lasers [73] suggest that the coupling of other forms of laser noise - such as frequency noise or beam geometry fluctuations - into intensity noise at a photodiode can limit the performance of an intensity noise feedback system. If some other form of laser noise was being sensed as intensity noise by the servo loop photodiode, the feedback loop would correct for this detected signal and thus impose some intensity noise on the laser light. An independent photodiode would thus sense a level of intensity noise not reduced by the full loop gain of the servo system.

To investigate whether the servo performance at low frequencies might be being limited in this way a signal generator was used to impose a test peak at approxi-

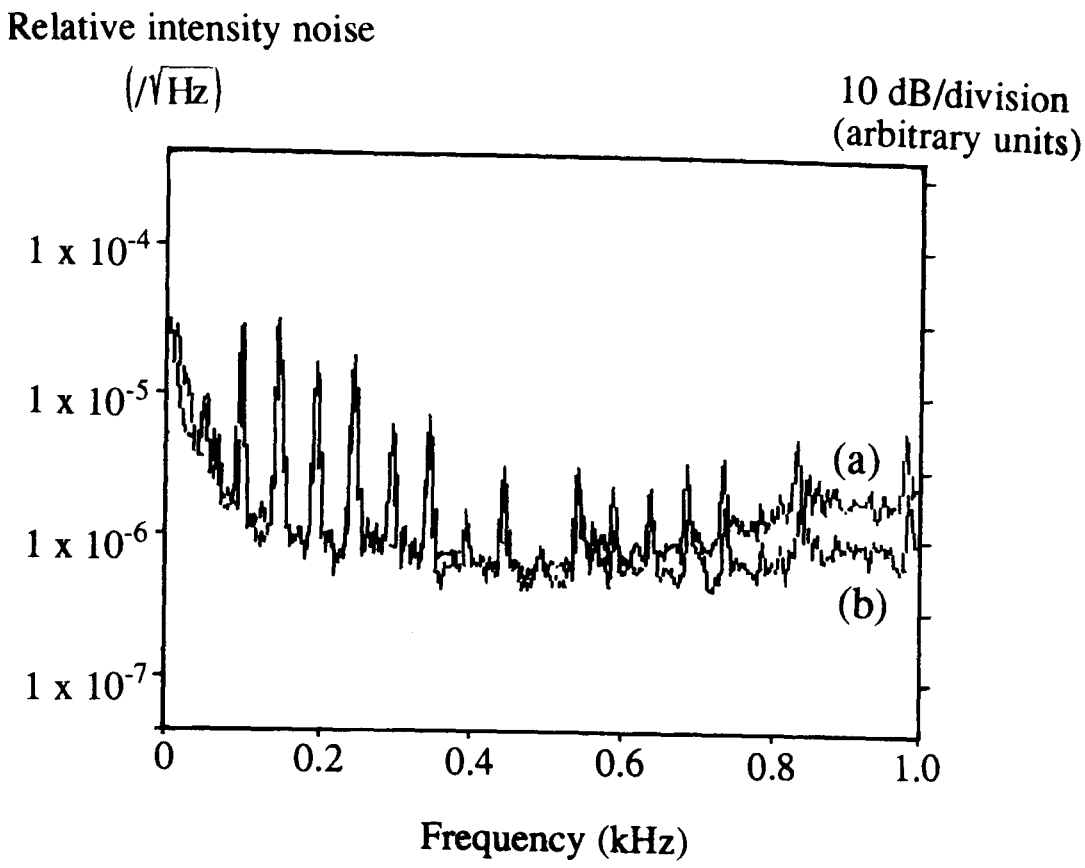


Figure 2.25: *Intensity spectra up to 1 kHz with the intensity stabilisation system operating. For curve* **(b)** *the servo gain was double that for curve* **(a)**.

mately 625 Hz inside the feedback loop onto the intensity of the laser. The effect of the intensity feedback system on the size of this peak with respect to the reduction in the background intensity noise close to this frequency was noted.

The effect of the intensity feedback system on the signals inside the feedback system was measured at the output of the servo photodiode. Spectra were taken with and without the feedback system operating and are shown in figure 2.26. It can be seen that the peak at 625 Hz was reduced by approximately 38 dB, this being the available loop gain of the system, while the background signals were reduced by approximately 30 dB. The background noise in the system was limited by a noise floor due to the electronic noise in the Levell amplifier used to amplify the feedback signal before the signal was displayed on a spectrum analyser.

The effect of the feedback system on the laser intensity noise as measured on the external photodiode is shown in figure 2.27. The peak at 625 Hz as viewed using the external photodiode is reduced by the full available loop gain of approximately 38 dB, while the background close to this frequency was only reduced by approximately 25 dB. The intensity noise spectra with the feedback system operating was not limited by electronic noise or shot noise. This suggested that the signal at 625 Hz

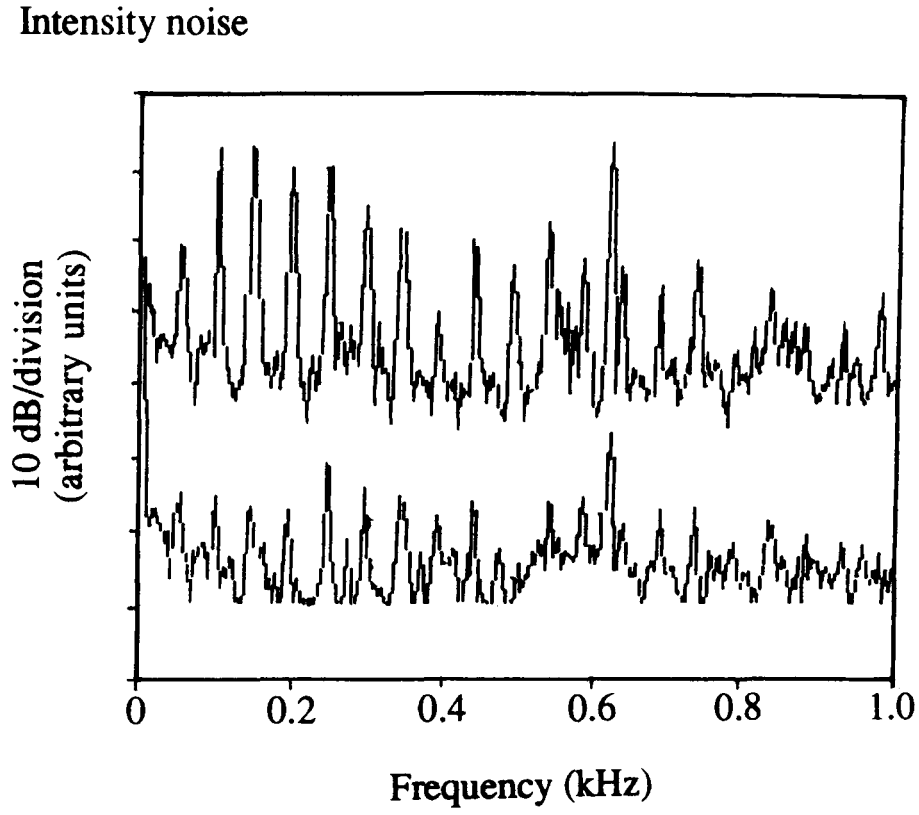


Figure 2.26: *Intensity spectra up to 1 kHz measured inside the intensity feedback servo showing the reduction of an applied peak at approximately 625 kHz by the loop gain of 38 dB, and the reduction of the background signals by approximately 30 dB.*

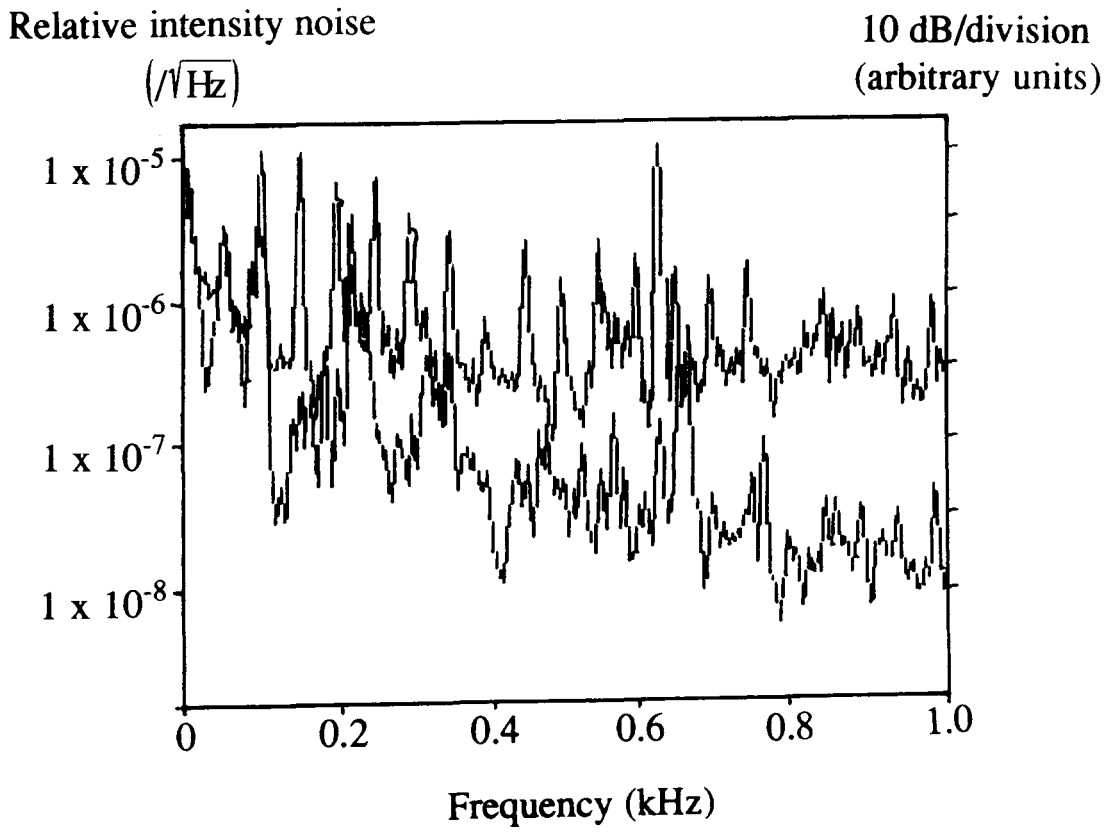


Figure 2.27: *Intensity spectra up to 1 kHz measured external to the intensity feedback servo loop showing the reduction of an applied peak at 625 Hz by the loop gain of 38 dB with the background intensity noise reduced by 25 dB.*

was purely due to intensity noise while the background noise spectrum was partly due to some other form of noise being detected as intensity noise.

### Effect of Laser Frequency Noise on Intensity Servo Performance

Any multiple reflections of the laser beam between optical components where the reflected beams interfere before detection at a photodiode could allow frequency noise of the laser to be converted into intensity noise. To determine whether this was the reason for the limited performance of the intensity feedback servo, a feedback system was constructed to reduce the frequency noise of the laser at low frequencies, and the effect of this feedback system on the performance of the intensity feedback system observed. A diagram of the frequency feedback servo is shown in figure 2.28.

The laser frequency was stabilised by using a a Fabry-Perot cavity of linewidth 15 MHz as a discriminator. The frequency of the laser was servo controlled to follow the resonant frequency of the cavity at low frequencies using an RF reflection locking technique [74]. This technique and experimental system is described briefly here and in more detail in chapter 3.

Light from the laser, after isolation using a Faraday effect device, passed through a half wave plate to rotate the polarisation to the correct direction for the electro-optic modulator which phase modulated the light at 10 MHz. A fraction of the light was used for the intensity feedback servo, another fraction of the light was used for the frequency stabilisation system and some light was also sent to a monitor photodiode.

The fraction of the light used for frequency stabilisation was modematched into the Fabry-Perot cavity using two lenses. The light was directed to the cavity via a polarising beamsplitter and quarter wave-plate. Light returning from the cavity was directed using the polarising beamsplitter and quarter wave-plate onto a photodiode and amplifier tuned to the RF modulation frequency. The signal from the photodiode was amplified, coherently demodulated at a mixer, filtered and sent to control a pzt transducer mounted directly onto the monolithic Nd:YAG crystal.

The servo filtering used a low pass filter with a corner at 0.18 MHz at the mixer output to remove any unwanted signals at 20 MHz. This signal was then amplified

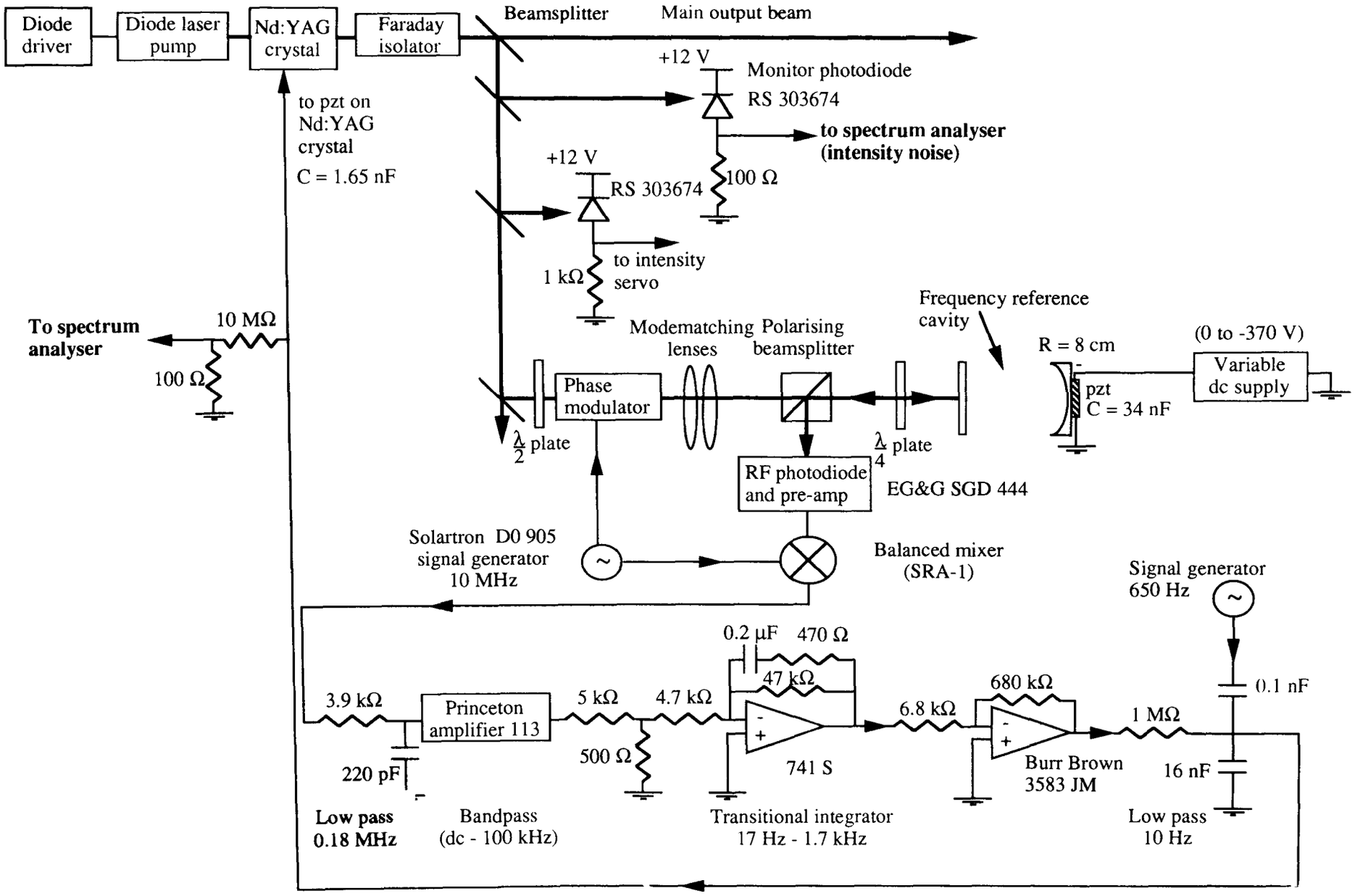


Figure 2.28: *Feedback system to reduce the frequency noise in a monolithic Nd:YAG ring laser.*

using a Princeton Model 113 amplifier (dc - 100 kHz) followed by a transitional integrator (17 Hz - 1.7kHz). The combination of the low pass filter formed by the 1 MΩ resistor and the 16 nF capacitance along with the 17 Hz corner allowed high servo gain at the low frequencies necessary to keep the servo locked, while the 1.7 kHz corner of the transitional integrator restored the slope of the transfer function to 6 dB per octave close to the unity gain point of the servo at $\simeq$ 10 kHz.

A voltage applied to the pzt resulted in strain being applied to the laser crystal causing a change in the lasing path in the cavity and thus a change in the resonant lasing frequency. The signal applied to the pzt with the servo system locked was a measure of the frequency noise of the laser within the bandwidth ( $\simeq$ 10 kHz) of the servo.

To measure the loop gain of the frequency servo a signal generator was used to apply a signal to the pzt at 650 Hz and a fraction of the feedback signal to the pzt displayed on a spectrum analyser with and without the servo system operating. The reduction of the size of the applied peak provided a measure of the servo loop gain. The signal at the monitor point of the frequency feedback system with and without the servo operating is shown in figure 2.29.

It can be seen from figure 2.29 that the applied peak in the frequency noise spectrum at 650 Hz was reduced by approximately 23 dB, suggesting that the frequency noise of the laser should also have been reduced by this amount.

The intensity noise spectrum of the laser with the intensity servo operating was then monitored with and without the frequency servo operating and is shown in figure 2.30. It can be seen from figure 2.30 that the operation of the frequency noise feedback system caused no significant improvement in the performance of the intensity noise feedback system, suggesting that the limited performance of the intensity servo was not a result of laser frequency noise at low frequencies being converted into intensity noise.

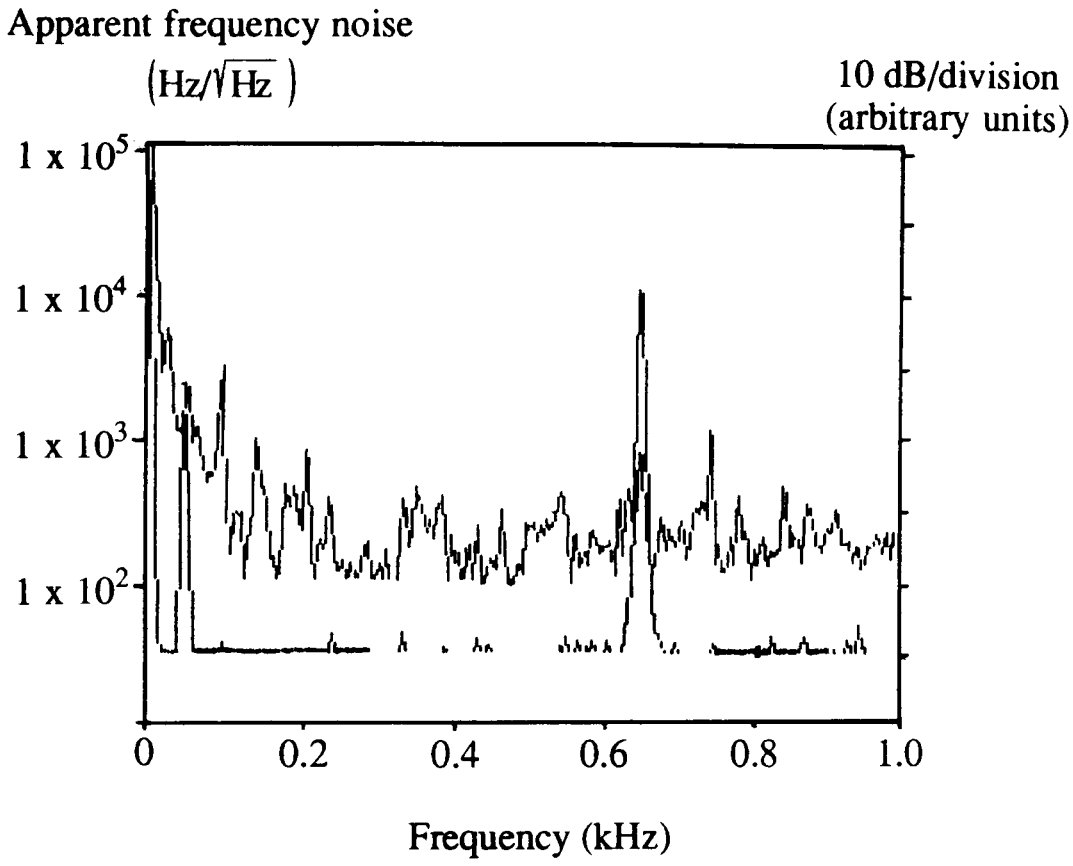


Figure 2.29: *Spectra showing the effect of a frequency stabilisation system on the frequency noise of a monolithic Nd:YAG ring laser. An applied peak in the frequency noise spectrum at ≃ 650 kHz is shown to be reduced by approximately 23 dB.*

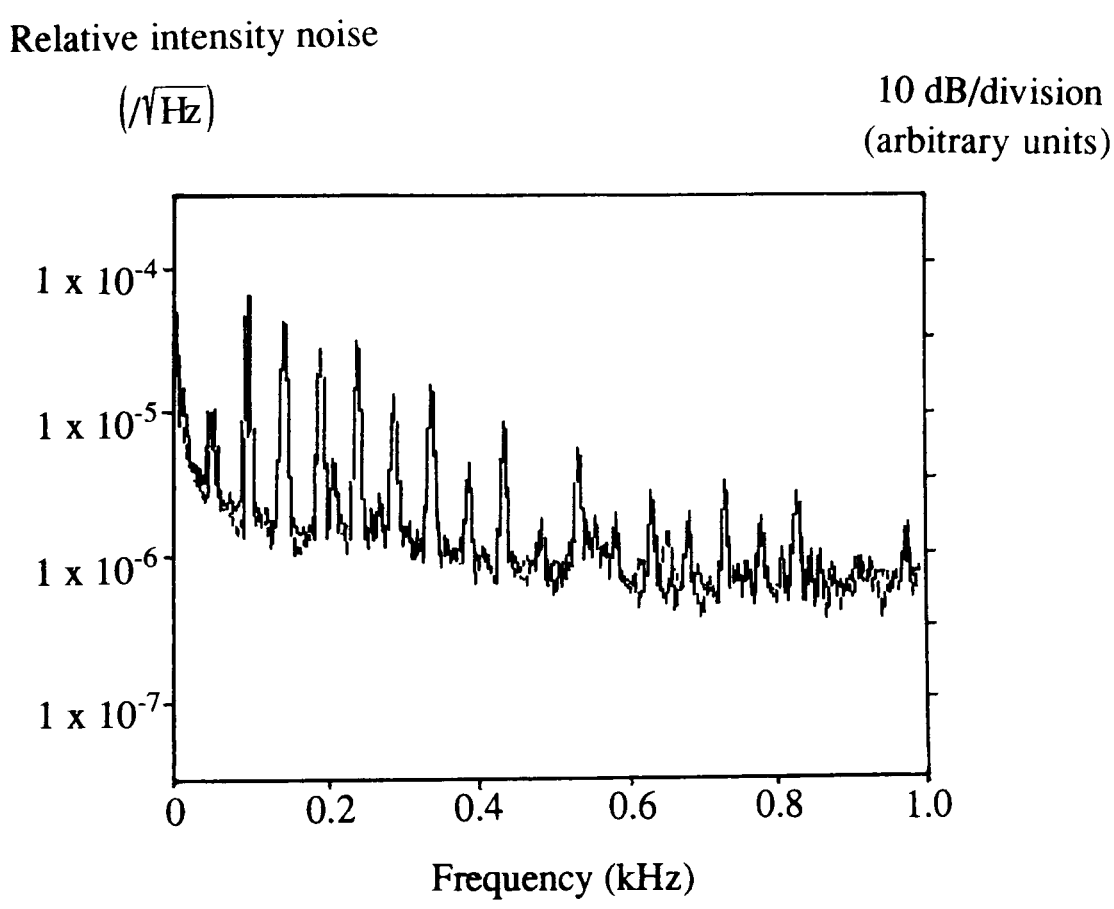


Figure 2.30: *Effect of frequency stabilisation system on performance of intensity noise feedback servo.*

### Effect of Laser Beam Geometry Fluctuations on Intensity Servo Performance

Further experiments were carried out mainly by A. M. Campbell and K. Skeldon in collaboration with myself to determine whether the performance of the intensity servo system was being limited as a result of the sensing of beam geometry fluctuations as apparent intensity noise. Positional fluctuations of a laser beam may be sensed as intensity noise at a photodiode due to the interference of scattered light with the main laser beam or as a result of variations in the response of a photodiode across its surface. Their investigations showed that when the laser light was passed through a piece of single mode optical fibre before a fraction of the laser light was split off to be used for the intensity noise feedback system, both an imposed peak in the intensity spectrum and the background intensity noise level monitored on an independent photodiode were reduced by the full available loop gain of the intensity servo system.

Passing the laser light through the piece of single mode fibre before splitting off a fraction of the light for use in the intensity servo would have reduced the level of laser beam geometry fluctuations present. This suggested that the performance of the servo system could thus have been limited by the conversion of laser beam geometry fluctuations into intensity noise at the servo photodiode.

Further, on removing the optical fibre and examining the mode structure of the laser using a scanning Fabry-Perot cavity it was noted that the laser output was alternating between several longitudinal and transverse modes. On examining the Faraday effect device at the laser output it was found that the isolation of the laser was not optimised and that a fraction of the laser output was returning to the laser after reflection from optical components in the beam path.

The conclusion was that the non-optimised laser isolation and subsequent multi-mode operation of the laser resulted in an increased level of laser beam geometry fluctuations, and hence the limited performance of the intensity servo. The laser isolation was improved so that the laser was operating in a single longitudinal, single spatial ($TEM_{00q}$) mode and the performance of the intensity servo was again observed operating with light split off from before and after a piece of single mode

optical fibre. The findings were that in each case, a peak imposed on the intensity spectrum of the laser was reduced by more than the background intensity noise level, but that in each case the servo performance was limited by shot noise and not by the action of beam geometry fluctuations.

It was desirable to demonstrate the operation of the stabilisation system without the added complexity of using an optical fibre and so the performance of the broadband intensity stabilisation system described in section 2.3.4 was obtained without passing the laser light through a fibre. The optical isolation was improved over that used in obtaining the results described in section 2.3.6. However it is interesting to note that the performance of the broadband servo was limited at a level approximately 5 dB above the expected performance and it seems that this was due to the laser isolation still being less than optimum.

### 2.3.7 Conclusions

The results of the experiments described in this chapter show that it is possible to construct a feedback system which simultaneously reduces the intensity noise of a miniature Nd:YAG ring laser at both the frequencies of interest for gravitational wave detection and at relaxation oscillation frequencies, to a level close to that necessary for proposed gravitational wave detectors.[1]

The stabilised relative intensity noise level of $4.6 \times 10^{-8}/\sqrt{Hz}$ at 500 Hz is very close to the final level required for the laser source for the GEO 600 interferometer of approximately $3 \times 10^{-8}/\sqrt{Hz}$, and is acceptable as the intensity of the laser light will undergo further amplification and stabilisation before injection into the interferometer [73]. The damped level of the intensity noise of $2.3 \times 10^{-6}/\sqrt{Hz}$ at the relaxation oscillation frequency is also considered to be sufficient for this laser to be used as a master laser source even if amplifiers or mixers with distortion levels of several percent were in use.

It is however also important that the frequency noise and beam geometry fluctuations of this type of laser are of a suitable level for it to be of use for large

[1] Broadband intensity stabilisation of a similar type of laser using a single feedback loop has independently been demonstrated by Harb et al [72]

gravitational wave interferometers. The results of investigations into these types of noise in a monolithic Nd:YAG ring laser are described in chapter 3.

# Chapter 3

# Investigations into the Frequency Noise of a Monolithic Nd:YAG Ring Laser

## 3.1 Introduction

As was discussed in chapter 2, it is important to have an accurate measure of the frequency noise of the light from a monolithic Nd:YAG ring laser both at the frequencies of interest for gravitational wave detection and at relaxation oscillation frequencies.

Recent measurements by Farinas et al [65] of the frequency noise of a 300 mW monolithic Nd:YAG ring laser at low frequencies give a level of approximately 30 $Hz/\sqrt{Hz}$ at 500 Hz. There is little information in the literature however about the expected level of frequency noise at relaxation oscillation frequencies; a single report by Kazovsky and Atlas [75] of a measurement for the 1320 nm transition in a diode-pumped Nd:YAG rod laser gives an upper limit to the frequency noise of approximately 200 $Hz/\sqrt{Hz}$ for a peak at the relaxation oscillation frequency. It is thus important to have a measure of the frequency noise at high frequencies for monolithic Nd:YAG ring lasers.

This chapter describes experiments to measure the levels of frequency noise at both low and relaxation oscillation frequencies for the monolithic Nd:YAG ring

laser described in chapter 2, and investigates the effect on the frequency noise of a stabilisation system to damp relaxation oscillations in the intensity of the laser. Also described are investigations of the noise performance at relaxation oscillation frequencies of a Lightwave Electronics 122 series monolithic Nd:YAG ring laser.

## 3.2 Frequency Noise at Low Frequencies

In chapter 2, a frequency stabilisation system was constructed to reduce the level of laser frequency fluctuations at low frequencies. This was achieved by locking the laser frequency to a Fabry-Perot cavity.

The frequency of the laser followed the resonant frequency of the cavity below the unity gain point of the locking servo which occurred at approximately 10 kHz, so that measurements of laser frequency noise below this point could be made by using the signal at the feedback point to the pzt. A calibration of the pzt response then allowed the measured voltage signal to be converted to a frequency signal.

Figure 2.29 shows the feedback signal up to 1 kHz measured at the feedback point. It should be noted that any mechanical vibrations of the cavity due to seismic or acoustic noise would result in changes in the feedback signal which were indistinguishable from laser frequency fluctuations. The measured levels of noise thus represent an upper limit to the frequency noise of the laser. From figure 2.29, an upper limit of the laser frequency fluctuations at 500 Hz was approximately $200Hz/\sqrt{Hz}$.

## 3.3 Frequency Noise at Relaxation Oscillation Frequencies

To measure the frequency noise at the relaxation oscillation frequency of the monolithic Nd:YAG laser a Fabry-Perot cavity of linewidth 15 MHz was used as a discriminator. In this case the cavity was servo controlled to the frequency of the laser for frequencies below approximately 1 kHz using an RF reflection locking technique and the error point of the system used to allow measurement of the laser frequency

noise at frequencies around that of the relaxation oscillation.

### 3.3.1 Principles of RF Reflection Locking

A brief description of the principles of the RF reflection locking technique is outlined here [74] [52].

Light from a laser of angular frequency $\omega$ is phase modulated at an angular frequency $\omega_m$, which has the effect of introducing sidebands onto the laser light at angular frequencies $\omega \pm \omega_m$. When the laser light is directed onto the reference cavity, most of the light is reflected directly from the input mirror of the laser cavity. The modulation frequency is chosen to be outside the angular frequency linewidth $\Delta\omega_L$ of the reference cavity; thus all the light at the frequency of the modulation sidebands is reflected but a small fraction of the laser light at the carrier frequency enters the cavity. The light entering the cavity resonates and the intensity of light inside the cavity builds up. Some of the light resonant inside the cavity then leaks back out of the input mirror to subtract from the beam directly reflected from the input mirror of the cavity. The combination of the beam reflected from the input mirror with its 10 MHz phase modulation, and the light leaking back out of the cavity on resonance results in a beam amplitude modulated at 10 MHz. The level of the 10 MHz amplitude modulation is a measure of the phase difference between the two beams and is thus a measure of the frequency noise of the laser.

When the resultant beam is detected and the signal demodulated using a fraction of the 10 MHz signal driving the electro-optic modulator, the effect of demodulation is to select only terms in the detected signal which are in phase with the driving signal. It can be shown [76] that this demodulated signal changes sign as the cavity resonant frequency is scanned through the frequency of the laser. This signal thus produces a suitable bipolar error signal to allow the resonant frequency of the cavity to be locked to the frequency of the laser light.

For the measurements of frequency noise at relaxation oscillation frequencies of several hundred kHz, the servo system chosen had a unity gain frequency of approximately 1 kHz. For frequency fluctuations occurring at several hundred kHz, well above the unity gain point of the servo system, the detected signal measured imme-

diately after demodulation, was directly proportional to the frequency fluctuations of the laser light.

### 3.3.2 Experimental Arrangement

The experimental arrangment for this measurement is shown in figure 3.1. Light from the laser first passed through a Faraday effect device to prevent any beams reflected back from the cavity entering the laser. The light then passed through a half wave plate to rotate the polarisation of the light to the correct polarisation (horizontal) for the electro-optic phase modulator (Gsanger PM-25 IR). The 10 MHz voltage drive for this modulator was produced using a tuned circuit driven by a signal generator. The laser light was thus phase modulated at 10 MHz. A fraction of the light was then split off for use in the servo to damp relaxation oscillations described in chapter 2, section 2.2.5, and some light was also split off to be sensed by an independent photodiode.

The fraction of the laser light used for frequency noise measurements was then modematched into the Fabry-Perot cavity using two lenses. The light entered the cavity via a polarising beamsplitter and quarter wave plate, this combination allowing separation of the beams incident on and reflected from the cavity. For these measurements the visibility was approximately 0.8, where visibility, V, is defined here as

$$V = \frac{I_{max} - I_{min}}{I_{max}} \tag{3.1}$$

where $I_{max}$ is the maximum intensity of light reflected from the cavity (occurring when the cavity is not on resonance), and $I_{min}$ is the intensity of light apparently reflected from the cavity when the cavity is on resonance.

The beamsplitter and quarter wave plate allowed the light reflected from the cavity to be directed onto a photodiode and amplifier tuned to the RF modulation frequency. The signal from the RF photodiode and amplifier was then coherently demodulated at the mixer, filtered and fed back to a pzt transducer on which one of the cavity mirrors was mounted. The feedback servo contained a parallel path to boost the dc and low frequency gain of the servo, and a facility for adding a small dc offset to the system to adjust for any offset of the locking point caused by

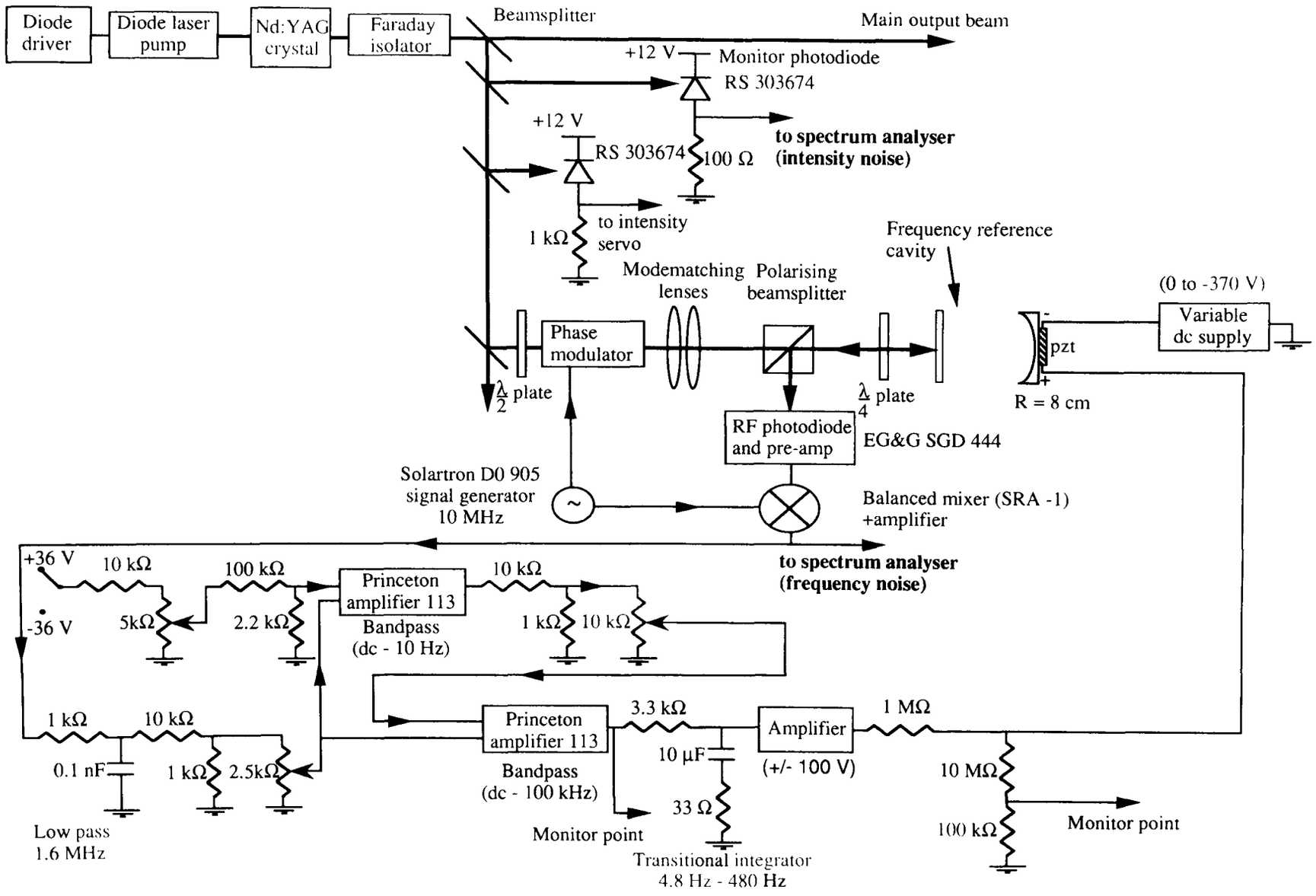


Figure 3.1: *Schematic diagram of the optical and electronic arrangement for the RF locking system used to measure frequency noise at relaxation oscillation frequencies.*

the demodulation of RF pickup or of spurious amplitude modulation of the light at 10 MHz by the electro-optic modulator. The other side of the pzt was connected to a battery driven variable dc supply to allow coarse steering of the cavity resonant frequency onto that of the laser.

With the system locked, the error point signals, i.e. the signals immediately after demodulation, were displayed, after amplification, on an RF spectrum analyser (Hewlett Packard 8590A). The frequency noise signals measured at the mixer output were calibrated in units of V/$\sqrt{\text{Hz}}$. It can be shown that the gradient of the RF fringes in V/Hz is given by

$$\text{Gradient} = \frac{2 \times \text{peak to peak height of RF fringes}}{\text{linewidth of cavity}} \tag{3.2}$$

The cavity was scanned through the laser resonant frequency and the peak to peak height of the RF fringes measured. This then allowed the frequency noise signals to be calibrated in units of Hz/$\sqrt{\text{Hz}}$.

### 3.3.3 Results and Discussion

The results of two sets of measurements of frequency noise of different sensitivity are discussed.

#### First measurement

The first measurement of the frequency noise is shown in figure 3.2. The peak in the centre of the screen is the zero Hz peak of the spectrum analyser and the left hand half of the screen is essentially a mirror image of the right half. The range of interest is from 0 Hz to 375 kHz. The peak in the spectrum at approximately 250 kHz is at the frequency of the relaxation oscillation peak in the intensity of the laser. This gives an upper limit on the apparent frequency noise due to relaxation oscillations of approximately 7 $Hz/\sqrt{Hz}$. However intensity noise in the laser may couple in to frequency noise measurements due to deviations of the servo from the correct locking point caused for example by the demodulation of RF pickup and so this apparent frequency noise could be due to intensity noise. Thus an intensity modulation signal was applied at 120 kHz by modulating the pump diode laser current at the diode

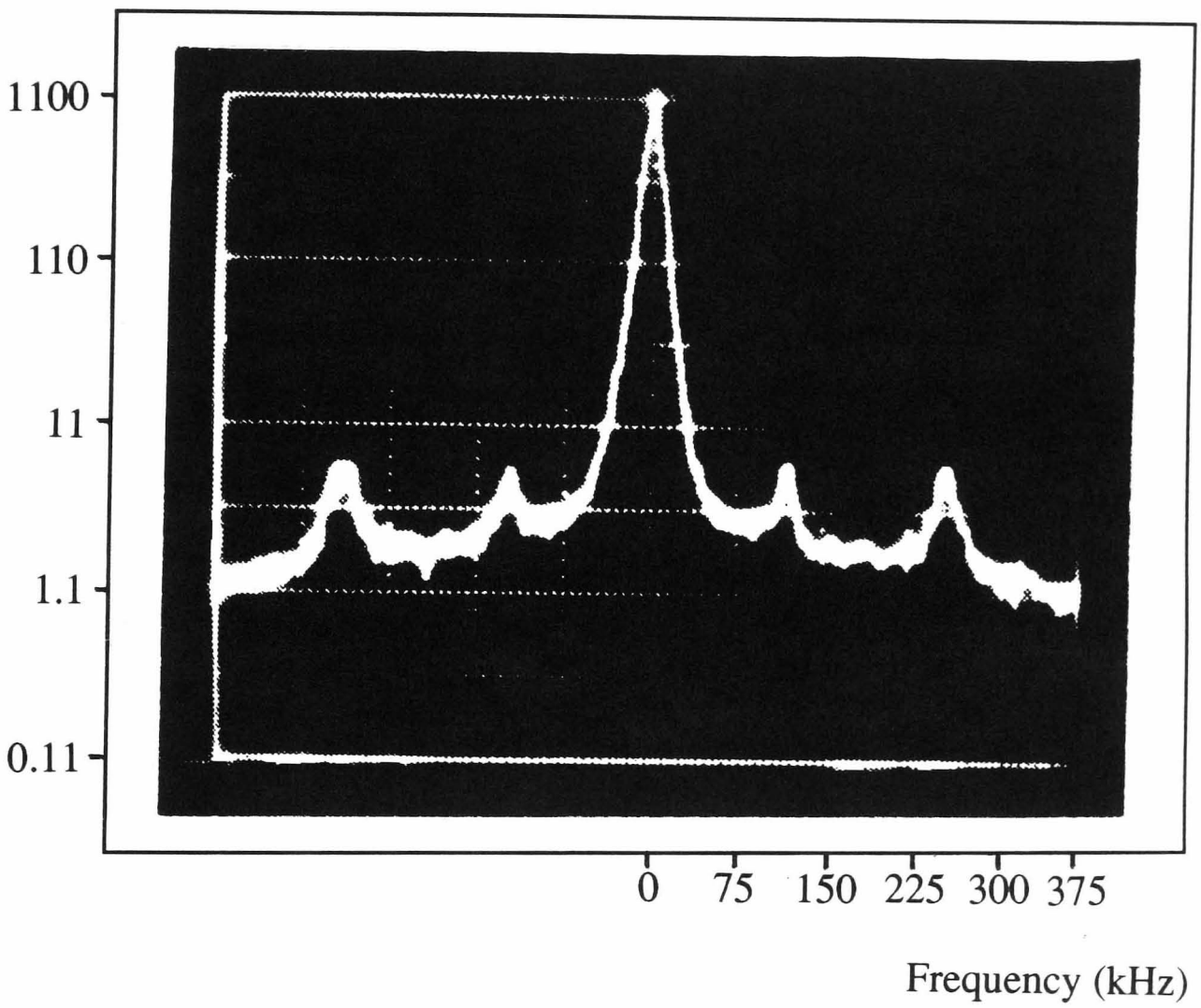


Figure 3.2: *First measurement of frequency noise spectrum showing a peak at the relaxation oscillation frequency of 250 kHz and at the frequency of an applied intensity peak of 120 kHz. The peak at the relaxation oscillation frequency corresponds to a frequency noise level of* $7Hz/\sqrt{Hz}$.

driver input, and the sensitivity of the system to intensity noise was minimised by adjusting the locking point of the servo using the variable dc offset in the servo loop.

An interesting effect was observed when the dc offset in the servo loop was altered to offset the locking point on either side of the position which minimised the applied 120 kHz intensity peak. Figures 3.3 and 3.4 show the relative size of the intensity modulation peak and the relaxation oscillation peak when the dc offset (and thus locking point) was set to be either side of the position which minimised the applied intensity peak. Here the relaxation oscillation peak occurs at 350 kHz as a higher diode pump current was used. The offset was set to increase the applied intensity peak by approximately 10 dB on either side of its minimum value. It can be seen that the peak associated with the relaxation oscillations did *not* increase by the same amount in the two cases. The difference in height of the relaxation peak and the applied peak being about 7 dB on one side and about 3 dB on the other side. This suggested that there was a difference in the type of noise associated with the applied intensity peak and with the relaxation oscillation peak. Consistent with this finding is the fact that different values of dc offset were required to minimise the relaxation oscillation peak and the applied intensity peak.

These results suggested that either the applied intensity peak or the peak at the relaxation oscillation frequency was at least partly due to frequency noise or to beam geometry fluctuations coupling into the observed frequency noise spectrum.

### Effect of the Intensity Noise Servo on Frequency Noise

An investigation was made into the effect on the apparent frequency noise of damping the relaxation oscillations in intensity. The intensity noise servo system used to damp the relaxation oscillations was the system described in chapter 2, section 2.2.4, with the feedback point being the input to the diode current driver. With the servo locking point offset to either side of the position minimising the applied peak the intensity and frequency noise spectra were observed simultaneously as the intensity noise servo was turned on. When the gain of the intensity servo was such that the relaxation oscillations observed in the intensity spectrum was reduced by 10 dB, the same magnitude of reduction of the peak at relaxation oscillation frequencies in

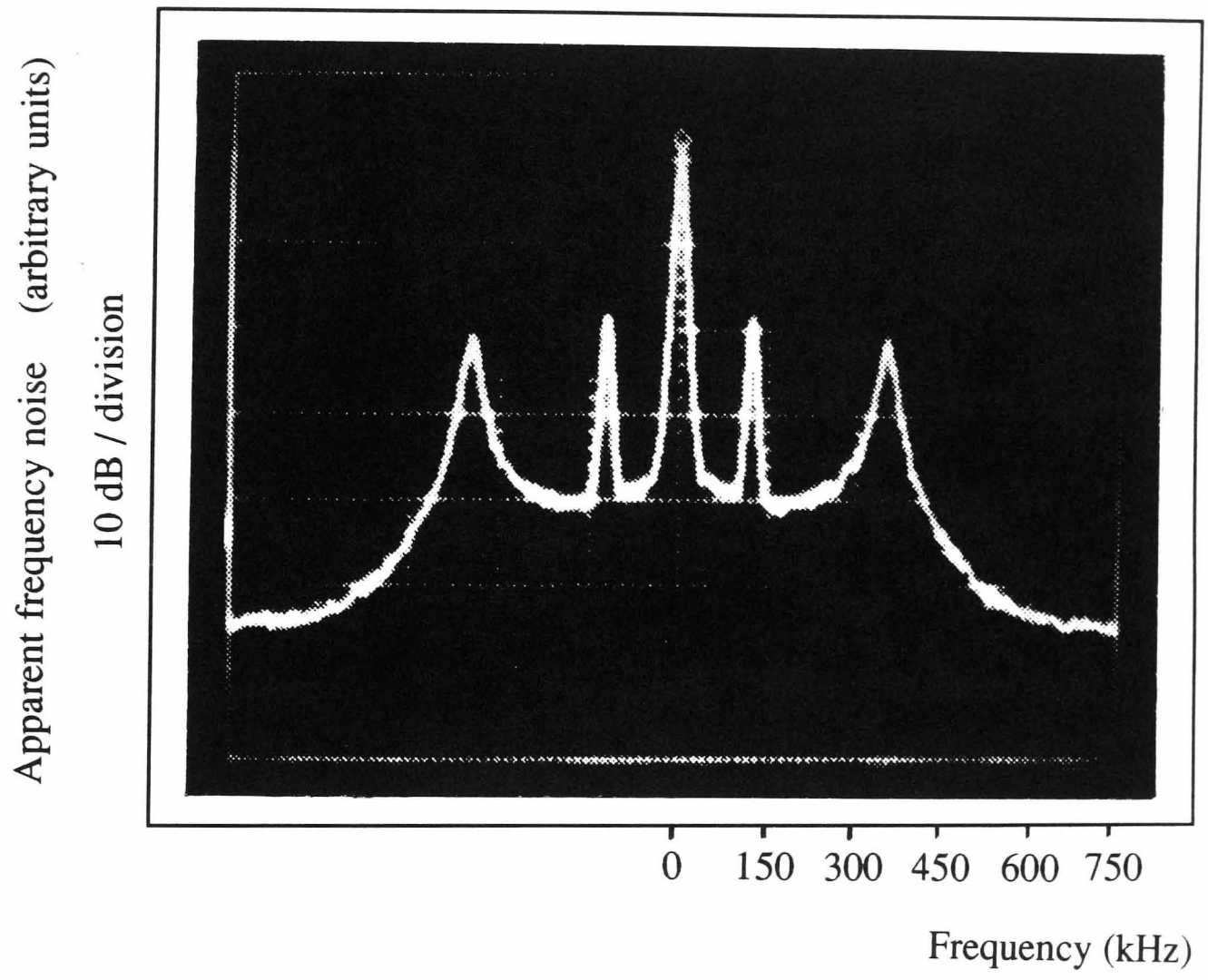


Figure 3.3: *Noise spectrum at the mixer output showing the difference in height of an applied intensity peak and the relaxation oscillation peak with the locking point offset to one side of the position which minimises the applied peak.*

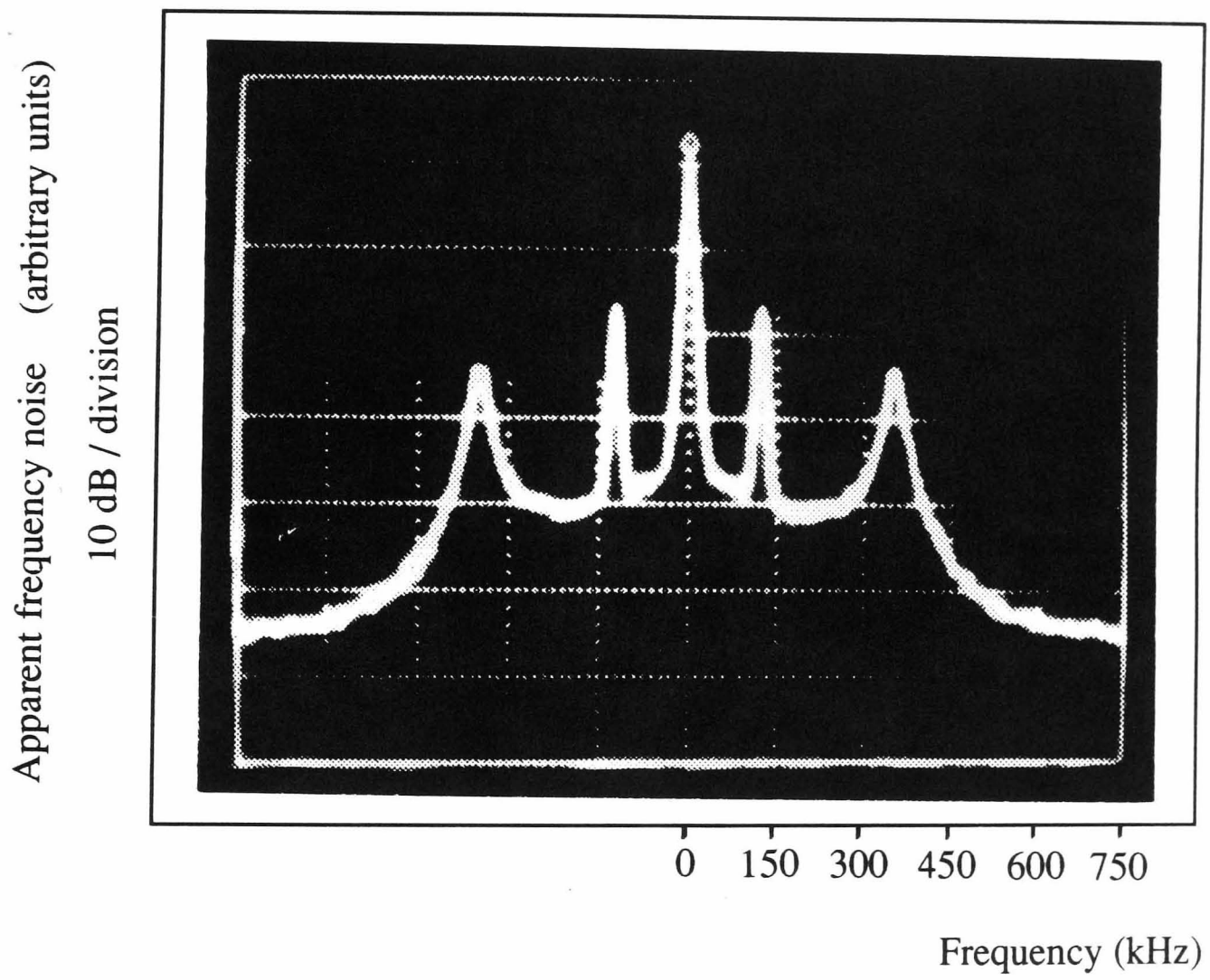


Figure 3.4: *Noise spectrum at the mixer output showing the difference in height of an applied intensity peak and the relaxation oscillation peak with the locking point offset to opposite side of the position which minimises the applied peak.*

the frequency noise spectrum was observed. If a signal input to the diode current driver could cause any change in the laser light (which was sensed) other than an intensity fluctuation (for example a frequency or beam geometry fluctuation) such a simple relation between the reduction in apparent frequency and intensity noise would not be expected. When the sensitivity of the system to intensity noise was minimised and the intensity noise servo was turned on, the peak in the frequency noise at the relaxation oscillation frequency shown in figure 3.2 was reduced into the background noise. The frequency noise spectrum with the intensity noise servo operating is shown in figure 3.5

The three following conclusions were thus drawn as the most likely explanation of these results:

1. A signal applied to the diode current driver produced *intensity* modulation with no evidence of any other form of noise being produced. The peak at 120 kHz produced by applying a signal at this point, as observed in the frequency noise spectrum, is thus caused by intensity noise in the laser.

2. The peak in the frequency noise spectrum at the relaxation oscillation frequency is partly due to frequency noise or beam geometry fluctuations in addition to some intensity noise.

3. Any fluctuations in frequency or beam geometry associated with the relaxation oscillations are reduced by the feedback sytem used to damp the relaxation oscillations in intensity.

### Second measurement

To further investigate these results the measurements were repeated. In an attempt to improve the sensitivity of the measurements the optics in the system were cleaned and the system realigned. For these measurements the visibility was 0.8 and the modulation index was approximately 0.24, with the modulation index defined here as the amplitude of the phase modulation of the light. The resulting frequency noise measurement is shown in figure 3.6. The level of apparent frequency noise at the relaxation oscillation frequency of 250 kHz was found here to be approximately

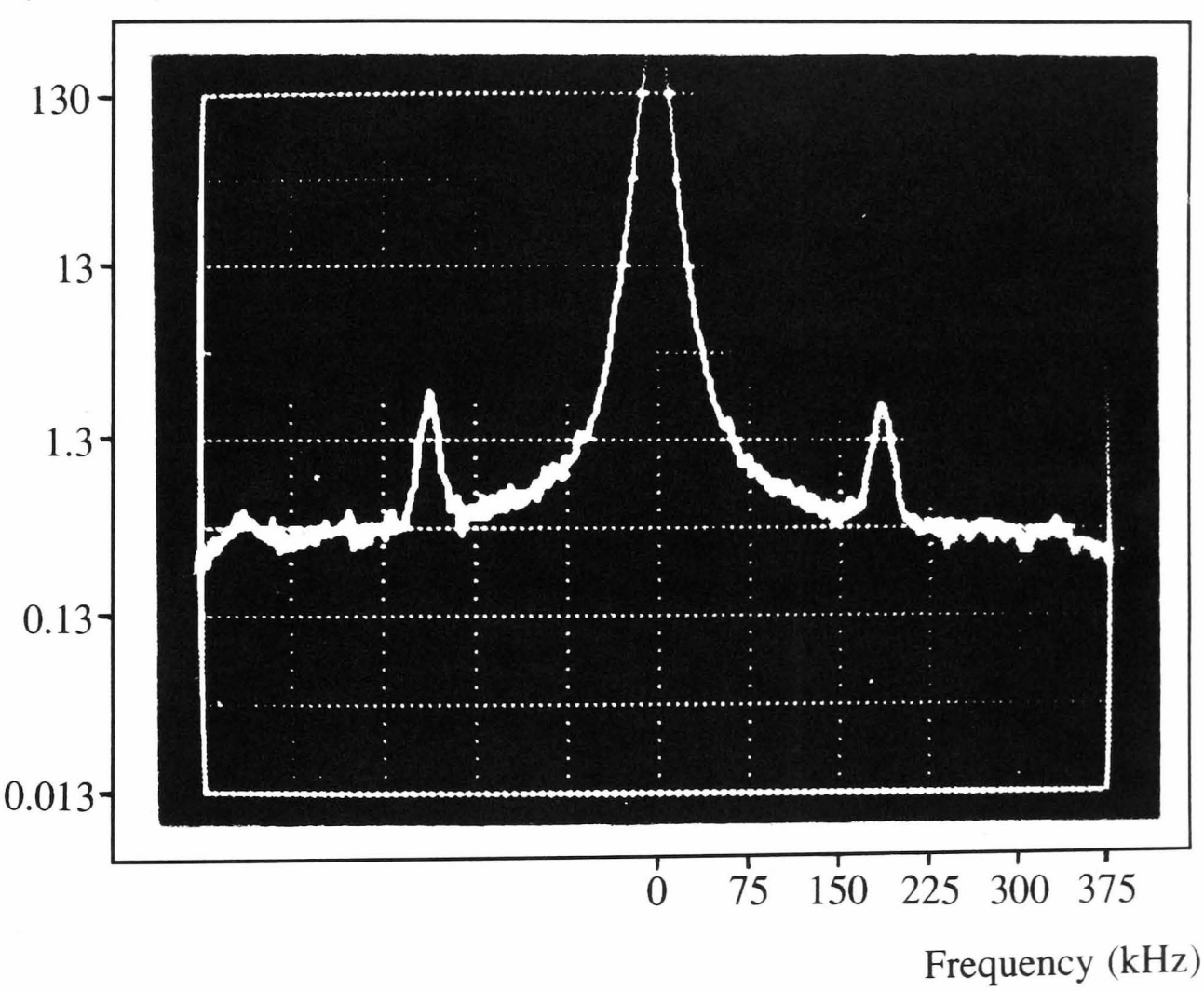


Figure 3.5: *Frequency noise spectrum with a servo to damp relaxation oscillations in intensity operating. A peak at the relaxation oscillation frequency in the frequency noise spectrum has been reduced into the background measurement noise.*

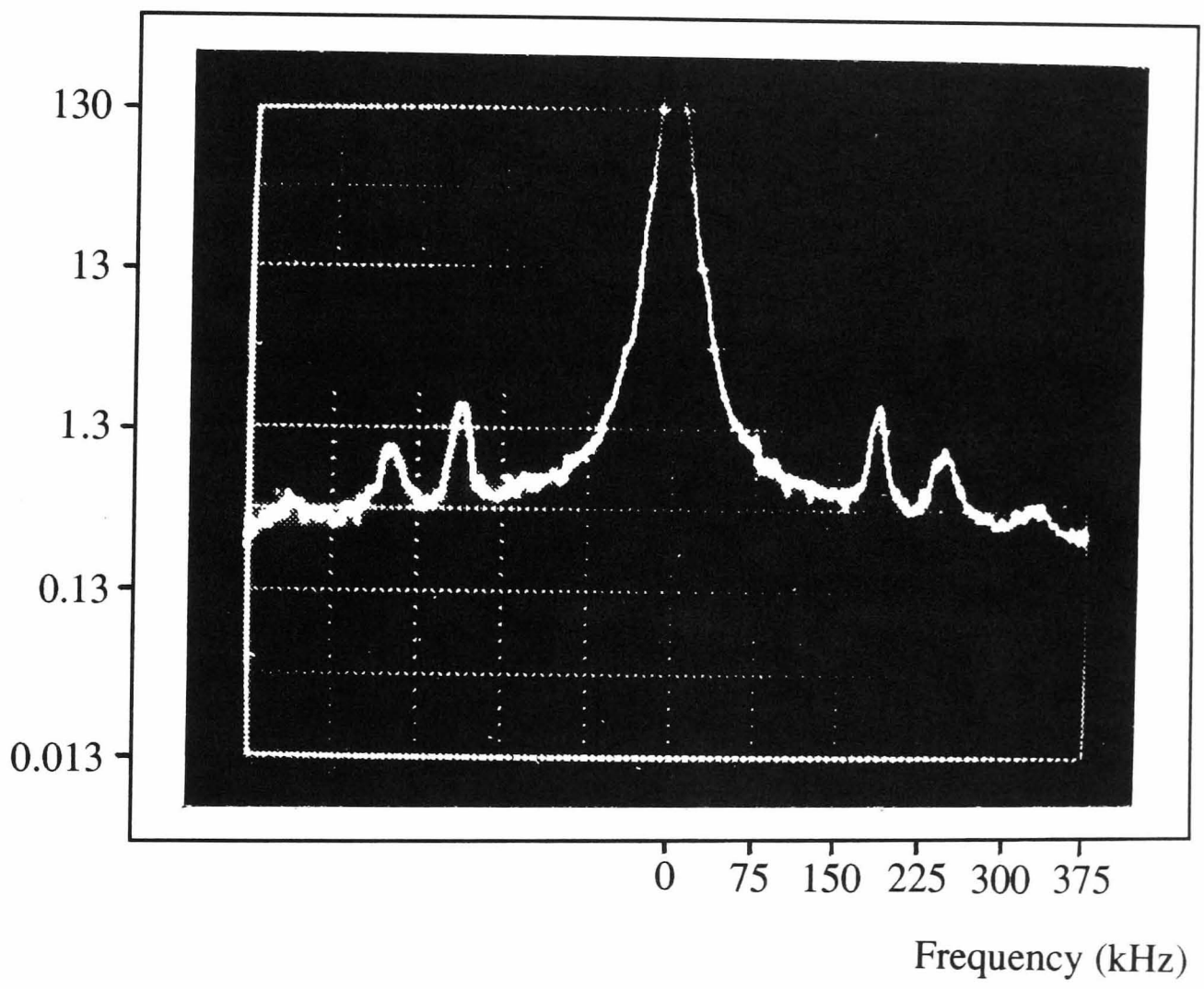


Figure 3.6: *Frequency noise spectrum showing a peak at the relaxation oscillation frequency of 250 kHz and at the frequency of an applied intensity peak of 180 kHz.*

1 $Hz/\sqrt{Hz}$. The measurement floor was approximately 0.4 $Hz/\sqrt{Hz}$ of which approximately 0.2 $Hz/\sqrt{Hz}$ was photon shot noise.

In this case it was noted that both the applied intensity peak and the peak due to relaxation oscillations were minimised at the same value of dc offset in the cavity servo loop, and when the dc offset was adjusted to be either side of the value which minimised the peaks there was no detectable difference in the relative size of the applied peak and the relaxation peak.

The above results suggest that

1. in the first measurement, the peak in the frequency noise spectrum at the relaxation oscillation frequency was mainly a result of the coupling of intensity noise into the measurement but there was some other noise present in addition. The noise could have been frequency noise or laser beam geometry fluctuations associated with the relaxation oscillation, perhaps resulting from imperfect isolation of the laser as was suggested by the experiments described in chapter 2, section 2.3.6.

2. the realigning of the optics reduced the level of laser beam geometry fluctuations and frequency noise present and/or the sensitivity of the system to beam geometry fluctuations with the residual peak in the frequency noise spectrum probably being caused by intensity noise.

High frequency intensity noise coupled into the measured frequency noise as a result of small deviations of the servo locking point from the centre of the cavity resonance. These deviations occurred at a frequencies of a few kHz, outside the bandwidth of the frequency locking servo.

A possible model for the way in which beam geometry fluctations - in particular beam positional fluctuations - may have coupled into the frequency noise measurement is considered below.

### A method for the Coupling of Beam Position Fluctuations into Frequency Noise Measurements

As was discussed above, a measurement of the frequency noise of the laser is obtained by demodulating the signal produced by the detected light from the Fabry-Perot cav-

ity in reflection, as this light contains a component at 10 MHz which is amplitude modulated by the frequency noise spectrum of the laser. If beam geometry fluctuations of the laser in any way result in the detected light being amplitude modulated at 10 MHz then on demodulation a signal will be produced which appears to be part of the frequency noise spectrum.

In section 3.3.3 it was concluded that the second frequency noise measurement, giving a noise level of 1 $Hz/\sqrt{Hz}$ at the relaxation oscillation frequency, was most likely to be purely a result of intensity noise coupling to the frequency noise measurement. In the first measurement it was concluded that the noise level of 7 $Hz/\sqrt{Hz}$ was due to a mixture of intensity noise coupling to the frequency noise measurement in addition to some frequency noise or beam position fluctuations. If it is assumed that the difference in these measurements of $\simeq 7\ Hz/\sqrt{Hz}$ was caused by the coupling of, for example, positional laser beam geometry fluctuations, it is possible to obtain an estimate of the magnitude of beam position fluctuations present at the relaxation oscillation frequency.

### Coupling due to a Misalignment of Cavity Mirrors

If one (or both) of the Fabry-Perot mirrors are misaligned by some angle $\alpha$ with respect to the input laser beam, then beam position fluctuations, $\delta x$, at the cavity input can result in phase fluctuations, $\delta\phi$, of the light at the input to the cavity. The magnitude of these fluctuations is given by

$$\delta\phi = \frac{2\pi}{\lambda}\alpha\delta x \tag{3.3}$$

Phase fluctuations of the input light occurring as a result of beam position fluctuations are indistinguishable from genuine phase fluctuations of the laser light and thus result in a signal in the measured frequency noise spectrum.

The measured figure of $\simeq 7\ Hz/\sqrt{Hz}$ gives the level of apparent frequency fluctuations, $|\delta f|$, at the input to the Fabry-Perot cavity. This can be converted into the corresponding level of phase fluctuations by noting that

$$|\delta f| = f_n|\delta\phi| \tag{3.4}$$

where $f_n$ is the noise frequency (250 kHz). The corresponding level of phase fluctuations at the cavity input is thus $2.8 \times 10^{-5}$ radians $/\sqrt{Hz}$.

Assuming a misalignment of the mirror of $\alpha \simeq 2 \times 10^{-4}$ radians means that beam geometry fluctuations at the cavity input (at $\simeq 2\ m$ from the laser), of the order of approximately $2.3 \times 10^{-8} m/\sqrt{Hz}$ would have been required to produce the measured frequency noise signal of $\simeq 7\ Hz/\sqrt{Hz}$.

Subsequent measurements of the positional laser beam geometry fluctuations at the relaxation oscillation frequency by K. Skeldon and Dr. A. Campbell set an upper limit for the fluctuations of approximately $1 \times 10^{-10} m/\sqrt{Hz}$ at $\simeq 1$ m from the laser. This is significantly lower than the figure of $1 \times 10^{-8} m/\sqrt{Hz}$ at 1 m calculated to be required for beam position fluctuations to couple into the measurement of laser frequency noise by the method described above. However it is likely that at the time the first measurement of apparent frequency noise was made, the isolation of the laser from light feeding back was inadequate and this effect could have increased the level of beam geometry fluctuations condiderably so that they were well above the levels of positional fluctuations subsequently measured.

Positional fluctuations are just one type of beam geometry fluctuation. However it is expected that the coupling other types of fluctuation would be very similar and similar results would be found.

## 3.4 Noise Performance of a Lightwave Electronics Non-planar Ring Laser

All the previous measurements were made on a monolithic Nd:YAG ring laser constructed at the Laser Zëntrum, Hannover. Some investigatons were also made into the noise properties of a commercial laser of a similar type, a Lightwave Electronics series 122 diode pumped monolithic Nd:YAG ring laser. The Lightwave laser had a maximum output power of 500 mW and could be operated with or without the operation of a built in intensity noise reduction system.

### Intensity Noise

The intensity noise of the laser was measured and the relaxation oscillation peak in the intensity noise spectrum found to be at approximately 700 kHz. A typical intensity spectrum in shown in figure 3.7. The level of intensity noise at the relaxation oscillation peak is approximately $2.3 \times 10^{-5}/\sqrt{Hz}$. With the intensity noise reduction system operating the intensity noise at the relaxation oscillation frequency was reduced by approximately 40 dB to a level of approximately $2.3 \times 10^{-7}/\sqrt{Hz}$.

It can be seen that the intensity noise of the laser is reduced from dc to frequencies over 1 MHz with no region in which the intensity noise of the laser is increased.

### Frequency noise

The frequency noise of the Lightwave laser was measured using the RF locking system described in section 3.3. Figures 3.8 and 3.9 show frequency noise spectra measured without and with the intensity noise reduction servo for the laser operating.

It can be seen that the frequency noise of the laser in both cases contains considerable structure. It is clear that the operation of the intensity noise reduction system affected the frequency noise of the laser. In particular comparing figures 3.9 and 3.8 shows that the peak in frequency noise at approximately 265 kHz is increased by 10 dB from 1.8 $Hz/\sqrt{Hz}$ to 5.6 $Hz/\sqrt{Hz}$.

The laser included an input to allow frequency tuning of the light; this was achieved by the use of a pzt element and associated circuitry within the laser. It was thought that the peaks in the frequency noise spectrum might be due to pzt resonances and that the increase of the peak at 265 kHz could be caused by some pickup of signals from the intensity noise reduction system further exciting a pzt resonance at this frequency.[1]

The effect of the intensity system on the frequency noise was examined in more detail close to the relaxation oscillation frequency, with the results shown in figures 3.10 and 3.11.

In figure 3.10, the top trace is an intensity spectrum showing the relaxation

[1]Modifications by Lightwave have been made to ensure this effect is no longer present.

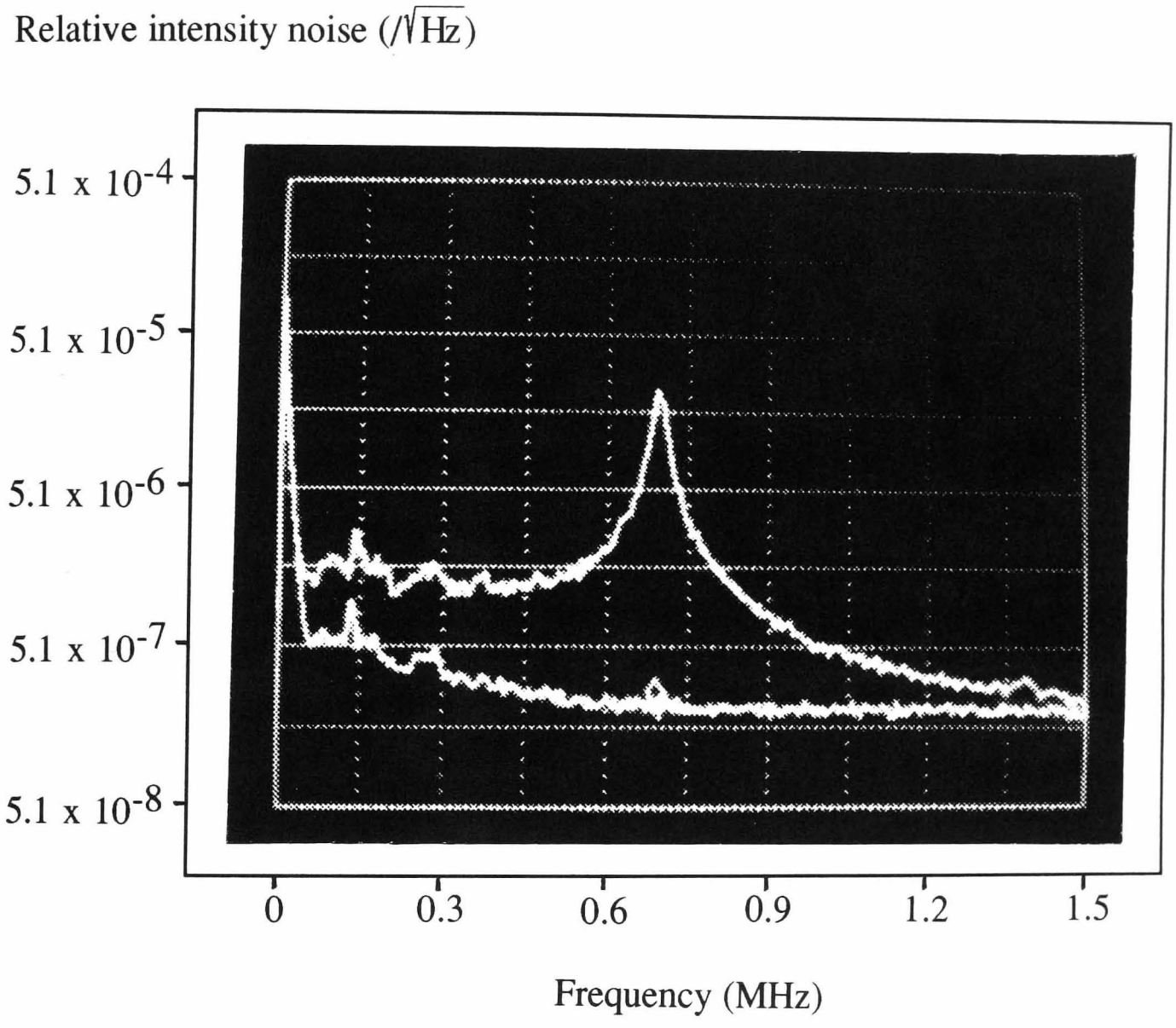


Figure 3.7: *Typical intensity noise spectrum for Lightwave Nd:YAG ring laser.*

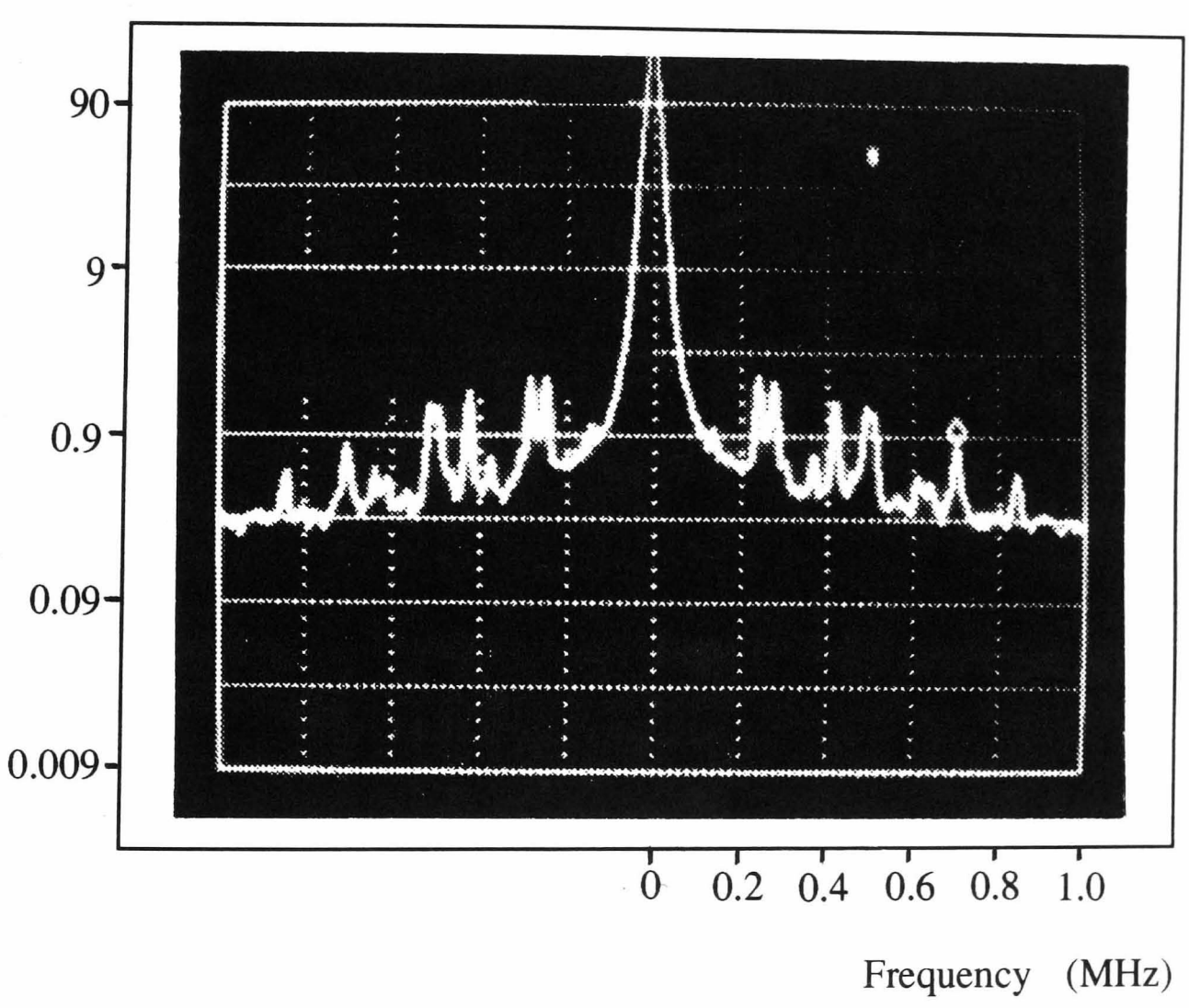


Figure 3.8: *Frequency noise spectrum for Lightwave Nd:YAG ring laser measured without intensity noise reduction system operating.*

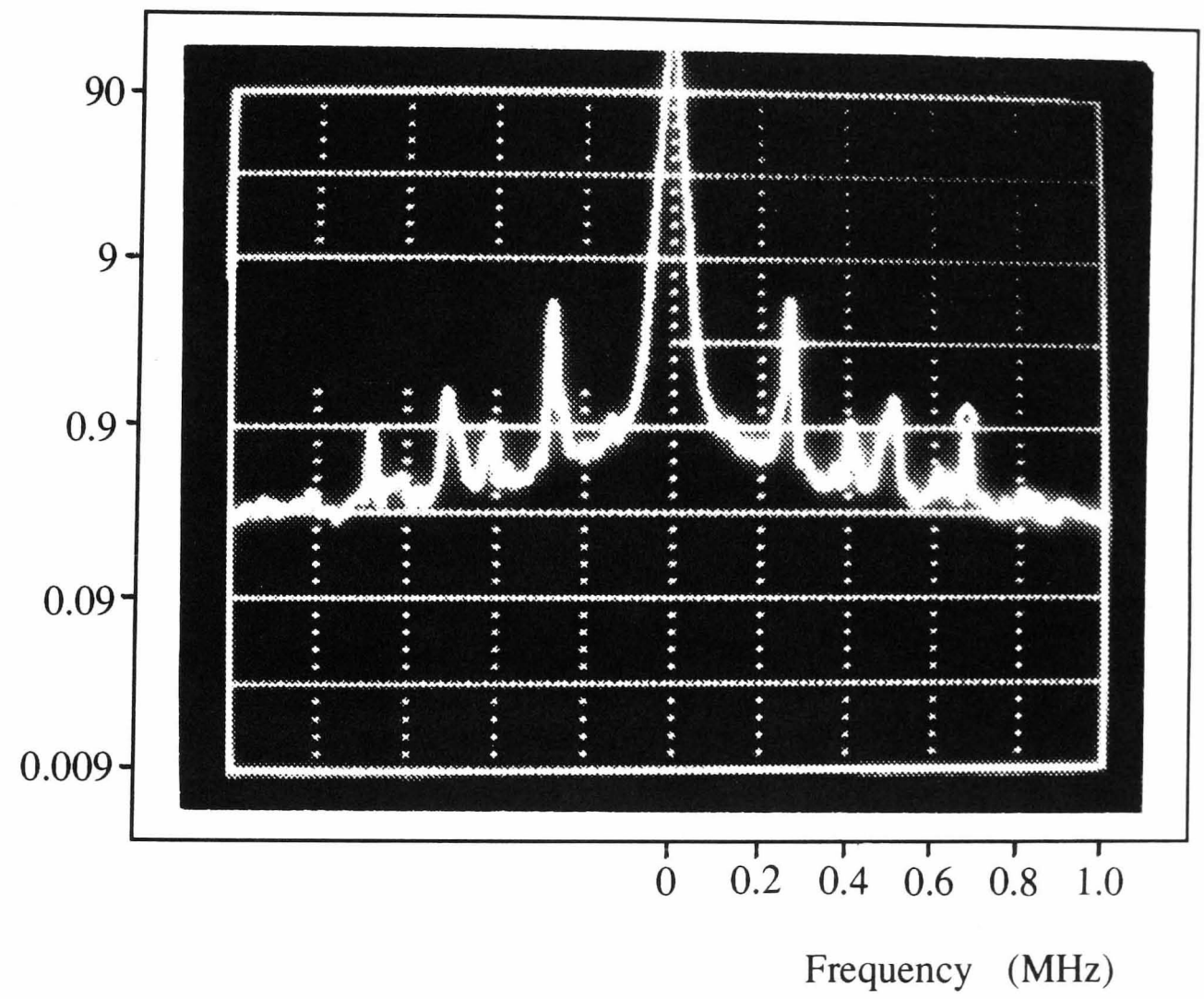


Figure 3.9: *Frequency noise spectrum for Lightwave Nd:YAG ring laser measured with intensity noise reduction system operating.*

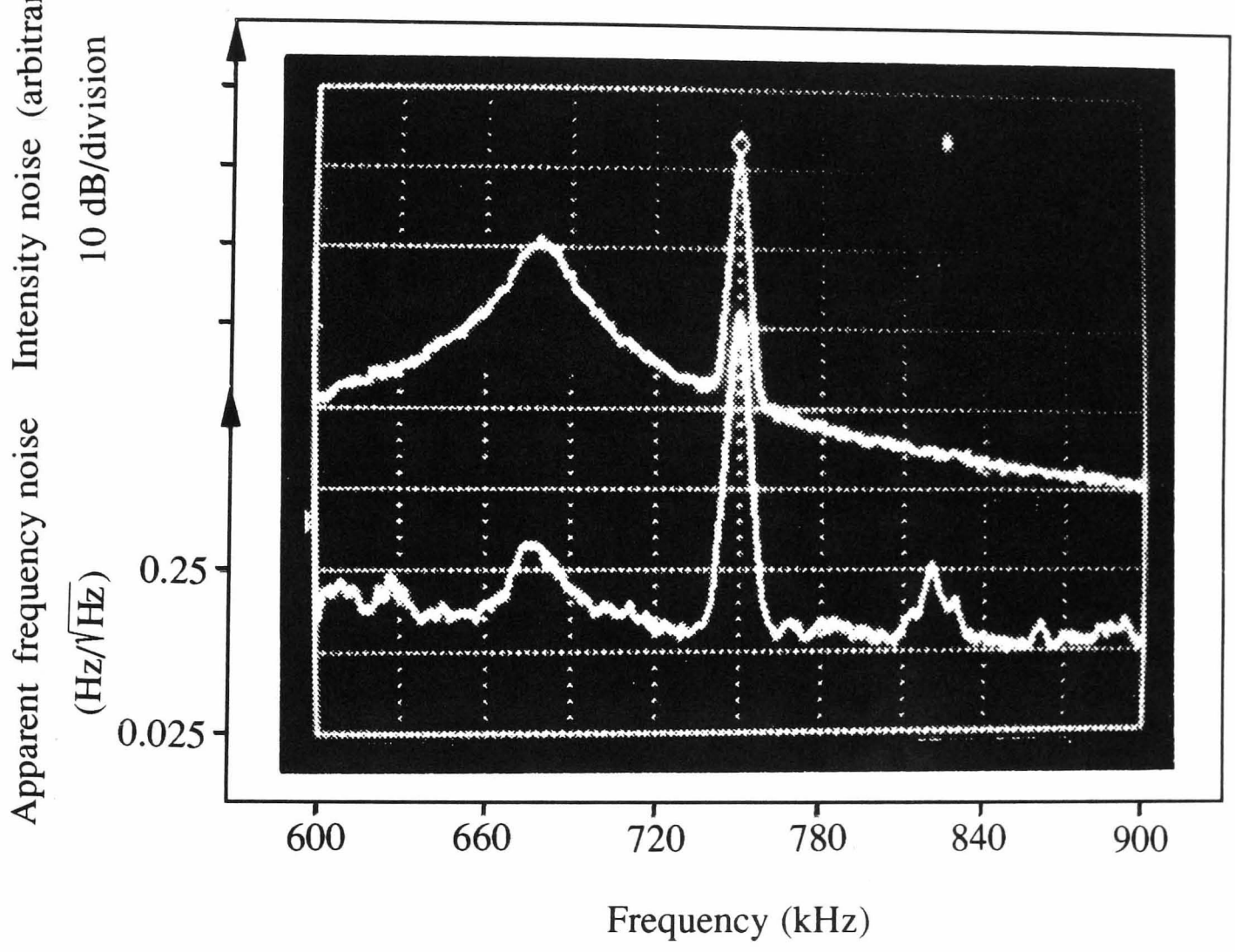


Figure 3.10: *The upper trace shows the intensity noise of the Lightwave laser close to the relaxation oscillation frequency. The lower trace shows the corresponding frequency noise at these frequencies without the intensity servo operating.*

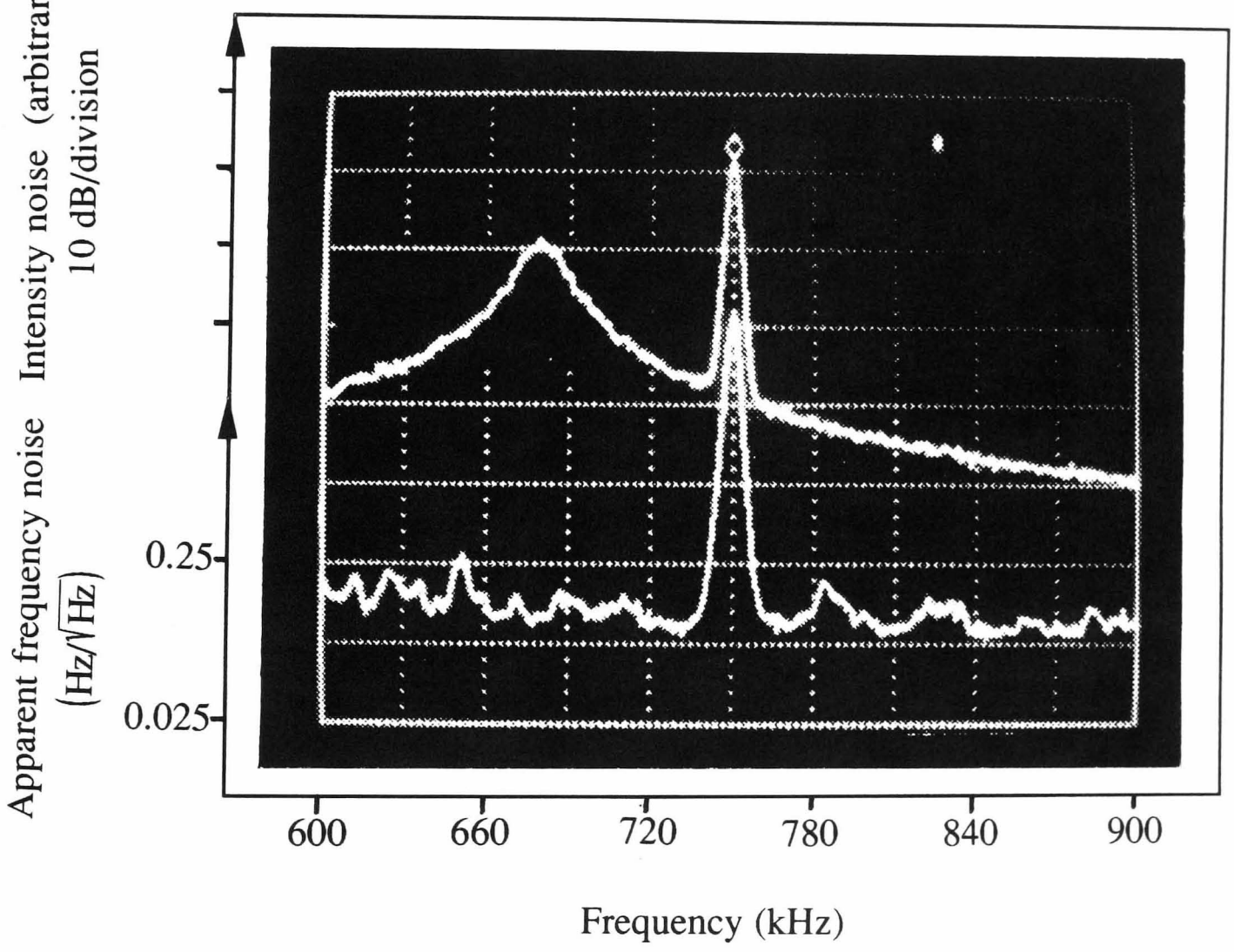


Figure 3.11: *The upper trace shows the intensity noise of the Lightwave laser close to the relaxation oscillation frequency. The lower trace shows the corresponding frequency noise at these frequencies of the laser with the intensity servo operating.*

oscillation peak along with a calibration peak. This peak was applied to signals just before injection into the spectrum analyser to allow the comparison of the position in frequency of structure in the frequency and intensity noise spectra. The lower trace shows the frequency noise of the laser again with an applied calibration peak but without the intensity servo operating.

It can be seen that there is a peak in the frequency noise spectrum very close to the relaxation oscillation frequency. Figure 3.11 shows the frequency spectrum when the intensity servo was turned on, with the peak close to the relaxation oscillation frequency having been reduced by 10 dB from $0.35Hz/\sqrt{Hz}$ to the shot noise limit of $0.1Hz/\sqrt{Hz}$. The reduction of this peak suggests it may possibly have been due to relaxation oscillations in intensity or beam geometry fluctuations coupling into the frequency noise measurement process.

## 3.5 Conclusions

In this chapter measurements of the frequency noise are outlined, both at frequencies below approximately 1 kHz and at relaxation oscillation frequencies, of monolithic Nd:YAG ring lasers, constructed at the Laser Zëntrum, Hannover, and supplied by Lightwave Electronics respectively.

For the Hannover laser an upper limit of the laser frequency fluctuations at 500 Hz was measured to be approximately $200Hz/\sqrt{Hz}$. This is clearly significantly higher than the final level of frequency fluctuations required in this frequency range for the proposed GEO600 interferometer of $\delta f \simeq 9 \times 10^{-6} Hz/\sqrt{Hz}$ for Nd:YAG light at approximately 1 kHz. The laser light would, however, undergo further amplification and frequency stabilisation before injection into the interferometer so this represents a satisfactory initial level of low frequency laser frequency noise.

In the initial measurement of frequency noise at high frequencies a peak was observed at the relaxation oscillation frequency of 250 kHz at a level of $\simeq 7\ Hz/\sqrt{Hz}$. When the optical alignment of the measurement system was adjusted this peak reduced in size to approximately 1 $Hz/\sqrt{Hz}$ (above a measurement floor of $\simeq$ 0.4 $Hz/\sqrt{Hz}$ of which 0.2 $Hz/\sqrt{Hz}$ was shot noise).

When a servo system was operating to damp the relaxation oscillation in intensity, the residual peak at the relaxation oscillation frequency in the frequency noise spectrum, was, in both cases reduced to the measurement background level. It was concluded that for the measurement with improved optical alignment, the residual peak in the frequency noise spectrum could probably be accounted for by the coupling of intensity noise into the frequency noise measurement. In the case of the initial measurement it was concluded that some other form of noise was present in addition to intensity noise: it is possible that imperfect optical isolation of the laser may have resulted in the presence either of real frequency noise or of beam geometry fluctuations which were coupling into the measurement of frequency noise.

These measurements of frequency noise show that any apparent relaxation oscillations observed in frequency noise are very small and can be reduced by damping the relaxation oscillation peak in intensity and so are unlikely to result in difficulties in measuring signals at lower frequencies.

Measurements of the frequency noise of a similar monolithic Nd:YAG ring laser, a Lightwave Electronics series 122 model, suggested that the apparent frequency noise close to the relaxation oscillation frequency of $\simeq$ 700 kHz was approximately $0.35 Hz/\sqrt{Hz}$ above a shot noise background of $0.1 Hz/\sqrt{Hz}$. This residual peak was reduced into the shot noise background when the intensity noise reduction system for the laser was operated. The levels of apparent frequency noise at relaxation oscillation frequencies were thus found to be similar in the two lasers.

The measured levels of frequency noise detailed above make this type of laser suitable for use as a master light source for a larger laser to illuminate a gravitational wave detector.

# Chapter 4

# Frequency Doubling of Light from a Nd:YAG laser for use in a Gravitational Wave Detector

## 4.1 Introduction

The technique of frequency doubling infra-red light is of great interest due to the possibilities it holds for producing an efficient solid-state source of green laser light. Sources of this type would be desirable for many applications but are of particular interest as potential light sources for the next generation of gravitational wave detectors. At present argon ion lasers are in use in several prototype gravitational wave detectors [55] and are the light sources proposed for use in the first stage of the LIGO Project [56]. Argon-ion lasers are however relatively inefficient in their use of electrical power and are inherently noisy compared with available infra-red solid-state lasers. It would thus be desirable to have a solid-state laser emitting several watts of continuous wave (cw) green light. One such possible source would be a frequency doubled Nd:YAG laser. The frequency doubling of Nd:YAG light using a doubling crystal in an external resonant cavity has been successfully demonstrated by Yang et al [60] with up to 6.5W of single frequency light at 532 nm being produced. Experiments on the intracavity frequency doubling of a cw Nd:YLF laser by Magni et al [77] have succeeded in producing up to 13.5 W of light at 523.5 nm.

Described in this chapter are experiments directed towards the development of an intracavity doubled flashlamp pumped Nd:YAG laser for use in a gravitational wave detector as an argon laser replacement. Also included is a brief review of the theory of second harmonic generation.

## 4.2 Second Harmonic Generation

### 4.2.1 Introduction

When an electric field is applied to a medium, the electrons in the medium are displaced due to the influence of the field. In a dielectric medium this can be considered as the creation of electric dipoles. The summed effect of the dipoles is the macroscopic polarisation of the medium. For weak applied electric fields this polarisation, P, is proportional to the applied E field and can be written

$$P = \varepsilon_0 \chi^{(1)} E \tag{4.1}$$

where $\varepsilon_0$ is the permittivity of free space and $\chi$ is the linear optical susceptibility, related to the refractive index of the medium, n, by $\chi^{(1)} = n^2 - 1$. This linear expression is however an approximation to the full expression for the polarisation

$$P = \varepsilon_0 \chi^{(1)} E + \varepsilon_0 \chi^{(2)} E^2 + ... \tag{4.2}$$

In the presence of strong E fields the nonlinear terms become important. In that case electromagnetic waves reradiated by the dipoles will contain components at different frequencies from that of the original applied E field. Second harmonic generation arises from the second order term in the polarisation equation. Consider an applied electric field of the form

$$E = E_0 \cos(kx + \omega t) \tag{4.3}$$

where k is the wave vector and $\omega$ the angular frequency. Substituting for E in the second term of equation 4.2 produces

1. a dc term

$$\varepsilon_0 \chi^{(2)} \frac{E_0^2}{2}$$

2. terms at twice the original frequency

$$\varepsilon_0 \chi^{(2)} \frac{E_0^2}{2} \cos(2kx + 2\omega t)$$

o it can be seen that the polarisation of the medium and subsequent reradiated lectromagnetic waves contain components at twice the frequency of the original pplied field. Clearly higher order terms in the polarisation will also give rise to omponents of the reradiated wave at different frequencies, and all these processes ill occur simultaneously. For the process of second harmonic generation to occur referentially, the applied and second harmonic waves must be phasematched.

## .2.2 Phasematching

or two waves of different frequencies passing through a medium to be phasematched ney must travel through the medium with the same phase velocity, i.e. the refractive idex for the waves in the medium must be the same. A common way to achieve his condition is to choose as a doubling material a birefringent crystal.

To illustrate how this works, consider a uniaxial birefringent crystal (a birefrin-ent crystal with a single optic axis). Now consider a monochromatic point source f light within the crystal at a point P shown in figure 4.1.

The expanding wavefronts of light originating at P will have different shapes de-ending on their polarisation. Light polarised with its electric vector perpendicular o the optic axis will have a spherical wavefront whereas light polarised such that a omponent of the electric vector is parallel to the optic axis will have an ellipsoidal avefront. This can be visualised in terms of the index surface for each wavefront. he index surfaces are formed such that the distance from the origin P to a point on e index surface is equal to the refractive index for a ray travelling in that direction.

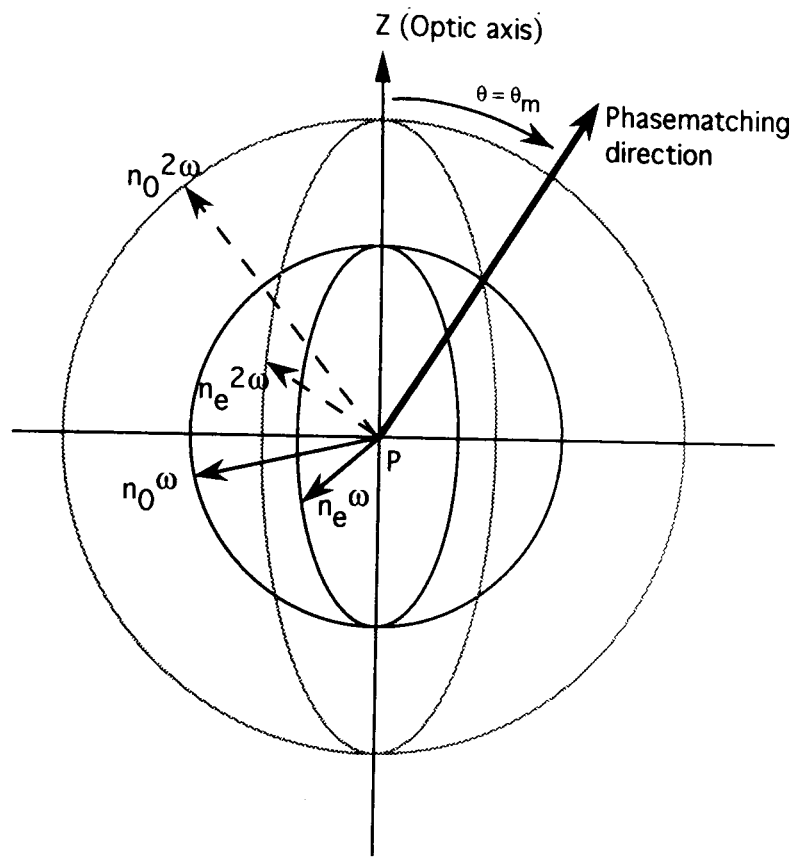


Figure 4.1: *Cross sections of the index surfaces in a uniaxial crystal for two angular frequencies, $\omega$ and $2\omega$.*

Thus the light which is polarised perpendicular to the optic axis travels through the crystal with a refractive index, $n_0$, independent of its direction of propagation. This is called the ordinary polarisation. The other polarisation has a refractive index which is dependent on the direction of propagation of the light through the crystal, this direction being defined in terms of the angle $\theta$ between the direction of propagation and the optic axis of the crystal. This refractive index is written $n_e(\theta)$, and this polarisation termed the extraordinary polarisation. Cross sections through the index surfaces for two different frequencies in a negative uniaxial crystal are shown in figure 4.1.

(Note, a negative uniaxial crystal is one for which $(n_e - n_o < 0)$ and for a positive uniaxial crystal $(n_e - n_0 > 0)$.)

Recall that we wish to have light of angular frequencies $\omega$ and $2\omega$ propagating with the same refractive index. From figure 4.1 it can be seen that there is a propagation direction through the crystal for which index surfaces for the different frequencies intersect, and for which

$$n_o^{\omega} = n_e^{2\omega}(\theta) \tag{4.4}$$

(For positive uniaxial crystals $n_e^{\omega}(\theta) = n_o^{2\omega}$) This is known as type I phasematching. In this case a linearly polarised ray of angular frequency $\omega$ is phasematched to generate an orthogonally polarised ray of angular frequency $2\omega$.

There is a second type of phasematching possible using the direction in which there is an intersection between the index surface for $n_e^{2\omega}$ and the surface made up of the *average* values of $n_e^{\omega}(\theta)$ and $n_o^{\omega}$. Thus

$$n_e^{2\omega}(\theta) = \frac{1}{2}[n_e^{\omega}(\theta) + n_o^{\omega}] \tag{4.5}$$

(For positive uniaxial crystals $n_o^{2\omega} = \frac{1}{2}[n_e^{\omega}(\theta) + n_o^{\omega}]$) This is known as type II phasematching. Here the input ray of frequency $\omega$ is made up of both an ordinary and an extraordinary component. These are types of *angular phasematching.* Note that angle $\theta$ specifies a locus of phasematching directions forming a cone about the optic axis. It should be noted that in the case of biaxial crystals there are three different refractive indices $n_x$, $n_y$ and $n_z$ defining three orthogonal axes, $x$, $y$ and $z$ in the crystal. In this case to identify completely the phasematching direction it is also necessary to specify the angle $\phi$, defined to be the angle between the projection of the propagation direction on the $xy$ plane and the $x$ axis.

### 4.2.3 Frequency Conversion

Consider again equation 4.2 for the polarisation of a medium. The second order nonlinear susceptibility $\chi^{(2)}$, is in fact a tensor and the second term of equation 4.2 can thus be written in the form

$$P_i(t) = \varepsilon_0 \sum_{jk} \chi_{ijk}^{(2)} E_j(t) E_k(t) \tag{4.6}$$

If we rewrite this with the E fields expressed in terms of their Fourier components, then for applied E fields of angular frequency $\omega$ we obtain an equation for the polarisation at the second harmonic frequency of the form

$$P_i(2\omega) = \varepsilon_0 \sum_{jk} \frac{\chi_{ijk}^{(2)}}{2}(2\omega, \omega, \omega) E_j(\omega) E_k(\omega) \times \exp i[(2k_{\omega} - k_{2\omega}) \cdot r] \tag{4.7}$$

This is often expressed in terms of the nonlinear tensor $d_{ijk}$. giving

$$P_i(2\omega) = \varepsilon_0 \sum_{jk} d_{ijk}(2\omega, \omega, \omega) E_j(\omega) E_k(\omega) \times \exp i[(2k_\omega - k_{2\omega}) \cdot r] \qquad (4.8)$$

For a particular type of interaction and nonlinear medium the nonlinear tensor $d_{ijk}$ can be reduced to an effective nonlinear coefficient, $d_{eff}$. Using Maxwell's equations and the expression for the polarisation given in equation 4.8 it is possible to derive the coupled wave equations driven by the nonlinear polarisation. For a plane wave travelling in the $z$ direction in a lossless nonmagnetic medium these are [78]

$$\frac{d}{dz} E(z, 2\omega) = i\kappa E(\omega) E(\omega) e^{-i\Delta k z} \qquad (4.9)$$

$$\frac{d}{dz} E(z, \omega) = i\kappa E(2\omega) E^*(\omega) e^{i\Delta k z} \qquad (4.10)$$

where $\kappa = \frac{\omega d_{eff}}{nc}$, n is the index of refraction, $E^*(\omega)$ is the complex conjugate of $E(\omega)$, c is the speed of light in vacuum and

$$\Delta k = k_{2\omega} - 2k_\omega \qquad (4.11)$$

In the low conversion efficiency limit (which is generally most appropriate when considering cw frequency doubling) the fundamental field changes negligibly with distance, and an expression for the efficiency of the frequency doubling process can thus be obtained by setting $\frac{d}{dz} E(z, \omega) = 0$, integrating equation 4.9 and noting that the intensity, $I \propto E^* E$. This produces [78]

$$\frac{I^{2\omega}}{I^\omega} = \frac{2\omega^2 d_{eff}^2 l^2 I^\omega}{n^3 c^3 \varepsilon_0} \times \frac{\sin^2(\frac{\Delta k l}{2})}{(\frac{\Delta k l}{2})^2} \qquad (4.12)$$

where $I^{2\omega}$ is the second harmonic intensity, $I^\omega$ is the fundamental intensity, and $l$ is the interaction length.

### 4.2.4 Efficiency

From equation 4.12 it can be seen that the conversion efficiency is proportional to the interaction length squared, the effective nonlinear coefficient squared and the intensity of the fundamental light.

The nonlinear coefficient is a property of the individual material used. When selecting a material however, factors such as whether the second harmonic process can be phasematched must also be taken into account. The interaction length may limited in several ways:

- by the size of crystals which can be grown without flaws
- by possible divergence of the fundamental and second harmonic beams due to double refraction (this phenomenon is known as walk-off)
- by the effect of absorption on the fundamental power in a resonant cavity.

The intensity of the fundamental beam can be maximised by focusing the beam. For a given length of crystal there is however a limit to the size to which the beam can profitably be focused. If the beam is made too small, the divergence of the beam through the crystal becomes large enough to limit the efficiency of the conversion. [69]

The phasematching conditions described in section 4.2.2 enter the conversion efficiency equation through the term

$$\frac{\sin^2(\frac{\Delta kl}{2})}{(\frac{\Delta kl}{2})^2} \tag{4.13}$$

When the beams are phasematched, $\Delta k = 0$ and the phasematching term shown in 4.13 tends to 1, its maximum value. If however the doubling crystal is *tilted* slightly away from the correct phasematching angle, there will be a mismatch in the refractive indices for the fundamental and second harmonic beams (see figure 4.1). The beams will thus be slightly out of phase, causing the phasematching term above and thus the conversion efficiency to drop from their maximum value.

The magnitude of this effect is usually described in terms of the angle through which a crystal must be tilted for the conversion efficiency of the particular doubling process to reach half its maximum value. This angle is called the acceptance angle. From equation 4.12, the conversion efficiency drops to half maximum when

$$\frac{\sin^2(\frac{\Delta kl}{2})}{(\frac{\Delta kl}{2})^2} = \frac{1}{2} \tag{4.14}$$

that is, when $\frac{\Delta kl}{2} = 1.39$ radians.

It is interesting to note the variation of $\Delta k$ with angular misalignment for the different types of phasematching process. For example consider a type I phasematching process in a negative uniaxial crystal with phasematching angle $\theta_m \neq 90$ degrees. It may be shown that

$$\Delta k = \frac{2\pi}{\lambda_\omega}(n_0^\omega)^2 \left[\frac{1}{(n_e^{2\omega})^2} - \frac{1}{(n_o^{2\omega})^2}\right] \sin 2\theta_m \delta\theta_{ext} \tag{4.15}$$

where $\lambda_\omega$ is the wavelength of the fundamental light, and $\delta\theta_{ext}$ is the half angular misalignment external to the doubling crystal.

For a similar type I phasematching process but with $\theta_m = 90$ degrees it can be shown that

$$\Delta k = \frac{2\pi}{\lambda_\omega} n_e^{2\omega} \left(\frac{1}{(n_e^{2\omega})^2} - \frac{1}{(n_o^{2\omega})^2}\right) \delta\theta_{ext}^2 \tag{4.16}$$

It can be seen that for $\theta_m \neq 90$ degrees, $\Delta k$ is a *linear* function of $\delta\theta_{ext}$, whereas for $\theta_m = 90$ degrees $\Delta k$ is a *quadratic* function of $\delta\theta_{ext}$. A phasematching angle of 90 degrees is thus desirable as it reduces the sensitivity of the conversion efficiency to angular misalignment of the crystal. This type of phasematching is often known as non-critical phasematching. For materials with temperature dependent refractive indices, deviations from the phasematching temperature also result in a change in $\Delta k$ and a subsequent drop in conversion efficiency. The magnitude of this effect is characterised for a particular phasematching process by the deviation in temperature which results in the conversion efficiency falling to half its maximum value. This deviation is known as the temperature bandwidth.

### 4.2.5 Choice of Doubling Crystal

A variety of crystals are available which can be used in frequency doubling the light from Nd:YAG lasers. For a crystal to be useful it must satisfy certain criteria. A crystal should be transparent at the frequencies of interest, be phase matchable at the correct wavelengths and be thermally and mechanically stable. The properties of two crystals commonly used for frequency doubling Nd:YAG light are briefly described below.

1. Lithium Triborate (LBO)

- LBO is a biaxial nonlinear crystal, i.e. it has two optic axes and refractive indices $n_x \neq n_y \neq n_z$.
- It is particularly attractive as a doubling crystal for Nd:YAG laser light as at the correct temperature the 1064nm to 532nm conversion process may be type I phasematched with angles $\theta = 90$ degrees and $\phi = 0$ degrees (that is, noncritically phasematched)
- The acceptance angles for an LBO crystal of length 23mm are shown in Table 4.1.
- LBO is reported to have a moderate nonlinear coefficient of around $1pm/V$ for this interaction but values in the literature are not consistent [79], [70]. In all calculations which follow the most conservative value reported of 0.83 $pm/V$ is used.
- The damage threshold of LBO is high, being approximately 2.5 $GW/cm^2$ [70]

The properties of LBO are described in more detail in [79], [80].

2. Potassium Titanyl Phosphate (KTP)

   - KTP is also a biaxial nonlinear crystal. The most efficient 1064 nm to 532 nm conversion process in KTP is type II phasematched which, as will be discussed later, can be undesirable for intracavity frequency doubling. The phasematching angles are $\theta = 90$ degrees and $\phi = 23.6$ degrees.
   - KTP is however reported to have a relatively large nonlinear coefficient of approximately 3.18 $pm/V$. The dependence of the conversion efficiency equation on the square of the effective nonlinear coefficient makes this an attractive property.
   - The acceptance angles for KTP crystal of different lengths are shown in Table 4.2.
   - The damage threshold for KTP is approximately 0.5 $GW/cm^2$ [70]

   The properties of KTP are described in more detail in [70] [81]

## 4.3 Experiments on Intracavity Frequency Doubling

The laser used in these experiments was a rebuilt SPECTRON SL903 flashlamp-pumped Nd:YAG laser. The cylindrical Nd:YAG rod was 10 cm long and 0.4 cm in diameter, with both ends anti-reflection coated for 1064 nm. The rod was water cooled, with a thermal lens of focal length of approximately 0.33 m for a lamp current of 21.5A. [82]

Previous intracavity frequency doubling experiments at Glasgow have used Potassium Titanyl Phosphate (KTP) cut for type II phasematching as the doubling crystal. These experiments resulted in the production of up to 1W of light at 532 nm. There was however evidence of damage to the KTP material [82]. The material Lithium Triborate (LBO) presents a promising alternative to KTP as it is reported to have a higher damage threshold [70] and is available cut for type I noncritical phasematching. Experiments were carried out using both types of crystal for comparison.

### 4.3.1 Linear Double Pass Cavity

Some investigations were made into the possibility of using a linear cavity for intracavity frequency doubling. A design was chosen with dimensions similar to the original model SL903 cavity dimensions. The design used is shown in figure 4.2.

The total cavity length was approximately 94.5 cm. The waists in the cavity were positioned at mirrors $m_1$ and $m_2$. Mirror $m_1$ was coated to be a high reflector at 1064 nm and mirror $m_2$ was coated to be reflecting at both 1064 nm and 532 nm with nominally zero phase shift between the two wavelengths on reflection. A plate was inserted into the cavity at the Brewster angle for 1064 nm to act as a polariser such that the laser light should be horizontally polarised. This plate was coated to be a highly transmitting for 1064 nm (p-polarisation) and highly reflecting for 532 nm (s-polarisation) so that it reflected the light at 532 nm out of the cavity.

The intracavity fundamental power was calculated by monitoring the power transmitted through the calibrated mirror $m_1$, and the second harmonic power mea-

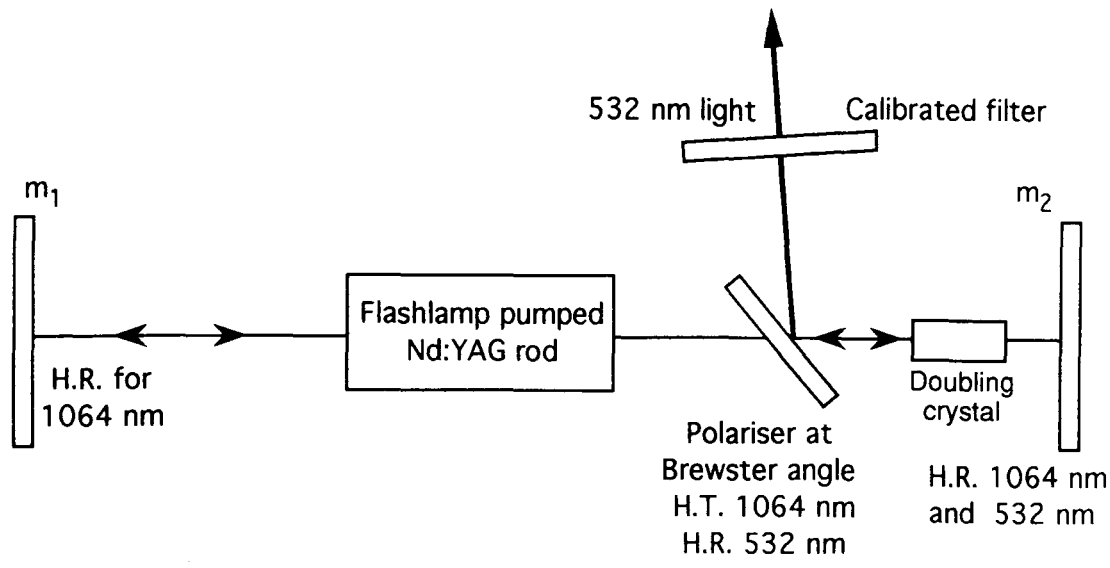


Figure 4.2: *Design of linear double pass cavity for intracavity frequency doubling.*

sured using a calibrated filter as shown in figure 4.2.

The doubling crystal used was inserted into the cavity between the coated Brewster plate and the doubly reflecting mirror. Second harmonic generation occurs as light at the fundamental frequency passes through the doubling crystal. Both the second harmonic and fundamental light are then reflected from mirror $m_2$ some distance away from the end of the crystal. The fundamental and second harmonic beams then both pass through the doubling crystal a second time with second harmonic generation occurring on the return pass. If the relative phase of the second harmonic light produced on each pass is such that the beams add in phase then the result should be light of double the amplitude and thus four times the intensity of that produced on a single pass through the crystal [83].

It should be noted that if the 1064nm and 532nm beams generated on the first path travel any distance in air before re-entering the crystal, dispersion of the beams will occur causing a relative phase shift between the beams of the order of 29 degrees per cm [70]. This phase shift can in principle be corrected by adjusting the position of mirror $m_2$ such that the total phase shift between the two beams is a multiple of $2\pi$ [84]. Mirror $m_2$ was mounted on a translation stage so that the distance between $m_2$ and the end of the doubling crystal could be altered.

### 4.3.2 Experiments with LBO

#### Cavity Description

Experiments were carried out using a crystal of LBO of dimensions $3 \times 3 \times 23$ mm as the doubling element. The crystal was cut was cut for type I non-critical phase-matching with both ends anti-reflection coated for light of 1064 nm and 532 nm. The crystal was placed in an oven constructed to hold the crystal at the correct phasematching temperature. The crystal and oven were inserted into the linear cavity between the plate at Brewsters angle and the doubly reflecting mirror. The waists, $\omega_0$, at mirrors $m_1$ and $m_2$ were approximately 320 $\mu$m in radius.

#### Temperature Profile

To investigate the performance of the oven controlling the temperature of the LBO crystal the temperature of the crystal was varied and the effect on the relative conversion efficiency of the second harmonic generation measured.[1] The variation of conversion efficiency with temperature is shown in figure 4.3. Also shown in figure 4.3 are plots of the expected variation of the conversion efficiency with temperature. These plots were obtained using values for the temperature bandwidth of the frequency doubling process of $\pm 0.78$ degrees C obtained from Koechner [70] and $\pm 1.14$ degrees C from Velsko et al [79] respectively. It can be seen from figure 4.3 that the experimental plot falls between the two theoretical plots and is thus in reasonable agreement with what is expected. This agreement shows that any self heating from the fundamental intracavity power did not significantly change the phasematching condition.

#### Spacing of Crystal and Doubly Reflecting Mirror

The arrangement described above with the fundamental and second harmonic beams being reflected from mirror $m_2$ before re-entering the doubling crystal leads to two problems in particular:

[1] This measurement was actually made using the LBO in the ring cavity described in section 4.3.4.

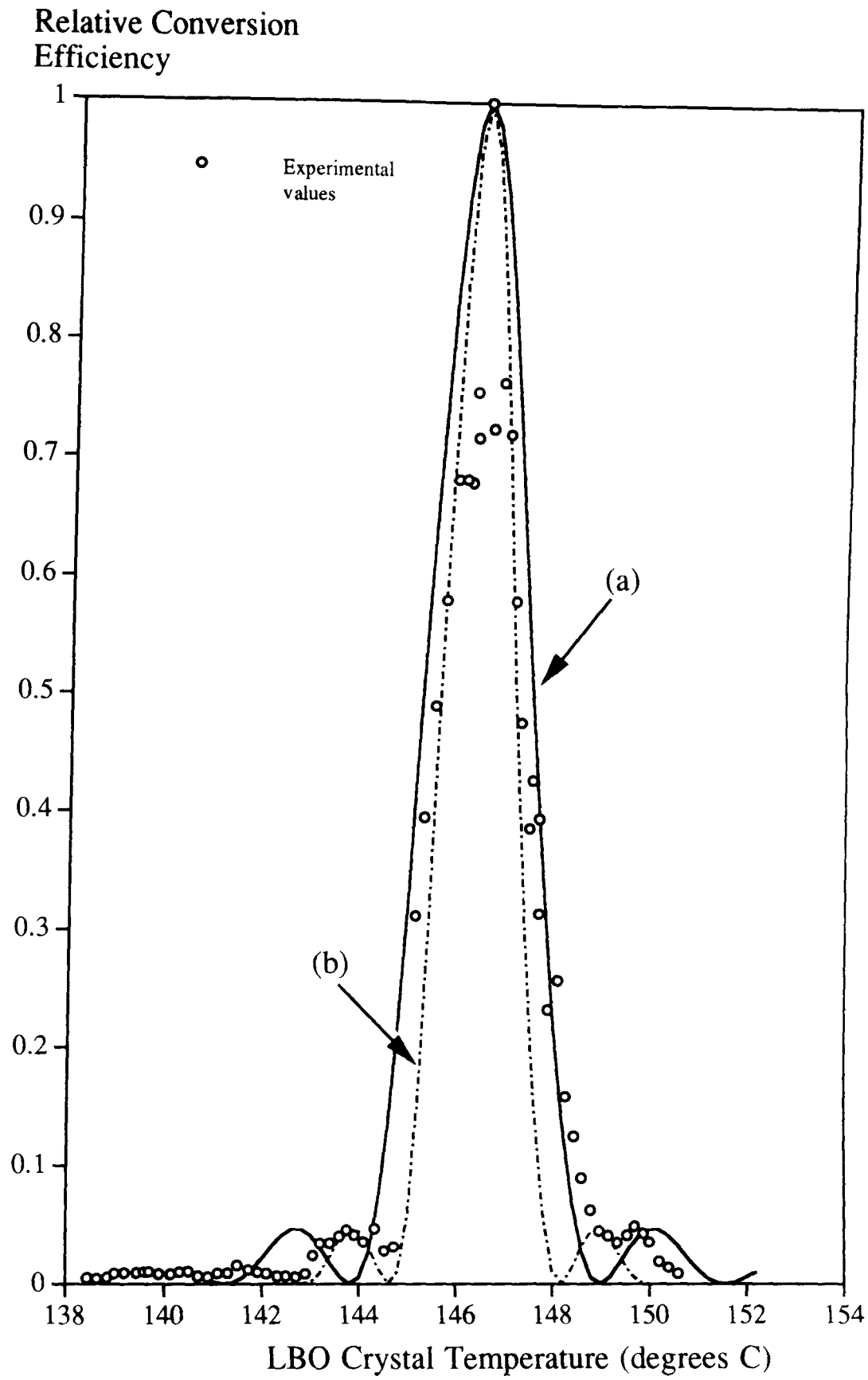


Figure 4.3: *Experimental and theoretical plots showing the relative conversion efficiency of the frequency doubling process as a function of temperature for a 23 mm crystal of LBO. The measured data points are shown as circles. Curve* **(a)** *shows the theoretical curve obtained assuming a temperature bandwidth for the process of* $\pm 1.14$ *degrees C. Curve* **(b)** *assumes a temperature bandwidth of* $\pm 0.78$ *degrees C.*

1. The fundamental and second harmonic beams may undergo a relative phase change on reflection at the mirror (despite there being nominally zero phase shift).

2. Any air gap between the end of the doubling crystal and the mirror results in the dispersion of the fundamental and second harmonic beams.

The effects of dispersion can be minimised by placing mirror $m_2$ as close as possible to the end of the doubling crystal but the possibility of a phase change of the light on reflection at $m_2$ leaves an uncertainty in the total phase change of the light when it re-enters the crystal.

A typical example of the effect of dispersion of the fundamental and second harmonic beams on the amount of second harmonic light generated is shown in figure 4.4.

This graph was obtained by initially placing mirror $m_2$ as close as possible to the doubling crystal (approximately 6 mm away from the crystal end) and adjusting the orientation and temperature of the doubling crystal to maximise the second harmonic power produced. Mirror $m_2$ was then moved to increase the distance between the crystal and mirror $m_2$ and thus alter the relative phase of the infra-red and green light. The effect on the conversion efficiency of the frequency doubling process was then measured.

It can be seen from this graph that changing the relative phase of the green and infra-red light between the first and second pass through the doubling crystal had a significant effect on the conversion efficiency. The graph shows the conversion efficiency maximised for the initial mirror-crystal spacing. The conversion efficiency then decreased as the total path length in air for the green and infra-red beams was increased until a minimum was reached when the path length was approximately 5.9 cm (i.e. the distance between mirror $m_2$ and the end of the doubling crystal was approximately 2.95 cm).

The difference in path length between the positions of minimum and maximum conversion efficiency was approximately 4.7 cm. With the dispersion of the green and infra-red light corresponding to a relative phase shift of 29 degrees per cm, this suggests that the phase change introduced by the air on moving between these

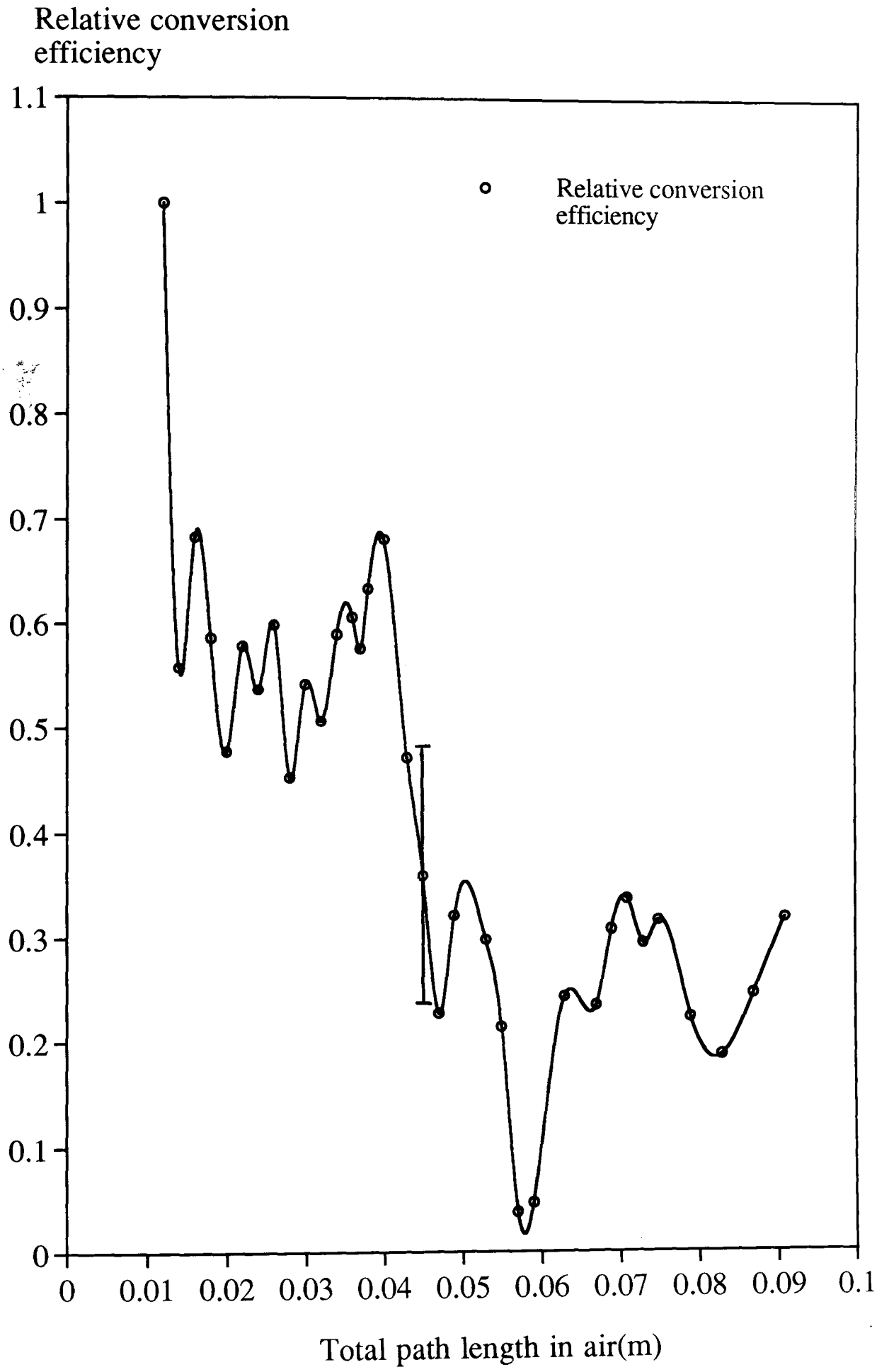


Figure 4.4: *Relative conversion efficiency as a function of dispersion for a double pass through a 23 mm LBO crystal.*

positions was approximately 136 degrees. A phase change of 180 degrees would be expected and the difference is probably due to experimental error.

It was noted that with mirror $m_2$ placed some distance away from the end of the doubling crystal the reduction in the amount of green power produced could to some extent be compensated by a combination of readjusting the orientation of the LBO crystal and adjusting the crystal temperature. These two actions both alter the phasematching of the second harmonic and fundamental light passing through the crystal. This suggested that the relative phase shift between the fundamental and second harmonic light produced by tilting and or changing the temperature of the crystal had partially compensated the phase shift introduced by the dispersion of the beams in air.

The relation between the tilt of the crystal away from the phasematching angle and the resulting phase mismatch can be obtained by adapting equation 4.16. Equation 4.16 describes $\Delta k$, the wave-vector mismatch of the fundamental and second harmonic beams as a function

of angular displacement in the case of type I, non-critical phasematching in a *uniaxial* crystal. A similar formula can be obtained for the case of interest of type I non-critical phasematching in biaxial LBO. The orientation of the LBO crystal axes with respect to the fundamental and second harmonic polarisations for this type of phasematching is shown in figure 4.5

The axes x, y and z are crystal axes. For the non-critically phasematched case shown the phasematching angles are $\theta_m = 90$ degrees and angle $\phi_m = 0$ degrees. The phasematching condition $n_z^\omega = n_y^{2\omega}$ is satisfied, where $n_z^\omega$ is the refractive index for the fundamental light which is plane polarised in the $z$ direction, and $n_y^{2\omega}$ is the refractive index for the second harmonic light plane polarised in the $y$ direction. Clearly the crystal may be tilted so as to change angle $\phi$ or angle $\theta$. This leads us to the equations

$$\Delta k_\theta = \frac{2\pi}{\lambda_\omega} n_z^\omega \left( \frac{1}{(n_x^\omega)^2} - \frac{1}{(n_z^\omega)^2} \right) \delta\theta_{ext}^2 \tag{4.17}$$

where $\Delta k_\theta$ is the wave vector mismatch caused by changing the phasematching angle $\theta$ by an angle $\delta\theta_{ext}$ external to the doubling crystal, and

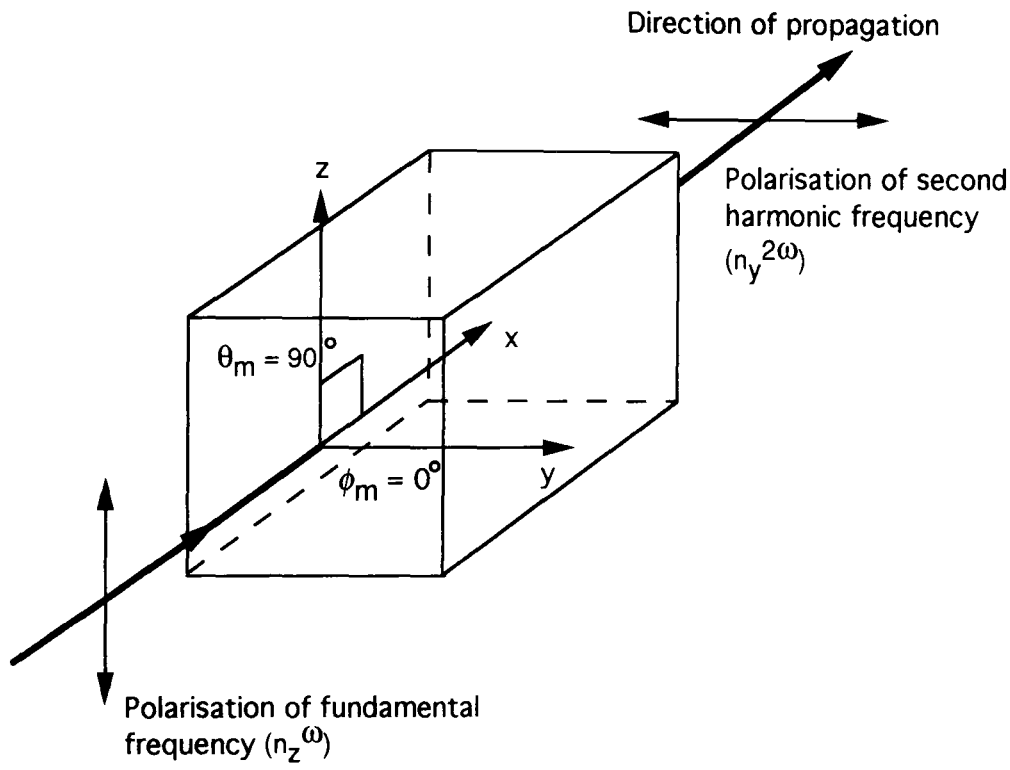


Figure 4.5: *Orientation of LBO crystal with respect to fundamental and second harmonic beams for type I noncritical phasematching.*

$$\Delta k_\phi = \frac{2\pi}{\lambda_\omega} n_y^{2\omega} \left( \frac{1}{(n_y^{2\omega})^2} - \frac{1}{(n_x^{2\omega})^2} \right) \delta\phi_{ext}^2 \tag{4.18}$$

where $\Delta k_\phi$ is the wave vector mismatch caused by changing the phasematching angle $\phi$ by $\delta\phi_{ext}$.

From these equations it is possible to deduce in each case the relative phase shift of the fundamental and second harmonic, $\Phi$, as a function of angular misalignment by noting that

$$\Phi = \frac{\Delta k l}{2} \tag{4.19}$$

The phase shift $\Phi_\theta$ produced by an angular misalignment $\delta\theta_{ext}$ can thus be written

$$\Phi_\theta = \frac{\pi l}{\lambda_\omega} n_z^{\omega} \left( \frac{1}{(n_x^{\omega})^2} - \frac{1}{(n_z^{\omega})^2} \right) \delta\theta_{ext}^2 \tag{4.20}$$

and the phase shift $\Phi_\phi$ produced by an angular misalignment $\delta\phi_{ext}$ written

$$\Phi_\phi = \frac{\pi l}{\lambda_\omega} n_y^{2\omega} \left( \frac{1}{(n_y^{2\omega})^2} - \frac{1}{(n_x^{2\omega})^2} \right) \delta\phi_{ext}^2 \tag{4.21}$$

Although the above equations describe the magnitude of angular displacement needed to produce a particular phase mismatch of the green and infra-red light, it is not

yet clear what size of phase mismatch best compensates a given dispersion. This information can be obtained by considering equation 4.22. As shown in Appendix A, the total resultant intensity $I_t^{2\omega}$ of the second harmonic light produced after the second pass of the laser light through the doubling crystal may be written as

$$I_t^{2\omega} \propto 4I_0^{2\omega}\frac{\sin^2\Phi}{\Phi^2}\cos^2\left(\frac{\psi}{2}+\Phi\right) \tag{4.22}$$

Where $\psi$ is the relative phase change between the fundamental and second harmonic beams on re-entering the doubling crystal, caused by dispersion of the beams in air. The relative intensity of the second harmonic $I_{rel}^{2\omega}$ as a function of phase mismatch and dispersion is thus

$$I_{rel}^{2\omega} = \frac{\sin^2\Phi}{\Phi^2}\cos^2\left(\frac{\psi}{2}+\Phi\right) \tag{4.23}$$

For a given dispersion $I_{rel}^{2\omega}$ can be plotted as a function of $\Phi$ allowing the optimum value of $\Phi$ to be found.

Consider the worst case example of dispersion such that $\psi = 180$ degrees. Figure 4.6 shows the relative intensity of green light obtained as $\Phi$ is varied. It can be seen that the optimum values of $\Phi$ to compensate the dispersion are approximately $\pm 65$ degrees and for these values the fraction of green light obtained is approximately 0.53 of the maximum possible intensity.

Using equations 4.20 and 4.21 the angular displacements necessary to produce relative phase shifts of $+65$ and $-65$ degrees were calculated and are shown in Table 4.1. It is interesting to note that the refractive indices of LBO are such that $n_z > n_y > n_x$ [79]. Thus for any value of $\delta\theta_{ext}$ the phase shift $\Phi_\theta$ is always positive and for any value of $\delta\phi_{ext}$ the phase shift $\Phi_\phi$ is always negative. To compensate for a dispersion of $\psi = 180$ degrees the LBO crystal may be tilted to change either $\theta$ or $\phi$. However when $I_{rel}^{2\omega}$ is plotted as a function of $\Phi$ for the case of dispersion $\psi = 90$ degrees it can be seen from figure 4.7 that the variation of $I_{rel}^{2\omega}$ with $\Phi$ is asymmetric about $\Phi = 0$. There is thus a single best value for $\Phi$ where $\Phi = -34$ degrees. To compensate the effect of dispersion the crystal must thus be tilted to change angle $\phi$ and not $\theta$.

Another way to compensate for some dispersion of the fundamental and second harmonic beams in air is to use the fact that the refractive indices of LBO at the frequencies of interest are temperature dependent. Thus by changing the temperature

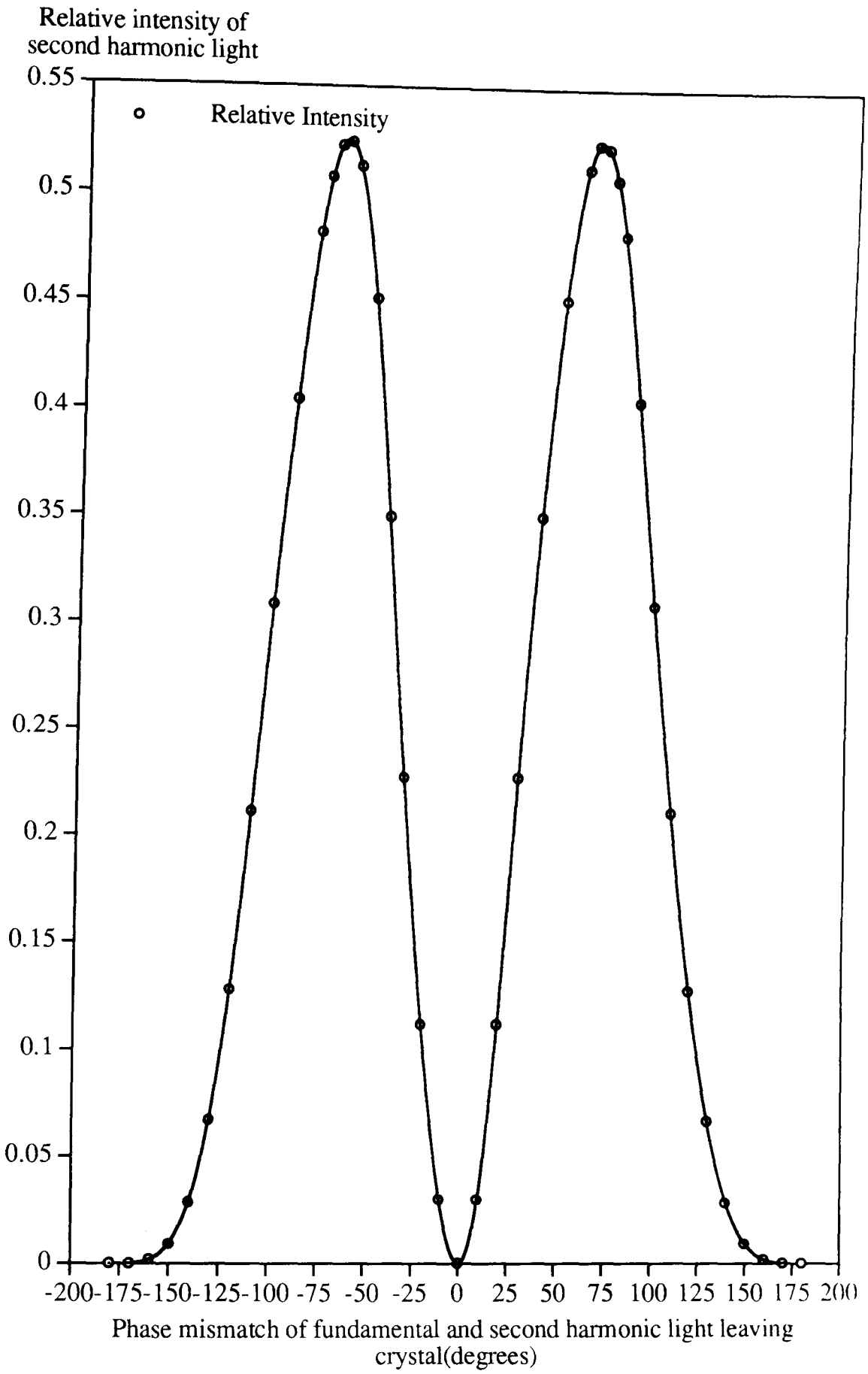


Figure 4.6: *Theoretical relative intensity of second harmonic light as a function of phase mismatch through crystal with dispersion of fundamental and second harmonic beams in air of 180 degrees.*

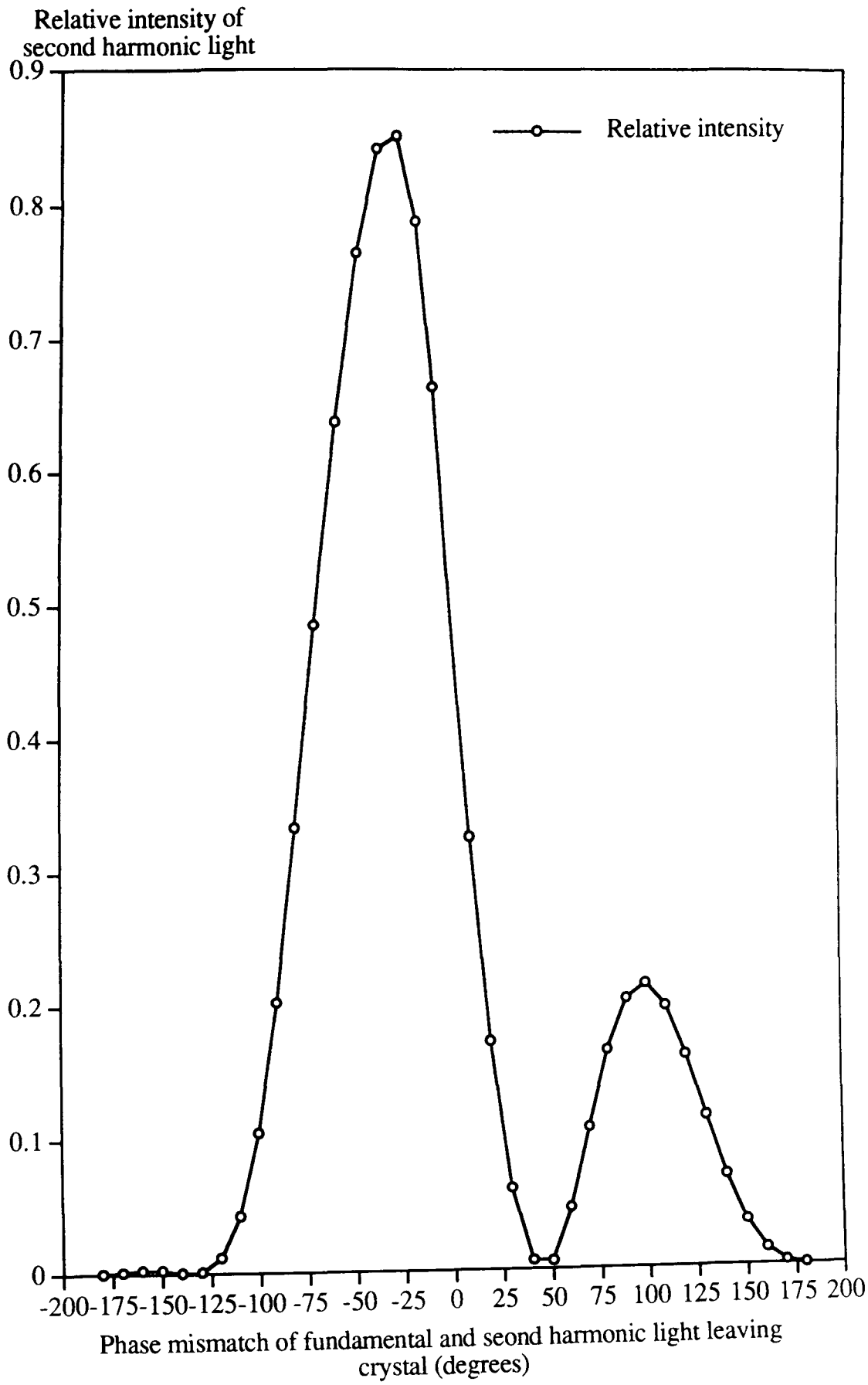


Figure 4.7: *Theoretical relative intensity of second harmonic light as a function of phase mismatch through crystal with dispersion of fundamental and second harmonic beams in air of 90 degrees*

| Doubling Crystal | | LBO (23 mm) | |
|---|---|---|---|
| Dispersion, $\psi$, (degrees) | | 180 | 90 |
| Phase mismatch, $\Phi$, (degrees) | | $\pm 65$ | -34 |
| $\delta\theta_{ext}$ (degrees) | | $\pm 1.3$ | - |
| $\delta\phi_{ext}$ (degrees) | | $\pm 1.62$ | $\pm 1.17$ |
| $\Delta T$ (degrees C) | | $\mp 0.94$ | $\mp 0.49$ |
| Acceptance angle | $\delta\theta_{ext}$ (degrees) | $\pm 1.44$ | |
| | $\delta\phi_{ext}$ (degrees) | $\pm 1.8$ | |
| Temperature bandwidth | | $\pm 1.14$ | |

Table 4.1: *This table shows the phase mismatches, $\Phi$ and corresponding angular misalignments $\delta\theta_{ext}$, $\delta\phi_{ext}$ and changes in temperature, $\Delta T$, needed to compensate for dispersions in air of 180 degrees and 90 degrees respectively along with the acceptance angles and temperature bandwidth for an LBO crystal of length 23 mm*

of the LBO crystal away from its phasematching temperature it should be possible to introduce a phase mismatch of the required size between the green and infra-red beams.

The relative phase shift $\Delta\Phi$ of the fundamental and second harmonic beams as a function of change in temperature is given by

$$\Delta\Phi = \frac{2\pi l}{\lambda_\omega}\left(\frac{\delta n_y^{2\omega}}{\delta T} - \frac{\delta n_z^{\omega}}{\delta T}\right)^{-1}\Delta T \tag{4.24}$$

Using values for $\frac{\delta n_z^{\omega}}{\delta T}$ and $\frac{\delta n_y^{2\omega}}{\delta T}$ from Velsko et al [79] the temperature changes needed to produce relative phase shifts of $+65$ degrees and $-65$ degrees respectively in a crystal of length $l = 0.023m$ were calculated and are shown in Table 4.1. Clearly the effects of dispersion may be to some extent compensated by either raising or lowering the temperature of the LBO crystal with respect to the phasematching temperature, however there will still be some reduction of the second harmonic power from the maximum possible power.

### Second Harmonic Power Obtained

The maximum second harmonic power obtained was approximately 4.6 W for an intracavity fundamental power of 343 W with the distance between the end of the doubling crystal and the doubly reflecting mirror equal to approximately 1.05 cm. This distance corresponds to a total path length in air for the fundamental and second harmonic beams of 2.1 cm, which is equivalent to a dispersion of approximately 61 degrees. This power was obtained with the laser operating in approximately 3 longitudinal modes and several spatial modes (see figure 4.8 and figure 4.9).

From equation 4.23 it can be seen that in the case of perfect phasematching ($\Phi = 0$), mirror $m_2$ should be as close as possible to the end of the doubling crystal to maximise the amount of green power produced. Since the maximum amount of power was produced when the dispersion was approximately 61 degrees, either

1. The relative phase shift of 61 degrees due to dispersion was compensating for a relative phase shift of -61 degrees occurring on reflection of the beams at mirror $m_2$

   or

2. The optimum phasematching condition could not be achieved experimentally and that some compensation for this is possible using the dispersion of the beams in air.

Consider point one above. The amount of second harmonic light expected from theory can be calculated using equation 4.22. Note that equation 4.22 assumes a single longitudinal mode and should be multiplied by a factor of $\frac{(2N-1)}{N}$ where $N$ is the number of longitudinal modes of the laser [83]. This gives a figure of approximately 5.7 W for the theoretical second harmonic power.

If, as suggested in point two, perfect phasematching cannot be achieved experimentally, for example because of difficulties in controlling the orientation or temperature of the crystal, then there will always be some phase mismatch $\Phi$ between the fundamental and second harmonic light. From equation 4.23 it can be seen that there is an optimum non-zero dispersion for any phase mismatch, so the maximum second harmonic power would be obtained for some non-zero dispersion. Assuming

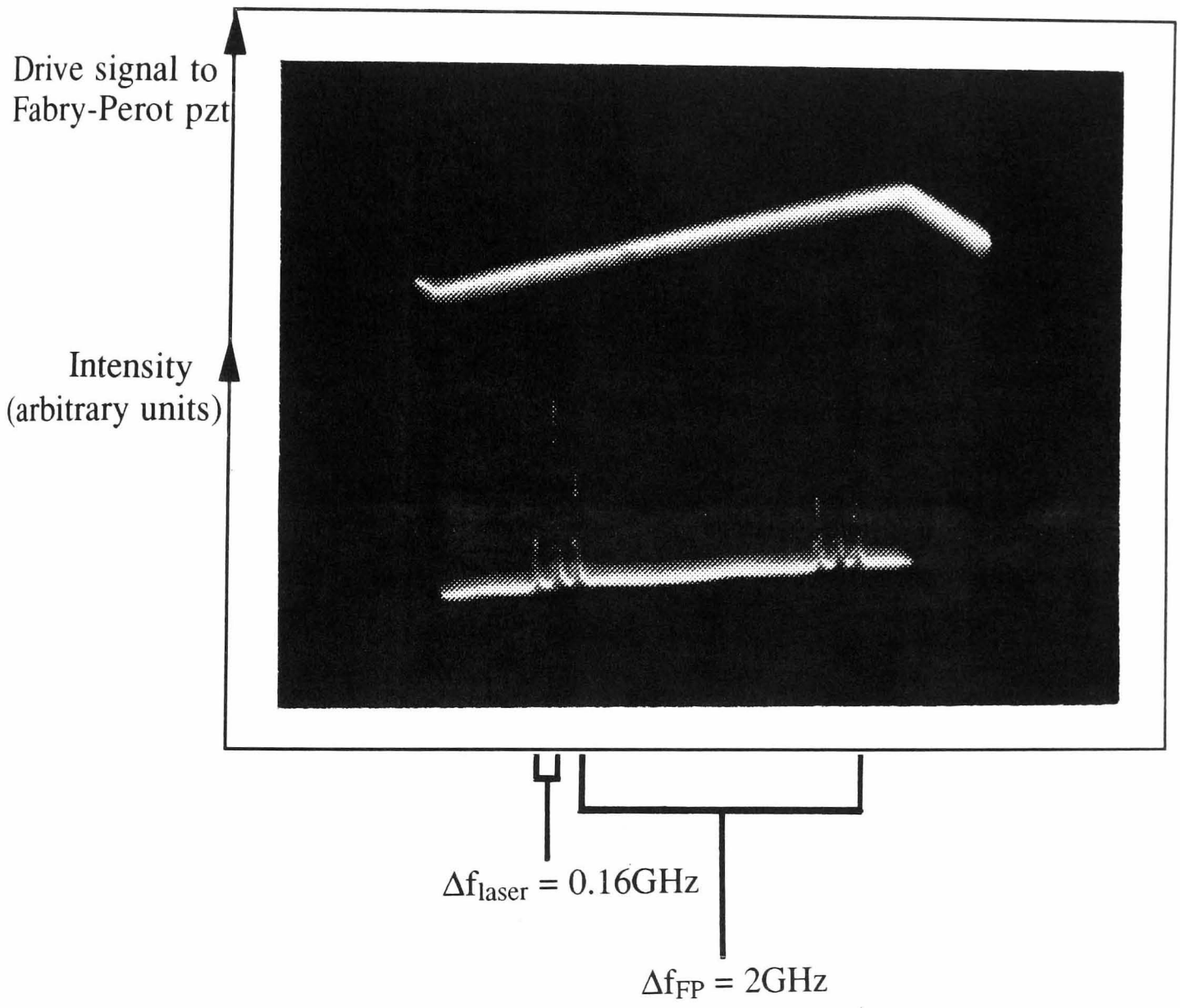


Figure 4.8: *Typical frequency spectrum of fundamental light in linear frequency doubling cavity containing LBO crystal of length 23 mm. The narrower mode spacing is set by the free spectral range of the laser cavity, $\Delta f_{laser}$, and the larger mode spacing set by the free spectral range of the Fabry-Perot analyser, $\Delta f_{FP}$.*

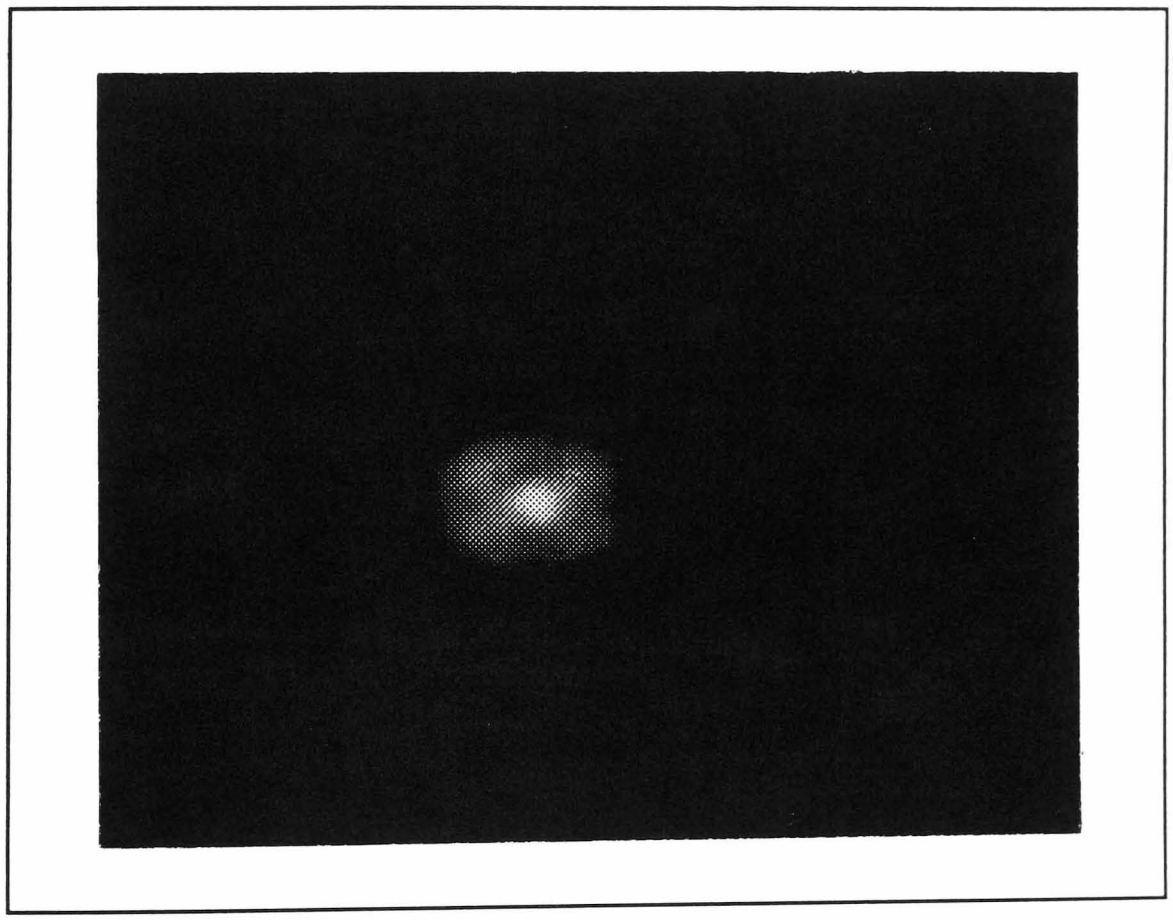

Figure 4.9: *Typical beam shape of second harmonic light produced by an LBO crystal of length 23 mm in linear doubling cavity.*

this is the case and starting with the experimental values for the maximum second harmonic power obtained and the corresponding dispersion, it is possible to determine the mismatch in angle or temperature limiting the phasematching using equations 4.21, 4.23 and 4.24. It can be shown that if the second harmonic power is obtained with dispersion equal to approximately 61 degrees, there must be an angular displacement of $\delta\phi_{ext} = 1.2$ degrees *or* a deviation in temperature of $\Delta T = +0.4$ degrees C. It should be noted that the value for the limiting angular displacement assumes the crystal is at the correct phasematching temperature and similarly the value for the limiting temperature mismatch assumes the crystal is perfectly oriented. From the magnitude of these values it seems possible that the phasematching was experimentally limited by the difficulties of both stabilising the temperature of the LBO crystal and controlling its position within the limits given above.

From equation 4.22 the theoretical second harmonic power is then 5.2 W, which is in reasonable agreement with the 4.6 W obtained.

### 4.3.3 Experiments with KTP

#### Introduction

Experiments were carried out using crystals of KTP cut for type II phasematching to frequency double the Nd:YAG light to compare the properties of KTP with those of LBO. The doubling cavity used was essentially the same as for the experiments with LBO as shown in figure 4.2.

#### Experiments with a 5mm KTP crystal

Experiments were carried out using a crystal of KTP of dimensions 2 x 2 x 5 mm. This crystal was inserted into the linear cavity shown in figure 4.2 between the plate at the Brewster angle and mirror $m_2$. It was found that as the separation of the mirror $m_2$ and the crystal was varied, altering the orientation of the KTP crystal allowed approximately the same amount of second harmonic power to be obtained over a range of mirror positions. The maximum amount of second harmonic power produced by this crystal was approximately 1.38 W with a fundamental circulating

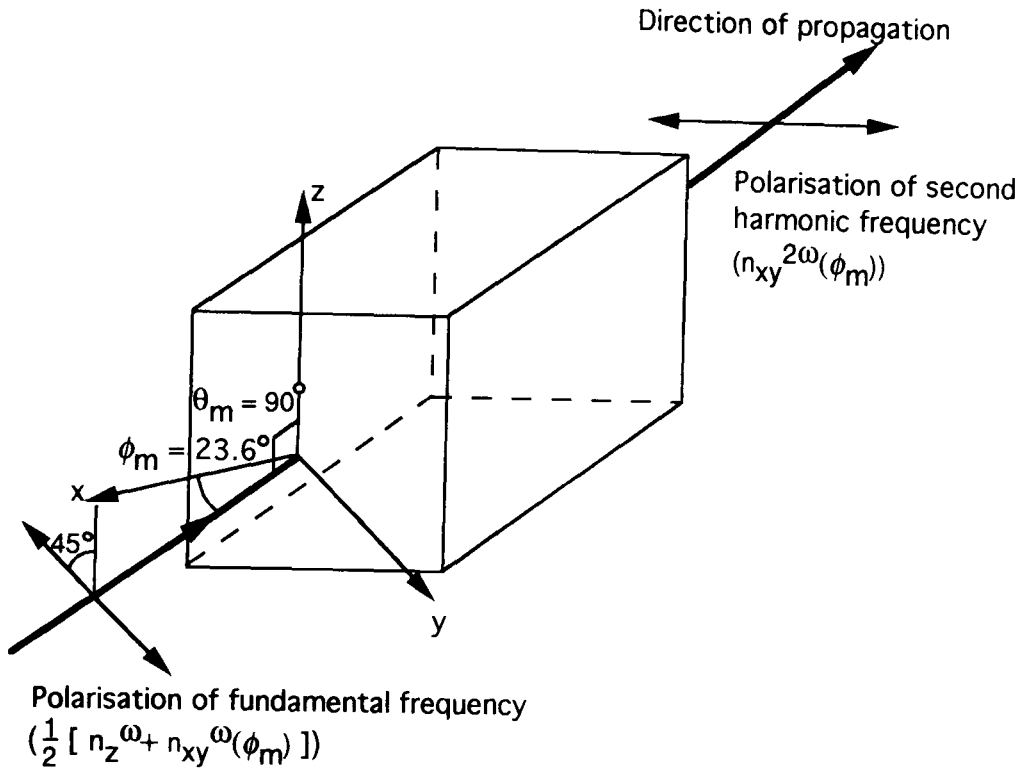


Figure 4.10: *Orientation of KTP crystal with respect to fundamental and second harmonic beams for type II phasematching.*

power of approximately 278 W obtained with mirror $m_2$ placed in the range 1.5 cm to 2.2 cm from the doubling crystal - that is a total path length in air of 3 cm to 4.4 cm.

This appeared to show the presence of an effect similar to that previously described for LBO where changing the orientation of the doubling crystal allowed some compensation of the effects of dispersion. In KTP this compensation is more complicated due to the particular phasematching conditions of this crystal - KTP is type II phasematched at room temperature. The effects of these phasematching conditions are considered below.

### Tilting the KTP crystal to compensate for dispersion

The orientation of the KTP crystal axes with respect to the fundamental and second harmonic beams for the case of type II phasematching is shown in figure 4.10. The axes x, y and z are crystal axes. For the case shown the phasematching angles are $\theta_m = 90$ degrees and $\phi_m = 23.6$ degrees, and the phasematching condition $\frac{1}{2}[n_z^{\omega} + n_{xy}^{\omega}(\phi_m)] = n_{xy}^{2\omega}(\phi_m)$ is satisfied. $n_z^{\omega}$ is the refractive index for the component of the fundamental beam plane polarised in the z direction, $n_{xy}^{\omega}(\phi_m)$ is the refractive

index for the fundamental component plane polarised in the xy plane and $n_{xy}^{2\omega}(\phi_m)$ is the refractive index for the second harmonic light plane polarised in the xy plane. The equations describing the angular misalignments $\delta\theta_{ext}$ and $\delta\phi_{ext}$ as a function of relative phase shift $\Phi$ are given by

$$\delta\theta_{ext} = n_{xy}^{2\omega}(\phi_m)\left[\frac{2\lambda_\omega}{\pi l (n_z^\omega)^3}\left(\frac{1}{(n_{xy}^\omega(\phi_m)^2} - \frac{1}{(n_z^\omega)^2}\right)^{-1}\Phi_\theta\right]^{\frac{1}{2}} \tag{4.25}$$

and

$$\begin{aligned}\delta\phi_{ext} &= n_{xy}^{2\omega}(\phi_m)\frac{\lambda_\omega}{\pi l \sin 2\phi_m}\left\{\frac{(n_{xy}^\omega(\phi_m))^3}{2(n_x^\omega)^2(n_y^\omega)^2}\left[(n_y^\omega)^2 - (n_x^\omega)^2\right]\right. \\ &- \left.\frac{[n_{xy}^{2\omega}(\phi_m)]^3}{(n_x^{2\omega})^2(n_y^{2\omega})^2}\left[(n_y^{2\omega})^2 - (n_x^{2\omega})^2\right]\right\}^{-1}\Phi_\phi \end{aligned} \tag{4.26}$$

Note that for KTP, $n_{xy}(\phi_m) < n_z$ so, for any tilt $\delta\theta_{ext}$ the phase shift produced is always positive, whereas positive and negative phase shifts can be obtained by varying $\delta\phi_{ext}$. Using equations 4.25 and 4.26 the angular displacements necessary to best compensate dispersions of 180 degrees and 90 degrees were calculated for a crystal of length 5 mm and are shown in Table 4.2.

### Tilting the KTP crystal to control fundamental polarisation

The type II phasematching condition for KTP means that the fundamental polarisation is made up of two perpendicular components with refractive indices $n_z^\omega$ and $n_{xy}^\omega(\phi_m)$ respectively. Since the components have different refractive indices the relative phase of the components changes as the light travels through the crystal, causing the overall polarisation of the infra-red light to change. When the fundamental light emerges from the crystal it may thus be in the wrong polarisation to resonate in the laser cavity. This results in a loss of fundamental power.

The polarisation in which the fundamental beam leaves the KTP crystal can be changed by changing the optical length of the crystal. This can be done by for example heating the crystal [82] or by tilting the crystal.

The relation between the difference in path length, $\Delta l$, seen by the fundamental components as a function of changes $\delta\theta_{ext}$ (measured external to the crystal) in the

| Doubling Crystal | | KTP (5mm) | | KTP (25mm) | |
|---|---|---|---|---|---|
| Dispersion, $\psi$, (degrees) | | 180 | 90 | 180 | 90 |
| Phase mismatch, $\Phi$, (degrees) | | $\pm$65 | -34 | $\pm$65 | -34 |
| $\delta\theta_{ext}$ (degrees) | | $\pm$2.95 | - | $\pm$1.25 | - |
| $\delta\phi_{ext}$ (degrees) | | $\mp$0.76 | 0.38 | $\mp$0.15 | -0.04 |
| $\Delta T$(degrees C) | | $\pm$19.7 | -10.3 | $\pm$3.9 | -2.06 |
| Acceptance angle | $\delta\theta_{ext}$ (degrees) | $\pm$3.27 | | $\pm$1.46 | |
| | $\delta\phi_{ext}$ (degrees) | $\pm$0.95 | | $\pm$0.19 | |
| Temperature Bandwidth(degrees) | | $\pm$24.1 | | $\pm$4.82 | |

Table 4.2: *This table shows the phase mismatches, $\Phi$ and corresponding angular misalignments $\delta\theta_{ext}$, $\delta\phi_{ext}$ and changes in temperature, $\Delta T$, needed to compensate for dispersions in air of 180 degrees and 90 degrees respectively along with the acceptance angles and temperature bandwidth for KTP crystals of length 5mm and 25mm*

phasematching angle $\theta$ can be shown to be

$$\delta\theta_{ext} = \left( \frac{2\Delta l}{l} \left[ \frac{1}{n_z^\omega} - \frac{1}{n_{xy}^\omega(\phi_m)} + n_z^\omega \left( \frac{1}{(n_{xy}^\omega(\phi_m)^2)} - \frac{1}{(n_z^\omega)^2} \right) \right]^{-1} \right)^{\frac{1}{2}} \tag{4.27}$$

The loss of fundamental power would be highest if after a double pass through the KTP crystal the fundamental polarisation was perpendicular to the polarisation resonant in the cavity. This situation would be equivalent to the relative phase of the components of the fundamental light having been shifted in phase by 180 degrees ($\lambda/2$) after passing twice through the crystal, thus being shifted by 90 degrees ($\lambda/4$) on a single pass. For a 5mm crystal, using equation 4.27 the tilt needed to compensate for this phase shift was calculated and found to be $\delta\theta_{ext} = \pm 3.52$ degrees, compared with the acceptance angle for tilts of this crystal $\delta\theta_{ext} = \pm 3.27$ degrees. Clearly, in a worst case the tilt needed to compensate the rotation of the fundamental polarisation lies outside the acceptance angle and thus would result in a significant loss of conversion efficiency.

**Temperature effects**

KTP is phasematched at room temperature. Thus self heating of the KTP crystal due to some absorption of the circulating intracavity fundamental power could interfere with the phasematching conditions. It can be shown that for type II phasematching the phase mismatch $\Delta\Phi$ as a function of change in temperature $\Delta T$ may be written [85]

$$\Delta\Phi = \frac{\pi l}{\lambda_\omega}\left[2\frac{\delta n_{xy}^{2\omega}(\phi_m)}{\delta T} - \left(\frac{\delta n_z^\omega}{\delta T} + \frac{\delta n_{xy}^\omega(\phi_m)}{\delta T}\right)\right]\Delta T \tag{4.28}$$

giving a temperature bandwidth of $\pm 24.1$ degrees for a 5mm long crystal. It can be shown that an estimate of the change in temperature due to self heating $\Delta T$, approximating the crystal as a cylinder, may be obtained from

$$\Delta T = \frac{1}{2\pi l K}\left(\frac{dQ}{dt}\right)[log_e(r_2) - log_e(r_1)] \tag{4.29}$$

where K is the thermal conductivity for KTP (2.3 W/m/K) [86], l is the crystal length, $\frac{dQ}{dt}$ is the power absorbed, $r_1$ is the beam radius in the crystal and $r_2$ is the radius of the doubling crystal. A value for $\frac{dQ}{dt}$ was obtained by using a measured value for the total loss per pass of the crystal for light at 1064 nm ($\simeq 0.2\%$) and the appropriate value for the fundamental intracavity power(278 W). Using equation 4.29 the temperature change and resulting phase mismatch due to self heating were calculated for the 2 x 2 x 5 mm KTP crystal and were found to be $\Delta T = 8.8$ degrees C and $\Phi = +29$ degrees respectively. Clearly this would slightly reduce the amount of second harmonic power which could be obtained.

The phase mismatches caused by temperature effects and tilts of the crystal as described above are effects which in practice occur simultaneously. The interaction of these effects means for example that compensating the effects of dispersion by tilting the KTP crystal will also have an effect on the fundamental intracavity power and thus self heating. This makes orienting the crystal to maximise the second harmonic power produced a very difficult process and may be why the maximum experimental power obtained was 1.38W compared with the theoretical maximum power for perfect phasematching and no dispersion of 2.4W.

### Experiments with 25mm KTP crystal

The 2 x 2 x 5 mm crystal was replaced with a crystal of dimensions 3 x 3 x 25 mm in an attempt to increase the second harmonic power obtained by increasing the interaction length.

The maximum amount of second harmonic power obtained was 4.2 W for a fundamental power of approximately 202 W with the distance between mirror $m_2$ and the end of the doubling crystal equal to 4 cm. The total path length in air was thus approximately 8 cm corresponding to a dispersion of 232 degrees. The theoretical maximum power for perfect phasematching and no dispersion was 27.2 W.

The angular displacements and temperature changes necessary to compensate for dispersions of 180 degrees and 90 degrees were calculated and are shown in Table 4.2.

The tilt necessary to change the fundamental polarisation by 90 degrees was calculated to be $\pm 1.8$ degrees. The temperature change and resulting phase mismatch due to self heating were calculated using a measured value for the loss per pass at 1064 nm of approximately 1% and found to be to be $\Delta T = 8.7$ degrees C and $\Phi = +143$ degrees, with the temperature bandwidth for the crystal being approximately $\pm 4.82$ degrees C.

Clearly the effects described in section 4.3.3 will also be present for the 25 mm KTP crystal with the associated difficulties in correctly orienting the crystal to optimise the second harmonic power. In general a long crystal is expected to be more difficult to set up than a short crystal because the same size of temperature or angular offset will have a significantly larger effect on the relative phase of the green and infra-red light. This certainly appeared to be borne out in practice.

## 4.3.4 Ring Cavity

### Introduction

While the linear cavity described in the previous section allowed the possibility of increasing the amount of second harmonic light produced from a doubling crystal using the double passing technique, it had the disadvantage that due to spatial hole burning it is difficult to obtain high powers of single frequency second harmonic

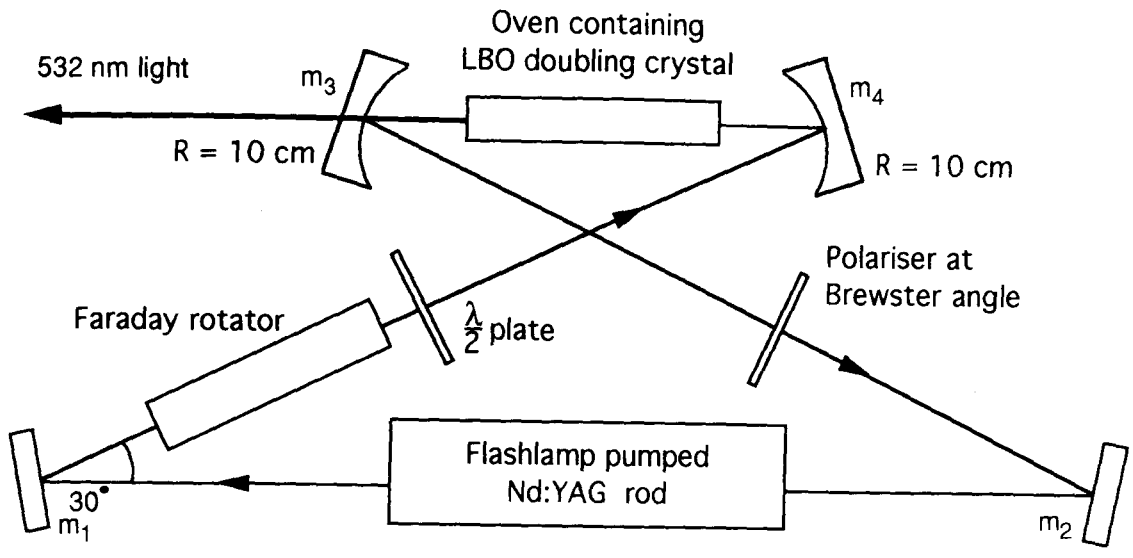


Figure 4.11: *Design of ring cavity used for intracavity frequency doubling.*

light. Investigations were thus made into using a 4 mirror ring cavity for intracavity frequency doubling.

### Cavity Description

A cavity was constructed made up of two plane mirrors, $m_1$ and $m_2$ and two spherical mirrors $m_3$ and $m_4$ arranged as shown in figure 4.11

The plane mirrors were coated to be high reflectors for light of 1064 nm and the curved mirrors coated to be highly reflecting for light of 1064 nm and highly transmitting for 532 nm. The beam size was a maximum approximately at the centre of the Nd:YAG laser rod and a waist was formed between the two curved mirrors. The cavity contained a plate at the Brewster angle to vertically polarise the fundamental intracavity light. The cavity also contained a Faraday rotator and a half wave plate to form an optical diode forcing the lasing to occur in one direction. The total cavity length was approximately 94.5 cm. The fundamental intracavity power was calculated by monitoring the power leakage through the calibrated mirror $m_2$ and the second harmonic power was measured after passing through a calibrated filter. The oven containing the LBO doubling crystal was inserted into the cavity between mirrors $m_3$ and $m_4$. Mirrors of radius of curvature 10 cm were initially used

for mirrors $m_3$ and $m_4$ and later replaced by mirrors of radius of curvature 8 cm in an attempt to reduce the waist size in the doubling crystal and thus increase the conversion efficiency. It was however noted that a similar decrease in waist size could be achieved by altering the spacing of the 10 cm mirrors.

### Second Harmonic Power Obtained

The maximum amount of second harmonic power obtained using this cavity was 2.8 W for a total intracavity fundamental power of approximately 207 W. Typically around 17 % of the power was not vertically polarised possibly as a result of birefringence in the Nd:YAG rod. The maximum second harmonic power was obtained using spherical mirrors of 10 cm radius of curvature as mirrors $m_3$ and $m_4$ giving a waist $\omega_0$ in the doubling crystal of approximately 68 $\mu$m x 61 $\mu$m. The waist was slightly astigmatic due to the non zero angle of incidence of the fundamental laser beam at the mirrors. The light obtained was observed to be contain many longitudinal and spatial modes.

Using equation 4.12 the amount of second harmonic light expected in theory was calculated to be approximately 10.6 W. Clearly there is a large discrepancy between the experimental and theoretical results. This is possibly due to the fact that the fundamental light was made up of a large number of spatial modes, so that the fundamental power was not concentrated into the $TEM_{00}$ mode assumed in equation 4.12.

The maximum single frequency ($TEM_{00q}$) second harmonic power obtained was approximately 980 mW for an intracavity power of approximately 72 W. The frequency spectrum and physical shape of the second harmonic beam are shown in figures 4.12 and 4.13. This single frequency power was obtained with mirrors $m_3$ and $m_4$ having radii of curvature of 8 cm, producing a waist in the doubling crystal $\omega_0$ of approximately 61 $\mu$m x 52 $\mu$m. The theoretical second harmonic power expected for the intracavity power of 72 W was calculated to be approximately 1.21 W. In this case the theoretical and experimental powers are in much closer agreement than for the multimode case.

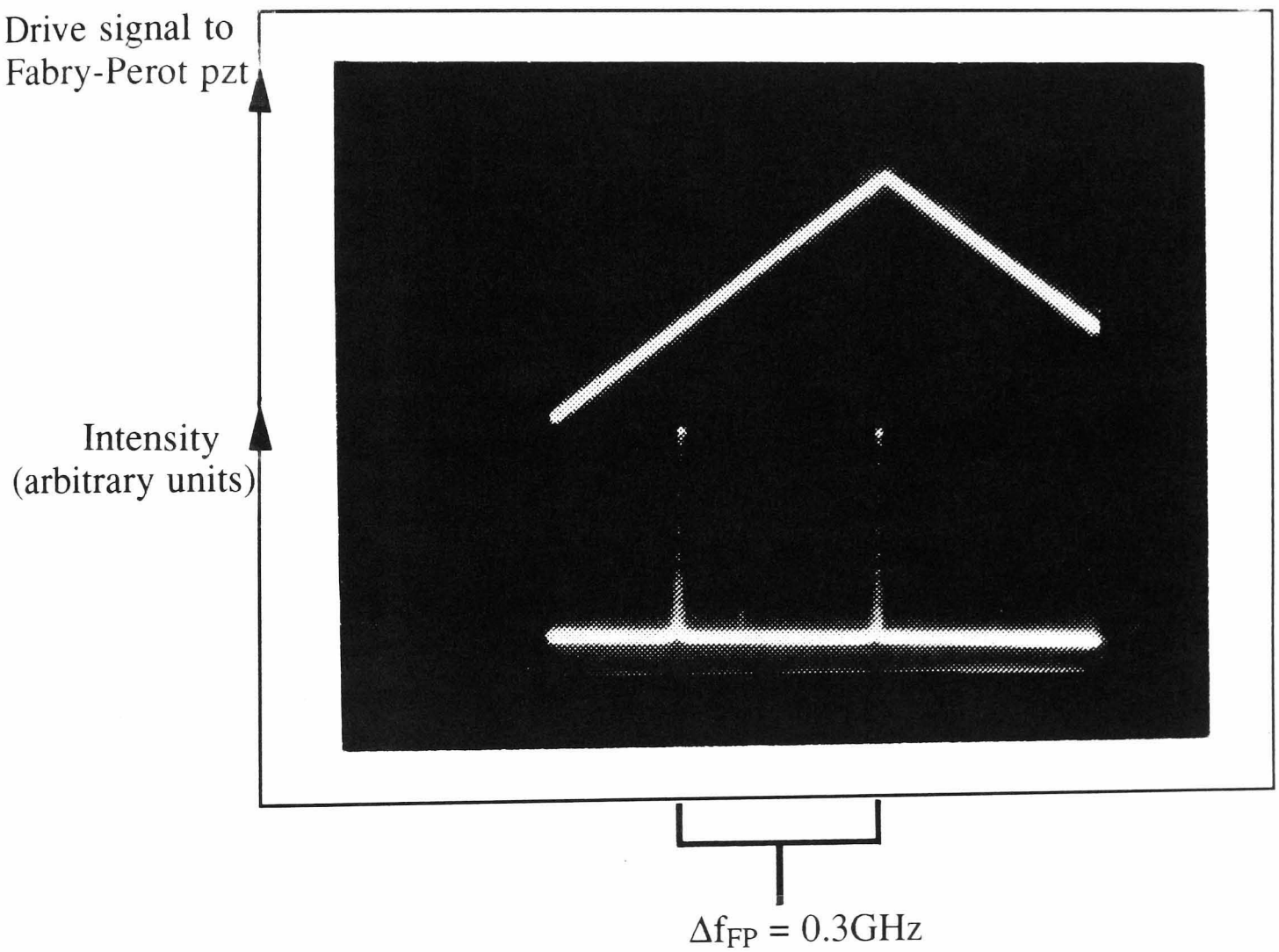


Figure 4.12: *Frequency spectrum of second harmonic light generated from four mirror ring cavity showing single frequency operation.*

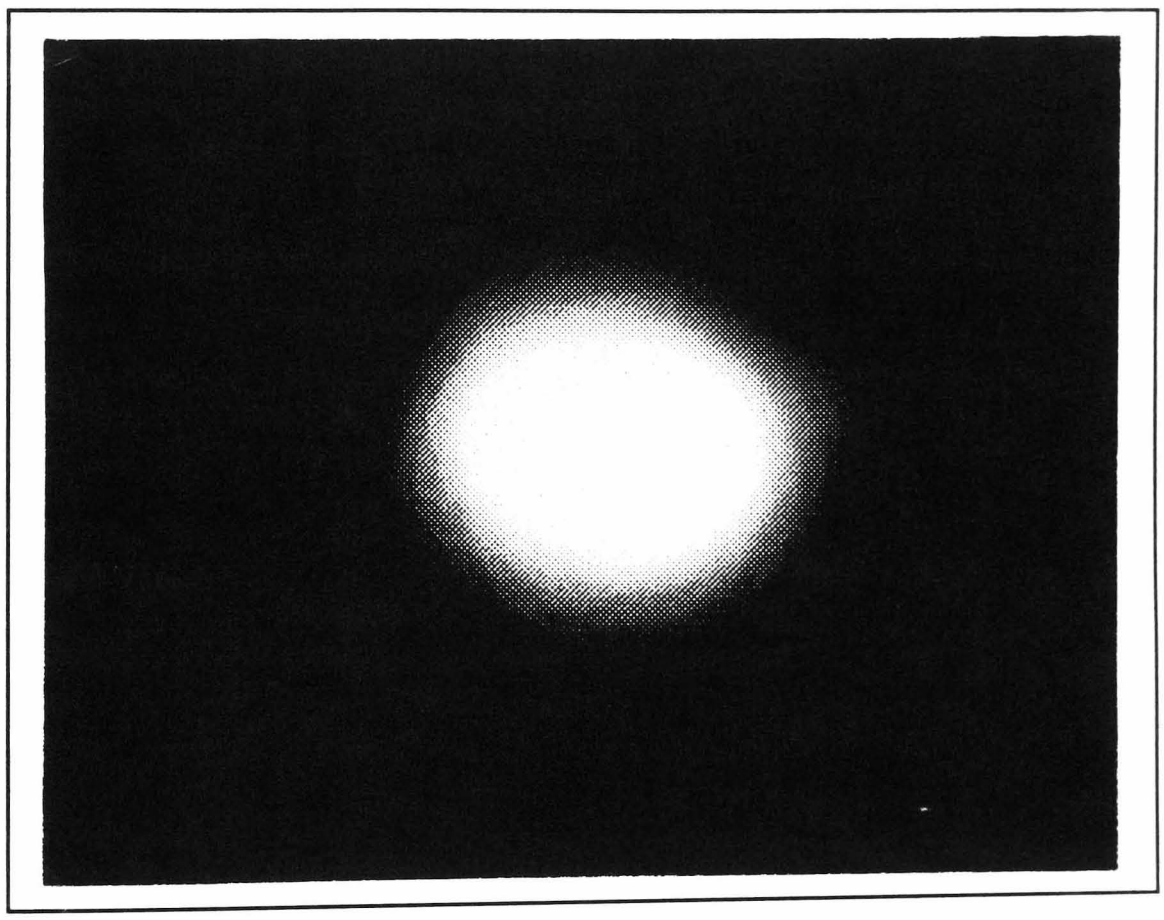

Figure 4.13: *Beam shape of second harmonic light obtained from four mirror ring cavity showing* $TEM_{00}$ *operation.*

## 4.4 Conclusions

From the investigations above the linear cavity in which the fundamental and second harmonic light was double passed through the doubling crystal appeared to be a relatively efficient way to obtain reasonable powers of *multimode* second harmonic light, avoiding the need to focus the fundamental beam to a very small waist in the doubling crystal and thus reducing the risk of damage to the crystal.

Intracavity frequency doubling in the linear cavity produced up to 4.6 W of second harmonic light using a 23 mm LBO doubling crystal and 4.2 W using a 25 mm KTP crystal. The advantages of the larger effective nonlinear coefficient of the KTP crystal were outweighed by the difficulties in aligning the crystal caused by the type II phasematching condition for KTP so that the LBO crystal was experimentally found to be more efficient in producing second harmonic light.

The difficulties of obtaining $TEM_{00q}$ operation in a linear cavity due to spatial hole burning meant that a ring cavity design seemed desirable. For the four mirror ring cavity design considered it was found that the maximum single frequency second harmonic power which could be obtained was approximately 980 mW for an intracavity power of approximately 72 W. This was in reasonable agreement with the theoretically expected power of 1.21 W. Disappointingly, this power was not high enough to allow the laser to be used as an argon ion laser replacement. At higher intracavity powers the laser could not be made to resonate in a $TEM_{00q}$ mode and the multi-spatial mode of the fundamental light at these high powers resulted in a significant decrease in the efficiency of the conversion process.

Subsequent investigations by P. McNamarra and J. Hough suggest that the failure of the laser to resonate in $TEM_{00q}$ mode may partially have been due to acoustic and vibrational noise coupling to the laser cavity mirrors from the laser power supply. Isolation of the cavity from this noise source might improve the mode structure and stability of the laser light and allow higher powers of $TEM_{00q}$ second harmonic light to be obtained. An alternative approach would be to use an external doubling cavity to allow the removal of the frequency conversion process from the laser resonator and thus relax the requirement of very high laser intracavity power in $TEM_{00q}$ mode [60].

# Chapter 5

# Conclusions and Future Prospects

In chapter 1 the criteria for choosing a suitable laser source to illuminate an interferometric gravitational wave detector were discussed, and it was concluded that the potential efficiency and high light powers available from Nd:YAG lasers made this type of laser a likely choice.

While Nd:YAG lasers are the proposed light sources for the GEO 600 and VIRGO projects, frequency doubled Nd:YAG light has been proposed for the illumination of the LIGO interferometer at a later stage in its operation. Frequency doubled Nd:YAG light offers a laser source which has the potential to provide the benefits which come from using a solid-state laser source with the added attraction of the increased sensitivity to power ratio and decrease in component size resulting from the shorter wavelength. This thesis thus detailed the results of investigations into aspects of Nd:YAG and frequency doubled Nd:YAG lasers for use in interferometric gravitational wave detectors.

A design of laser being proposed to illuminate long-baseline gravitational wave detectors uses a monolithic Nd:YAG ring laser as a master oscillator to seed a higher power Nd:YAG laser. It had been previously shown by Farinas et al [65] that the noise properties of the light from the slave laser are dominated by those of the master laser light. It was thus important to characterise the noise properties of monolithic Nd:YAG ring lasers and to demonstrate that it was possible to stabilise the levels of laser noise to those required for proposed gravitational wave detectors.

It is well known that solid state lasers are prone to a type of high frequency

intensity noise in the form of relaxation oscillations. Large amounts of noise at high frequencies may couple into measurements at low frequencies as a result of any nonlinearities in the detection process so it is important to be able to control noise at relaxation oscillation frequencies. This thesis extends previous work by Kane [68] on the damping of relaxation oscillations in low power monolithic Nd:YAG ring lasers to higher power lasers suitable for use as master oscillators for the injection locking of high power systems.

To this end an electronic feedback system was designed and constructed to damp relaxation oscillations in monolithic Nd:YAG ring lasers supplied by the Laser Zëntrum, Hannover. It was shown that this type of noise could be suppressed to a level of $1.9 \times 10^{-6}/\sqrt{Hz}$ which is acceptable for a laser of this type to be used as a master oscillator for a gravitational wave detector.

Experiments were also carried out on the design and construction of a dual loop feedback servo system to reduce the noise of a monolithic Nd:YAG ring laser at both relaxation oscillation frequencies (a few hundred kHz) and in the frequency range of interest for gravitational wave detection (from a few tens of Hz to a few kHz). The stabilised levels of intensity noise achieved of $4.6 \times 10^{-8}/\sqrt{Hz}$ at 500 Hz and $2.3 \times 10^{-6}/\sqrt{Hz}$ at the relaxation oscillation frequency of around 260 kHz to 270 kHz were low enough to make this type of laser a good candidate for a seed laser.

It was also important to characterise the frequency noise of this type of laser. Measurements were made of the frequency noise of monolithic Nd:YAG ring lasers supplied by the Laser Zëntrum, Hannover and by Lightwave Electronics respectively. For the Hannover laser an upper limit to the laser frequency fluctuations at 500 Hz was measured to be $\simeq 200\ Hz/\sqrt{Hz}$. Also of interest was the frequency noise at relaxation oscillation frequencies. Measurements of this noise set an upper limit of $1\ Hz/\sqrt{Hz}$ (above a background of $0.4\ Hz/\sqrt{Hz}$) for the frequency noise. When a servo operating to damp the relaxation oscillations in intensity was operated the residual peak at the relaxation oscillation frequency in the frequency noise spectrum was reduced to the level of the measurement background. Experiments using the Lightwave laser set an upper limit on the frequency noise at the relaxation oscilla-

tion frequency (in this case $\simeq$ 700 kHz) of 0.35 $Hz/\sqrt{Hz}$ above a background of 0.1 $Hz/\sqrt{Hz}$. This residual peak also reduced into the background when an intensity noise reduction system for the laser was operated. It was thus concluded that frequency noise at relaxation oscillation frequencies was unlikely to cause problems with any measurements at the frequencies of interest for gravitational wave detection.

Investigations were made into the intra-cavity frequency doubling of light from a high power flashlamp pumped Nd:YAG laser using linear and ring designs of cavity. The linear cavity design allowed both the fundamental and second harmonic light to pass twice through the doubling crystal before the second harmonic light was extracted from the cavity. If the cavity was arranged so that the second harmonic and fundamental beams were in phase on re-entering the doubling crystal then in theory the beams of second harmonic light could add to produce up to four times the power which was expected on a single pass. Results were obtained using a 23 mm crystal of LBO, and, for comparison, KTP crystals of lengths 5 mm and 25 mm. The maximum second harmonic power obtained using the LBO crystal was 4.6 W, and the maximum using the 5 mm and 25 mm KTP crystals was 1.38 W and 4.2 W respectively.

In each case the light obtained was in several spatial and longitudinal modes and no single mode operation was observed. It was thus concluded that while the linear design of doubling cavity was a relatively simple and efficient way of obtaining reasonably high powers of multi-mode frequency doubled light, it seemed desirable to use a cavity - a ring - in which single frequency light necessary for the illumination of gravitational wave detectors could be obtained.

The maximum total second harmonic power obtained using the LBO crystal in the ring cavity was 2.8 W. This, however, was again in several spatial and longitudinal modes. $TEM_{00q}$ operation could be achieved at lower intra-cavity fundamental powers and the maximum single frequency second harmonic power obtained was approximately 980 mW. It seemed that the limit to the amount of second harmonic single frequency power which could be obtained was set by the intra-cavity power of the laser. Subsequent investigations suggested that the failure of the laser to res-

onate in $TEM_{00q}$ mode at high powers may have partially been due to acoustic and vibrational noise coupling to the laser cavity mirrors from the laser power supply. Isolation of the laser cavity from this noise source may improve the mode structure and stability of the laser light and allow higher powers of single frequency second harmonic light to be obtained.

An alternative approach to improving performance would be to place the doubling crystal in an external resonant cavity. This would allow separation of the lasing and doubling processes, allowing each of the processes to be more easily optimised.

It is also possible that high powers of second harmonic light may be more easily achieved through the use of new nonlinear materials currently under development.

# Appendix A

# Intensity of Second Harmonic Light Produced in a Linear Double Pass Cavity

In this Appendix an equation is derived for the resultant intensity of second harmonic light $I_t^{2\omega}$ produced in the case of linear intra-cavity frequency doubling when a mirror some distance away from the doubling crystal is used to reflect both the fundamental and second beams through the doubling crystal for a second time before the second light is extracted from the cavity. The situation described is shown in figure 4.2

The intensity, $I_1^{2\omega}$ of the second harmonic light produced after a single pass of the fundamental beam through a doubling crystal may, from equation 4.12 be written

$$I_1^{2\omega} = (I^{\omega})^2 \frac{2\omega^2 d_{eff}^2 l^2}{n^3 c^3 \varepsilon_0} \times \frac{\sin^2(\frac{\Delta kl}{2})}{(\frac{\Delta kl}{2})^2} \tag{A.1}$$

or equivalently

$$I_1^{2\omega} = I_0^{2\omega} \frac{\sin^2(\frac{\Delta kl}{2})}{(\frac{\Delta kl}{2})^2} \tag{A.2}$$

The above equation is obtained from an electric field vector $A_1^{2\omega}$ for the second harmonic at this point which has the form

$$A_1^{2\omega} = A_0^{2\omega} \frac{\sin(\frac{\Delta kl}{2})}{\frac{\Delta kl}{2}} e^{-i\frac{\Delta kl}{2}} \tag{A.3}$$

where $A_1^{2\omega} A_1^{2\omega *} \propto I_1^{2\omega}$ and $\frac{\Delta kl}{2}$ is the phase shift of the second harmonic light with respect to the fundamental light.

Note that from equation 4.11 for the second harmonic light *leading* the fundamental, $\Delta k$ is negative and when the harmonic light *lags* the fundamental, $\Delta k$ is positive.

We can thus rewrite equation A.3 as

$$A_1^{2\omega} = A_0^{2\omega} \frac{\sin \Phi}{\Phi} e^{-i\Phi} \tag{A.4}$$

where $\Phi = \frac{\Delta k l}{2}$. If the fundamental and second harmonic beams travel some distance $d$ in air before re-entering the crystal, dispersion causes the second harmonic beam to lag the fundamental by some phase shift $\psi$. On re-entering the crystal the electric field $A_2^{2\omega}$ of the second harmonic beam is thus described by

$$A_2^{2\omega} = A_0^{2\omega} \frac{\sin \Phi}{\Phi} e^{-i(\Phi+\psi)} \tag{A.5}$$

The fundamental and second harmonic fields then pass through the doubling crystal for a second time. On this return pass through the crystal it is necessary to consider two effects

1. The second harmonic beam $A_2^{2\omega}$ on passing through the crystal is shifted in phase with respect to the fundamental beam by a further $2\Phi$ and can be written

$$A_2^{2\omega} = A_0^{2\omega} \frac{\sin \Phi}{\Phi} e^{-i(\psi+3\Phi)} \tag{A.6}$$

2. As the fundamental beam passes through the crystal there is further second harmonic generation producing a beam described by

$$A_3^{2\omega} = A_0^{2\omega} \frac{\sin \Phi}{\Phi} e^{-i\Phi} \tag{A.7}$$

The total resultant second harmonic light $A_t$ produced after a double pass of the light throught the doubling crystal is thus

$$A_t^{2\omega} = A_2^{2\omega} + A_3^{2\omega} = A_0^{2\omega} \frac{\sin \Phi}{\Phi} \left[ e^{-i\Phi} + e^{-i(\psi+3\Phi)} \right] \tag{A.8}$$

which may be written

$$A_t^{2\omega} = \underbrace{2A_0^{2\omega} \frac{\sin \Phi}{\Phi} \cos\left(\frac{\psi}{2} + \Phi\right)}_{amplitude} \underbrace{e^{-i\Phi} e^{-i(\frac{\psi}{2}+\Phi)}}_{phase} \tag{A.9}$$

The resultant intensity $I_t^{2\omega}$ of the second harmonic as a function of phase mismatch of the fundamental and second harmonic beams in the crystal and dispersion of the fundamental and second harmonic beams in air is then given by

$$I_t^{2\omega} \propto 4(A_0^{2\omega})^2 \frac{\sin^2 \Phi}{\Phi^2} \cos^2 \left( \frac{\psi}{2} + \Phi \right) \tag{A.10}$$

The *relative* intensity of the second harmonic with respect to the maximum possible value, as a function of phase mismatch and dispersion is thus

$$I_{rel}^{2\omega} = \frac{\sin^2 \Phi}{\Phi^2} \cos^2 \left( \frac{\psi}{2} + \Phi \right) \tag{A.11}$$

# Bibliography


[1] J.H. Taylor and J.M. Weisberg, *The Astrophysical Journal*, **253** 908 (1982)

[2] D. Blair, in *The detection of gravitational waves*, Cambridge University Press, Cambridge (1991)

[3] B.F. Schutz, *Proc. of First Edoardo Amaldi Conf. on Grav. Wave Exp.*, in press, World Scientific (1995)

[4] K.S. Thorne in S.W. Hawking and W. Israel, *300 Years of Gravitation*, Cambridge University Press, Cambridge (1987)

[5] S. Bonazzola and J.-A. Marck, *Annu. Rev. Nucl. Part. Sci.*, **45** 655-717 (1994)

[6] J. Weber, *Phys. Rev. Lett.*, **22** (24) 1320 (1969)

[7] A.G. Lyne and D.R. Lorimer, *Nature*, **369** L17 (1991)

[8] J. Hough, B.J. Meers, G.P. Newton, N.A. Robertson, H. Ward, B.F. Schutz, I.F. Corbett and R.W.P. Drever, *Vistas in Astronomy*, **30** 109-134 (1987)

[9] B.F. Schutz, *Frontiers in Astrophysics*, 45-68 (1995)

[10] B.F. Schutz, *Nature*, **323** 310-311 (1986)

[11] S.J. Curran and D.R. Lorimer, *Mon. Not. R. Astron. Soc.*, in press (1995)

[12] A. Tutukov and L. Yungelson, *Mon. Not. R. Astron. Soc.*, **260** 675 (1993)

[13] K. Danzmann et al, *LISA: Proposal for a Laser-Interferometric Gravitational Wave Detector in Space, Max-Planck-Institut für Quantenoptik, Preprint 177.* Garching, Germany (1993)

[14] W.H. Press and K.S. Thorne, *Ann. Rev. Astron. and Astrophys.*, **10** 335 (1972)

[15] R.V. Wagoner, *The Astrophysical Journal*, **278** 345 (1984)

[16] P. Astone, J.A. Lobo and B.F. Schutz, *Class. Quantum Grav.*, **11** 2093-2112 (1994)

[17] B. Allen and E.P.S. Shellard, *Phys. Rev. D*, **45** 1898-1912 (1992)

[18] R.W. Hellings, P.S. Callahan, J.D. Anderson and A.T. Moffett, *Phys. Rev. D*, **23** 844 (1981)

[19] V.M. Kaspi, J.H. Taylor and M.F. Ryba, *The Astrophysical Journal*, **428** 713-728 (1994)

[20] B. Bertotti et al, *Astronomy and Astrophysics*, in press

[21] R.L. Garwin and J.L. Levine, *Phys. Rev. Lett.*, **31** 176 (1973)

[22] R.W.P. Drever, J. Hough, R. Bland and G.W. Lessnoff, *Nature*, **246** 340 (1973)

[23] H. Billing, P. Kafka, K. Maischberger, F. Meyer and W. Winkler, *Lett. Nuovo Cim.*, **12** 111 (1975)

[24] B. Hamilton, *Proc. MG7 Meeting*, Stanford (1994) in press.

[25] G. Frossati, *Proc. MG7 Meeting*, Stanford (1994) in press.

[26] R.L. Forward, *Phys. Rev. D*, **17** 379 (1978)

[27] R. Weiss, *Massachusetts Institute of Technology Quarterly Progress Report*, **105** 54 (1972)

[28] D.I. Robertson, E. Morrison, J. Hough, S. Killbourn, B.J. Meers, G.P. Newton, N.A. Robertson, K.A. Strain and H. Ward, *Rev. Sci. Instrum.*, in press (1995)

[29] D. Shoemaker, R. Schilling, L. Schnupp, W. Winkler, K. Maischberger and A. Rüdiger, *Phys. Rev. D*, **38** (2) (1988)

[30] A. Gillespie, *PhD Thesis*, California Institute of Technology, (1995)

[31] L. Livas, R. Benford, D. Dewey, A. Jeffries, P. Linsay, P. Saulson, D. Shoemaker and R. Weiss, *Proc. MG4 Meeting*, Rome, (1985)

[32] H. Mizuno et al, *Proc. MG7 Meeting*, Stanford (1994) in press.

[33] D.B. Blair, *private communication* (1995)

[34] K. Tsubono, *Proc. MG7 Meeting*, Stanford (1994) in press.

[35] D.E. McClelland, D.B. Blair, *Proc. MG7 Meeting*, Stanford (1994) in press.

[36] W.A. Edelstein, J. Hough, J.R. Pugh, W. Martin, *J. Phys. E: Sci. Instrum.*, **11** (1978)

[37] K. Danzmann et al, *GEO 600: Proposal for a 600m Laser-Interferometric Gravitational Wave Antenna, Max-Planck-Institut für Quantenoptik, Report 190*, Garching, Germany (1994)

[38] J.E. Logan, *PhD Thesis*, University of Glasgow, (1993)

[39] N. A. Robertson, in *The detection of gravitational waves*, Cambridge University Press, Cambridge (1991)

[40] A. Brillet, A. Giazotto, M. Jacquemet et al, *VIRGO Final Conceptual Design* (1992)

[41] K.S. Thorne, *Light scattering and the proposed baffle configuration for the LIGO, California Institute of Technology Report GRP-299* (1989)

[42] L. Schnupp, *poster at GR12*, Boulder, Colorado

[43] B.J. Meers and K.A. Strain, *Phys. Rev. A*, **44** (7) 4693 (1991)

[44] T.M. Niebauer, R. Schilling, K. Danzmann, A. Rüdiger and W. Winkler, *Phys. Rev. A*, **43** (9) 5022 (1991)

[45] W. Winkler, *private communication*

[46] R.W.P. Drever et al, *Proceedings of the Ninth International Conference on General Relativity and Gravitation*, Ed. by E. Schmutzer, (VEB Deutscher Verlag der Wissenschaften, Berlin (1983)

[47] R.W.P. Drever, *Proceedings of the Les Houches NATO Advanced Study Institute*, Ed. by T. Piran and N. Derouelle, North Holland Publishing Company, Amsterdam (1983)

[48] B.J. Meers, *Phys. Rev. D*, **38** 2317 (1988)

[49] J. Mizuno, K.A. Strain, P.G. Nelson, J.M. Chen, R. Schilling, A. Rüdiger, W. Winkler and K. Danzmann, *Phys. Lett. A*, **175** 273-276 (1993)

[50] J. Hough, *private communication*

[51] R.W.P. Drever, J.L. Hall, F.V. Kowalski, J. Hough, G.M. Ford, A.J. Munley and H. Ward, *Appl. Phys. B*, **31** 97-105 (1983)

[52] J. Hough et al, in *The detection of gravitational waves*, Cambridge University Press, Cambridge (1991)

[53] A. Rüdiger, R. Schilling, L. Schnupp, W. Winkler, H. Billing and K. Maischberger, *Optica Acta*, **26** (5) 641-658 (1981)

[54] A. Rüdiger, *private communication* (1995)

[55] E. Morrison, J. Hough, B.J. Meers, G.P. Newton, D.I. Robertson, K.A. Strain, P.J. Veitch and H. Ward, *Proc. of MG6 Meeting*, Part B, 1505, World Scientific (1992)

[56] R.E. Vogt, R.W.P. Drever, K.S. Thorne, F.J. Raab, and R. Weiss, *A Laser Interferoneter Gravitational-Wave Observatory (LIGO)*, Proposal to The National Science Foundation (1989)

[57] G.A. Kerr and J.Hough, *Appl. Phys. B*, **49**, 491-495 (1989)

[58] I. Freitag, D. Golla, S. Knoke, W. Schöne, H. Zellmer, A. Tünnermann and H. Welling, *Optics Letters*, **20** (5) 462-464 (1995)

[59] R.J. Shine Jr., A.J. Alfrey and R.L. Byer, *Optics Letters*, **20** (5) 459-461 (1995)

[60] S.T. Yang, C.C. Pohalski, E.K. Gustafson, R.L. Byer, R.S. Feigelson, R.J. Raymakers, and R.K. Route, *Optics Letters*, **16** 1493 (1991)

[61] S. Rowan, A.M. Campbell, G.P. Newton, J. Hough, M. Gray and J. Hong, *Proc. MG7 Meeting*, Stanford (1994) in press.

[62] V.B. Sigachev, M.I. Timoshechkin and M.N. Shkunov, *Bull. Russ. Ac. Sci.*, **58** (2) 185-188

[63] J. Hough, G.P. Newton, N.A. Robertson, H. Ward, A.M. Campbell, J.E. Logan, D.I. Robertson, K.A. Strain, K. Danzmann, H. Lück, A. Rüdiger, R. Schilling, M. Schrempel, W. Winkler, J.R.J. Bennet, V. Kose, M. Khüne, B.F. Schutz, D. Nicholson, J. Shuttleworth, H. Welling, P. Aufmuth, R. Rinkleff, A. Tünnermann, B. Wilke, *Proc. of MG 7 Meeting*, Stanford (1994) in press.

[64] A. Abramovici, W.E. Althouse, R.W.P. Drever, Y. Gürsel, S. Kawamura, F.J. Raab, D. Shoemaker, L. Sievers, R.E. Spero, K.S. Thorne, R.E. Vogt, R. Weiss, S. E. Whitcomb, and M.E. Zucker, *Science*, **256** (1992)

[65] A.D. Farinas, E.K. Gustafson and R.L. Byer, *J. Opt. Soc. Am. B*, **12** (2) 328-334 (1995)

[66] T.J. Kane and R.L. Byer, *Optics Letters*, **10** (2) 65-67 (1985)

[67] A.E. Siegmann, *Lasers*, Oxford University Press (1986)

[68] T.J. Kane, *IEEE Phot. Tech. Lett.*, **2** (4) 244-245 (1990)

[69] A. Yariv, *Quantum Electronics*, Third Edition, John Wiley & Sons (1989)

[70] W. Koechner, *Solid-State Laser Engineering*, 3rd Edition, Springer-Verlag (1992)

[71] I. Kröpke, *private communication* (1991)

[72] C.C. Harb, M.B. Gray, H.-A. Bachor, R. Schilling, P. Rottengatter, I. Freitag and H. Welling, *IEEE Journal of Quantum Electronics*, **30** 12 (1994)

[73] N.A. Robertson, S. Hoggan, J.B. Mangan and J. Hough, *Appl. Phys. B*, **39** 149-153 (1986)

[74] R.W.P. Drever, J.L. Hall, F.V. Kowalski, J. Hough, G.M. Ford, A.J. Munley and H. Ward *Appl. Phys. B.* **31** 97-105 (1983)

[75] L.G. Kazovsky and D.A. Atlas, *J. Light. Tech.*, **8** (3) 294-301 (1990)

[76] G.A. Kerr, *PhD Thesis*, University of Glasgow, (1986)

[77] V. Magni, G. Cerullo, S. De Silvestro, O. Svelto, L.J. Qian, and M. Danailov, *Optics Letters*, **18** 2111 (1993)

[78] R.L. Byer In *Nonlinear Optics*, Proceedings of the Sixteenth Scottish Universities Summer School in Physics 1975, Academic Press, London, (1977)

[79] S.P. Velsko, M. Webb, L. Davies and C. Huang, *IEEE J. Qu. Elect.*, **27** (9) 2182 (1993)

[80] S. Lin, Z. Sun, B. Wu and C. Chen, *J. Appl. Phys.*, **67** (2) 634 (1990)

[81] R.C. Eckardt, H. Masuda, Y.X. Fan and R.L. Byer, *IEEE J. Qu. Elect.*, **26** (5) 922 (1990)

[82] A. Carmichael, *PhD Thesis*, University of Glasgow (1992)

[83] R.G. Smith, *IEEE J. Qu. Elect.*, **Qu-E 6** (4) 215 (1970)

[84] J.M. Yarborough, J. Falk and C.B. Hitz, *Appl. Phys. Lett.*, **18** (3) 70 (1971)

[85] K. Kato, *IEEE J. Qu. Elect.*, **28** (10) (1992)

[86] H. Minemoto, Y. Ozaki and N. Sonoda, *J. Appl. Phys.*, **76** (7) 3975 (1994)

Physics Letters A 170 (1992) 363–369
North-Holland

PHYSICS LETTERS A

# Apparent relaxation oscillations in the frequency noise of a diode-pumped miniature Nd:YAG ring laser

A.M. Campbell, S. Rowan and J. Hough
*Department of Physics and Astronomy, University of Glasgow, Glasgow G12 8QQ, Scotland, UK*

Received 21 August 1992; accepted for publication 10 September 1992
Communicated by J.P. Vigier

We have set an upper limit to apparent relaxation oscillations in the frequency noise of a diode-pumped single-mode monolithic Nd:YAG ring laser using an RF reflection locking technique, and have observed the effect on the frequency noise spectrum of a servo system which damps relaxation oscillations as observed in intensity noise.

## 1. Introduction

The development of a high power stable continuous wave Nd:YAG laser operated at its fundamental wavelength of 1064 nm, or frequency doubled to 532 nm, is of great interest for use in the next generation of gravitational wave detectors [1]. Diode-pumped monolithic Nd:YAG ring lasers, which show very low noise characteristics at low frequencies [2], could be ideal candidates for seeding such a high power cw Nd:YAG laser. However, above about 100 kHz, relaxation oscillations produce intensity noise in these lasers. Although the relaxation oscillation frequencies are well above the frequencies of interest for gravitational wave detectors ($<100$ Hz to a few kHz), large fluctuations in intensity or frequency at these frequencies could couple into measurements at lower frequencies through nonlinearities in the detection system.

Relaxation oscillations observed in the intensity noise of Nd:YAG lasers are well known, and it is relatively easy to damp them in diode pumped lasers by servo controlling the diode current [3]. However, as far as we are aware, there is only one report in the literature of frequency noise at relaxation oscillation frequencies [4] in Nd:YAG lasers. This was for the 1320 nm transition in a diode-pumped Nd:YAG rod laser. These measurements gave an upper limit to frequency noise of about 200 Hz/$\sqrt{\text{Hz}}$ due to a peak at the relaxation oscillation frequency. It is important to have a more accurate measure of this noise for miniature diode-pumped ring lasers.

In this Letter we present our results of the measurement of frequency noise at the relaxation oscillation frequency in a miniature Nd:YAG ring laser, and of the effect on this noise of a servo system used to damp relaxation oscillations in the intensity noise.

## 2. Experimental system

The laser we used was a monolithic diode-pumped miniature Nd:YAG ring laser built at the Laser Zentrum in Hannover, Germany, based on the original design by Kane and Byer [5]. This laser emits up to 400 mW in the $TEM_{00}$ mode, but for measurements made here was run at 200 mW.

To measure frequency noise we used a Fabry–Pérot cavity of linewidth 15 MHz as a discriminator. The resonant frequency of the cavity was servo controlled to the frequency of the laser at low frequencies ($<1$ kHz) using RF reflection locking [6] and the error point of the system was used to allow measurement of frequency noise at high frequencies. The RF reflection locking technique provides a high degree of rejection of cross-coupling of intensity noise into the frequency noise signal provided that the cavity is locked at the centre of its resonance.

The experimental apparatus is shown in fig. 1. Light from the laser, after isolation by a Faraday effect device, is passed through a half wave plate to rotate the polarisation to the correct direction for the electro-optic modulator which phase modulates the light at 10 MHz for the RF reflection locking. Some light is split off for a servo which may be used to damp the relaxation oscillations as observed in the intensity noise spectrum (this is discussed in the appendix), and some light goes to a monitor photodiode. The fraction of the light used to make frequency noise measurements is mode-matched into the Fabry–Pérot discriminating cavity using two lenses; the visibility was about 0.8. The polarising beam splitter and quarter wave plate allow the light reflected from the cavity to be directed onto a pho-

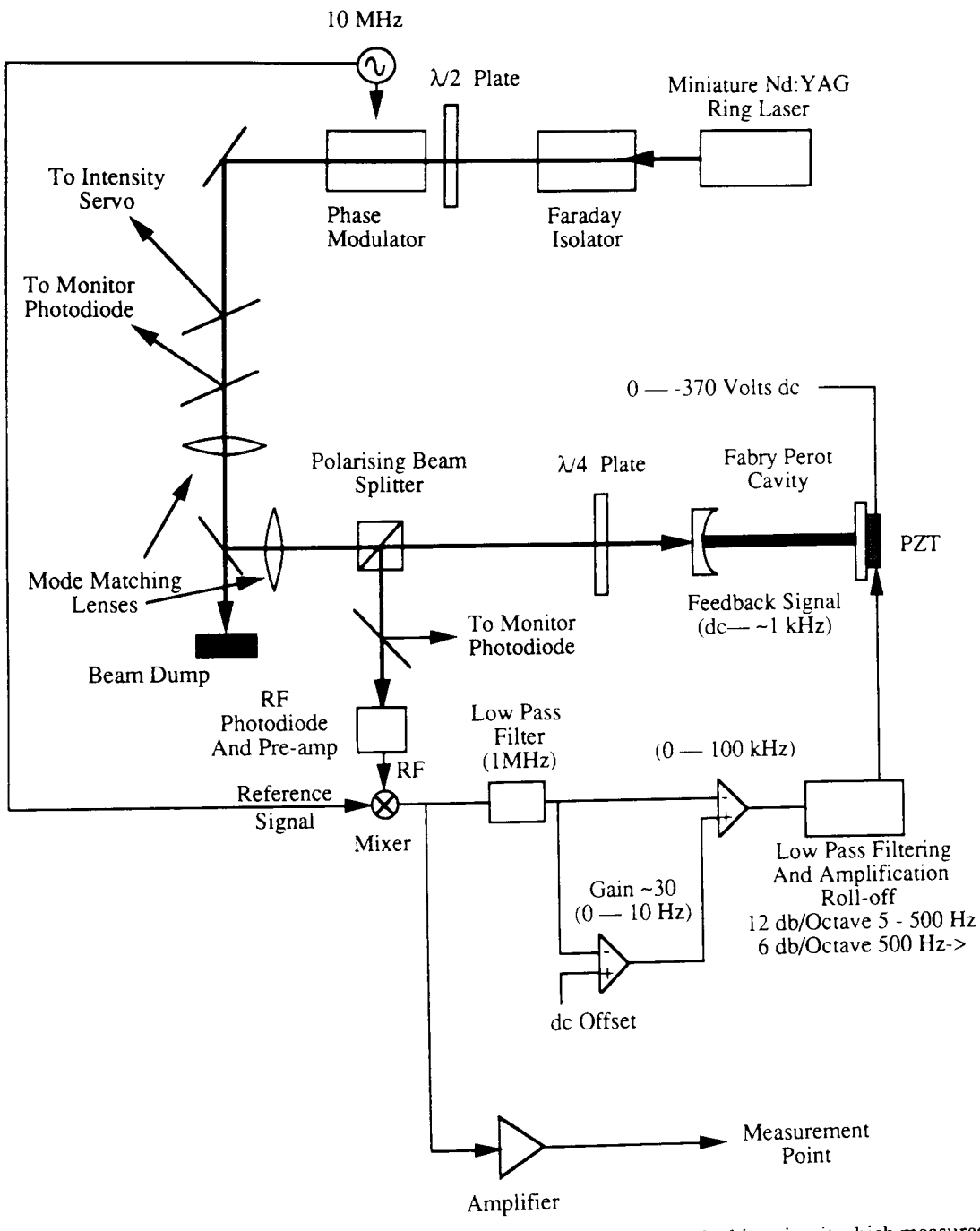


Fig. 1. Schematic diagram of the optical and electronic arrangement for the RF reflection locking circuit which measures frequency noise at the relaxation oscillation frequency.

todiode and amplifier tuned to the RF modulation frequency and to another monitor photodiode. The signal from the photodiode and amplifier is amplified, coherently demodulated at the mixer, filtered and fed back to a piezo-electric device on which one of the cavity mirrors is mounted. This ensures the resonant frequency of the cavity remains locked to the frequency of the laser over a bandwidth of about 1 kHz. Measurements of noise at hundreds of kHz are made at the error point of the system, directly after the mixer. Included in the feedback is a parallel path to boost the dc and low frequency gain, and a facility for adding in a small amount of dc to adjust for any offset of the locking point caused by RF pickup or by spurious amplitude modulation of the light at 10 MHz by the electro-optic modulator. The other side of the PZT is connected to a battery driven variable dc supply to allow coarse adjustment of the cavity resonant frequency so that lock can be achieved.

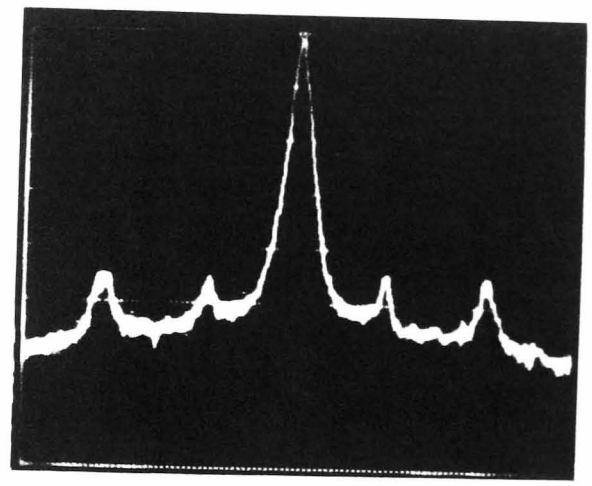

Fig. 2. First frequency noise measurement of the laser showing a peak at the relaxation oscillation frequency (250 kHz) and an intensity peak at 120 kHz resulting from a signal applied to the diode current driver. The relaxation oscillation peak corresponds to a frequency noise level of 7 Hz/$\sqrt{\text{Hz}}$. The centre of the diagram is 0 Hz, with a full screen frequency span of 750 kHz. The resolution bandwidth is 10 kHz. One side of the screen is a mirror image of the other side. The calibration of the vertical scale is 10 dB/division.

## 3. Results

We made two sets of measurements on this laser, one with better sensitivity; but both sets of results are of interest and will be discussed.

### *3.1. First measurement*

The first measurement is shown in fig. 2. This is a spectrum of the frequency noise measured using a Hewlett Packard 8590A RF spectrum analyser. An instrumental peak at 0 Hz is at the centre of the screen and one half of the screen is essentially a mirror image of the other. The full screen span is 750 kHz: the region of interest spans 375 kHz. The peak at 250 kHz is at the relaxation oscillation frequency: this peak represents an upper limit on the apparent frequency noise due to relaxation oscillations and we calibrated its level to be about 7 Hz/$\sqrt{\text{Hz}}$ from measurement of the slope of the discriminator curve of the cavity. The fractional intensity noise at this freyuency is about $10^{-5}/\sqrt{\text{Hz}}$. The other peak at 120 kHz is due to an intensity modulation signal imposed by us on the laser by modulating the diode pump current at the diode driver input. This signal allowed us to minimise sensitivity to intensity noise in the system by adjusting the dc offset in the servo loop.

An interesting effect was observed when the dc offset in the servo loop was adjusted to either side of the value which minimised the applied 120 kHz intensity modulated signal. Figure 3 shows the relative size of the two peaks (intensity modulation and relaxation oscillation) when the dc offset was adjusted to increase the applied intensity peak by about 10 dB on either side of its minimum value. The peak associated with the relaxation oscillations did not increase by the same amount in the two cases, the difference in heights between the relaxation oscillation peak and the applied peak being about 7 dB on one side, and about 3 dB on the other side. This suggests that there is some difference in the type of noise associated with the applied intensity peak and with the relaxation oscillation peak. Consistent with this finding is the fact that different values of dc offset were required to minimise the relaxation oscillation peak and the applied intensity peak.

From the above measurements it seems likely that either the applied intensity peak or the relaxation oscillation peak is at least partly due to frequency noise

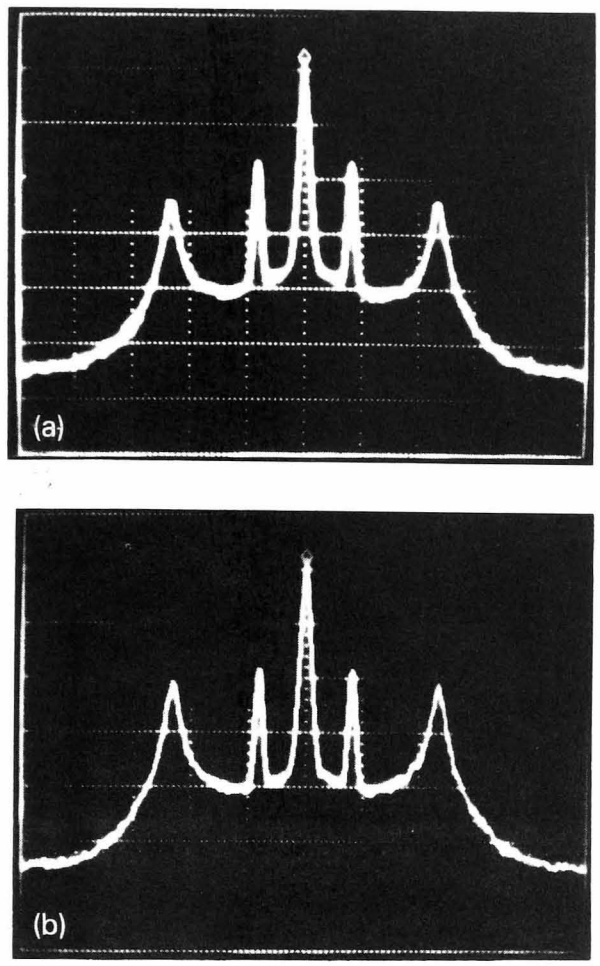


Fig. 3. Noise spectrum on (a) one side and (b) the other side of the dc position which minimised the 120 kHz intensity peak, showing an asymmetry in the relative sizes of the relaxation oscillation peak and the applied peak. The relaxation oscillation peak is at 350 kHz because a higher diode pumping current was used for these measurements. Screen centre is at 0 Hz, with a full screen frequency span of 1.5 MHz. The resolution bandwidth is 10 kHz. The calibration of the vertical scale is 10 dB/division.

or beam geometry fluctuations (which can couple into the observed frequency noise spectrum). In order to investigate the situation further we observed the effect of actively damping the relaxation oscillations as observed in intensity noise. The feedback signal from the servo system was applied to the diode pump current driver, where previously we had applied our intensity peak. (A diagram of this servo system and its Nyquist plot is shown in fig. 4 and is discussed in the appendix.) We observed the intensity and the frequency noise spectra simultaneously as the intensity servo was turned on. The relaxation oscillation reduced in exactly the same way in both spectra: a 10 dB reduction in the relaxation oscillation peak in the intensity noise spectrum corresponded to a 10 dB reduction in the relaxation oscillation peak in the frequency noise spectrum. If the signal at the input to the diode driver caused anything other than intensity noise in the laser light (for instance frequency noise or beam geometry fluctuations) we would not expect such a simple relationship. We therefore draw the following three conclusions as the most likely explanation of these observations:

- A signal applied to the diode current driver does produce intensity modulation with few, if any, side effects. Hence the 120 kHz peak, produced by a signal applied to the diode current driver, as observed in the frequency noise measurement system, is indeed caused by intensity noise in the laser;
- The peak in the frequency noise spectrum associated with the relaxation oscillations is partly due to frequency noise or beam geometry fluctuations in addition to some intensity noise;
- Fluctuations in frequency or beam geometry associated with the relaxation oscillations are reduced by the feedback system used to damp the relaxation oscillations observed in intensity noise.

### *3.2. Second measurement*

We repeated the measurements in order to investigate our findings more fully at improved sensitivity. We cleaned and realigned the optics (in particular we realigned the beam through the electro-optic modulator). We operated with a mode-matching which gave a visibility of 0.8, and with a modulation index of 0.24. These experiments gave us an improved measurement of the level of the apparent frequency noise due to relaxation oscillations, this being about 1 Hz/$\sqrt{\text{Hz}}$ at 250 kHz. The measurement floor was about 0.4 Hz/$\sqrt{\text{Hz}}$ of which about 0.2 Hz/$\sqrt{\text{Hz}}$ was photon shot noise. This measurement is shown in fig. 5a, where the applied peak is also shown at a frequency of 180 kHz.

In this case, however, both the applied intensity peak and the peak due to relaxation oscillations minimised at the same value of dc offset in the cavity servo loop, and when we altered the dc offset on either side of the value that minimised the peaks, we could discern no difference in the relative size of the applied peak and the peak due to relaxation oscil-

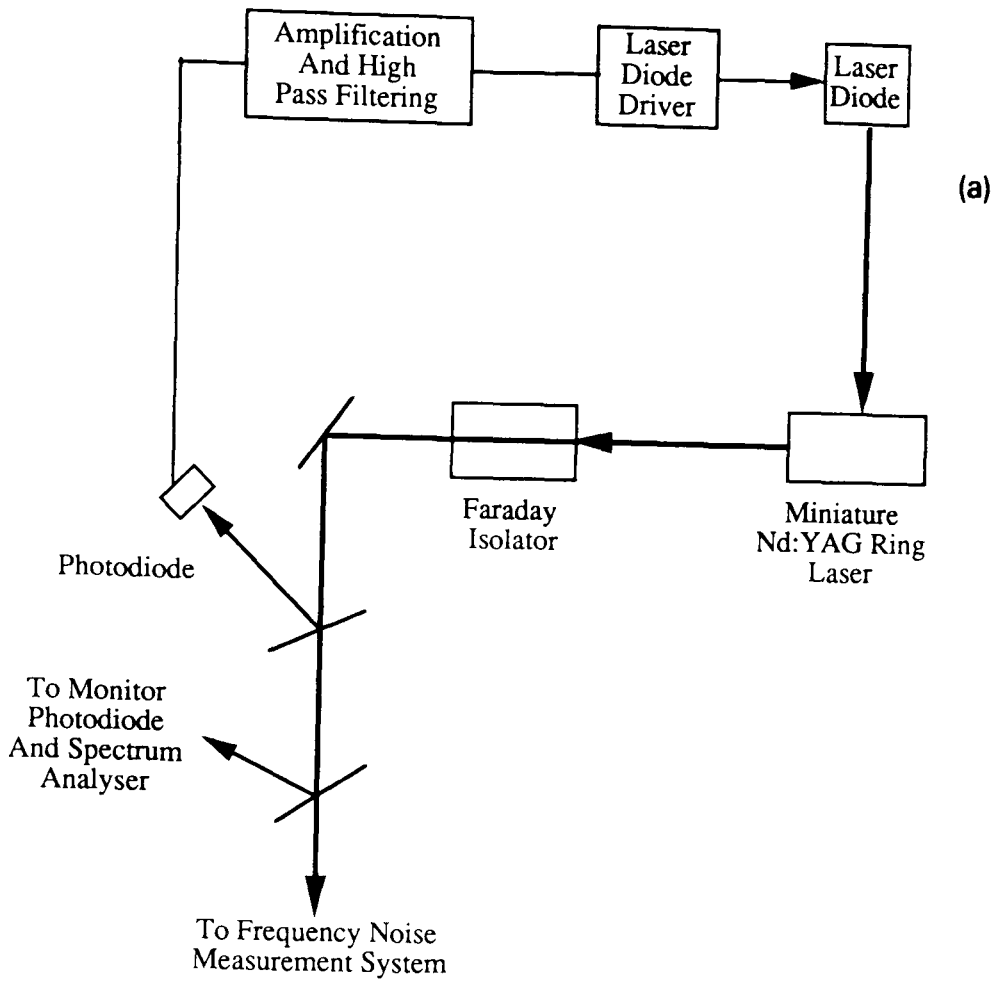


Fig. 4. Feedback circuit for damping relaxation oscillations in intensity noise. (a) Schematic diagram of the servo loop. The high pass filtering consists of four differentiating circuits, operating over the ranges 13–630 kHz, 230 kHz–2.3 MHz, 66– 660 kHz, 100 kHz–3 MHz. (b) Schematic Nyquist plot for the open loop transfer function of the servo loop.

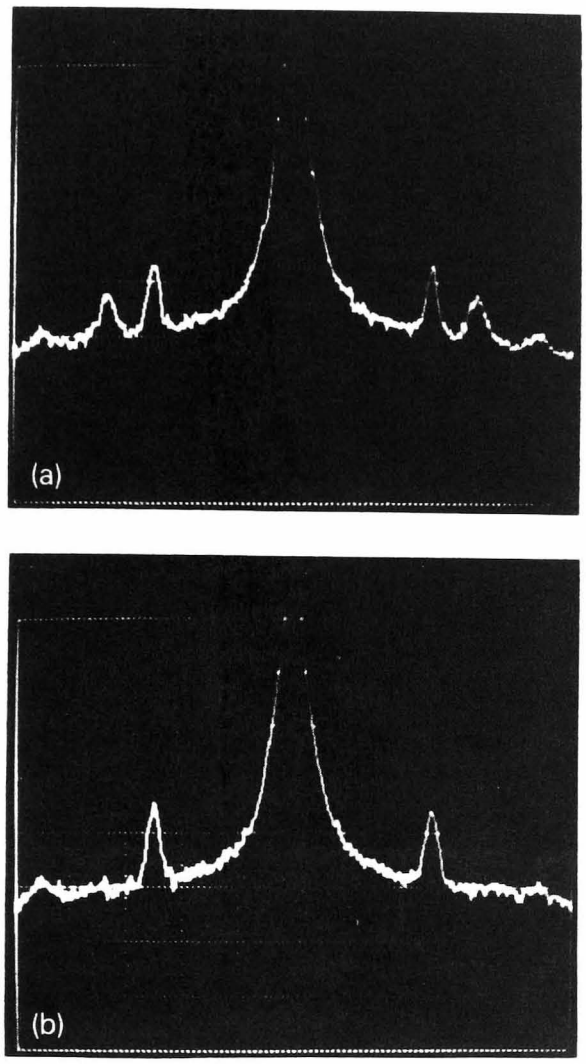


Fig. 5. Frequency noise spectra. Diagram centres are at 0 Hz with a full screen span of 750 kHz. The applied intensity signal is at 180 kHz. The resolution bandwidth is 10 kHz. The calibration of the vertical scale is 10 dB/division. (a) Frequency noise spectrum showing the apparent relaxation oscillation peak at a level of $\sim 1$ Hz/$\sqrt{\text{Hz}}$ without intensity servo operating; (b) Frequency noise spectrum when the relaxation oscillations in intensity noise are damped by the servo. The peak at the relaxation oscillation frequency is reduced into the background noise.

lations at the two values of dc offset. We conclude from this that our first measurements were probably affected by beam geometry fluctuations introduced by imperfect alignment of the beam through the electro-optic modulator. Beam geometry fluctuations caused by relaxation oscillations would have imposed intensity modulation of the beam at 10 MHz, modulated at the relaxation oscillation frequency and thus would appear on the demodulated signal: this would not have been the case for the applied peak which was purely an intensity signal. When we realigned the beam we reduced the sensitivity of our measurement system to beam geometry fluctuations. The apparent residual relaxation oscillations in the frequency noise spectrum in the improved measurement are likely to be caused by intensity noise, since both the applied peak and the peak at the relaxation oscillation frequency behave in exactly the same way. High frequency intensity noise coupled into the measured frequency spectrum because of small deviations of the servo locking point from the centre of the cavity resonance. These deviations occurred at a few kHz, outside the bandwidth of the servo.

When we applied the servo to damp relaxation oscillations in intensity noise, the relaxation oscillations were damped in both the intensity noise spectrum and the frequency noise spectrum (figs. 5b and 6a and 6b). The applied peak was slightly increased in each spectrum because the servo for intensity noise damped close to the relaxation oscillation frequency only and caused a very small amount of positive feedback at lower frequencies. (This is discussed in more detail in the appendix.) In the frequency noise, the relaxation oscillation peak was reduced into the background noise.

The upper limit to frequency noise of this laser at the frequency of the relaxation oscillations is therefore about 1 Hz/$\sqrt{\text{Hz}}$, which reduces to an upper limit of about 0.4 Hz/$\sqrt{\text{Hz}}$ when a servo to reduce relaxation oscillations in intensity noise is operating.

## 4. Conclusions

In our initial measurement we observed a residual relaxation oscillation in the frequency noise spectrum, probably caused by beam geometry fluctuations and intensity noise. In our later measurement, where greater care was taken with optical alignment, the residual peak at the relaxation oscillation frequency could probably be accounted for by intensity noise only. In both cases, the residual peak reduced when a servo system was operating which damped relaxation oscillations as observed in intensity noise.

For gravitational wave research we are particularly interested in using a miniature Nd:YAG ring laser to seed a high power Nd:YAG laser. These frequency noise measurements have shown that appar-

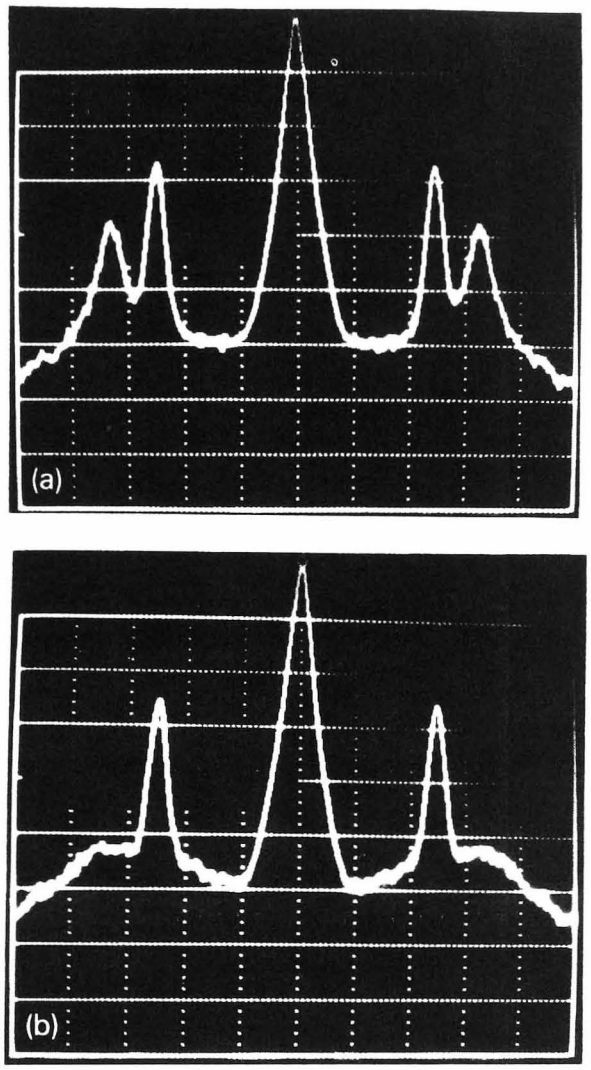


Fig. 6. Intensity noise spectra. Diagram centres are at 0 Hz with a full screen span of 750 kHz. The applied intensity signal is at 180 kHz. The resolution bandwidth is 10 kHz. The calibration of the vertical scale is 10 dB/division. (a) Intensity noise of the free-running laser; (b) Intensity noise of the laser when the intensity servo is operating. These measurements correspond to the frequency noise measurements shown in fig. 5.

ent relaxation oscillations in frequency noise are very small and can be reduced by damping the relaxation oscillation in intensity, and so are unlikely to cause problems in gravitational wave measurements at lower frequencies. Therefore. these miniature ring lasers can have very low noise at intermediate frequencies in addition to low noise at lower frequencies and look very attractive as master light sources for larger lasers in gravitational wave detectors.

## Acknowledgement

We are very grateful to K.Danzmann from the Max-Planck Institute in Garching, Germany, from whom we borrowed the laser, and to I. Kröpke from the Laser Zentrum in Hannover, Germany, for advising us on many aspects of miniature Nd:YAG ring laser characteristics. We also wish to thank A. Carmichael and other members of our group in Glasgow for help and advice. A.M. Campbell and S Rowan are supported by SERC. We are grateful to the University of Glasgow and SERC for equipment support.

## Appendix

The servo system used to damp relaxation oscillations observed in intensity noise is shown in fig. 4a. The relaxation oscillations are detected by monitoring some of the light on a photodiode. The signal from the photodiode is amplified and filtered using four differentiators to provide the large amount of phase lead needed to compensate for the 180° phase lag at the relaxation oscillation frequency, for a phase lag above about 11 kHz due to a low pass filter effect in the diode current driver, and for a few microseconds of time delay in the diode current driver. The amplified and filtered signal was fed back to the diode driver to control the diode laser pump current.

Some light was also split off to a separate photodiode which independently monitored the effects of the intensity servo.

In fig. 4b a schematic Nyquist plot for the open loop transfer function of the servo to reduce intensity noise is shown. At the frequency of the relaxation oscillation, the servo can reduce intensity noise by up to 20 dB and the relaxation oscillation is critically damped. At frequencies below about 150 kHz the servo system causes a slight increase in the noise background due to a small amount of positive feedback.

## References

[1] J. Hough et al., Max-Planck-Institut für Quantenoptik/University of Glasgow Report, MPQ 147 GWD/137/JH(89).
[2] P. Fritschel, A. Jeffries and T.J. Kane, Opt. Lett. 14 (1989) 993.
[3] T.J. Kane, IEEE Phot. Lett. 2 (1990) 244.
[4] L.G. Kazovsky and D.A. Atlas, J. Lightwave Technol. (1990) 294.
[5] T.J. Kane and R.L. Byer, Opt. Lett. 10 (1985) 65.
[6] R.W.P. Drever, J.L. Hall, F.V. Kowalski, J. Hough, G.M. Ford, A.J. Munley and H. Ward, Appl. Phys. B 31 (1983) 97.

JOURNAL OF MODERN OPTICS, 1994, VOL. 41, NO. 6, 1263–1269

# Broadband intensity stabilization of a diode-pumped monolithic miniature Nd:YAG ring laser

S. ROWAN, A. M. CAMPBELL, K. SKELDON and J. HOUGH

Department of Physics and Astronomy, University of Glasgow, Glasgow G12 8QQ, Scotland

(*Received 1 October 1993; revision received 18 November 1993*)

**Abstract.** We have built an electronic servo system to reduce the intensity noise in a diode-pumped single-mode monolithic Nd:YAG ring laser with a maximum output power of 350 mW. The servo used two stabilization systems operating simultaneously over two different frequency ranges, each of which detected a fraction of the laser output, amplified and phase shifted the detected signals and used the resultant signals to control the current to the laser diode pump. We achieved a reduction in intensity noise of up to a factor of 30 for frequencies up to about 1 kHz, with some noise reduction observable up to about 30 kHz. At frequencies between around 30 and 200 kHz the intensity noise was increased by a factor of approximately 1·4. In the frequency range 200 to 300 kHz, around the relaxation oscillation frequency of 260 kHz, the intensity noise was suppressed, the reduction factor being approximately 14 at 260 kHz.

## 1. Introduction

The development of a high power stable continuous wave Nd:YAG laser operated at its fundamental wavelength of 1064 nm, or frequency doubled to 532 nm, is of great interest for use in the next generation of gravitational wave detectors [1]. Diode-pumped monolithic Nd:YAG ring lasers, which exhibit low-noise characteristics [2, 3], could be ideal candidates for seeding such a high-power c.w. Nd:YAG laser. Such lasers do exhibit relaxation oscillations in their intensity, but Kane [4] has demonstrated in the case of a low-power system operating at 1·32 μm that noise around the relaxation oscillation frequency can be significantly reduced by electronic feedback. We have previously examined the frequency noise of a higher power laser operating at 1064 nm at frequencies around the relaxation oscillation and found it to be small [3]. In this paper we examine the intensity noise of a very similar laser and show that it can be reduced simultaneously at the frequency range of interest for gravitational wave detection (<100 Hz to a few kHz), and at the relaxation oscillation frequency (260 kHz). Although relaxation oscillation frequencies are well above the frequency range of interest for gravitational wave detection, large fluctuations in intensity at those frequencies could couple into measurements at lower frequencies through nonlinearities in the detection system.

Similar work has been performed by Harb *et al.* [5] and commercial systems available from Lightwave Inc. have intensity noise reduction systems installed.

## 2. Experimental system

The laser we used was a monolithic diode-pumped miniature Nd:YAG ring laser built at the Laser Zentrum in Hannover, Germany, based on the original

design by Kane and Byer [6]. This laser emits up to 350 mW in the $TEM_{00}$ mode, but for measurements made here was run at 200 mW.

To control the intensity noise of the laser we used a two-loop servo system which operated over two frequency ranges simultaneously (figure 1). Light from the laser, after isolation using a Faraday effect device, is split off from the main beam and directed onto two photodiodes. The signal from each of these photodiodes is amplified, phase shifted and then the resultant signals are added. The combined signal then controls the laser diode pump current directly at the pins to the diode laser. One loop of the intensity servo system operates primarily at low frequencies, from near d.c. to about 30 kHz, with most reduction obtained at frequencies of a few hundred Hz. The other servo loop operates solely at frequencies around the relaxation oscillation. The amount of light falling on the photodiode in the servo loop operating primarily at low frequencies was approximately 7 mW. The amount of light falling on the photodiode in the loop operating in the high frequency range was approximately 13 mW. A separate photodiode is used for each loop only so that the loops can easily be operated independently: future systems would be likely to use one photodiode for both loops. In addition to this, some light was split off to a photodiode which independently monitored the effects of the intensity servo system. The amount of light falling on the external photodiode was approximately 7 mW.

The low-frequency loop consists of two Princeton model 113 amplifiers, one operating over frequencies from 10 to 100 Hz, and the other operating from d.c. to 300 kHz. The signal is then sent to the power pins of the diode laser via a high pass filter with a corner of 7 Hz. The maximum gain of this loop was about 160 at about 200 Hz. The high frequency loop consists of two amplifiers and three differentiators operating over relatively narrow frequency bands around the relaxation oscillation, and a buffer amplifier to take the signal into the diode laser. The low-frequency and high-frequency signals are added together before injection into the diode laser.

In figure 2 Nyquist plots for the open loop transfer function of the two-loop

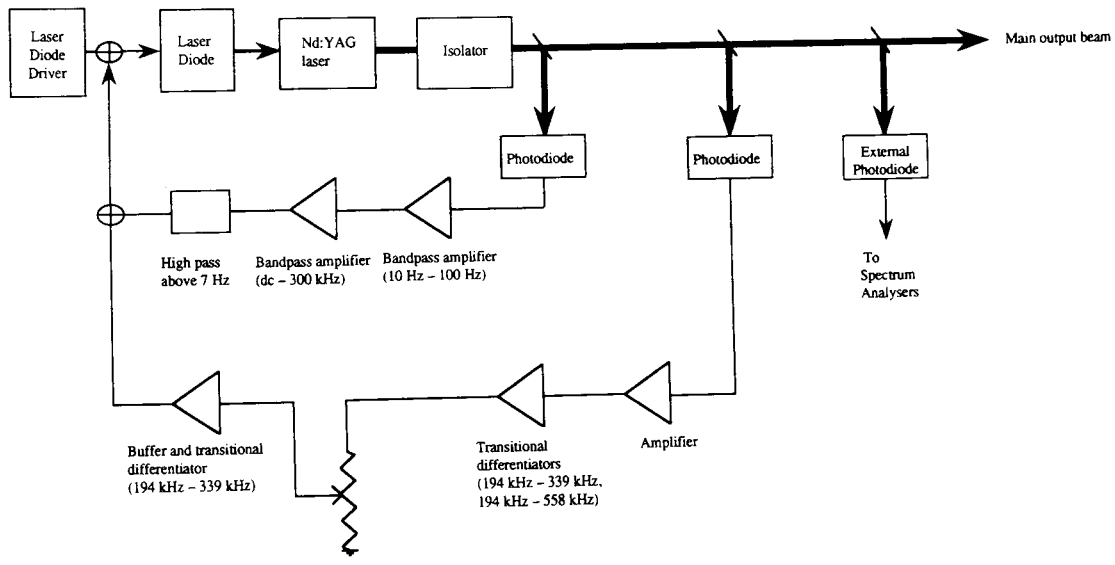


Figure 1. Schematic diagram of the two-loop intensity stabilization system.

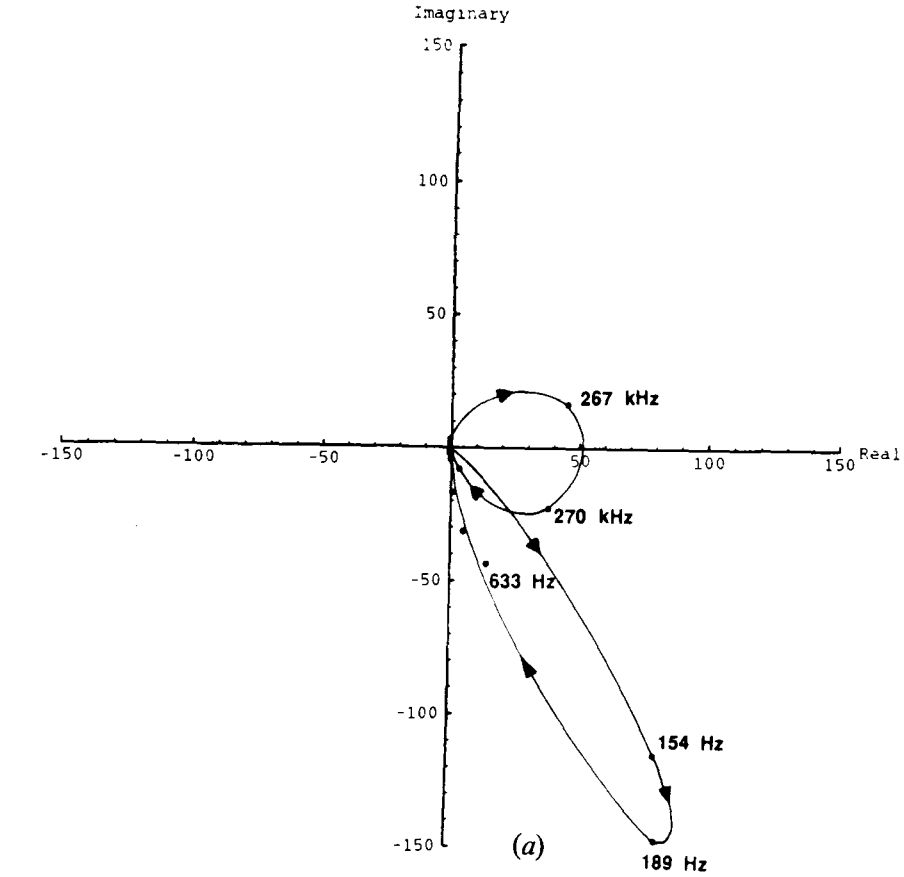


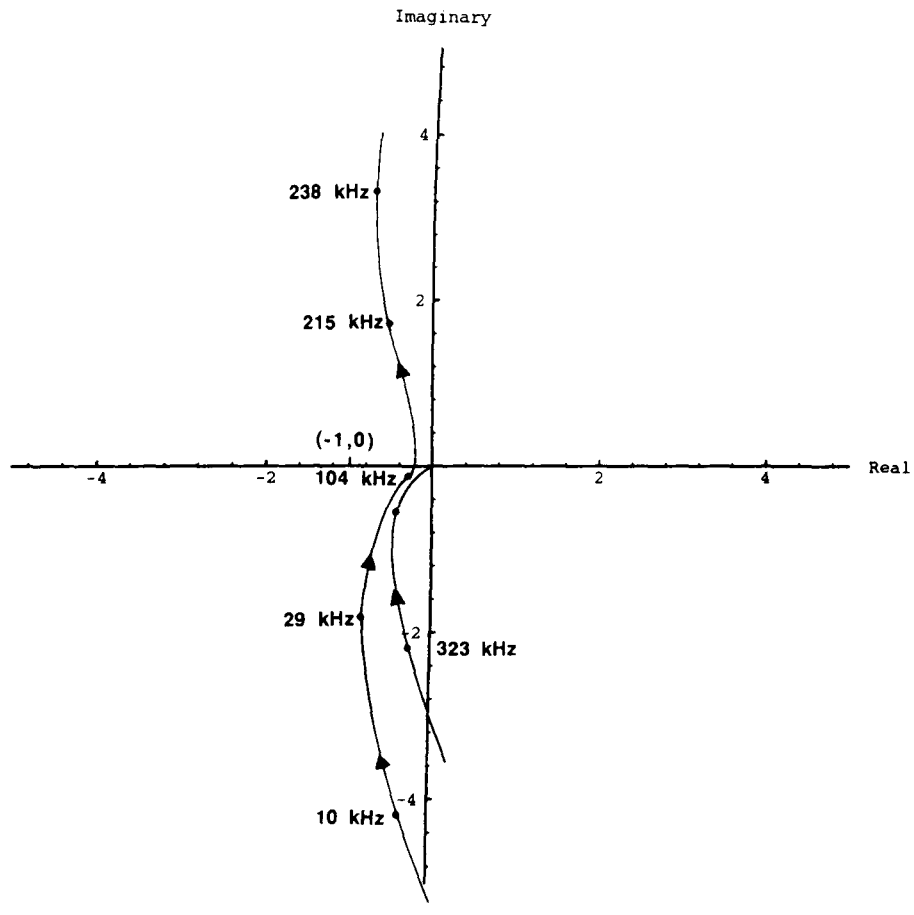


Figure 2. Nyquist plots for the intensity stabilization servo loop. (*a*) Nyquist plot for the open loop transfer function of the complete stabilization system. (*b*) Detail of Nyquist plot showing behaviour of transfer function close to the point $(-1, 0)$.

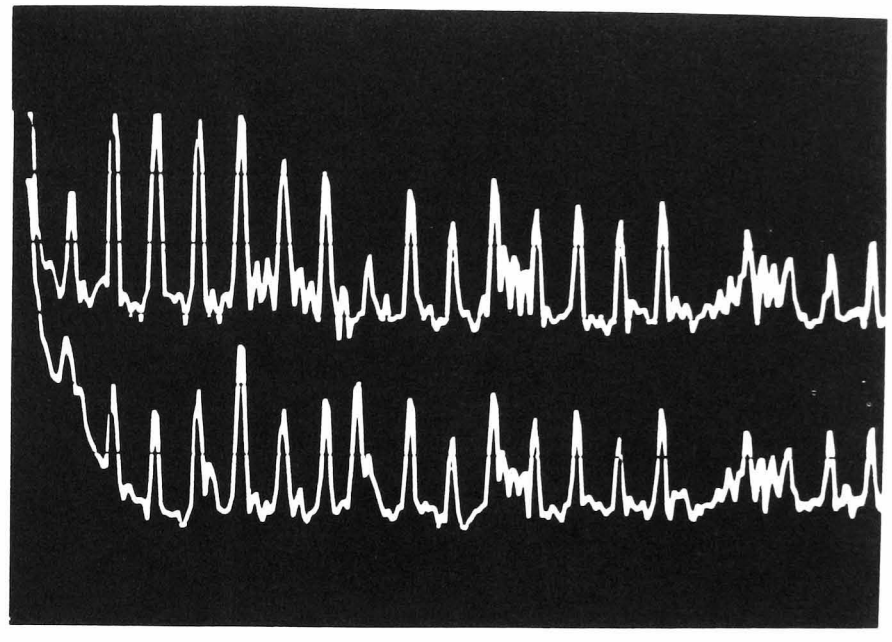

Figure 3. Spectra showing intensity noise with and without the intensity stabilization system. The full screen span is from 0 to 1 kHz. The resolution bandwidth is 6 Hz. The calibration of the vertical scale is 10 dB/division. At 500 Hz the relative intensity noise with the stabilization system operating corresponds to a level of $4{\cdot}6 \times 10^{-8}$ $(\mathrm{Hz})^{-1/2}$. Note that the 50 Hz peak and harmonics are on the laser light.

servo system are shown. Figure 2(*a*) shows the Nyquist plot for the whole frequency range, while figure 2(*b*) shows the region around the $(-1, 0)$ point. From figure 2(*a*) we would expect to have significant gain available from a few Hz to a few kHz, with maximum gain and thus maximum reduction in intensity noise at a few hundred Hz. We would also expect to have gain available in the range 200

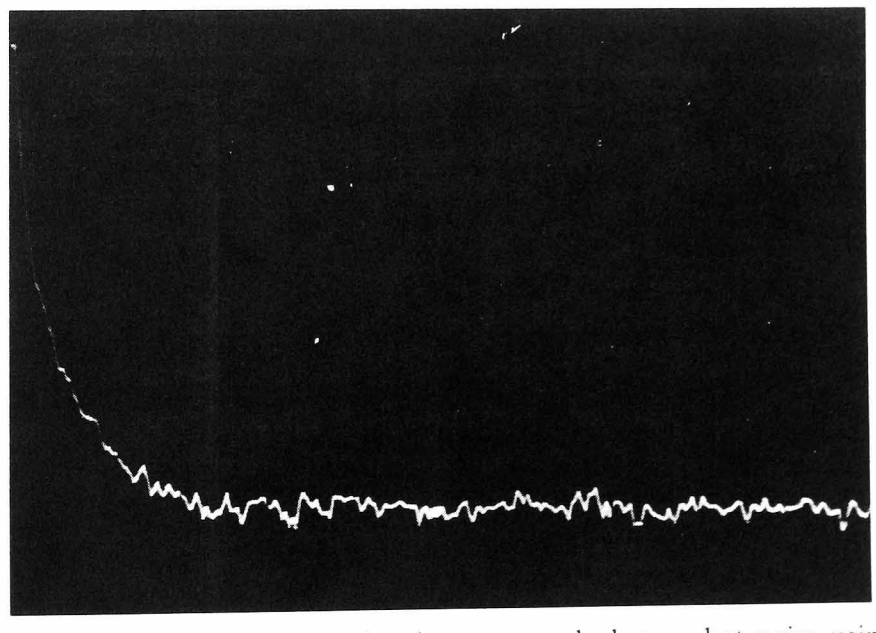

Figure 4. Intensity noise spectrum showing measured photon shot noise using a white light source. The full screen span is from 0 to 1 kHz. The resolution bandwidth is 6 Hz. The calibration of the vertical scale is 10 dB/division. At 500 Hz the measured photon shot noise corresponds to a level of $1{\cdot}5 \times 10^{-8}\,(\mathrm{Hz})^{-1/2}$.

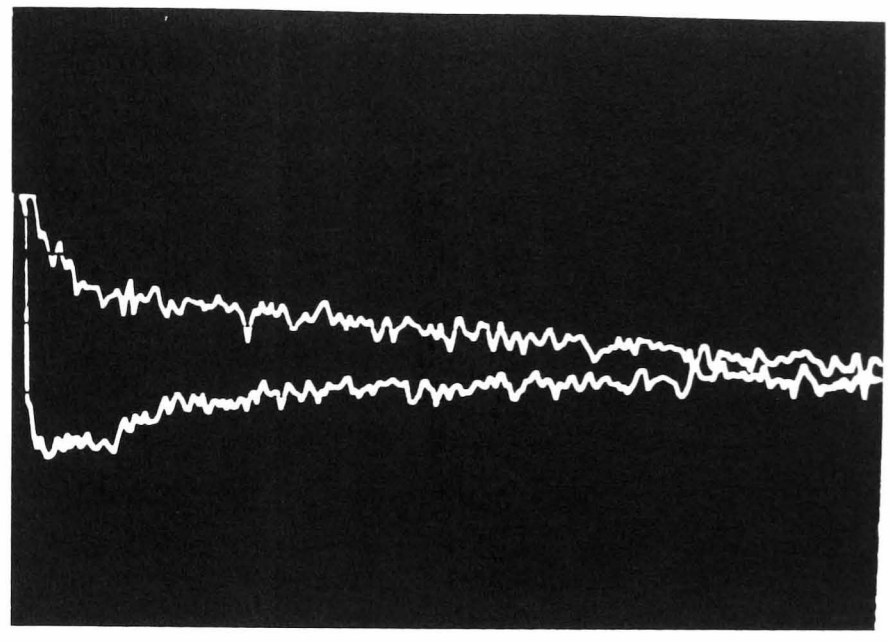

Figure 5. Spectra showing intensity noise with and without the intensity stabilization system. The full screen span is from 0 to 25 kHz. The resolution bandwidth is 150 Hz. The vertical scale is 10 dB/division.

to 300 kHz and thus expect the intensity noise at the relaxation oscillation frequency of 260 kHz to be reduced. Figure 2 (*b*) shows that the open loop transfer function is close to $(-1, 0)$ for frequencies between 30 and 200 kHz; however the gain of the loop at these frequencies is small and the transfer function does not encircle the $(-1, 0)$ point. We would thus expect there to be a slight increase in the intensity noise at these frequencies.

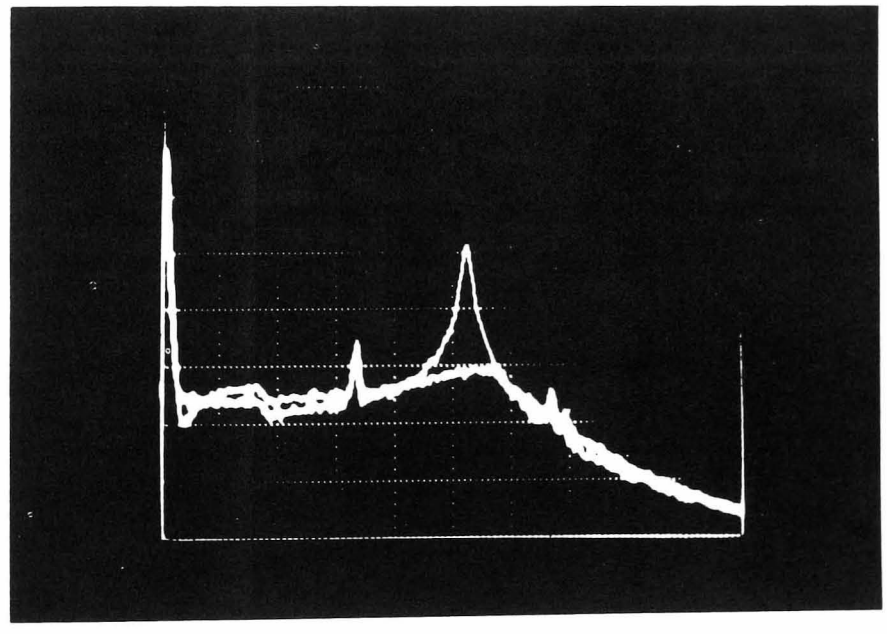

Figure 6. Spectra showing intensity noise with and without the intensity stabilization system. The full screen span is from 0 to 500 kHz. The resolution bandwidth is 3 kHz. The vertical scale is 10 dB/division.

## 3. Results

Our results are shown in figures 3, 4, 5 and 6. Figure 3 shows spectra of the laser intensity noise in the region 0–1 kHz with and without the intensity reduction system operating. The intensity noise was reduced by up to factor of 30 over this frequency range. The noise was reduced to $4{\cdot}6 \times 10^{-8}\,(\mathrm{Hz})^{-1/2}$ at 500 Hz of which $1{\cdot}5 \times 10^{-8}\ (\mathrm{Hz})^{-1/2}$ was photon shot noise in 7 mW of detected light. Figure 4 shows a spectrum of the measured photon shot noise over the same frequency range using a white light source.

Figure 5 shows the reduction in intensity noise over the region 0–25 kHz. This figure clearly shows the intensity servo working over this range.

A spectrum of the intensity noise up to 500 kHz is shown in figure 6. The locked intensity noise is slightly higher than the unlocked intensity noise for frequencies between 30 and 200 kHz. This is to be expected from the Nyquist plot. The relaxation oscillation at 260 kHz is reduced by a factor of 14, bringing down the relative intensity noise to $2{\cdot}3 \times 10^{-6}\,(\mathrm{Hz})^{-1/2}$ at that frequency.

## 4. Discussion and conclusions

From the results above it can be seen that in the frequency range 0–1 kHz, with the intensity noise servo operating, the intensity noise was reduced to a level within 10 dB of the shot noise limit for the detected light. We would not expect to be able to reduce the intensity noise further than a level of about 5 dB above the shot noise limit for the light detected on the external photodiode due to a contribution to the laser noise from the shot noise and amplifier noise of the low frequency servo loop. (Note that due to the relatively low gain of the high-frequency servo loop at low frequencies, noise in this loop did not contribute to the intensity noise discussed above.) The loop gain available should have allowed reduction to the limit above but our experience with other lasers [7] has suggested that the coupling of beam geometry fluctuations into intensity noise at a photodiode can limit performance.

It was noted that the performance of the stabilization system was limited more severely if the external optical isolation of the laser was not optimized. This poorer performance could be improved by passing the light through a piece of single mode optical fibre before extracting the fraction of the light for the intensity stabilization system. We conclude from this that lack of isolation may increase the level of higher-order modes in the system and these may couple into intensity noise at the photodiode.

**Acknowledgments**

We are very grateful to K. Danzmann from the Laser Zentrum in Hannover, Germany, from whom we borrowed the laser, and to I. Kröpke and I. Freitag from the Laser Zentrum in Hannover, for advising us on many aspects of miniature Nd:YAG ring laser characteristics, and we wish to thank to Charles Harb for technical advice. We also wish to thank other members of our group in Glasgow for help and advice. A. M. Campbell and S. Rowan are supported by the Science and Engineering Research Council (SERC). K. Skeldon is in receipt of a University of Glasgow Scholarship. We are grateful to the University of Glasgow and SERC for equipment support.

## References

[1] HOUGH, J., WALTHER, H., SCHUTZ, B. F., EHLERS, J., WELLING, H., CORBETT, I. F., KOSE, V., *et al.*, 1989, Proposal for a Joint German–British Interferometric Gravitational Wave Detector, *Max-Planck-Institut für Quantenoptik/University of Glasgow Report*, MPQ 147 GWD/137/JH(89).

[2] FRITSCHEL, P., JEFFRIES, A., and KANE, T. J., 1989, *Optics Lett.*, **14,** 993.

[3] CAMPBELL, A. M., ROWAN, S., and HOUGH, J., 1992, *Phys. Lett.* A, **170,** 363.

[4] KANE, T. J., 1990, *IEEE Phot. Tech. Lett.*, **2,** 244.

[5] HARB, C. C., GRAY, M. B., BACHOR, H.-A., SCHILLING, R., ROTTENGATTER, P., FREITAG, I., and WELLING, H., 1993, *IEEE J. Quant. Electron.*, (submitted for publication).

[6] KANE, T. J., and BYER, R. L., 1985, *Optics Lett.*, **10,** 65.

[7] ROBERSTON, N. A., HOGGAN, S., MANGAN, J. B., and HOUGH, J., 1986, *Appl. Phys.* B, **39,** 149.